

E. Soriano  
J. Marco-Contelles *Editors*

# Computational Mechanisms of Au and Pt Catalyzed Reactions



Springer

## **Topics in Current Chemistry**

**Editorial Board:**

**A. de Meijere • K.N. Houk • C.A. Hunter • J.-M. Lehn  
S.V. Ley • M. Olivucci • J. Thiem • B.M. Trost • M. Venturi  
P. Vogel • C.-H. Wong • H. Wong • H. Yamamoto**

# Topics in Current Chemistry

## Recently Published and Forthcoming Volumes

### **Computational Mechanisms of Au and Pt Catalyzed Reactions**

Volume Editors: Elena Soriano,  
José Marco-Contelles  
Vol. 302, 2011

### **Reactivity Tuning in Oligosaccharide Assembly**

Volume Editors: Bert Fraser-Reid,  
J. Cristóbal López  
Vol. 301, 2011

### **Luminescence Applied in Sensor Science**

Volume Editors: Luca Prodi, Marco Montalti,  
Nelsi Zaccheroni  
Vol. 300, 2011

### **Chemistry of Opioids**

Volume Editor: Hiroshi Nagase  
Vol. 299, 2011

### **Electronic and Magnetic Properties of Chiral Molecules and Supramolecular Architectures**

Volume Editors: Ron Naaman,  
David N. Beratan, David H. Waldeck  
Vol. 298, 2011

### **Natural Products via Enzymatic Reactions**

Volume Editor: Jörn Piel  
Vol. 297, 2010

### **Nucleic Acid Transfection**

Volume Editors: Wolfgang Bielke,  
Christoph Erbacher  
Vol. 296, 2010

### **Carbohydrates in Sustainable Development II**

Volume Editors: Amélia P. Rauter,  
Pierre Vogel, Yves Queneau  
Vol. 295, 2010

### **Carbohydrates in Sustainable Development I**

Volume Editors: Amélia P. Rauter,  
Pierre Vogel, Yves Queneau  
Vol. 294, 2010

### **Functional Metal-Organic Frameworks: Gas Storage, Separation and Catalysis**

Volume Editor: Martin Schröder  
Vol. 293, 2010

### **C-H Activation**

Volume Editors: Jin-Quan Yu, Zhangjie Shi  
Vol. 292, 2010

### **Asymmetric Organocatalysis**

Volume Editor: Benjamin List  
Vol. 291, 2010

### **Ionic Liquids**

Volume Editor: Barbara Kirchner  
Vol. 290, 2010

### **Orbitals in Chemistry**

Volume Editor: Satoshi Inagaki  
Vol. 289, 2009

### **Glycoscience and Microbial Adhesion**

Volume Editors: Thisbe K. Lindhorst,  
Stefan Oscarson  
Vol. 288, 2009

### **Templates in Chemistry III**

Volume Editors: Broekmann, P., Dötz, K.-H.,  
Schalley, C.A.  
Vol. 287, 2009

### **Tubulin-Binding Agents: Synthetic, Structural and Mechanistic Insights**

Volume Editor: Carlomagno, T.  
Vol. 286, 2009

### **STM and AFM Studies on (Bio)molecular Systems: Unravelling the Nanoworld**

Volume Editor: Samorì, P.  
Vol. 285, 2008

### **Amplification of Chirality**

Volume Editor: Soai, K.  
Vol. 284, 2008

# Computational Mechanisms of Au and Pt Catalyzed Reactions

Volume Editors: Elena Soriano · José Marco-Contelles

With Contributions by

B. Alcaide · P. Almendros · T.M. Campo · L. Cavallo · A. Correa ·  
O.N. Faza · L. Fensterbank · V. Gandon · F. López · A.R. de Lera ·  
A. Lledós · M. Malacria · J. Marco-Contelles · J.L. Mascareñas ·  
V. Michelet · S. Montserrat · S.P. Nolan · E. Soriano · P.Y. Toullec ·  
G. Ujaque

*Editors*

Dr. Elena Soriano  
Laboratorio de Radicales Libres y Química  
Computacional  
Instituto de Química Orgánica  
General (CSIC)  
Juan de la Cierva, 3  
28006 Madrid  
Spain  
esoriano@iqog.csic.es

Dr. José Marco-Contelles  
Laboratorio de Radicales Libres y Química  
Computacional  
Instituto de Química Orgánica  
General (CSIC)  
Juan de la Cierva, 3  
28006 Madrid  
Spain  
jlmarco@iqog.csic.es

ISSN 0340-1022 e-ISSN 1436-5049  
ISBN 978-3-642-21082-2 e-ISSN 978-3-642-21083-9  
DOI 10.1007/978-3-642-21083-9  
Springer Heidelberg Dordrecht London New York

Library of Congress Control Number: 2011929696

© Springer-Verlag Berlin Heidelberg 2011

This work is subject to copyright. All rights are reserved, whether the whole or part of the material is concerned, specifically the rights of translation, reprinting, reuse of illustrations, recitation, broadcasting, reproduction on microfilm or in any other way, and storage in data banks. Duplication of this publication or parts thereof is permitted only under the provisions of the German Copyright Law of September 9, 1965, in its current version, and permission for use must always be obtained from Springer. Violations are liable to prosecution under the German Copyright Law.

The use of general descriptive names, registered names, trademarks, etc. in this publication does not imply, even in the absence of a specific statement, that such names are exempt from the relevant protective laws and regulations and therefore free for general use.

*Cover design:* WMXDesign GmbH, Heidelberg, Germany

Printed on acid-free paper

Springer is part of Springer Science+Business Media ([www.springer.com](http://www.springer.com))

---

## Volume Editors

**Dr. Elena Soriano**

Laboratorio de Radicales Libres y Química  
Computacional  
Instituto de Química Orgánica  
General (CSIC)  
Juan de la Cierva, 3  
28006 Madrid  
Spain  
*esoriano@iqog.csic.es*

**Dr. José Marco-Contelles**

Laboratorio de Radicales Libres y Química  
Computacional  
Instituto de Química Orgánica  
General (CSIC)  
Juan de la Cierva, 3  
28006 Madrid  
Spain  
*jlmarco@iqog.csic.es*

## Editorial Board

**Prof. Dr. Armin de Meijere**

Institut für Organische Chemie  
der Georg-August-Universität  
Tammanstr. 2  
37077 Göttingen, Germany  
*ameijer1@uni-goettingen.de*

**Prof. Dr. Steven V. Ley**

University Chemical Laboratory  
Lensfield Road  
Cambridge CB2 1EW  
Great Britain  
*Svl1000@cus.cam.ac.uk*

**Prof. Dr. Kendall N. Houk**

University of California  
Department of Chemistry and Biochemistry  
405 Hilgard Avenue  
Los Angeles, CA 90024-1589, USA  
*houk@chem.ucla.edu*

**Prof. Dr. Massimo Olivucci**

Università di Siena  
Dipartimento di Chimica  
Via A De Gasperi 2  
53100 Siena, Italy  
*olivucci@unisi.it*

**Prof. Dr. Christopher A. Hunter**

Department of Chemistry  
University of Sheffield  
Sheffield S3 7HF, United Kingdom  
*c.hunter@sheffield.ac.uk*

**Prof. Dr. Joachim Thiem**

Institut für Organische Chemie  
Universität Hamburg  
Martin-Luther-King-Platz 6  
20146 Hamburg, Germany  
*thiem@chemie.uni-hamburg.de*

**Prof. Dr. Jean-Marie Lehn**

ISIS  
8, allée Gaspard Monge  
BP 70028  
67083 Strasbourg Cedex, France  
*lehn@isis.u-strasbg.fr*

**Prof. Dr. Barry M. Trost**

Department of Chemistry  
Stanford University  
Stanford, CA 94305-5080, USA  
*bmtrost@leland.stanford.edu*

**Prof. Dr. Margherita Venturi**

Dipartimento di Chimica  
Università di Bologna  
via Selmi 2  
40126 Bologna, Italy  
*margherita.venturi@unibo.it*

**Prof. Dr. Pierre Vogel**

Laboratory of Glycochemistry  
and Asymmetric Synthesis  
EPFL – Ecole polytechnique fédérale  
de Lausanne  
EPFL SB ISIC LGSA  
BCH 5307 (Bat.BCH)  
1015 Lausanne, Switzerland  
*pierre.vogel@epfl.ch*

**Prof. Dr. Chi-Huey Wong**

Professor of Chemistry, Scripps Research  
Institute  
President of Academia Sinica  
Academia Sinica  
128 Academia Road  
Section 2, Nankang  
Taipei 115  
Taiwan  
*chwong@gate.sinica.edu.tw*

**Prof. Dr. Henry Wong**

The Chinese University of Hong Kong  
University Science Centre  
Department of Chemistry  
Shatin, New Territories  
*hncwong@cuhk.edu.hk*

**Prof. Dr. Hisashi Yamamoto**

Arthur Holly Compton Distinguished  
Professor  
Department of Chemistry  
The University of Chicago  
5735 South Ellis Avenue  
Chicago, IL 60637  
773-702-5059  
USA  
*yamamoto@uchicago.edu*

# Topics in Current Chemistry

## Also Available Electronically

*Topics in Current Chemistry* is included in Springer's eBook package *Chemistry and Materials Science*. If a library does not opt for the whole package the book series may be bought on a subscription basis. Also, all back volumes are available electronically.

For all customers with a print standing order we offer free access to the electronic volumes of the series published in the current year.

If you do not have access, you can still view the table of contents of each volume and the abstract of each article by going to the SpringerLink homepage, clicking on "Chemistry and Materials Science," under Subject Collection, then "Book Series," under Content Type and finally by selecting *Topics in Current Chemistry*.

You will find information about the

- Editorial Board
- Aims and Scope
- Instructions for Authors
- Sample Contribution

at [springer.com](http://springer.com) using the search function by typing in *Topics in Current Chemistry*.

*Color figures* are published in full color in the electronic version on SpringerLink.

## Aims and Scope

The series *Topics in Current Chemistry* presents critical reviews of the present and future trends in modern chemical research. The scope includes all areas of chemical science, including the interfaces with related disciplines such as biology, medicine, and materials science.

The objective of each thematic volume is to give the non-specialist reader, whether at the university or in industry, a comprehensive overview of an area where new insights of interest to a larger scientific audience are emerging.



Thus each review within the volume critically surveys one aspect of that topic and places it within the context of the volume as a whole. The most significant developments of the last 5–10 years are presented, using selected examples to illustrate the principles discussed. A description of the laboratory procedures involved is often useful to the reader. The coverage is not exhaustive in data, but rather conceptual, concentrating on the methodological thinking that will allow the non-specialist reader to understand the information presented.

Discussion of possible future research directions in the area is welcome.

Review articles for the individual volumes are invited by the volume editors.

In references *Topics in Current Chemistry* is abbreviated *Top Curr Chem* and is cited as a journal.

Impact Factor 2009: 4.291; Section “Chemistry, Multidisciplinary”: Rank 20 of 138

# Preface

The homogeneous platinum- and gold-catalyzed transformation of unsaturated precursors is a very active area in the field of catalysis research. Indeed information about new novel reactions and modified, improved, metal complexes is published every week. These findings involve interesting and sometimes surprising changes in the molecular connectivity, which can often be applied to a growing number of applications in total synthesis.

The rapid expansion of this field is due to the peculiar Lewis acid properties of the concerned metals. The alkynophilic character of these soft metals and the  $\pi$ -acid carbophilic activation of unsaturated groups promote the intra- or intermolecular attack of nucleophiles to form carbon-carbon and carbon-heteroatom bonds.

The pioneering efforts in this area in the early 1990s utilized simple metal salts, such as halides because of their apparent insensitivity under aqueous conditions and ability to successfully promote a diversity of synthetic transformations. But a decade later, Au(I) cationic species have proven to be superb catalysts. The chemistry of  $\pi$ -complexes of gold finally underwent an explosive growth when novel complexes were used successfully as catalysts for a rapidly growing number of important reactions or transformations of alkynes, alkenes and allenes.

These catalysts allow us to overcome additional problems associated with other metal complexes that also promote the same transformations, such as Hg salts, since they are considered essentially nontoxic. Furthermore, they combine high affinity to the  $\pi$  system with the advantages of a kinetically labile carbon-metal bond that can be readily cleaved under the reaction conditions. These reactions provide an atom-economical entry into functionalized cyclic and acyclic scaffolds useful for the synthesis of natural and non-natural products under mild conditions with excellent chemoselectivity and high synthetic efficiency.

Although this protocol gives rise to a wide range of transformations and shows a large versatility, an array of mechanistic hypotheses has been formulated to account for the results, leading many times to a diversity of mechanistic proposals for the same reaction. Therefore, a mechanistic interpretation is needed to direct and improve a given process. The theoretical underpinnings have been considered recently and, despite computational analyses being less abundant, they have become a useful

tool for rationalizing the role of the molecular structure of precursor and catalyst and accounting for the versatility of these reactions.

In this book, we provide a perspective on the mechanisms as suggested by theoretical calculations and discuss the most significant physical features and results obtained in this fascinating research area. In particular, the description of the probable intermediates, given their transient nature, has provided critical information about the reaction pathways.

The layout of this book is as follows. Chapter 1 presents an overview of the theoretical properties of the reactant complexes and of the nature of the likely key reaction intermediates. It is focused on the results reported on the structure, bonding and reactivity. A correlation of the catalytic behavior with the available structural data, coordination chemistry, and reactivity patterns, including relativistic effects, is provided which allows the underlying principles of catalytic carbophilic activation by  $\pi$ -acids to be formulated.

In Chapter 2 a review of the recent and seminal advances in 1,*n*-enynes cycloisomerization reactions in the presence of carbophilic transition metals is described. These compounds have emerged as highly useful and important precursors for this synthetic protocol. The recent mechanistic insights, the enantioselective versions and the applications in total synthesis are highlighted.

Chapter 3 analyzes the rearrangement of propargylic esters, a block of essential and versatile precursors. The description of different mechanisms taken from the recent literature in which stereoselectivity, with special focus on chirality transfer and memory of chirality phenomena, is shown. The chapter starts with reactions involving simpler rearrangements and adds steps until more complex reaction cascades with highly functionalized substrates.

Chapter 4 focuses on N-heterocyclic carbenes (NHC), a family of complexes as effective alternatives to classical tertiary phosphines as catalysts in transition metal catalyzed transformations. The rapid development of this area is a result of synergic interactions between experimental and computational chemists. The authors detail how computer modeling has proven extremely useful to rationalize the experimental data and to accelerate the pace at which this chemistry is being developed.

Chapter 5 provides an insight into the activation of allenes and allenynes by gold complexes toward nucleophilic attack. It is focused on the various possible geometries of allene-gold species. While some retain the stereochemical information of the starting optically active allenes, others may lose it by planarization. To shed light on this, the factors governing axial-to-center chirality transfer are described. Some concepts are illustrated by selected examples of transformations analyzed computationally.

Chapter 6 shows how computational studies can be a useful complementary tool to experimental methodology. In this case, the elucidation of mechanisms and regioselectivity of heterocyclization of allenes catalyzed by late transition metals.

Finally, the theoretical analyses of the reaction mechanisms for gold-catalyzed cycloaddition reactions involving allenes and dienes have been assessed in the Chapter 7. This family of reactions gives different products, six- and seven-membered rings depending on the nature of the catalyst. According to the published

theoretical studies, the mechanisms proposed for the [4C+3C] and [4C+2C] intramolecular cycloadditions are detailed.

We have tried to cover the most relevant computational studies on the main topics in this research area, from the physical properties of the noble-metal catalysts to the most important transformations catalyzed by them. In some cases this has required more detailed theoretical chapters. Other topics have focused more on the practical application of computational chemistry as a valuable and complementary tool to the experimental research.

We sincerely appreciate and acknowledge the first-class contributions of the authors who collaborated in producing this book and the encouragement, help and support of the team at the publisher, Springer.

Spain  
May 2011

Elena Soriano  
José Marco-Contelles



# Contents

<b>Structure, Bonding, and Reactivity of Reactant Complexes and Key Intermediates</b> .....	1
Elena Soriano and José Marco-Contelles	
<b>Cycloisomerization of 1,<i>n</i>-Enynes Via Carbophilic Activation</b> .....	31
Patrick Yves Toullec and Véronique Michelet	
<b>DFT-Based Mechanistic Insights into Noble Metal-Catalyzed Rearrangement of Propargylic Derivatives: Chirality Transfer Processes</b> .....	81
Olalla Nieto Faza and Angel R. de Lera	
<b><i>N</i>-Heterocyclic Carbene Complexes of Au, Pd, and Pt as Effective Catalysts in Organic Synthesis</b> .....	131
Andrea Correa, Steven P. Nolan, and Luigi Cavallo	
<b>Activation of Allenes by Gold Complexes: A Theoretical Standpoint</b> ...	157
Max Malacria, Louis Fensterbank, and Vincent Gandon	
<b>Heterocyclization of Allenes Catalyzed by Late Transition Metals: Mechanisms and Regioselectivity</b> .....	183
Benito Alcaide, Pedro Almendros, Teresa Martínez Campo, Elena Soriano, and José Marco-Contelles	
<b>Gold-Catalyzed Cycloadditions Involving Allenes: Mechanistic Insights from Theoretical Studies</b> .....	225
Sergi Montserrat, Gregori Ujaque, Fernando López, José L. Mascareñas, and Agustí Lledós	
<b>Index</b> .....	249



# Structure, Bonding, and Reactivity of Reactant Complexes and Key Intermediates

Elena Soriano and José Marco-Contelles

**Abstract** Complexes of Pt and Au (gold(III) and cationic gold(I)) have shown an exceptional ability to promote a variety of organic transformations of unsaturated precursors due to their peculiar Lewis acid properties: the alkynophilic character of these soft metals and the  $\pi$ -acid activation of unsaturated groups promotes the intra- or intermolecular attack of a nucleophile. In this chapter we summarize the computational data reported on the structure, bonding, and reactivity of the reactant  $\pi$ -complexes and also on the key intermediate species.

**Keywords** Carbophilic activation · Computational analysis · Electronic structure · Gold · Platinum

## Contents

1	Introduction .....	2
2	Theoretical Considerations .....	2
2.1	Relativistic Effects .....	2
2.2	Theoretical Chemistry of Gold: Differences from Neighbor Elements .....	3
3	Reactivity and Selectivity in Homogeneous Catalysis .....	5
4	Bonding Properties of the Reactant Complexes .....	9
4.1	Metal–Alkene Complexes .....	9
4.2	Metal–Alkyne Complexes .....	10
4.3	Preference for Alkyne Group .....	12
5	Structure of M-Alkyne and M-Alkene Reactant Complexes .....	12
6	Structure and Bonding of Key Intermediates: Carbene Versus Carbocation Model .....	18
7	Conclusions .....	24
	References .....	25

---

E. Soriano (✉) and J. Marco-Contelles

Laboratorio de Radicales Libres y Química Computacional, Instituto de Química Orgánica General (CSIC), Juan de la Cierva, 3, 28006 Madrid, Spain

e-mail: esoriano@iqog.csic.es



## 1 Introduction

Transition metals exhibit significant efficacy for catalyzing the formation of carbon–carbon and carbon–heteroatom bonds, and in particular, Pt and Au (gold(III) and cationic gold(I)) show an exceptional capacity to promote a growing variety of organic transformations of unsaturated precursors. These processes result from the unique ability of these metal species to activate carbon–carbon multiple bonds as soft, carbophilic Lewis acids, thus promoting the intra- or intermolecular attack of a nucleophile.

In this chapter we describe the electronic factors that explain the reactivity of the catalyst systems and their behavior as “soft” Lewis acids, hence preferentially activating “soft” electrophiles such as  $\pi$ -systems. The increase of electrophilicity resulting from the coordination of the  $\pi$ -acceptor ligand at the metal center triggers the intra- or intermolecular attack of nucleophiles such as alkene, allene, arene groups or heteroatoms.

In the last few years, many comprehensive reviews have appeared on different aspects of homogeneous noble metal catalysis and its applications in organic synthesis. The reader is directed to them to get a more detailed view on the subject (for recent reviews, see [1–7], for a review on computational results, see [8]).

Here we present a brief review on theoretical studies carried out to describe structure, bonding, and reactivity of the reactant  $\pi$ -complexes, mainly alkynes and also alkenes. For theoretical studies on other types of catalyzed reactions concerning allenes, see other chapters within this special issue.

Moreover, given the size of the systems considered in the calculations, the majority of the studies have been carried out within the framework of DFT. Therefore, we will not describe any methodological issues because our main interest is on the chemical concepts obtained from the calculations. When necessary, methodology issues will be mentioned for specific cases.

## 2 Theoretical Considerations

### 2.1 Relativistic Effects

The electronic configuration of gold(0) is  $5d^{10}6s^2$ , which would justify the relative stability of gold(I) compounds, with ten electrons in a closed set of 5d orbitals.

Gold has an electrochemical potential which is the lowest of any metal. This means that gold in any cationic form will accept electrons from virtually any reducing agent to form metallic gold. It is the most electronegative of all metals, which confirms its noble character.

Post-lanthanide elements, such as platinum and gold, contain a large number of protons in their atomic nuclei. Therefore, the electrons move in a field of very high nuclear charge, which leads to velocities approaching that of light and,

consequently, they have to be treated according to Einstein's theories of relativity. This is particularly true for electrons that are in *s* orbitals, which have wavefunctions that correspond to a finite electron density at the atomic nucleus, but it is less important for electrons in *p* or *d* orbitals. Electrons moving at a speed close to the speed of light cannot be treated in terms of classical physics, but they are assigned a relativistic mass that is larger than the mass of the electron at rest. Therefore, the term relativistic effect refers to any phenomenon resulting from the need to take into account velocity as significant relative to the speed of light. The effect on the 6s electrons, in the post-lanthanide elements, is that the orbital radius is contracted and the distance of the electron from the nucleus is reduced. In addition, these electrons have greater ionization energies. For compounds of the neighboring element platinum (and also mercury), relativistic effects are still large [9], but are expected to be smaller compared to similar compounds of gold.

Some of the consequences of this effect in gold chemistry are: (1) a marked reduction in the lengths of covalent bonds involving gold atoms is often found, and the covalent radius of gold is smaller than that of silver; likewise, the relativistic contraction of the 6s orbital results in greatly strengthened Au-L bonds, where L is the ligand [10]; (2) the small difference in energy between the *s*, *p* and *d* orbitals leads to the efficient formation of linear two-coordinate complexes in gold(I), in contrast with the prevalence of tri- and tetracoordinate Cu(I) and Ag(I) complexes [11, 12]; (3) the destabilization of the 5d orbitals allows the easy formation of the oxidation state III in gold to be explained; (4) tendency for Au–Au interactions to be stabilizing of the order of hydrogen bonds; this property is known as *aurophilicity* [13].

Theoretical calculations have played a key role in understanding the origin of these properties and also in the development of gold chemistry. Bonding between closed-shell atoms was successfully traced in several early theoretical investigations by extended Hückel quantum chemical calculations [14–16]. Based on the hybridization concept, the nature of the bonding interaction could be qualitatively rationalized. The introduction of relativistic effects in more advanced calculations has shown that bonding between closed-shell metal atoms or ions may be strongly enhanced by these effects [17–27]. Since relativistic effects have been known to reach a local maximum for gold, *aurophilicity* was accepted as a logical consequence of these contributions. In fact, *aurophilic* bonding was considered as an effect based largely on the electron correlation of closed-shell components, similar to van der Waals interactions but unusually strong [24, 25]. All these studies have consistently shown that calculations will only reproduce the attractive forces between the gold atoms if relativistic effects are included.

## 2.2 Theoretical Chemistry of Gold: Differences from Neighbor Elements

In the last 30 years, the chemistry of gold has undergone an expansion as not only well-established areas of research have been developed, but also new innovative

approaches have enabled the progress of other fields of research. The metal and its complexes also have special characteristics that make them suitable for several uses. Gold presents special characteristic features that make it unique, such as high chemical and thermal stability, softness, and high electrical conductivity. These attributes give rise to a variety of relevant applications [28]. For example, gold is an essential element for nanoscale electronic devices because it is resistant to oxidation and mechanically robust. Gold compounds have been used successfully for the treatment of rheumatoid arthritis [29–31]. Gold is also an outstanding element for use as a heterogeneous catalyst operating at ambient temperature because it is catalytically active at low temperature (200–350 K, compared with Pd and Pt at 400–800 K) [32]. However, in the last few years several uses in homogeneous catalysis and in a wide variety of organic transformations have been reported [1–8].

Among the gold species, the chemistry of gold(I) is by far the most developed. It is difficult to say which types of complexes are more stable and important for gold. Those of phosphine or polyphosphine ligands have been studied in depth, as have organometallic gold complexes or species with chalcogenolate or chalcogenide ligands. The chemistry of gold(I) complexes is dominated by linear two-coordinate complexes of the form  $[\text{AuXL}]$  most notably in phosphane complexes [33–35]. Although higher coordinate gold–phosphane complexes are known, gold is the least predisposed amongst the Group 11 elements to increase its coordination number any further [12, 36].

Despite being known for a long time,  $[\text{AuXL}]$  complexes have returned to prominence because they display short intermolecular gold–gold contacts that associate the monomeric units. These *aurophilic* interactions, together with other secondary bonds such as hydrogen bonds, play a role in determining the solid state arrangement of Au(I) complexes. These Au...Au interactions generally occur perpendicular to the principle axis of the linearly arranged two-coordinate Au(I) centers, with typical values ranging from 2.75 to 3.4 Å [37]. The binding energies of such *metallophilic* contacts are comparable to that of a prototypical hydrogen bond, despite the fact that both metal centers carry charges of the same sign and have no valence electrons available to make covalent bonds. According to Pyykkö, the simplest picture to describe *aurophilicity* is “just another dispersive (van der Waals) interaction”, but a (virtual) charge transfer, again enhanced by relativistic effects, was invoked to explain this seeming contradiction [25]. The pronounced “*aurophilicity*” of gold directs the formation of a large number of gold clusters and diverse supramolecular aggregates with a variety of coordination numbers and geometries [12, 25, 36, 38–42]. The formation of aggregates with gold–gold bonds and nanoparticles is currently an active area of research.

The main and practical consequence of the limited coordination modes observed in Au(I) chemistry is the need to abstract a ligand from neutral bicoordinate Au(I) species so as to induce catalytic reactivity. Theoretical studies have indicated that, as a comparison, the Au 5d electrons are of greater energy than the Cu 3d electrons due to decreased electron/electron repulsion in the diffuse 5d orbitals, resulting in less nucleophilic metal species that do not tend to undergo oxidative addition [43].

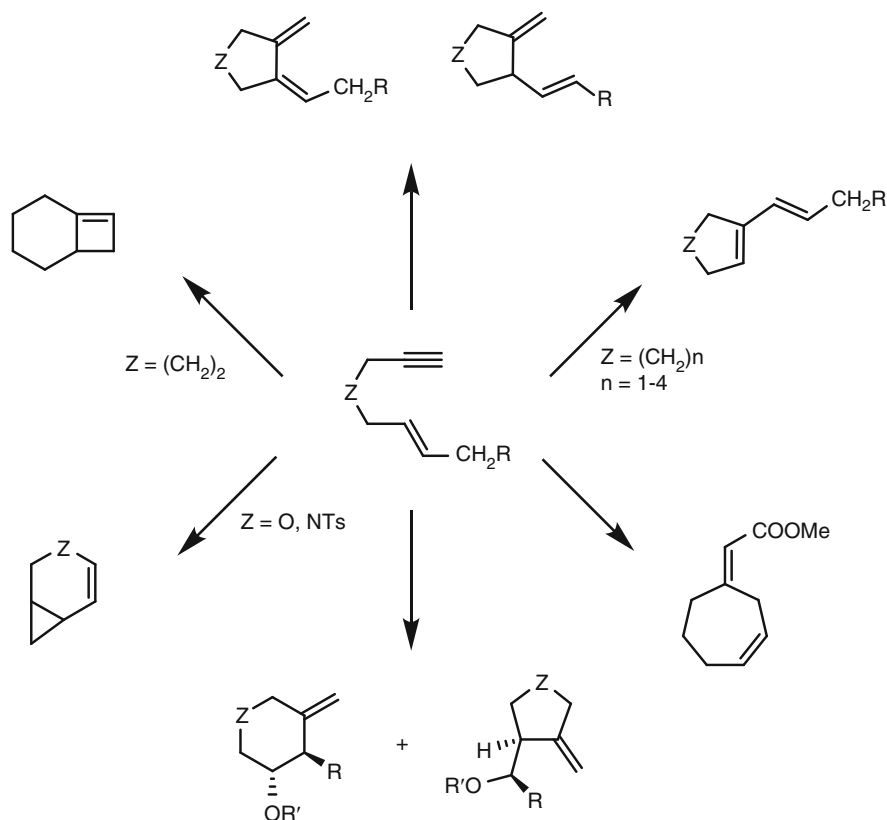
Computational and experimental results on reductive elimination from Au(III)LR<sub>3</sub> complexes have revealed that such process seems disfavored [44, 45]. These evidences are consistent with the reactivity of Au(I) and Au(III) complexes, which do not readily cycle between oxidation states. In this context, the redox stability of Au(I) species implies tolerance to oxygen and hence allows the development of modes of reactivity under ambient conditions by precluding the well-known oxidative addition/reductive elimination cycles common to other late transition-metal catalysis, such as Pd-catalysis.

### 3 Reactivity and Selectivity in Homogeneous Catalysis

Catalytic organometallic chemistry represents a powerful tool in the development of efficient strategies for the stereocontrolled synthesis of complex functionalized hetero- and carbocycles [46]. The transition metals from groups 10–12 exhibit significant efficacy for catalyzing the formation of carbon–carbon and carbon–heteroatom bonds. In particular, complexes and salts derived from Pt and Au (gold(III) and cationic gold(I)) have shown an exceptional ability to promote a variety of organic transformations of unsaturated precursors as homogeneous catalyst (Scheme 1) [1–8]. These processes result from the peculiar Lewis acid properties of these metals: the alkynophilic character of these soft metals and the  $\pi$ -acid activation of unsaturated groups promote the intra- or intermolecular attack of a nucleophile.

The isolation and characterization of Zeise's salt, K[PtCl<sub>3</sub>(C<sub>2</sub>H<sub>4</sub>)], the first well-defined organometallic compound prepared [47] and model of a  $\pi$  complex, provided direct evidence for the ability of Pt(II) to remove electron density from ethylene, thereby rendering it susceptible to nucleophilic attack [48–50]. This insight provided the impetus for the development of numerous platinum and palladium catalyzed reactions. In contrast, homogeneous Au(I) and Au(III) complexes have only recently emerged as highly competent and selective catalysts for the activation of  $\pi$ -bonds [1–8].

Although the pioneering efforts in this area employed simple metal salts, such as halides (PtCl<sub>2</sub> and AuCl<sub>3</sub>) due to their apparent insensitivity under aqueous conditions and ability to promote a diversity of transformations, Au(I) cationic species have proven to be superb catalysts for both carbon–carbon and carbon–heteroatom bond formations. Because the activation process invokes electrophilicity enhancement, a move toward cationic metal templates, which may be stabilized by a suitable spectator ligand (phosphane, N-heterocyclic carbene, pyridine derivative), results in increased activity. Among the cationic phosphine Au(I) species, R<sub>3</sub>PAuX (X = trifluoromethanesulfonate (<sup>−</sup>OTf) or other weakly coordinating counterions), formed in situ by the abstraction of Cl<sup>−</sup> from R<sub>3</sub>PAuCl by AgX or by the protonolysis of R<sub>3</sub>PAuCH<sub>3</sub> with acid, show superior catalytic activity for a series of C–C bond-forming reactions.



**Scheme 1** Example of the versatility of the Au and Pt-catalyzed cycloisomerization of polyunsaturated precursors (1,6-enynes)

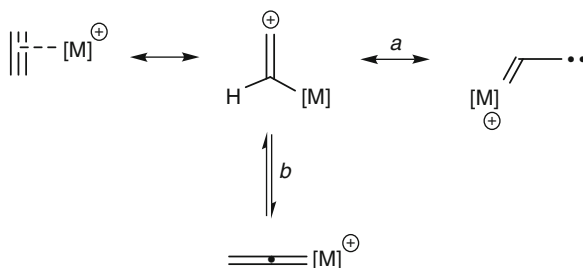
These late-transition metal complexes also combine high affinity to the  $\pi$  system with the advantages of a kinetically labile carbon–metal bond that can be readily cleaved under the reaction conditions, thus ensuring efficient turnover [3]. Therefore, these reactions provide an atom-economical entry into functionalized cyclic and acyclic scaffolds useful for the synthesis of natural and non-natural products under mild conditions with excellent chemoselectivity and high synthetic efficiency.

During the last years an explosive increase of interest in Au and Pt catalysis has taken place, thus becoming an extremely dynamic and innovative field of catalysis research. In this context, rationalization of the reactivity and selectivity observed is usually based on qualitative concepts such as steric bulk, electronic influence of the ligands, acidity of the bonds to be broken, etc. However, these valuable tools to build a qualitative picture lack the required quantitative aspects to draw effectively the subtle influences of the ligand set, the metal, and the substituents on the reactants.

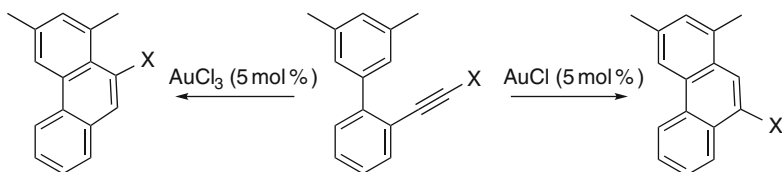
Computational studies of the structure and reactivity of organometallic complexes have now proven to be an essential tool in homogeneous catalysis [51–56]. A wealth of comparative studies has now established density functional theory (DFT) as a reliable method to study organometallic reactivity [57, 58] (for an interesting paper on the application of DFT methodology in the design of Au-catalyzed transformations, see [59]). In addition, the increase in computing power has allowed us to model systems closer to the actual experimental situation.

For gold-catalysis, oxidation state can induce different reaction paths. Thus, it was observed that the regioselectivity was reversed for the intermolecular hydroarylation of alkynes with arenes in the presence of Au(I) as opposed to Au(III) [60, 61]. The metal- $\pi$ -complex may evolve through the usual carbenoid species (Scheme 2, path a) or also via back-donation down through a 1,2-shift (hydride, halide, etc.) that results in the formation of a metal-vinylidene complex (Scheme 2, path b). Then the carbon atom bound to the metal center, rather than that at the vicinal position, would suffer initial nucleophilic attack. The generation of vinylidenes from alkynes has been described for other metals [62–64], but has recently been evidenced to play a role in the platinum and gold catalysis.

An example of the dichotomy in the catalytic behavior of Au(I) and Au(III) can be seen in the synthesis of phenanthrenes from biaryls bearing a halo-alkyne moiety [61]. As AuCl<sub>3</sub> is less able to back-donate, the reactive intermediate undergoes a Friedel–Crafts type hydroarylation of the triple bond. In contrast, the more electron-rich AuCl back-donates to a degree sufficient to enable a vinylidene pathway to become active, thereby resulting in the formation of the regioisomeric phenanthrene (Scheme 3). Theoretical studies on these mechanisms corroborate this proposed explanation and reveal a kinetic preference for the formation of the



**Scheme 2** Possible evolutions of a metal- $\eta$ -complex



**Scheme 3** Dichotomy in the catalytic behavior of Au(I) and Au(III) in the synthesis of phenanthrenes

vinylidene intermediate for the AuCl-catalyzed transformation (energy difference of  $6.6 \text{ kcal mol}^{-1}$ , B3LYP/LANL2DZ(Au)) [65].

Although it is supposed that no conventional redox chemistry is involved in gold catalysis, some ambiguity can remain as to the actual nature of the active species (Au(I) or Au(III)). On the one hand, it has been proposed that Au(I) can disproportionate in situ to Au(0) and Au(III) [66]. On the other hand, there is evidence that unsaturated substrates might lead to an in situ reduction of Au(III) to Au(I) [67].

Interestingly, a recent computational study on the catalytic performance of Au complexes in different oxidation states (as AuCl and AuCl<sub>3</sub>) in the cycloisomerization of  $\alpha$ -aminoallenes as well as the effects of the counterion on the catalytic activities has concluded that the Au(III)-catalyzed path does not involve an oxidation state change from Au(III) to Au(I). These calculated results rationalize the experimental findings and overthrow the previous conjecture about Au(I) serving as the catalytically active species for Au(III)-catalyzed transformation [68].

The complexes of transition metals can act as bifunctional Lewis acids activating, in addition of C–C, multiple bonds via  $\pi$ -binding, generating  $\sigma$ -complexes with heteroatoms, as conventional Lewis acids, such as BF<sub>3</sub>, do [69]. Accordingly, the oxophilic character of gold complexes and their activation of oxygen compounds have also been explored. Hence, it is thought that a proper choice of a Lewis acid, which may exhibit a dual role, can lead to the activation of both C–C and C–X multiple bonds in a single transformation [70, 71]. A study on this subject with gold (III) has been recently reported by Jin and Yamamoto [72].

Gevorgyan and co-workers have also observed from a study on a bromoallenyl ketone an enhanced oxophilic behavior for gold(III) with respect to the more carbophilic gold(I), namely, with Au(I) a product consistent with activation of the allene was observed, whereas with Au(III) the product formed was consistent with activation of the ketone moiety [73]. Calculations by Straub support this notion of functional group discrimination and indicate that Au(III) exhibits a thermodynamic preference for aldehyde over alkyne coordination by  $21.3 \text{ kJ mol}^{-1}$  [74]. However, this preference does not preclude Au(III)-catalyzed transformations that proceed through alkyne activation pathways. Nolan, Maseras, and co-workers have recently reported an experimental and computational study on the Au(I)-catalyzed formation of  $\alpha,\beta$ -unsaturated carbonyl compounds from propargylic acetates in the presence of water, and their results suggest a preferred catalytic cycle featuring a transfer of the OH moiety bound to the gold center to the triple bond to form a gold allenolate [75]. There are other recent examples in the literature on the activation of oxygen compounds by gold(I), most of them dealing with carbonyl compounds [76, 77], but also with epoxides [78, 79], where the catalyst acts as a Lewis acid and as a result promotes the inter- or intramolecular nucleophilic attack. Remarkably, a recent computational study in the rearrangement of (3-acyloxyprop-1-ynyl)oxiranes [80] to functionalized divinyl ketones under gold(I) catalysis (B3LYP/6-311G(d,p), LANL2TZ(f) level of theory), suggested that all the groups act in synergy, and sequential gold coordination to the CC  $\pi$ -system and the lone pairs of oxygen is needed for the transformation [81].

Additionally, ligand effects can influence reaction outcome. The relativistic bond contractions are sensitive to the nature and electronegativity of the ligand, as one might expect. For example, they are much more pronounced for a bound phosphane than for a chloride ligand [12, 36], a fact with potential implications for catalysis. Au(I)-phosphine species are well studied [12, 82], offering a tunable ligand set for optimizing catalyst reactivity. In the Au(I)-catalyzed ring expansion of propargylcyclopropanols, [(4-CF<sub>3</sub>-C<sub>6</sub>H<sub>4</sub>)<sub>3</sub>P]AuCl was shown to be superior to other Au-phosphines [83]. Buchwald-type ligands were most effective in the intramolecular hydroamination of allenes [84], whereas N-heterocyclic carbene (NHC) ligands were optimal for an indene synthesis [85].

## 4 Bonding Properties of the Reactant Complexes

As noted above, the coordinating behavior of these late transition metals can be accounted for by relativistic effects: relativity causes the contraction of the atomic *s* orbitals and expansion of the atomic *d* and *f* orbitals, because of an increased shielding effect by the contracted core. These effects lead to higher ionization potentials, strong acidity, and a net contraction and strengthening of the M–L bonds. It is worth mentioning that this effect is dependent on the nature and electronegativity of the ligand. The decreased electron/electron repulsion in the diffuse 5d orbitals qualitatively explains the chemically soft character of these transition metals [6]. Thus, the complexes may be considered as “soft” Lewis acids, preferentially activating “soft” electrophiles such as  $\pi$ -systems.

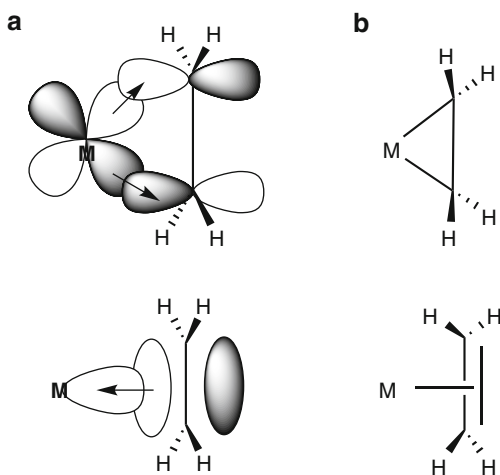
### 4.1 Metal–Alkene Complexes

The electrophilic activation of alkenes by transition-metal catalysts such as Pt, Au, or Pd is a fundamental step in a rapidly growing number of catalytic processes. Although palladium is the best known metal for this purpose, the special properties of its third-row cousin platinum (strong metal–ligand bonds and slow substitution kinetics) have enabled the development of transformations that are initiated by addition to the activated C=C bonds nitrogen, oxygen, and phosphorus nucleophiles, as well as alkene or arene nucleophiles [86].

The bonding in these metal–ethylene complexes can be described by the Dewar–Chatt–Duncanson model [87, 88] as a synergistic combination of  $\sigma$ -donor and  $\pi$ -acceptor interactions between the metal and the ethylene  $\pi$ -system (Fig. 1a) [89]. Figure 1b shows the limiting bonding schemes in which the ethylene–metal-ion interaction is weak and typically dominated by the ethylene-to-metal-ion  $\sigma$ -donation (leading to the T-shaped structure) (bottom). At the other extreme (Fig. 1b, top),



**Fig. 1** (a) Schematic representation of the metal–ethylene bonding model: donation to a vacant orbital of a metal from the filled  $\pi$ -orbital of ethylene (*bottom*); back-donation to the empty antibonding  $\pi^*$ -orbital of ethylene from a filled metal d-orbital (*top*). (b) Limiting structures of a metal–ethylene complex: T-shaped structure (*bottom*) and metallacyclopropane (*top*)



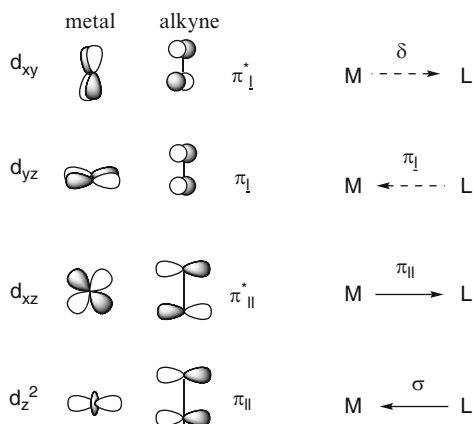
$\sigma$ -donation and, more importantly, the metal-ion-to-ethylene  $\pi$ -back-donation is dominant, and it results in a metallacyclopropane ring structure and a C=C bond with a bond order approaching unity. Note that both the  $\sigma$ -donor and  $\pi$ -back-bonding contributions lead to the lengthening of the C=C bond. Thus, metal–ethylene adducts should show C=C distances that are longer than that of free ethylene, although the extent of lengthening depends on a number of factors such as the charge on the metal and the nature of any auxiliary ligands.

## 4.2 Metal–Alkyne Complexes

While these catalysts have been used with some success to activate alkenes, dienes, and allenes (see other chapters within this special issue), the most important application concerns the activation of alkynes. The C–C triple bond alkyne functional group is characterized by two orthogonal  $\pi$ -bonds, high in energy, that easily interact with the  $d$  orbitals in transition metals (electrophiles). At the same time, the LUMO in alkynes is low in energy, which allows the attack of strong nucleophiles. When the alkyne is activated by coordination to the electrophilic metal complex, it may undergo easier attack of weaker nucleophiles.

To shed light into the bonding of these complexes, computational studies using bond decomposition energy analysis reveals roughly similar contributions to electrostatic and covalent ( $\sigma$ -donor and  $\pi$ -back-bonding components) bonding interactions, and a very slightly higher electrostatic terms is observed [90–92]. Alkynes interact with gold and platinum through the  $\sigma$  overlap of a  $\pi$  orbital with an empty  $d$  orbital on the metal with the appropriate symmetry. In addition, back-donation of a filled orbital on the metal to the corresponding alkyne in plane  $\pi_{//}^*$  takes place. Other contributions to the bonding can involve the orthogonal  $\pi_{\perp}$  and  $\pi_{\perp}^*$  orbitals donating charge ( $\pi$  symmetry) and accepting it ( $\delta$  symmetry, very

**Fig. 2** Qualitative orbital diagram showing the interaction between a transition metal and an alkyne ligand



weak interaction due to low overlap) from orbitals at the metal center, respectively (Fig. 2). Generally, the  $\sigma$  interaction makes the largest contribution to bonding, followed by the in plane  $\pi_{\parallel}$  back-donation, a much smaller  $\pi_{\perp}$ -ligand donation to the metal and a negligible metal- $\pi_{\perp}^*$  back-donation, making alkynes in gold(I) and platinum(II) complexes good  $\sigma$  donors and only weak  $\pi$  acceptors.

Gold frequently exhibits a higher catalytic activity than platinum and, therefore, transformations catalyzed by Pt(II) are usually carried out at higher temperatures than the Au(I) catalyzed counterparts. Sometimes both types of catalysts lead to different products [93–95], and sometimes they afford the same products following different reaction mechanisms [96, 97]. The differences in mechanism usually obey the difference in electrophilicity of the catalytic species. Gold complexes being more electrophilic, they tend to displace the system towards more cationic key intermediates (in the carbene-carbocation continuum), resulting preferentially in cation cyclizations and cationic rearrangements over the C-H insertions and cyclopropanations through carbenoid key intermediates (in the carbene-carbocation continuum) favored by platinum.

A recent relativistic *ab initio* study of model gold ( $\text{AuCl}_3$ ) and platinum ( $\text{PtCl}_2(\text{H}_2\text{O})$ )-alkyne complexes in the catalysis of nucleophilic additions to alkyne, where both metals show similar steric effects and possess a  $d^8$  electron configuration, assigns the difference in their reactivity to differences in the metal  $d$  populations in the outer valence space, resulting in large structural changes in the LUMOs. Gold complexes exhibit a high LUMO density on carbon together with considerably low LUMO energies, both favoring nucleophilic attack, while platinum complexes have higher energy LUMOs and no LUMO density on carbon, leading to a less favorable overlap with a nucleophilic frontier orbital [98].

Numerous experimental and theoretical investigations support the intuitive view that a positive charge on the metal center results in enhanced electrophilicity of the bound  $\pi$  ligand relative to the neutral analogs [99]. That is to say, catalysts imparting higher charge density onto the ligated  $\pi$ -system lead to higher rates, which explains

why cationic Pt templates [100] and, notably, cationic gold complexes turn out to be particularly effective.

It is also worth mentioning at this point that catalysts favoring ligation of a single  $\pi$ -system should be more reactive, which may be another reason why  $\text{LAu}^+$  constitutes a privileged catalyst fragment as it will bind to only one  $\pi$  ligand, in contrast to Pt(II) or Au(III).

### 4.3 Preference for Alkyne Group

A remarkable property of these catalyzed reactions is the preference of the metal complexes for activating alkyne over alkene moieties and other functional groups. This effect is known as *alkynophilicity*.

Studies on  $\text{Au}^+$ -ethylene and  $\text{Au}^+$ -ethyne bonding indicate a greater stabilization, by 10 kcal mol<sup>-1</sup> for the ethylene complex over the ethyne  $\pi$ -complex [92, 101]. Because Au(I) apparently does not selectively complex alkynes over other  $\pi$ -systems, the observed reactivity is supposedly kinetic in origin. That is, the pronounced alkynophilicity of the late transition metal catalysts likely reflects the discrimination by the incoming nucleophile in selecting between activated electrophiles and the preference for attack at the coordinated triple bond [3, 6].

On the basis of the soft nature of these metals, one might expect orbital rather than charge interactions to dominate in binding to an unsaturated C–C fragment [102]. The lowest unoccupied molecular orbital (LUMO) contains the  $\pi^*$ -metal (back-donation) interaction. Hence, such selectivity can be understood by taking into account the LUMO energy for the catalyst coordinated to ethyne and ethylene. The former shows a LUMO energy lower than the latter (by 0.39 and 0.37 eV, for  $\text{PtCl}_2$  and  $\text{AuPH}_3^+$ , respectively), a gap slightly lower than that for the uncoordinated organic fragments (by 0.62 eV). Consequently, the  $\pi$ -M-alkyne complexes are more electrophilic than the  $\pi$ -M-alkene complexes, so the orbital overlap with the nucleophile should be more efficient.

## 5 Structure of M-Alkyne and M-Alkene Reactant Complexes

As noted above, binding of metal complex to the alkene appears as thermodynamically favored over the alkyne moiety. However, indirect evidence suggests that it is coordination to the alkyne unit that triggers the subsequent chemical transformation. In this context, complexes of metal acetylides are known in the literature (for several trigonal planar Au(I) complexes coordinated to organometallic 1,4-diynes, see [103]; see also [104]; for a gold(I)-[2]catenane containing a linear ( $\eta^1$ -alkyne)-Au-( $\eta^2$ -alkyne) moiety [105]; for a supramolecular complex containing a linear ( $\eta^1$ -alkyne)-Au-( $\eta^2$ -alkyne) moiety [106]; and also [107]), but very few gold (for a linear N-heterocyclic carbene-Au-( $\eta^2$ -alkyne) that has been

characterized by NMR and IR spectroscopy, see [108]; [109]; for two trigonal planar strained cycloheptyne-Au(I) complexes [110]; for some neutral and cationic 14-electron gold alkyne  $\pi$  complexes [111]<sup>1</sup> and platinum [3] complexes of regular alkynes have been isolated in pure form. In the case of Pt complexes, the alkyne adopts a perpendicular arrangement to the plane defined by the  $L_3Pt^{2+}$  fragment. In the case of gold, the dicoordinated gold(I) complexes adopt a linear geometry, the second stabilizing ligand being either a phosphane [102] or an N-heterocyclic carbene [111].

The  $\pi$ -complexation of  $C=C$  or  $C\equiv C$  bonds at Au(I) and Au(III) centers (for a mini-review on coinage-metal-ethylene complexes, see [112], for a review on gold  $\eta^2$ -coordination to unsaturated and aromatic hydrocarbons [113]) with an incomplete residual ligand sphere L is the crucial step of the activation of the substrates. However, few species of this type could be directly observed or isolated for further investigation. For alkenes, although the experimental [114–116] and computationally estimated (MP2 and CCSD(T) levels [66, 75]) bond dissociation energy values (BDE) of  $M^+-C_2H_4$  ( $M = Cu, Ag, Au$ ) are relatively high, and  $M-C_2H_4$  adducts are expected to be thermodynamically stable, the labile nature of the metal-ethylene interaction has plagued the isolation of “bottle-able” coinage-metal-ethylene compounds for many years.

Besides electronic and energetic properties, complex formation alters the structures of the metal fragment and the ligand. The Dewar–Chatt–Duncanson model predicts an elongation of the double or triple C–C bonds due to the net shift of electron density from the bonding  $\pi$  orbital into the antibonding  $\pi^*$  orbital. A partial pyramidalization (of alkenes) or bending (of alkynes) then occurs as a consequence of the ensuing rehybridization. Hence, the degree of distortion from the geometry of the unbound ligand may be taken as an observable indication for the degree of back-bonding in the structure of the complex.

Zeise’s salt (1, Fig. 3) is considered a prototype of complexes of transition metals with unsaturated hydrocarbons. It was recognized early on that the complexation of an olefin to a metal center such as platinum leads to a significant activation of the  $C=C$  multiple bond, which provides a basis for metal catalysis of olefin transformations. The structural parameters ( $\Phi = 90.0^\circ$  and slight elongation of the  $C=C$  upon coordination) [117] and theoretical calculations [118] suggest that ethylene acts as a strong  $\sigma$ -donor but very weak  $\pi$ -acceptor. Remarkably, only minor structural changes are observed upon formal replacement of the olefin by either a terminal or internal alkyne (Fig. 3) [119] (for a review, see [120]).

For a long time,  $\pi$ -complexes of gold in any of its oxidation states were ignored because of the unknown stoichiometry, low stability, and limited relevance, and thus the common gold halides  $AuX$  and  $AuX_3$  surprisingly appeared to show no reactions similar to those of its Pt or Pd neighbors. It was not until the 1990s that the structural chemistry of (alkyne)gold compounds was clarified, mainly in work on the oligomeric gold(I) alkynyls  $(RC\equiv CAu)_n$  by Mingos et al. [105], on the

<sup>1</sup>For a 14-electron Au(I)-phosphine- $(\eta^2$ -alkyne) complex, see [102].

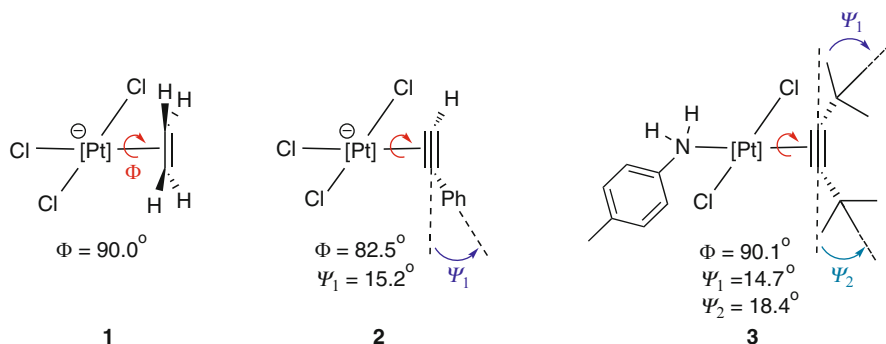


**Fig. 3** Examples of platinum(II)- $\eta^2$ -alkenyl (**1**) and alkynyl (**2**, **3**) complexes: crystal structure of the complex anion of Zeise's salt (**1**); crystal structure of the anion  $[\text{PtCl}_3(\text{PhC}\equiv\text{CH})]^-$  (**2**,  $r_{\text{C}\equiv\text{C}} = 1.23$  (1) Å (as compared to 1.208(1) Å in free phenylacetylene; crystal structure of  $[\text{PtCl}_2(\text{tBuC}\equiv\text{CtBu})(\text{MeC}_6\text{H}_4\text{NH}_2)]$  (**3**,  $r_{\text{C}\equiv\text{C}} = 1.24$  Å)

interaction of diacetylene “pincers” with gold salts by H. Lang et al. [103, 104], and on the complexation of cyclic functional alkynes by AuCl by Schulte and Behrens, providing insight into a variety of bonding modes [110]. In these compounds, the  $\text{C}\equiv\text{C}$  triple bond lengths of the ligands are generally elongated quite considerably, e.g., from 1.194 to 1.259 Å, upon complexation of  $\text{O}_2\text{S}(\text{CH}_2\text{CMe}_2)_2\text{C}_2$  to AuCl, and the  $\nu(\text{C}\equiv\text{C})$  stretching vibration is lowered from 2,188 to 1,930/1,910  $\text{cm}^{-1}$  (Fig. 4). In addition, a significant reduction of the  $\text{C}\equiv\text{C}-\text{C}$  angle (values between  $160^\circ$  and  $168^\circ$  for coordinated alkynes vs  $175\text{--}180^\circ$  for free alkynes) is also observed. Overall, with alkynes, the critical Au–C distances are about 2.10 Å, associated with lengthened  $\text{C}\equiv\text{C}$  distances of ca. 1.23 Å.

For alkenes, the range of the Au–C distances in the complexes is more variable (between 2.20 and 2.30 Å) and consequently a larger spread of  $\text{C}=\text{C}$  distances of  $1.40 \pm 0.05$  Å are observed [113].

It should be noted that for a long time there was no evidence for  $\pi$ -complexation of gold in any of its oxidation states to neutral arenes such as benzene. The first examples indeed were reported only very recently, while analogs with copper [121–123] and silver [124, 125] had been known for at least half a century. For arenes the Au–C distances are well beyond 2.30 Å and depend on the different hapticities ( $\eta^1\text{--}\eta^3$ ), associated with intra-ring C–C distances at ca. 1.425 Å. Not surprisingly, therefore, the deviation from linearity of the alkynes is more dramatic than that from planarity of the alkenes, which suggests that a description of the former as metallacyclopropenes is more justified than that of the latter as metallacyclopropanes (Fig. 5).

Recently, Toste and Shapiro have isolated and characterized, by X-ray crystallography, linear ( $\eta^2$ -alkyne)- and ( $\eta^2$ -alkene)-Au(I)-phosphine dimeric complexes (**4**, Fig. 4) [102], and Dias et al. have synthesized and characterized a linear gold(I) complex featuring a simple, unstrained alkyne (3-hexyne) bonded to AuCl (**5**, Fig. 4) [109]. Other structurally characterized gold alkyne complexes are **6**

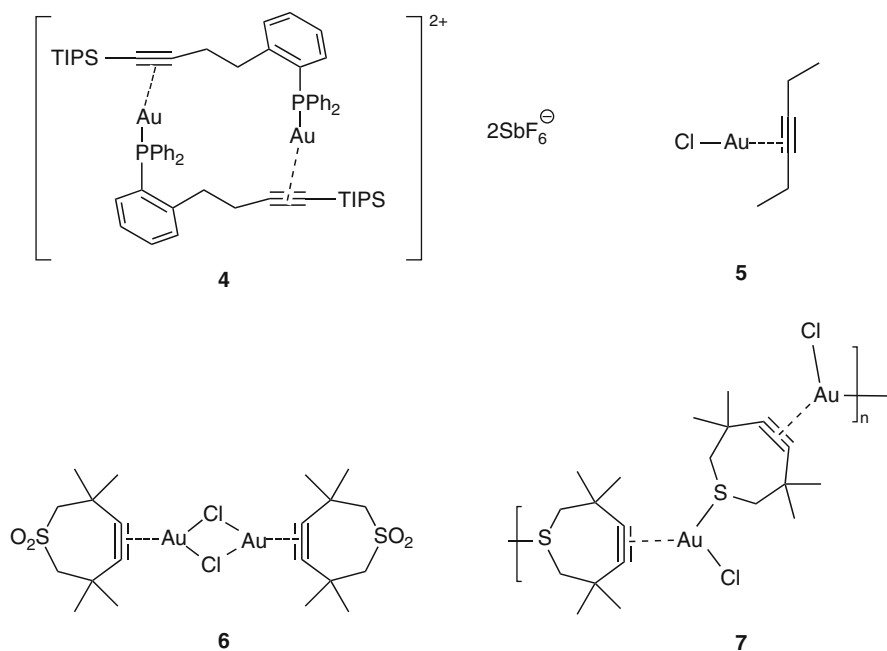


**Fig. 4** Structurally characterized gold(I)-alkyne complexes

**Fig. 5** Limiting structures of cationic Au(I)-ethylene (top) and ethyne (bottom) complexes

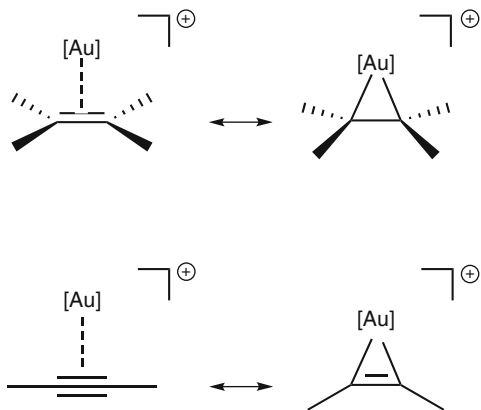


(Fig. 4) and 7 (Fig. 4), each incorporating a highly strained cycloalkyne as ligand [110].

Fürstner and co-workers have reported the structure and bonding properties for a series of complexes formed by coordination of the unstrained cyclododecyne to either the neutral  $\text{AuCl}$  or to two different cationic  $[\text{Au}-\text{NHC}]^+$  moieties (**8–10**, Fig. 6) [111].

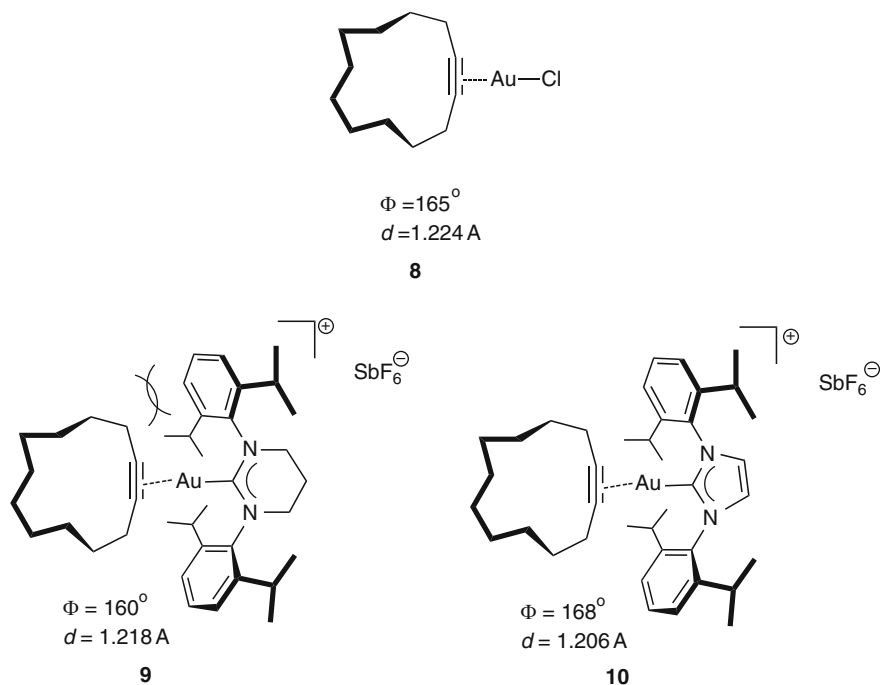
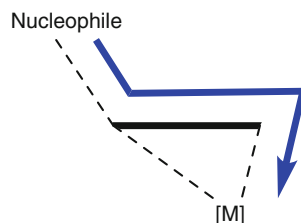


**Fig. 6** Structural changes imposed on cyclododecyne by either the neutral  $[\text{AuCl}]$  or the cationic  $[\text{Au}(\text{NHC})]^+$  fragment;  $d$  refers to the  $\text{C}\equiv\text{C}$  bond length,  $\Phi$  denotes the  $\text{C}\equiv\text{C}-\text{CH}_2-$  bond angle

**Fig. 7** Representation of the slippage or  $\eta^2-\eta^1$  deformation by redistribution of electrons upon nucleophilic attack onto a CC unsaturated group bound to a  $\pi$ -acidic metal complex



Computational studies on model complex–ligand systems indicate that the transition state for nucleophilic addition reactions is distorted regarding the ground-state. That is, even if a partial slipped ground-state ( $\eta^2$  structure for symmetric  $\pi$  ligand) is expected for asymmetric  $\pi$  ligands, the pertinent transition state is far from a  $\eta^2$  structure. It is now widely accepted that slippage of the  $\text{ML}_n$  fragment along the axis of the bound alkyne or alkene accompanies ligand activation [126] (the role of slippage has been reconfirmed by Car-Parrinello molecular dynamics calculations; see [127]). The electrophilicity is enhanced upon  $\eta^2-\eta^1$  deformation, as relaxation of the symmetry allows mixing of previously orthogonal orbitals and facilitates charge transfer from the nucleophile to the  $\pi$  ligand and finally to the metal center, especially in cationic complexes (Fig. 7) [128–130]. In other words, it is the partial

slippage away from the symmetrical  $\eta^2$  coordination in the transition state which engenders productive overlap of the orbitals of the nucleophile with the distorted  $\pi$  system. Overall,  $\pi$ -acidic metal fragments can be regarded as the “soft” counterparts to the conventional Lewis acids. Interactions between alkynes or alkenes with “ $\pi$  acidic” metal fragments result in a larger loss of  $\pi$ -electron density than is gained through back-donation; also, electrostatic contributions to bonding are essential.

The main structural characteristics of the electrophilic complexes resulting from interaction between alkynes or alkenes with  $\pi$ -acidic metal fragments are: (1) elongation of the C–C bond in the coordinated vs the free ligand; (2) configuration of the carbon atoms is changed from trigonal planar and linear toward pyramidal and bent, for alkyne and alkene ligands, respectively; (3) rehybridization of the unsaturated C atoms; (4) low inherent barriers for the rotation of the ligand around the metal–ligand centroid axis.

A recent experimental and computational study (BP86/def2-TZVP level) by Fürstner et al. on the structure and bonding of 14 electrons gold alkyne  $\pi$  complexes with a variety of gold(I) species (neutral and cationic complexes, **8–10** in Fig. 6) and the pertinent comparison with the uncomplexed alkyne (cyclododecyne) have shown that  $\pi \rightarrow \sigma^*$  donation clearly dominates over  $d \rightarrow \pi^*$  back-donation, and thus explains the highly electrophilic character of the alkyne within the coordination sphere of the Au(I) fragment [111]. These observations agree with previous theoretical results (B3LYP/LANL2DZ(Au), ccpVDZ(C,H), and AUG-ccpVDZ(Cl) levels of theory) by Dias et al. on the Au(I) chloride complex coordinated to the simple, unstrained 3-hexyne (**5**, Fig. 4) [109]. Likewise, Toste et al. have isolated, characterized by X-ray crystallography and analyzed by DFT approach (B3PW91/LANL2DZ(Au), LANL2DZdp(Si,P), ccpVDZ(C,H)) the structure of a phosphine Au(I)  $\pi$  complex (**4**, Fig. 4) [102], and, in this context, phosphine-Au(I)-chloride complexes ( $\text{Ph}_3\text{PAuCl}$ ), as 16-electron complexes upon alkyne coordination, are typically much less catalytically active than their cationic analogs and must be activated by addition of a silver salt (such as  $\text{AgSbF}_6$ ), which serves to remove the chloride ligand and replace it with a less coordinating counteranion. Second order perturbative analysis on the related Ag(I) and Cu(I) complexes revealed that  $\pi \rightarrow \sigma^*$  donation is of the largest magnitude for Au, as is metal  $d \rightarrow \pi^*$  back-donation. For all three metals,  $\sigma$ -donation to the metal dominates, augmenting the electrophilicity of the alkyne, although the difference between the two bonding interactions is the largest for Au.

While most of these observations are not very different from those of  $\pi$ -complexes of the neighboring elements of gold (Pd, Pt, Ag), differences in coordination numbers and oxidation states, which inter alia have their origin in particularly strong relativistic effects, provide gold species with their special reactivity properties. In its standard environment, gold(I) has the lowest possible coordination number, lower than Pt(II) or Pd(II), which gives substrates ready access to the metal center. Hence, the specific electrophilic nature of  $\text{LAu}^+$  units is governed by only one ligand L and thus can easily be tuned by a suitable combination of steric and donor/acceptor properties and by the choice of the counterion and the solvent.

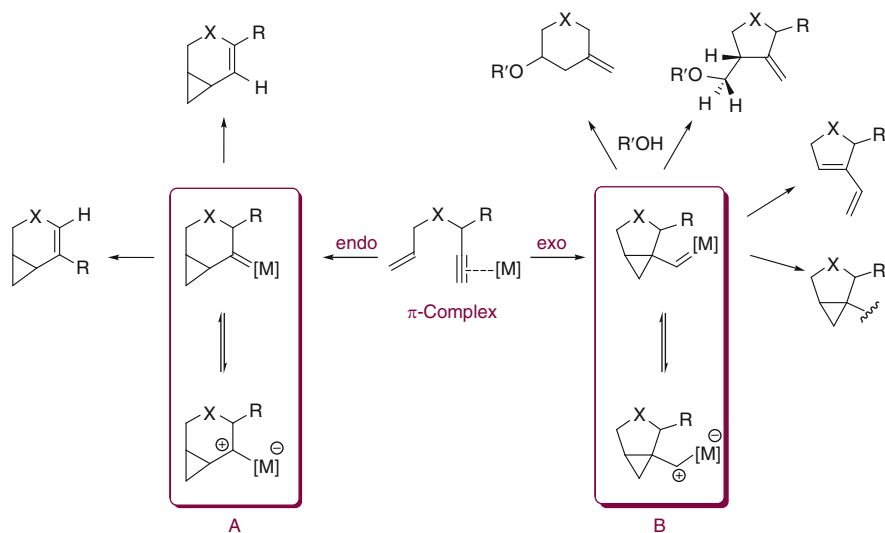


Biphenyl-substituted phosphines and NHC ligands induce greater reactivity and modulate selectivity among competing reaction pathways [131].

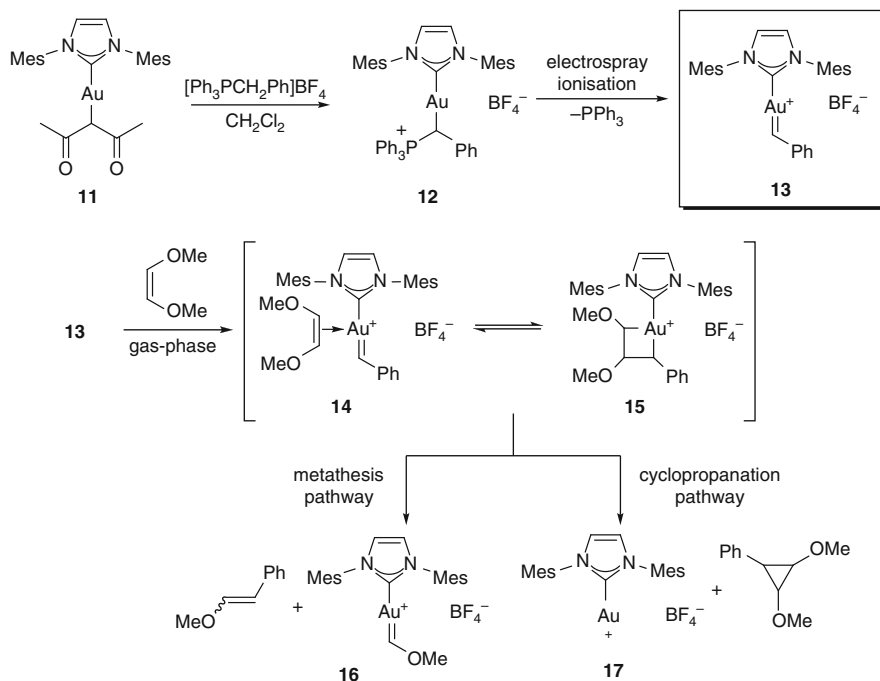
## 6 Structure and Bonding of Key Intermediates: Carbene Versus Carbocation Model

On the basis of the versatility, reactivity, and selectivity patterns observed in this synthetic protocol, several mechanistic pathways and bonding models for key intermediates have been proposed, including intermediates ranging from metal carbenes to metal-stabilized carbocations.

The electrophilic activation of the triple bond by the catalyst generates, as described above, highly electrophilic species and triggers the nucleophilic attack of other functionalities. An asymmetric alkyne implies two differently activated carbon positions, which accounts for the high versatility found in this field, although other structural factors come into play. Theoretical calculations have shown that the nucleophilic attack of an alkene onto a Pt-alkyne complex can take place through *exo-dig* or *endo-dig* pathways (Scheme 4) upon slippage of the  $\eta^2$ -coordinated alkyne, to afford the key cyclopropyl metallocarbenoid intermediates [132]. The involvement of these structures (very recently a gold-carbene complex has been isolated in the gas phase [133]) was previously speculated on the basis of trapping reactions [134].

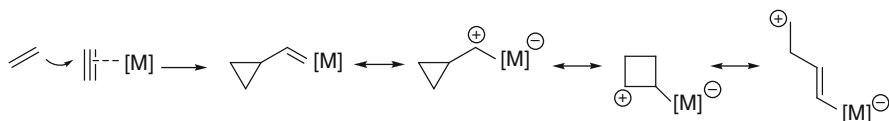


**Scheme 4** Versatility of the catalyzed cycloisomerization of 1,6-enynes likely from only two key intermediates, A and B



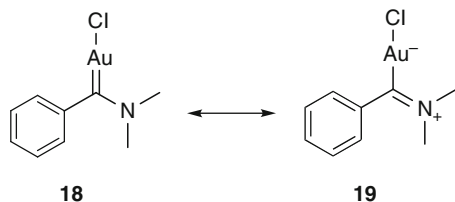
**Scheme 5** Synthesis of gold(I) benzylidene complex **13** and reactivity in gas phase according to mass spectroscopy data [133]

Despite gold carbenes have been usually proposed as key reactive intermediates, very little data relative to their characterization and reactivity have been reported to date [133], as only the synthesis of Au(I) carbenes in the gas phase along with their reactivity in the presence of alkenes (Scheme 5) have been reported. Gold complex **11** reacts with the phosphonium salt  $[\text{Ph}_3\text{PCH}_2\text{Ph}]\text{BF}_4$  to generate the gold ylide adduct **12**. Later, a submission of this species to electrospray ionization and detection of the ion corresponding to the gold benzylidene complex **13** by tandem mass spectroscopy have been carried out. The value predicted by DFT calculations using the M06-L functional is in agreement with the experimental activation energy. Introduction of alkenes into the ion guide allowed the assessment of the reactivity of these transient species. Upon generation and selection of complex ion **13** in the presence of 1,2-dimethoxyethene, the formation of three signals can be observed: (1) the first signal corresponding to the 1:1 adduct of the two reactants has been assigned either to the  $\eta^2$ -complex **14** or to the metalacyclobutane **15**; (2) the second signal corresponds to the gold methoxylidene carbene complex **16** – its formation is indicative of the existence of an alkene metathesis reactivity; (3) the third signal corresponds to the (NHC)Au cation **17** formed upon loss of both the benzylidene and the dimethoxyethene moieties from the gold complex **14/15** and has been proposed to account for a competitive cyclopropanation pathway. To sum



**Scheme 6** Resonance forms for the intermediate formed by nucleophilic attack of an alkene over an activated alkyne

**Fig. 8** Structure of a Fischer-type gold “carbene”



up, the nature of the synthesized carbene is demonstrated by its characteristic reactivity with olefins, including cross-metathesis and cyclopropanation.

Füstrner was first to propose that these key intermediates can be described in terms of either cationic or carbenoid resonance extremes (Scheme 6) depending on the metal template [3]. Thus, while calculations show a short C–Pt(II) bond (1.88–1.90 Å), resembling a double bond, the C–Au(I) bond length (2.02–2.04 Å) falls within the range for a single bond. A priori, the gold intermediates may thus be more appropriately described as gold-stabilized carbocations rather than “gold-carbenes”.

On the other hand, gold catalysis has been applied successfully to transformations that are traditionally carried out with carbene systems [135–138]. In this regard, it should be noted that the widespread formation of cyclopropanes, which is frequently invoked as an indication of the carbene character of the reactive intermediate species, in the reaction between activated alkynes and alkenes, can also occur in a stepwise, nonconcerted fashion via charged intermediates [139].

Therefore, the nature of bonding in these intermediates remains unclear and is still material of intense debate.

It has been observed that Fischer-carbene complexes of chromium, molybdenum, and tungsten readily undergo carbene transfer on reaction with gold salts, thus indicating that the gold–carbene complexes are thermodynamically highly stable [140, 141]. Both Au(I)– as well as Au(III)–carbene complexes are known, and in the former case show the expected linear coordination geometry (Fig. 8) [142]. However, it has been deduced from the molecular structures in the solid state (18/19, Fig. 8) that the C–Au “carbene” bond shows single – rather than double bond character [143]. In fact, the bond length (2.067(4) Å) even exceeds that of some prototypical C(sp<sup>2</sup>)–Au single bonds; hence, considerable partial positive charge will reside on the “carbenoid” C atom [144]. Moreover, it has been described that the C–N distance which is relatively short ([145]; for a theoretical analysis of the bonding situation in NHC–AuX complexes, see [146]; [147]), thus indicating that

the stabilization of the “carbene” is due mainly to the  $p_{\pi}$ – $p_{\pi}$  interaction with the heteroatom. However, as the nitrogen substitution induces electronic effects on the complex, this model cannot be considered fully satisfactory (Fig. 8).

The data accumulated suggest that the conceivable cationic and carbene extremes make very different contributions to the actual character of the reactive intermediates.

Ab initio calculations involving multireference configuration interaction [148] and DFT [149] levels of theory of  $[M=CH_2]^+$  systems have shown that carbenes of the 5d transition metals are distinguished by particularly high bond energies, which is maximum for Pt. Thereby, the bonding situation for platinum and gold is close to a purely dative case [148]. If seen within the framework of the Dewar–Chatt–Duncanson model, the overlap between a lone pair of electrons on a singlet methylene entity with an empty (hybrid) orbital on the metal has  $\sigma$  symmetry. This dative bond is counterbalanced by overlap of a metal  $d_{xz}$  orbital with the empty  $p_x$  orbital of the ligand to form the  $\pi$  bond. In other words, Au as well as Pt can engage in electron back-donation from the metal atom to a carbene ligand. This picture contrasts the low ability of the same metal templates to back-donate into the  $\pi^*$  orbital of an alkyne or alkene ligand. Hence, gold and platinum fragments activate a  $C\equiv C$  triple (double) bond toward nucleophilic attack yet are able to stabilize incipient “carbene intermediates.”

On other hand, one must also bear in mind that, in the case of gold, the acute different size of the frontier orbitals in relation to those of carbon might preclude significant back-donation from the metal to the ligand, rendering a dipolar bonding picture more likely than a carbon–metal “double bond.”

To get deeper insights into the nature of the chemical bond in gold-carbenes, Frenking and co-workers [146] analyzed mixed carbene–halogen and bis(carbene) complexes at the BP86 level of theory using an energy decomposition analysis (EDA) with the simple imidazol-1-ylidene as model carbene ligand. They concluded that, although the metal–ligand  $\pi$ -back-bonding interaction is not “negligible” compared to the  $\sigma$ -interaction, it usually constitutes less than 20% of the total orbital interaction energy which in turn, however, accounts for only 22–25% of the total attractive interaction between the metal and this ligand. These results are consistent with those observed by Meyer on tris(carbene) ligand systems using a “fragment approach” [150]. Energy decomposition analysis indicates that  $\pi$ -bonding in such gold carbene complexes is responsible for ca. 15% of the total orbital interaction.

In support of these findings, Jacobsen compared (at BP86 level of DFT) N- and P-heterocyclic carbenes and found that cationic complexes of Au form stronger bonds than neutral ones [151]. In addition, methyl substituents on the nitrogens of NHCs increase the metal–carbene bond strength by 25–35  $\text{kJ mol}^{-1}$  and, although PHCs (P-heterocyclic carbenes) form bonds comparable in strength to NHCs, they are better  $\pi$ -acceptors and the  $\pi$ -bonding makes up a larger percentage of the total orbital contribution (“intrinsic bond strength”) – up to 45% compared to less than 20% when considering NHCs.

Other interesting computational analysis has been reported by Pyykkö and Runeberg [152] who, working at the BP86 level of theory, have compared the bonding dissociation energy of  $\text{Au}^+\text{-L}$  and  $\text{ClAu-L}$  systems for a chosen series of ligands, L. The two sets of calculations indicate virtually the same trend with the NHC ligands top of the scale and the cyclic diphosphinocarbenes (PHCs) filling the second position (for an interesting review on the latest computational studies on gold, see [153]).

In the last year, theoretical investigations [154] and experimental observations [155] have further polarized the discussion surrounding the carbenoid or cationic character of organogold species, mostly in support of their carbocationic character. Thus, recent NMR spectroscopic data [156] by Fürstner et al. support this proposal. They analyzed the synthesis of stabilized gold allylic carbocations by the reaction of acetalcyclopropenes with cationic  $[(\text{PPh}_3)\text{Au}]\text{NTf}_2$  complex. Formation of the vinylaurate (*Z*)-**21** has been characterized by  $^1\text{H}$  and  $^{13}\text{C}$  NMR spectroscopies. Isomerization to the diastereoisomer (*E*)- has been observed by temperature dependent NMR measurements and corresponds to a barrier of rotation of about  $30 \text{ kcal mol}^{-1}$ . Their findings have suggested a rapid rotation about the C2–C3 bond on the NMR timescale, and that the C1–C2 rather than the C2–C3 bond has a very high degree of double-bond character, results inconsistent with a carbene structure of type **20** and compatible with a delocalized allylic carbenium cation of type **21** (Fig. 9).

A recent computational study by Toste et al. based on the same arguments, namely the estimation of molecular structure and energetics [154], has also shed light onto this duality carbene/carbocation. Barrier to bond rotational energies have been estimated as descriptors to evaluate the strength of  $\pi$ -bonds. At the same time, they validated the M06 functional of DFT by comparison with the Fürstner's results described above as appropriate theoretical methodology. In this sense, it was

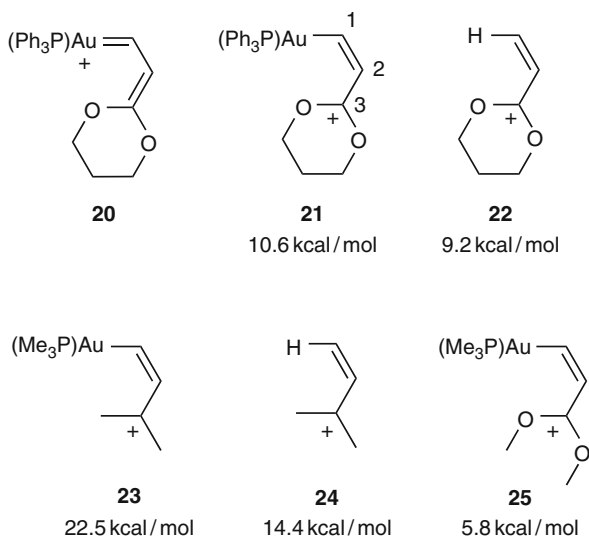


**Fig. 9** Calculated activation energies to C2–C3 bond rotation

concluded that other usual functionals like B3LYP or BP86 are unable to resolve the effects of different Au ligands.

While the results on the barrier to bond rotation energy confirm the conclusion of Fürstner and co-workers [156] that the gold moiety has little effect on the barrier to rotation in (Z)-**21** (1.4 kcal mol<sup>-1</sup> higher than for free-metal structure **22**, Fig. 9), this conclusion only appears valid in the presence of the highly carbocation-stabilizing oxygen atoms. When these heteroatoms are absent, the effect of the gold moiety is clearly large (8.1 kcal mol<sup>-1</sup> lower for the cationic metal-free structure **24** than for **23**). Therefore, the reactivity of these key intermediates seems highly dependent upon the carbene substituents.

The computed differences in structural parameters (gold–carbon bond length) and NPA charges agree with the increased barrier to C2–C3 bond rotation in **23** (Fig. 9). To verify these conclusions, the authors confirmed experimentally a difference in reactivity since **25** reacts as a gold-stabilized carbocation, whereas **23** react more as a gold-stabilized carbene. Furthermore, in the latter case, the yield of the reaction was highly dependent on the ancillary ligand, so the authors also examined the effect of this ligand on the nature of the Au–C1 bond [157].

An electron-withdrawing ligand such as P(OMe)<sub>3</sub> diminishes the electron density on the metal center, weakens the  $\pi$ -back-donation to the C $\alpha$ , and thus leads to carbocationic reactivity, while a good  $\sigma$ -donating ligand such as an *N*-heterocyclic carbene increases the electron density on the gold(I) center and allows a better  $\pi$ -back-donation to the C $\alpha$ , thus favoring a carbene reactivity. Remarkably, this mechanistic rationale has been confirmed experimentally [154].

Focusing on the bonding properties, the components of the L–Au–C bonding are (Fig. 10): (1) a three-center–four-electron  $\sigma$ -hyperbond (where hyperbond refers to bonding beyond the reduced 12-electron valence space) formed for the P–Au–C triad as [P:Au–C  $\leftrightarrow$  P–Au:C] (or C–Au–C triad for the NHC ligand) [158] – this bonding interaction implies that the Au–C1 bond order decreases with increasing *trans* ligand  $\sigma$ -donation (*trans* influence); (2) the metal center forms two  $\pi$ -bonds by donation from perpendicular filled d-orbitals into empty  $\pi$ -acceptors on the

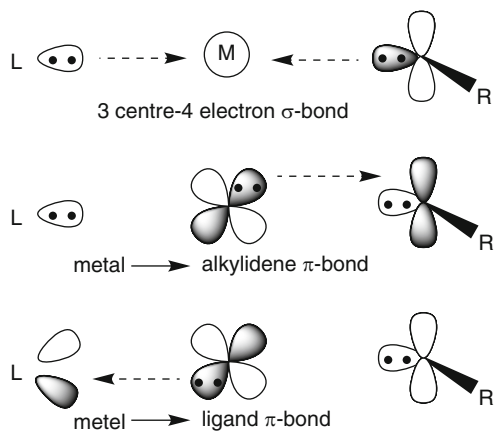


**Fig. 10** Schematic representation of the most important bonding interactions in [L–Au(I)–C]<sup>+</sup> systems

ligand and C1, so they both compete for electron density from gold. Accordingly,  $\pi$ -acidic ligands decrease back-donation to the substrate, resulting in longer Au–C1 bonds, while  $\pi$ -donating ligands (as chloride) increase back-donation to C1, resulting in a very short Au–C. Therefore,  $\pi$ -acidic ligands are expected to increase carbocation-like reactivity by decreasing gold-to-C1  $\pi$ -donation.

In general, the strength of the back-donation to C1 is dependent on both ligand and the electrophilicity of the  $\pi$ -acceptor on C1.

To sum up, the authors suggest that the reactivity in gold(I)-coordinated carbenes is best accounted for by a continuum ranging from a metal-stabilized singlet carbene to a metal-coordinated carbocation. The position of a given gold species on this continuum is largely determined by the carbene substituents and the ancillary ligand.

Finally, it should be emphasized that the influence of the heteroatom substituents inducing the system toward the cationic form may be assisted by the aurophilicity [156]. Alkenylgold species with a heteroatom substituent are thought to be key intermediates in gold-catalyzed additions of protic nucleophiles to alkynes. Fürstner et al. have proposed that the scarcity of such compounds likely lies in the non-innocence of the neighboring heteroatom, which may enforce the uptake of a second gold fragment with formation of robust species with a *gem*-digold unit adjacent to a largely cationic center [159]. Related *gem*-digold intermediates have been proposed recently by Houk et al. [160] whose calculations reveal that, in gold-catalyzed cycloisomerization reactions of 1,5-allenynes, a mechanism via nucleophilic addition of an allene double bond to a gold-complexed gold acetylide is more likely than oxidative cyclization or simple nucleophilic addition to gold-complexed substrate.

## 7 Conclusions

Transition metals exhibit significant efficacy for catalyzing the formation of carbon–carbon and carbon–heteroatom bonds and, in particular, Pt and Au (gold (III) and cationic gold(I)) show an exceptional capacity to promote a growing variety of organic transformations of unsaturated precursors. These processes result from their unique ability to activate carbon–carbon multiple bonds as soft, carbophilic Lewis acids, thus promoting the attack of a nucleophile.

In this chapter, we have provided an overview of the structure, bonding properties, and reactivity for the main reactant complexes and key intermediates involved in the most important transformations promoted by Pt and Au of unsaturated precursors, on the basis of computational studies performed in the last few years. A correlation of the catalytic behavior with the available structural data, coordination chemistry, and reactivity patterns, including relativistic effects, is provided which allows the underlying principles of catalytic carbophilic activation by  $\pi$ -acids to be formulated.

We have described the electronic factors that explain the reactivity of the catalyst systems and their behavior as “soft” Lewis acids, hence preferentially

activating “soft” electrophiles such as  $\pi$ -systems. The increase of electrophilicity resulting from the coordination of the  $\pi$ -acceptor ligand at the metal center triggers the intra- or intermolecular attack of nucleophiles such as alkene, heteroatom, allene, or arene groups, which can occur by exo- or endo- pathways.

The differences in the operating mechanism sometimes found for platinum and gold usually obey the difference in electrophilicity of the catalytic species. Gold complexes being more electrophilic, they tend to displace the system in the carbene-carbocation continuum towards more cationic species, resulting preferentially in cation cyclizations and cationic rearrangements over the C-H insertions and cyclopropanations (carbenoid derived products) favored by platinum.

The notable chemo-, regio-, and stereoselectivity of these transformations can be accounted for by structural and electronic effects on the key steps, so the computational methodology currently represents a valuable tool for the development of a solid conceptual framework and a better understanding of these processes.

**Acknowledgments** ES thanks the Spanish MICINN (Project CTQ2009-10478) for financial support.

## References

1. Bruneau C (2005) *Angew Chem Int Ed* 44:2328–2334
2. Zhang L, Sun J, Kozmin SA (2006) *Adv Synth Catal* 348:2271–2296
3. Fürstner A, Davies PW (2007) *Angew Chem Int Ed* 46:3410–3449
4. Hashmi ASK, Rudolph M (2008) *Chem Soc Rev* 37:1766–1775
5. Jimenez-Núñez E, Echavarren AM (2008) *Chem Rev* 108:3326–3350
6. Gorin DJ, Toste FD (2007) *Nature* 446:395–403
7. Michelet V, Toullec PY, Genêt J-P (2008) *Angew Chem Int Ed* 47:4268
8. Soriano E, Marco-Contelles J (2009) *Acc Chem Res* 42:1026–1036
9. Wahlgren U, Schimmelpfennig B, Jusuf S, Strömsnes H, Gropen O, Maron L (1998) *Chem Phys Lett* 287:525
10. Desclaux JP, Pykkö P (1976) *Chem Phys Lett* 39:300–303
11. Carvajal MA, Novoa JJ, Alvarez S (2004) *J Am Chem Soc* 126:1465–1477
12. Schwerdtfeger P, Hermann HL, Schmidbaur H (2003) *Inorg Chem* 42:1334–1342
13. Scherbaum F, Grohmann A, Huber B, Krüger C, Schmidbaur H (1988) *Angew Chem Int Ed Engl* 27:1544–1546
14. Dedieu A, Hoffmann R (1978) *J Am Chem Soc* 100:2974
15. Janiak C, Hoffmann R (1990) *J Am Chem Soc* 112:5924
16. Burdett JF, Eisenstein O, Schweizer WB (1994) *Inorg Chem* 33:3261
17. Mingos DMP, Slee T, Shenyang L (1990) *Chem Rev* 90:383
18. Häberlen OD, Schmidbaur H, Rösch N (1994) *J Am Chem Soc* 116:8241
19. Rösch N, Görling A, Ellis DE, Schmidbaur H (1991) *Inorg Chem* 30:3986
20. Rösch N, Görling A, Ellis DE, Schmidbaur H (1989) *Angew Chem Int Ed* 28:1357
21. Pykkö P, Assmann B, Schmidbaur H (1995) *Chem Commun* 1889
22. Pykkö P, Runerberg N, Mendizabal F (1997) *Chem Eur J* 3:1451
23. Pykkö P, Mendizabal F (1997) *Chem Eur J* 3:1458
24. Pykkö P (1997) *Chem Rev* 97:597
25. Pykkö P (2004) *Angew Chem Int Ed* 43:4412–4456
26. Schwerdtfeger P, Bruce AE, Bruce MRM (1998) *J Am Chem Soc* 120:6587



27. Kaltsoyannis N (1997) *J Chem Soc Dalton Trans* 1
28. Laguna A (ed) (2008) *Modern supramolecular gold chemistry: gold-metal interactions and applications*. Wiley-VCH, Weinheim
29. Shaw CF III (1999) *Chem Rev* 99:2589
30. Sadler PJ, Guo Z (1998) *Pure Appl Chem* 70:863
31. Gielen M, Tiekink ERT (eds) (2005) *Metallotherapeutic drugs of metal-based diagnostic agents. The use of metals in medicine*. Wiley, New York
32. Bond GC, Louis C, Thompson DT (2006) *Catalysis by gold*. Catalytic science series, vol 6. Imperial College Press, London
33. Puddephatt RJ (1987) In: Wilkinson G, Gillard RD, McCleverty JA (eds) *Comprehensive coordination chemistry: the synthesis, reactions, properties and applications of coordination compounds*, vol 5. Pergamon, Oxford, pp 861–923
34. Gimeno MC, Laguna A (1997) *Chem Rev* 97:511–522
35. Grohmann A, Schmidbaur H (1995) In: Abel EW, Stone FGA, Wilkinson G (eds) *Comprehensive organometallic chemistry II*, vol 3. Pergamon, Oxford, pp 1–56
36. Bowmaker GA, Schmidbaur H, Krüger S, Rösch N (1997) *Inorg Chem* 36:1754–1757
37. Schmidbaur H, Graf W, Müller G (1988) *Angew Chem Int Ed Engl* 27:417–419
38. Pyykkö P (2002) *Angew Chem Int Ed* 41:3573–3578
39. Schmidbaur H (1990) *Gold Bull* 23:11–21
40. Schmidbaur H (1995) *Chem Soc Rev* 24:391–400
41. Schmidbaur H (2001) *Nature* 413:31–33
42. Hall KP, Mingos DMP (1984) *Prog Inorg Chem* 32:237–326
43. Nakanishi W, Yamanaka M, Nakamura E (2005) *J Am Chem Soc* 127:1446–1453
44. Komiy S, Kochi JK (1976) *J Am Chem Soc* 98:7599–7607
45. Komiy S, Albright TA, Hoffmann R, Kochi JK (1976) *J Am Chem Soc* 98:7255–7265
46. Tsuji J (2002) *Transition metal reagents and catalysts: innovations in organic synthesis*. Wiley, New York
47. Zeise WC (1827) *Poggendorff's Ann Phys* 9:632
48. Wunderlich JA, Mellor DP (1954) *Acta Crystallogr* 7:130
49. Jarvis JAJ, Kilbourn BT, Owsten PG (1971) *Acta Crystallogr B* 27:366–372
50. Love RA, Koetzle TF, Williams GJB, Andrews LC, Bau R (1975) *Inorg Chem* 14:2653–2657
51. Dedieu A (1999) *Top Organomet Chem* 4:69
52. Niu S, Hall MB (2000) *Chem Rev* 100:353
53. Torrent M, Sola M, Frenking G (2000) *Chem Rev* 100:439
54. Dedieu A (2000) *Chem Rev* 100:543
55. Sakaki S (2005) *Top Organomet Chem* 12:31
56. Balcells D, Clot E, Eisenstein O (2010) *Chem Rev* 110:749–823
57. Siegbahn PEM (1996) *Adv Chem Phys* 93:333
58. Görling A, Trickey SB, Gisdakis P, Rösch N (1999) *Top Organomet Chem* 4:109
59. Dudnik AS, Xia Y, Li Y, Gevorgyan V (2010) *J Am Chem Soc* 132:7645–7655
60. Reetz MT, Sommer K (2003) *Eur J Org Chem* 3485–3496
61. Mamane V, Hannen P, Fürstner A (2004) *Chem Eur J* 10:4556–4575
62. Bruneau C, Dixneuf PH (2006) *Angew Chem Int Ed* 45:2176–2203
63. Trost BM, Rhee YH (2002) *J Am Chem Soc* 124:2528–2533
64. Kim H, Lee C (2006) *J Am Chem Soc* 128:6336–6337
65. Soriano E, Marco-Contelles J (2006) *Organometallics* 25:4542–4553
66. Vogler A, Kunkely H (2001) *Coord Chem Rev* 219–221:489–507
67. Hashmi ASK, Blanco MC, Fischer D, Bats JW (2006) *Eur J Org Chem* 1387–1389
68. Zhu RX, Zhang DJ, Guo JX, Mu JL, Duan CG, Liu CB (2010) *J Phys Chem A* 114:4689–4696
69. Kobayashi S, Manabe K (2002) *Acc Chem Res* 35:209–217
70. Yamamoto Y (2007) *J Org Chem* 72:7817–7831
71. Asao N, Nogami T, Takahashi K, Yamamoto Y (2002) *J Am Chem Soc* 124:764–765

72. Jin T, Yamamoto Y (2008) *Org Lett* 10:3137–3139
73. Xia Y, Dudnik AS, Gevorgyan V, Li Y (2008) *J Am Chem Soc* 130:6940–6941
74. Straub BF (2004) *Chem Commun* 1726–1728
75. Marion N, Carlqvist P, Gealageas R, de Fremont P, Maseras F, Nolan SP (2007) *Chem Eur J* 13:6437–6451
76. Lin CC, Teng T-M, Odedra A, Liu R-S (2007) *J Am Chem Soc* 129:3798–3799
77. Dudnik AS, Sromek AW, Rubina M, Kim JT, Kel'in AV, Gevorgyan V (2008) *J Am Chem Soc* 130:1440–1452
78. Hashmi ASK, Sinha P (2004) *Adv Synth Catal* 346:432
79. Shu X-Z, Liu X-Y, Xiao H-Q, Ji K-G, Guo L-N, Qi C-Z, Liang Y-M (2007) *Adv Synth Catal* 349:2493
80. Cordonnier MC, Blanc A, Pale P (2008) *Org Lett* 10:1569
81. Gonzalez Perez A, Silva Lopez C, Marco-Contelles J, Nieto Faza O, Soriano E, de Lera AR (2009) *J Org Chem* 74:2982–2991
82. Schwerdtfeger P, Boyd PDW, Burrell AK, Robinson WT, Taylor MJ (1990) *Inorg Chem* 29:3593–3607
83. Markham JP, Staben ST, Toste FD (2005) *J Am Chem Soc* 127:9708–9709
84. Zhang Z, Liu C, Kinder RE, Han X, Qian H, Widenhoefer RA (2006) *J Am Chem Soc* 128:9066–9073
85. Marion N, Diez-Gonzalez S, de Fremont P, Noble AR, Nolan SP (2006) *Angew Chem Int Ed* 45:3647–3650
86. Chianese AR, Lee SJ, Gagné SR (2007) *Angew Chem Int Ed* 46:4042–4059
87. Dewar MJS (1951) *Bull Soc Chim Fr* 18:C71–C79
88. Chatt J, Duncanson LA (1953) *J Chem Soc* 2939–2947
89. Dias HVR, Wu J (2010) *Eur J Inorg Chem* 509–522
90. Frenking G, Fröhlich N (2000) *Chem Rev* 100:717
91. Dedieu A (2000) *Chem Rev* 100:8372
92. Hertwig R, Koch W, Schröer D, Schwarz H, Hrušák J, Schwerdtfeger P (1996) *J Phys Chem* 100:12253–12260
93. Shi X, Gorin DJ, Toste FD (2005) *J Am Chem Soc* 127:5802
94. Nieto-Faza O, Silva-López C, Álvarez R, de Lera AR (2006) *J Am Chem Soc* 128:2434
95. Soriano E, Marco-Contelles JL (2007) *J Org Chem* 72:1443
96. Nieto-Oberhuber C, López S, Jiménez-Núñez E, Echavarren AM (2006) *Chem Eur J* 12:5916
97. Soriano E, Ballesteros P, Marco-Contelles JL (2005) *Organometallics* 24:3172
98. Pernpointner M, Hashmi ASK (2009) *J Chem Theory Comput* 5:2717–2725
99. Kurosawa H, Yamamoto A (eds) (2003) *Fundamentals of molecular catalysis. Current methods in inorganic chemistry*, vol 3. Elsevier, Amsterdam
100. Hahn C, Cucciolito ME, Vitagliano A (2002) *J Am Chem Soc* 124:9038–9903
101. Nechaev MS, Rayon VM, Frenking G (2004) *J Phys Chem A* 108:3134–3142
102. Shapiro ND, Toste FD (2008) *Proc Natl Acad Sci USA* 105:2779–2782
103. Lang H, Köhler K, Zsolnai L (1996) *Chem Commun* 2043–2044
104. Köhler K, Silverio SJ, Hyla-Kryspin I, Gleiter R, Zsolnai L, Driess A, Huttner G, Lang H (1997) *Organometallics* 16:4970–4979
105. Mingos DMP, Yau J, Menzer S, Williams DJ (1995) *Angew Chem Int Ed Engl* 34:1894–1895
106. Yip S-K, Cheng EC-C, Yuan L-H, Zhu N, Yam VW-W (2004) *Angew Chem Int Ed* 43:4954–4957
107. Chui SSY, Ng MFY, Che C-M (2005) *Chem Eur J* 11:1739–1749
108. Akana JA, Bhattacharyya KX, Müller P, Sadighi JP (2007) *J Am Chem Soc* 129:7736–7737
109. Wu J, Kroll P, Dias HVR (2009) *Inorg Chem* 48:423–425
110. Schulte P, Behrens U (1998) *Chem Commun* 1633–1634
111. Flügge S, Anoop A, Goddard R, Thiel W, Fürstner A (2009) *Chem Eur J* 15:8558–8565
112. Dias HVR, Wu J (2008) *Eur J Inorg Chem* 509–522

113. Schmidbaur H, Schier A (2010) *Organometallics* 29:2–23
114. Schroeder D, Schwarz H, Hrusak J, Pykkö P (1998) *Inorg Chem* 37:624–632
115. Schroeder D, Hrusak J, Hertwig RH, Koch W, Schwerdtfeger P, Schwarz H (1995) *Organometallics* 14:312–316
116. Stringer KL, Citir M, Metz RB (2004) *J Phys Chem A* 108:6996–7002
117. Jarvis JA, Kilbourn BT, Owsten PG (1971) *Acta Crystallogr Sect B* 27:366–372
118. Chang TH, Zink JI (1984) *J Am Chem Soc* 106:287–292
119. Steinborn D, Tschoerner M, von Zweidorf A, Sieler J, Bögel H (1995) *Inorg Chim Acta* 234:47–53
120. Belluco U, Bertani R, Michelin RA, Mozzon M (2000) *J Organomet Chem* 600:37–55
121. Turner RW, Amma EL (1966) *J Am Chem Soc* 88:1877
122. Dines MB, Bird PH (1973) *J Chem Soc Chem Commun* 12
123. Pasquali M, Floriani C, Gaetani-Manfredotti A (1980) *Inorg Chem* 19:1191
124. Schmidbaur H, Bublak W, Huber B, Reber G, Müller G (1986) *Angew Chem Int Ed Engl* 25:1089
125. (1975) *Gmelin handbook of inorganic chemistry*, 8th ed. Springer, Berlin, Silver (Part B5: Organosilver compounds)
126. Eisenstein O, Hoffmann R (1981) *J Am Chem Soc* 103:4308–4320
127. Senn HM, Blöchl PE, Togni A (2000) *J Am Chem Soc* 122:4098–4107
128. Cameron AD, Smith VH Jr, Baird MC (1988) *J Chem Soc Dalton Trans* 1037–1043
129. Fujimoto H, Yamasaki T (1986) *J Am Chem Soc* 108:578–581
130. Sakaki S, Maruta K, Ohkubo K (1987) *Inorg Chem* 26:2499–2505
131. Gorin DJ, Sherry BD, Toste FD (2008) *Chem Rev* 108:3351–3378
132. Nevado C, Cardenas DJ, Echavarren AM (2003) *Chem Eur J* 9:2627–2635
133. Fedorov A, Moret ME, Chen P (2008) *J Am Chem Soc* 130:8880–8881
134. Trost BM, Hashmi ASK (1993) *Angew Chem Int Ed* 32:1085–1087
135. Johansson MJ, Gorin DJ, Staben ST, Toste FD (2005) *J Am Chem Soc* 127:18002–18003
136. Fructos MR, Belderrain TR, de Frémont P, Scott NM, Nolan SP, Díaz-Requejo MM, Pérez PJ (2005) *Angew Chem Int Ed* 44:5284–5288
137. Lopez S, Herrero-Gomez E, Perez-Galan P, Nieto-Oberhuber C, Echavarren AM (2005) *Angew Chem Int Ed* 45:6029–6032
138. Fedorov A, Chen P (2009) *Organometallics* 28:1278–1281
139. Boger DL, Brotherton CE (1984) *Tetrahedron Lett* 25:5611–5614
140. Fischer EO, Böck M, Aumann R (1983) *Chem Ber* 116:3618–3623
141. Aumann R, Fischer EO (1981) *Chem Ber* 114:1853–1857
142. Schubert U, Ackermann K, Aumann R (1982) *Cryst Struct Comm* 11:591–594
143. Fernandez EJ, Laguna A, Olmos ME (2005) *Adv Organomet Chem* 52:77–141
144. Raubenheimer HG, Esterhuysen MW, Timoshkin A, Chen Y, Frenking G (2002) *Organometallics* 21:3173–3181
145. Lin IJB, Vasam CS (2005) *Can J Chem* 83:812–825
146. Nemcsok D, Wichmann K, Frenking G (2004) *Organometallics* 23:3640–3646
147. Liu B, De Brabander JK (2006) *Org Lett* 8:4907–4910
148. Irikura KK, Goddard WA (1994) *J Am Chem Soc* 116:8733–8740
149. Heinemann C, Hertwig RH, Wesendrup R, Koch W, Schwarz H (1995) *J Am Chem Soc* 117:495–500
150. Hu X, Castro-Rodriguez I, Olsen K, Meyer K (2004) *Organometallics* 23:755–764
151. Jacobsen H (2005) *J Organomet Chem* 690:6068–6078
152. Pykkö P, Runeberg N (2006) *Chem Asian J* 1:623–628
153. Pykkö P (2008) *Chem Soc Rev* 37:1967–1997
154. Benitez D, Shapiro ND, Tkatchouk E, Wang Y, Goddard WA III, Toste FD (2009) *Nat Chem* 1:482–486
155. Fürstner A, Morency L (2008) *Angew Chem Int Ed* 47:5030–5033
156. Seidel G, Mynott R, Fürstner A (2009) *Angew Chem Int Ed* 48:2510–2513

157. Padwa A, Austin DJ (1994) *Angew Chem Int Ed Engl* 33:1797–1815
158. Landis CR, Weinhold F (2007) *J Comput Chem* 28:198–203
159. Seidel G, Lehmann CW, Fürstner A (2010) *Angew Chem Int Ed Engl* 49:8466–8470
160. Cheong PH-Y, Morganelli P, Luzung MR, Houk KN, Toste FD (2008) *J Am Chem Soc* 130:4517–4526



# Cycloisomerization of 1,*n*-Enynes Via Carbophilic Activation

Patrick Yves Toullec and Véronique Michelet

**Abstract** Metal-catalyzed cycloisomerization of 1,*n*-enynes has appeared as a highly attractive methodology for the synthesis of original carbo- and heterocycles. This chapter intends to propose an overview of the recent and seminal advances in 1,*n*-enynes cycloisomerization reactions in the presence of carbophilic transition metals. The recent mechanistic insights, the enantioselective versions, and the applications in total synthesis are highlighted.

**Keywords** 1,*n*-Enyne · Carbophilic activation · Cycloisomerization · Gold · Platinum

## Contents

1	Introduction .....	31
2	Carbophilic Lewis Acids: Reactivity Principles .....	32
3	Enyne Cycloisomerization Reactions in the Absence of Nucleophiles .....	37
3.1	Formation of Dienes .....	37
3.2	Conia Ene Type Reactions .....	47
3.3	Formation of Bicyclic Derivatives Via Cycloisomerization Reactions .....	50
4	Domino Enyne Cycloisomerization-Nucleophile Addition Reaction .....	60
4.1	Oxygen Nucleophiles .....	60
4.2	Carbon Nucleophiles .....	68
4.3	Nitrogen Nucleophiles .....	73
5	Conclusion .....	75
	References .....	75

## 1 Introduction

Metal-catalyzed cycloisomerization reactions of 1,*n*-enynes have appeared as conceptually and chemically highly attractive processes as they contribute to the thrill towards atom economy and offer the opportunity to develop new reactions [1–8].

---

P.Y. Toullec and V. Michelet (✉)

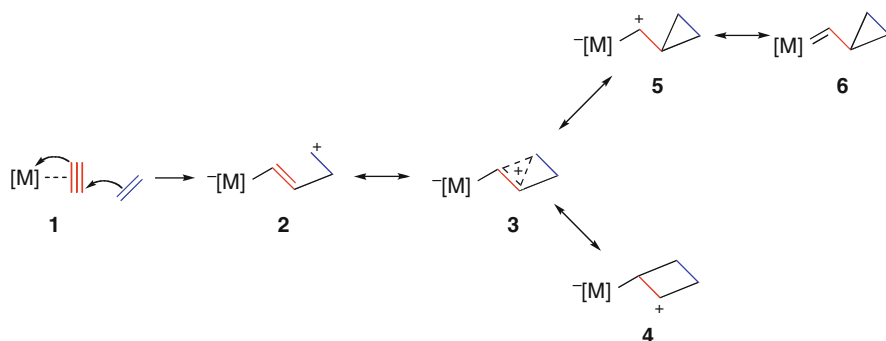
Laboratoire Charles Friedel, UMR 7223, Ecole Nationale Supérieure de Chimie de Paris, Chimie ParisTech, 11, rue P. et M. Curie, 75231 Paris cedex 05, France

e-mail: veronique-michelet@chimie-paristech.fr

Although various reaction mechanisms including metallacycles, hydrometalation or metathesis of enynes and relying on the specific reactivities of transition metal complexes have been reported over the years, the recent upsurge of interest associated with the studies involving carbophilic Lewis acids such as gold or platinum (for representative examples and seminal references, see [9–29]) has opened the way to the development of families of highly active and selective catalysts presenting a unique reactivity. A wide variety of carbo- and heterocycles presenting a high degree of structural complexity can be formed using these new catalytic systems. The emergence of sophisticated theoretical DFT studies has contributed to the understanding of plausible reaction pathways and to the optimization or design of highly efficient catalysts [30]. This highlight aims at presenting the mechanistic rationale associated with carbophilic Lewis catalysts in the context of their reactivity in the presence of 1,*n*-enynе substrates. The skeletal rearrangements will be presented putting the stress on similarities between transition metals, following the reaction type in the absence and then presence of nucleophiles. The formation of 1,3-dienes and 1,4-dienes will be followed by the reactivity of activated alkenes and then the synthesis of bicyclic derivatives. The presence of internal or external nucleophiles has led to the discovery of novel rearrangements, which will be then presented. The development of enantioselective variants of these transformations [31–33] along with their applications in natural products synthesis [18] will also be discussed. The reactions implying propargylic esters [34, 35] will not be presented.

## 2 Carbophilic Lewis Acids: Reactivity Principles

At the initial stage of all mechanisms invoked in the literature to explain enyne cycloisomerization reactions in the presence of carbophilic late transition metals, the  $\eta^2$ -coordination of the alkyne moiety by the metal complex activates the C–C unsaturated bond (Scheme 1, intermediate 1) (for an excellent review dealing with gold  $\eta^2$ -coordination to unsaturated hydrocarbons, see [36]). Since the pioneering



**Scheme 1** General mechanism for the metal-catalyzed addition of an alkene to an alkyne

studies of Utimoto on the hydroalkoxylation [37] and hydroamination [38] of alkynes catalyzed by gold complexes, the *anti* nucleophilic attack of a large variety of nucleophiles has been investigated in the presence of “soft” carbophilic transition metal Lewis acids. Alkenes can act as nucleophiles, the net *anti* addition of an alkene either intra- or intermolecularly by an outer-sphere mechanism results, upon slippage (for a theoretical investigation of  $\pi$ -systems slippage, see [39]) of the  $\eta^2$ -coordinated alkyne, in the formation of a vinylmetal intermediate **2** possessing a carbocation at the  $\delta$  position. This non-classical organometallic cation can best be viewed as a delocalized three center cation **3** whose mesomeric extremes can also be seen as cyclobutyl carbocation **4** or cyclopropyl carbocation **5**. The latter form has often been described as a cyclopropyl carbene **6** or more cautiously as a cyclopropyl carbenoid as the involvement of metal to carbon back donation is still a matter of debate. The cationic to carbenoid controversy arises from the possibility of observing reaction products that are best understood by one of the two ways to describe the bonding properties of these intermediates but is to some extent artificial.

Recent reports from the literature deal with the isolation and characterization of Pt(II)- or Au(I)-alkyne complexes (Fig. 1). In the case of Pt complexes, the alkyne adopts a perpendicular arrangement to the plane defined by the  $L_3Pt^{2+}$  fragment. In the case of gold, the dicoordinated gold complexes adopt a linear geometry, the second stabilizing ligand being either a phosphane [40, 41] (for recent NMR studies highlighting a carbophilic modulation of cationic Au complexes, see [42]) or an *N*-heterocyclic carbene [43]. X-ray analyses of complexes **7–11** show only marginal C $\equiv$ C bond shortening compared to the free alkyne but significant reduction of the C $\equiv$ C–C angle (values between 160° and 168° for coordinated alkynes vs 175–180° for free alkynes). Theoretical calculations also support a good  $\sigma$ -donation from the

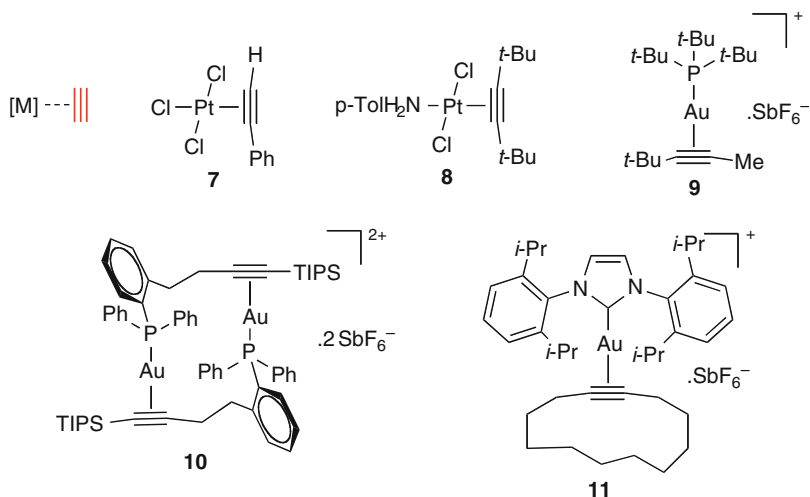


**Fig. 1** Examples of Pt(II)- and Au(I)- $\eta^2$ -alkynyl complexes



alkyne to the metal center and a relatively weak  $\pi$ -back donation from the metal to the alkyne, resulting in a depletion of the electron density on the alkyne. Comparison of the data for Au with the related ones for Ag and Cu complexes [40] highlights the superior activation obtained with cationic Au complexes and the superior electrophilicity of the coordinated alkyne.

The involvement of cyclopropyl carbocation **5** or the cyclopropyl carbene **6** (Scheme 1), revealing the nature of the carbon-metal bond, has recently been under debate in the literature, the discussion being concentrated on gold complexes. The selectivity observed in domino enyne cycloisomerization/nucleophile addition has led Fürstner and coworkers [44, 45] to invoke a mechanistic rationale involving a concerted transition state analogous to that involved in carbocation-induced polyene cyclization reactions (see Sect. 4.1) [46–48]. The authors also support their hypothesis by discussing structural parameters associated with the crystal structure analysis of the Fisher-type gold carbene **12** [49] (Fig. 2). The reported bond lengths are consistent with the existence of an Au–C single bond and are best described as gold iminium species **13**. As the nitrogen substitution induces electronic effects in the complex, this model cannot be considered as satisfactory for a comparison with enyne cycloisomerization intermediates depicted in Scheme 1. Nevertheless, crystallographic data seem to favor the involvement of intermediate **5**.

To get further insight into the bonding situation of gold “carbenoid” species, the group of Fürstner then investigated the synthesis of stabilized gold allylic carbocations by the reaction of acetalcyclopropenes such as **14** with cationic  $[(PPh_3)Au]NTf_2$  complex [50] (Scheme 2). Formation of the vinylaurate (Z)-**15** is cleanly observed at  $-78^\circ C$  and has been characterized by  $^1H$  and  $^{13}C$  NMR spectroscopies (1). Isomerization to the diastereoisomer (E)-**15** has been observed by temperature dependent NMR measurements and corresponds to a barrier of rotation of about  $30\text{ kcal mol}^{-1}$ . These data are consistent with the observation on the NMR timescale of a delocalized allylic carbenium structure **16** whereas the carbene form **17** has no significant contribution. This understanding of the bonding situation of compounds of general formula  $(LAu-CRR')^+$  has been further supported by the group of Toste [51] (Scheme 2). Using DFT calculations, the authors have shown that the bonding model involved in Au(I) carbenoids is strongly affected by both the substitution pattern of the organic moiety and the stereoelectronic parameters of the second coordinating ligand L on the gold center. The authors propose a bonding model, defined as a “double half bond” as both  $\sigma$ -donation and  $\pi$ -back donation as defined by the Chatt–Duncanson model are involved, but both contributions are relatively weak. The authors have studied analogous structures of **15**. Bond lengths

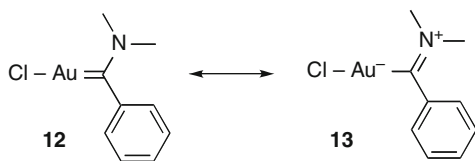
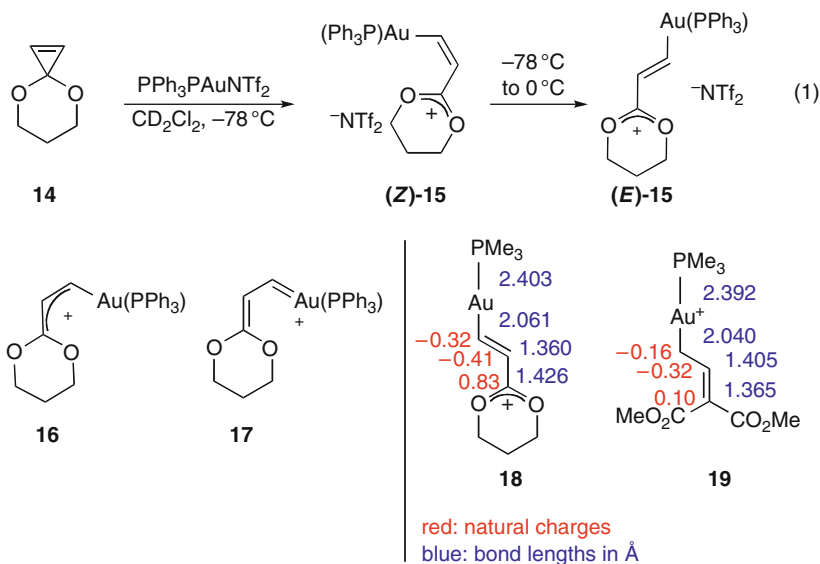
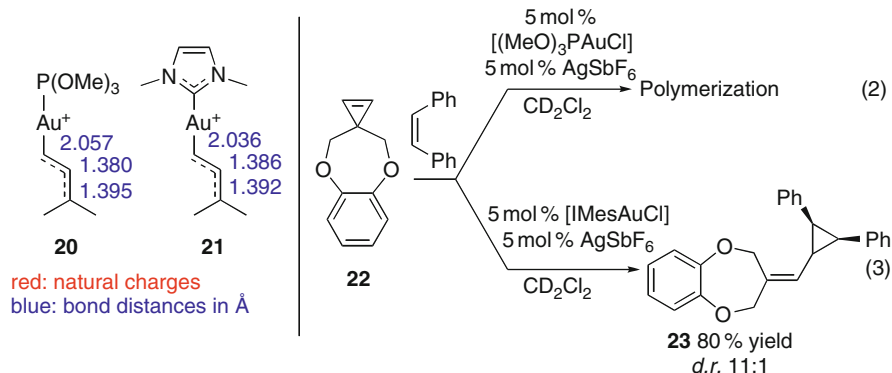


**Fig. 2** Fisher-type gold carbene



**Scheme 2** Reaction of acetalcyclopropene with cationic Au(I) complex



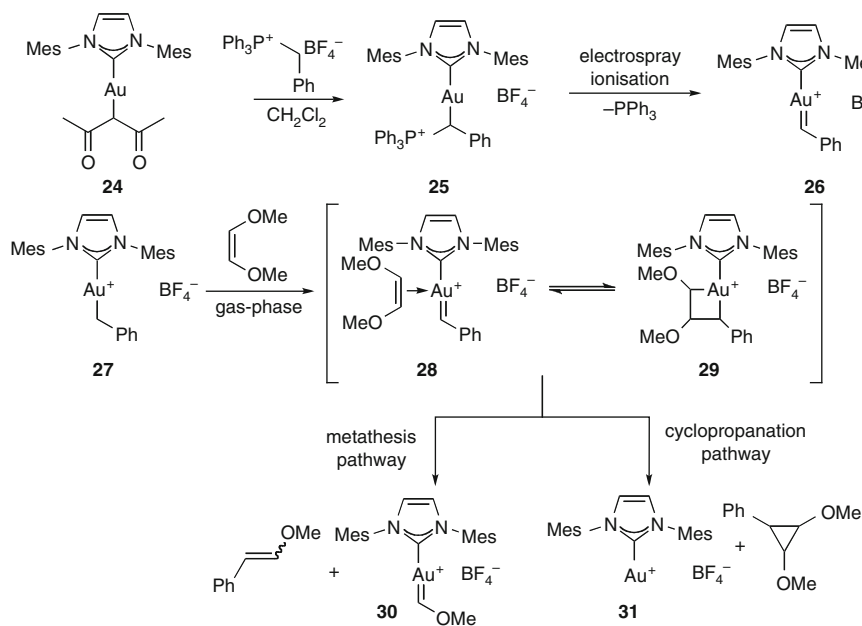
**Scheme 3** Influence of the ligand on cationic Au(I) carbene complexes

and charge distributions are clearly indicative of respectively a vinyl aurate complex **18** when  $\gamma$ -stabilizing groups are present (i.e., methoxy substituents) and an  $\eta^1$ -allyl complex **19** when  $\gamma$ -destabilizing groups are present.

DFT calculations and correlations of the theoretical data with experimental ones have also pointed out the strong influence of the ligand on Au(I) cationic complex [51] (Scheme 3). An electron-withdrawing ligand such as P(OMe)<sub>3</sub> diminishes the electron density on the metal center, weakens the  $\pi$ -back donation to the C $\alpha$ , and thus leads to carbocationic reactivity (complex **20**), whereas a good  $\sigma$ -donating ligand such as an *N*-heterocyclic carbene increases the electron density on the Au(I) center and allows a better  $\pi$ -back donation to the C $\alpha$ , thus favoring a carbene

reactivity (complex **21**). This mechanistic rationale is, remarkably, confirmed when the two aforementioned types of complexes are reacted with cyclopropene **22** and 1,2-diphenylethene. Whereas the use of the  $\text{P(OMe)}_3\text{Au}^+$  cation only leads to polymerization (2), the  $(\text{NHC})\text{Au}^+$  cation **23** gives the cyclopropanation product in 80% yield and excellent diastereoselectivity (3).

Gold carbenes being highly reactive intermediates, very little data relative to their characterization and reactivity have been reported in the literature. Recently the group of Chen [52–54] reported the synthesis of Au(I) carbenes in the gas phase along with their reactivity in the presence of alkenes (Scheme 4). Gold complex **24** reacts with the phosphonium salt  $[\text{Ph}_3\text{PCH}_2\text{Ph}]\text{BF}_4^-$  to generate the gold ylide adduct **25**. Upon submission of this species to electrospray ionisation, detection of the ion corresponding to the gold benzylidene complex **26** by tandem mass spectroscopy has been accomplished. Introduction of alkenes into the ion guide allowed the assessment of the reactivity of these transient species. Upon generation and selection of ion **26** in the presence of 1,2-dimethoxyethene, formation of three signals is observed. The first signal corresponding to the 1:1 adduct of the two reactants has been assigned either to the  $\eta^2$ -complex **27** or to the metalacyclobutane **28**. The second signal corresponds to the gold methoxylidene carbene complex **29**. Its formation is indicative of the existence of an alkene metathesis reactivity unprecedented in gold catalysis. The third signal corresponds to the  $(\text{NHC})\text{Au}^+$  cation **30** formed upon loss of both the benzylidene and the dimethoxyethene moieties from the gold complex **27/28** and has been proposed to account for



**Scheme 4** Synthesis and reactivity of Au(I) carbenes in the gas phase

a competitive cyclopropanation pathway, well described for Au(I) species in solution (see (3) and Sect. 4.2.1).

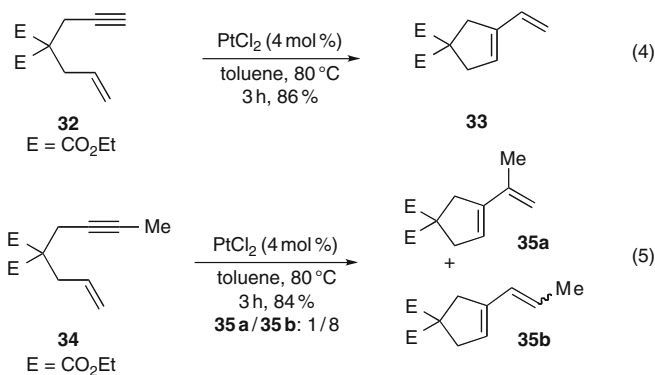
According to all these recent data, the specific behavior of Au complexes is offering the complete array of intermediate reactivity between the two mesomeric extremes **5** and **6** representing respectively the carbocationic and carbenic renditions. The reactivity in a given organic transformation catalyzed by gold can be explained preferentially by one of the two canonical pictures depending on the substitution pattern of the organic substrate or the stereoelectronic parameter of the metal fragment  $L_nM$ .

### 3 Enyne Cycloisomerization Reactions in the Absence of Nucleophiles

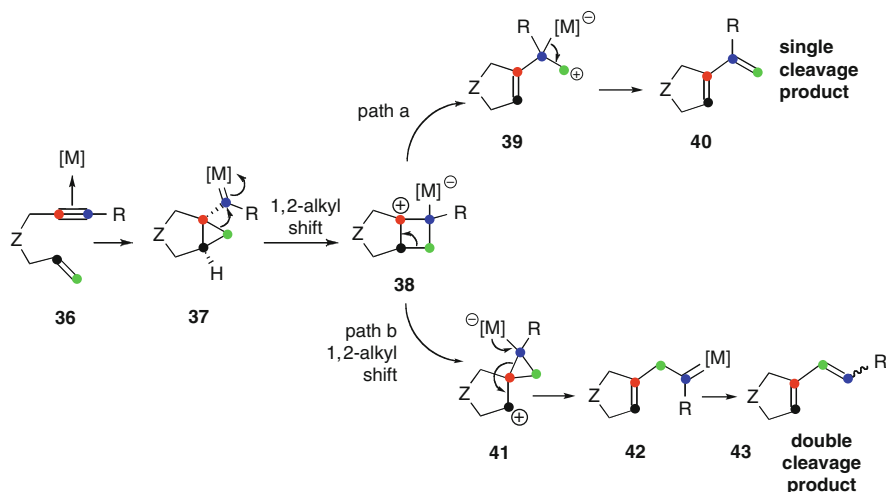
#### 3.1 Formation of Dienes

##### 3.1.1 Formation of 1,3-Dienes

The first report ([55]; earlier on, the group of Murai stated in a paper devoted to a Ru-catalyzed skeletal rearrangement of 1,6- and 1,7-enynes to 1-vinylcycloalkanes : “Interestingly, some other metal halides such as  $[RhCl(CO)_2]_2$ ,  $ReCl(CO)_5$ ,  $[IrCl(COD)]_n$ ,  $PtCl_2$ , and  $AuCl_3$  can cause a similar skeletal reorganization and some of these complexes exhibited characteristic substrate specificity.”, see [56]) of the transformation of an enyne in the presence of a carbophilic Lewis acid catalyst dates from 1996, when the group of Murai treated 1,6-enyne **32** with 5 mol%  $PtCl_2$  in toluene at 80 °C [57] (Scheme 5). Cyclization occurs via the 5-*exo* mode of cyclization to give 1,3-diene **33** in 86% yield. Since this seminal contribution, various metal salts or complexes have been evaluated in this reaction. Pt(II) [58] including a



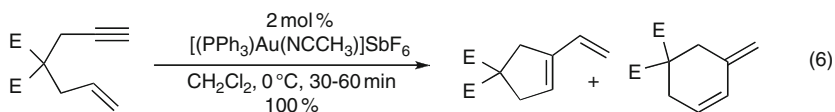
**Scheme 5** Cycloisomerization of 1,6-enynes leading to 1,3-dienes



**Scheme 6** Single cleavage and double cleavage reaction pathways

dicationic one [59], Pt(IV) [60], Rh(II) [61], Ir(I) [62], Hg(II) [63], Au(I) or Au(III) [64–66], In(III) [67], and Ga(III) [68] catalysts have shown very high activities, allowing the reaction to be run at room temperature or below.

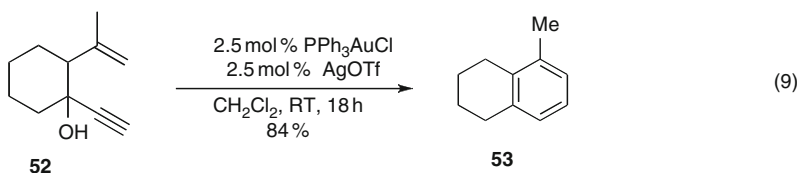
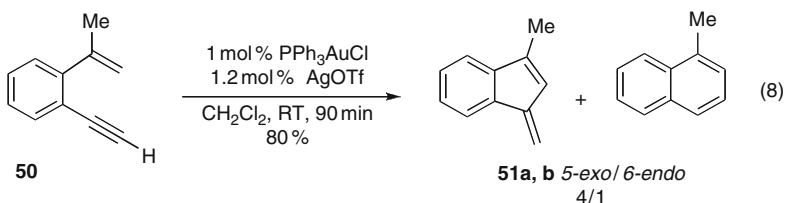
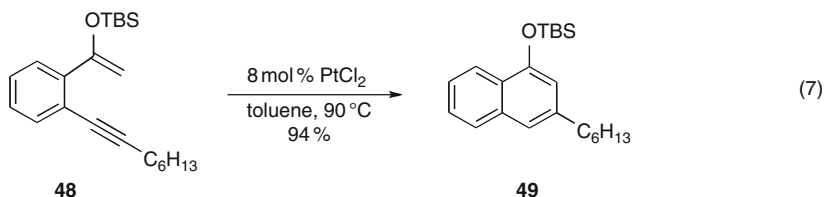
In the case of disubstituted alkynes, the cycloisomerization leads to a mixture of two different isomers depicted as “single cleavage” **40** and “double cleavage” **43** skeletal rearrangement products (Scheme 6). The “single to double cleavage” products ratio proved to be dependent on the metal catalyst used. The regiochemical outcome of this transformation has been confirmed by  $^2\text{H}$ - and  $^{13}\text{C}$ -labeling experiments [69]. Based on the experimental data collected [70] and DFT calculations independently realized by Soriano, Marco-Contelles and Echavarren groups [30, 71, 72] (for a discussion on 1,6-enynes bearing propargylic carboxylate moiety, see [73]), a mechanistic rationale has been proposed. The formation of “single cleavage” and “double cleavage” dienic products involves a competition between two different pathways. At the initial stage of the catalytic cycle,  $\eta^2$  coordination of the alkynyl function by the metal fragment initiates the *anti* attack of the alkene nucleophile. The cyclopropanation step occurs via the 5-*exo* mode of cyclization to give the cyclopropyl carbene intermediate **37**. A first 1,2-alkyl shift leads to the formation of the zwitterionic cyclobutane **38**. Depending on the nature of the alkene substitution, this species can either evolve by fragmentation through path a to give complex **39** or by a second 1,2-alkyl shift through path b to form the cyclopropyl intermediate **41**. Ring opening of this cyclopropyl zwitterion gives the carbene **42** that upon 1,2-hydride shift and elimination furnishes the double cleavage product **43**. Recent theoretical studies also compared the performance of homogeneous vs heterogeneous catalysis for the cycloisomerization of 1,6-enynes [74]. The authors showed that the activation of alkynyl substrates has a kinetic origin in the homogeneous case and a thermodynamic origin in the heterogeneous case.



44 E = CO<sub>2</sub>Me  
45 E = SO<sub>2</sub>Ph

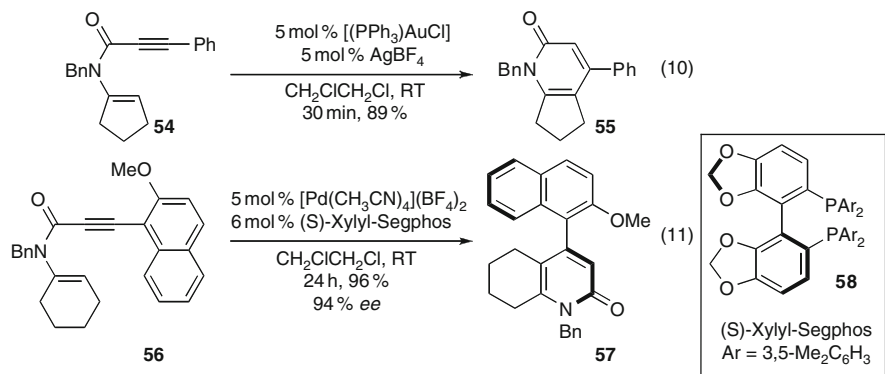
E = CO<sub>2</sub>Me  
E = SO<sub>2</sub>Ph

46a, b 1/4 5-*exo*/6-*endo*  
47a, b 10/1 5-*exo*/6-*endo*



**Scheme 7** Cycloisomerization of 1,6- and 1,5-enynes leading to dienes and indenes and naphthalenes

In the presence of cationic Au(I) species, the 6-*endo* mode of cyclization can be observed as a major path for specific 1,6-enynes [75]. The electronic nature of the C4 substituents plays a key role in orienting the regioselectivity of the cyclization event (Scheme 7). Whereas the malonate substrate **44** is cycloisomerized in the presence of 2 mol% [(PPh<sub>3</sub>)Au(NCCH<sub>3</sub>)](SbF<sub>6</sub>) at 0 °C in 97% yield with an *exo/endo* ratio of 1/4, the bissulfone **45** is transformed to the dienic products **47a,b** in 100% yield with an *exo/endo* selectivity of 10/1 under the same conditions. According to the same methodology, the synthesis of indenes and naphthalenes has been successfully described starting from aromatic enynes. Silyl enol ether **48** has been converted to the silyl-protected 1-naphthol **49** in 94% yield upon reaction in toluene at 90 °C in the presence of 8 mol% PtCl<sub>2</sub> (7) [76]. This methodology has been applied to the synthesis of a family of acridine derivatives using Rh(I) catalysts [77]. Enyne **50** reacts in the presence of a combination of PPh<sub>3</sub>AuCl and AgOTf in dichloromethane at room temperature to give a mixture of 5-*exo* and 6-*endo* products **51a,b** in a 4/1 ratio (8) [78].



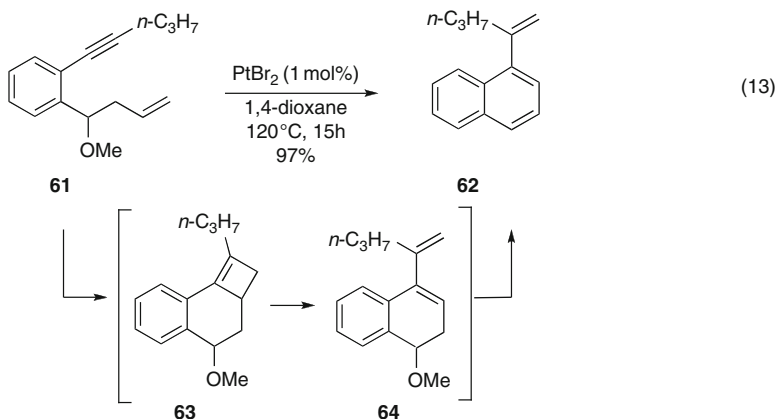
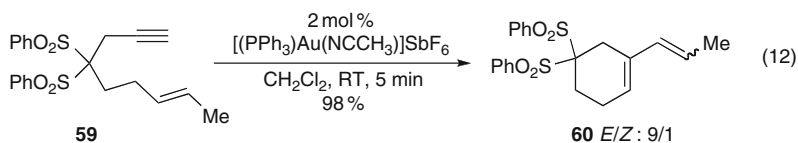
**Scheme 8** Cycloisomerization reaction of *N*-alkenyl alkynylamides

Similar results were obtained in the preparation of tetrahydronaphthalenes starting from 3-hydroxy-5-en-1-ynes **52**, taking advantage of the quaternary alcohol at the propargylic position [79].

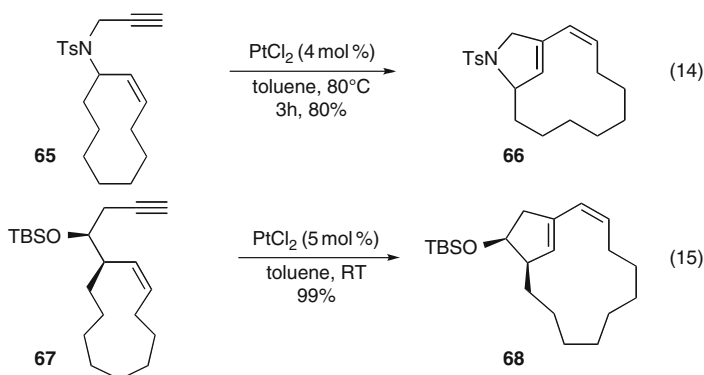
The cycloisomerization of 1,5-enynes and more specifically of *N*-alkenyl alkynylamides (**54** and **56**) was recently reported [80] (Scheme 8, (10, 11)). 2-Pyridones are formed in moderate to high yields in the presence of cationic Au(I) catalysts following a 6-*endo* mode of cyclization. The same group recently described an asymmetric version of this transformation leading to axially chiral 2-pyridones **57** using a combination of the bidentate phosphorus ligand **58** and the dicationic palladium precursor  $[Pd(CH_3CN)_4](BF_4)_2$ .

This type of skeletal rearrangements has not been limited to 1,5- or 1,6-enynes, and has been reported in the case of 1,7-enynes in the presence of gold and platinum catalysts (Scheme 9). Bissulfone-based enyne **59** cyclizes in a 6-*exo* fashion when reacted in the presence of a cationic Au(I) catalyst to furnish the vinylcyclohexene product **60** in 98% yield (12) [81]. This result is in agreement with the exclusive involvement of the single cleavage pathway in the case of 1,7-enynes. In the case of 1,7-enynes, which contain an aromatic ring and a benzylic leaving group in the tether such as **61**, the cycloisomerization reaction led to vinylnaphthalene **62** in 97% yield in the presence of  $PtBr_2$  at 120 °C for 15 h [82].

The mechanism proposed involves the initial formation of a cyclobutene intermediate **63** by a formal [2 + 2] cycloaddition (see Sect. 3.3.2 for the carbophilic Lewis acid-catalyzed formation of such intermediates) which would thermally rearrange to give the 1,3-diene **64** after cyclobutene ring opening; methanol elimination and aromatization leading to **62** (13). Skeletal rearrangement has most notably found applications in macrocyclic synthesis. Under optimized reaction conditions in the presence of  $PtCl_2$  as a catalyst, the synthesis of the 12-membered ring **66** was performed in 80% yield (Scheme 10, (14)) [83]. The reaction is rather versatile as the cyclization of carbon-, oxygen-, and nitrogen-tethered substrates lead to the corresponding bicyclic compounds in high yields (15).



Scheme 9 Cycloisomerization reaction of 1,7-enynes



Scheme 10 Synthesis of macrocycles

This strategy has been applied to the construction of the bicyclic unit of prodiginine antibiotics such as streptorubin B **70** [83], metacycloprodiginosin **71** [83], or roseophilin **69** [84] (Fig. 3).

The group of Sarpong exploited the Ga(III)-catalyzed skeletal rearrangement of enynes [85] and presented applications to the total synthesis of ( $\pm$ )-salviasperanol **74** [86] or ( $\pm$ )-icetexone [87] (Scheme 11, (16)). Treatment of alkynyl indene **72** with 20 mol%  $\text{GaCl}_3$  in benzene at  $40^\circ\text{C}$  gives cycloheptatriene **73** in 90% yield.



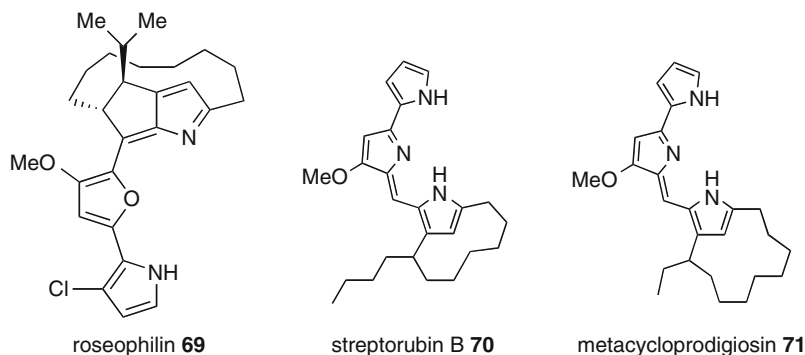
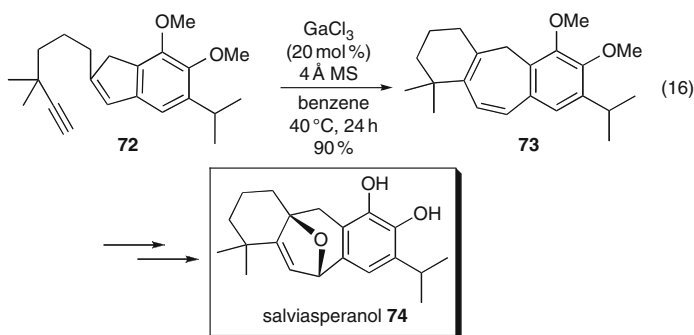


**Fig. 3** Applications in total synthesis

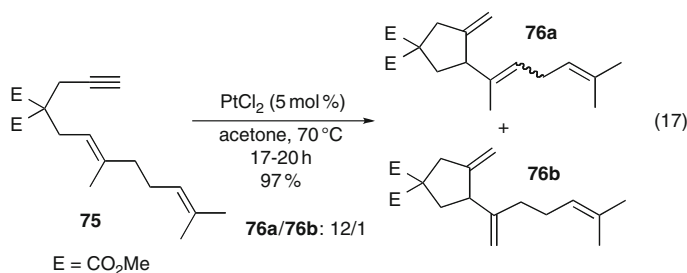


**Scheme 11** Ga-catalyzed cycloisomerization reaction

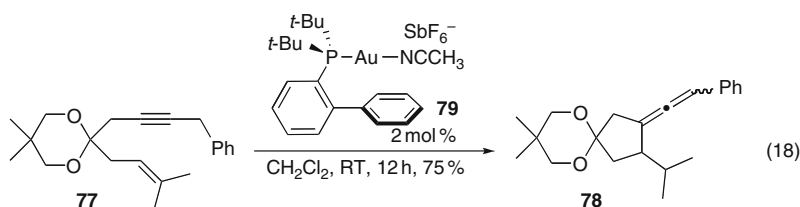
### 3.1.2 Formation of 1,4-Dienes

In contrast to the numerous palladium-catalyzed Alder-ene methodologies supported by palladacyclopentene or hydropalladation/carbopalladation mechanisms [4, 8], only rare reports of carbophilic Lewis acid-based systems have been reported. Echavarren and coworkers [88] have described the cycloisomerization of 1,6-enynes, such as **75**, to give a mixture of 1,4-dienes **76a** and **76b** by using  $\text{PtCl}_2$  as a catalyst in acetone at 70 °C (Scheme 12). This type of transformation is limited to trisubstituted alkenes. In complete analogy with the selectivity observed in the Pd-catalyzed reaction, a good regioselectivity for the  $\beta$ -hydride elimination step in favor of diene **76a** is observed. It was recently reported that bismuth(III) chloride (20 mol%) was an efficient catalyst for this transformation [89].

The 5-*exo* cyclization process may be followed by some hydride shift instead of elimination to form dienes (Scheme 13). For example, the cycloisomerization of enyne **77** afforded the cyclic allene **78** in 75% yield and implied a 1,5-*H* migration, which is favored by the presence of an electron-rich group at the propargylic position [90].



**Scheme 12** Cycloisomerization of 1,6-enynes leading to dienes



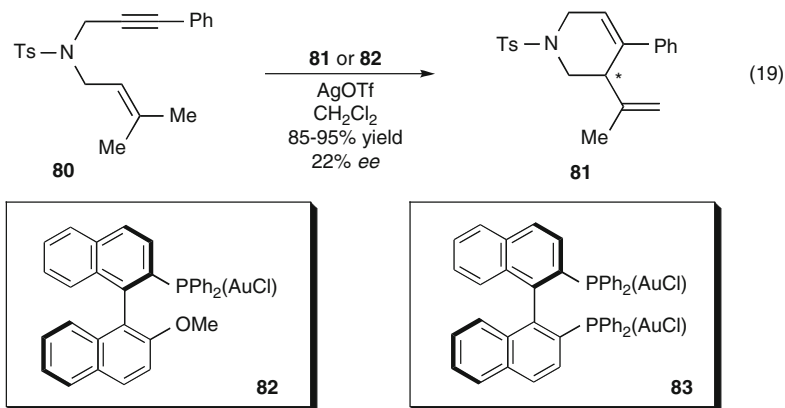
**Scheme 13** Example of hydride shift instead of elimination to form diene

Nitrogen-tethered 1,6-enynes are generally transformed to dienes via a 6-*endo* cycloisomerization process [64–66]. An enantioselective variant of this transformation was reported on **80** (Scheme 14, (19)) [91, 92]. In the presence of the monometallic complex [((*R*)-MOP)AuCl **82**] or the bimetallic complex [((*R*)-BINAP)(AuCl)<sub>2</sub> **83**] in combination with AgOTf in CH<sub>2</sub>Cl<sub>2</sub>, tetrahydropyridine **81** is obtained in good yields and modest enantioselectivities.

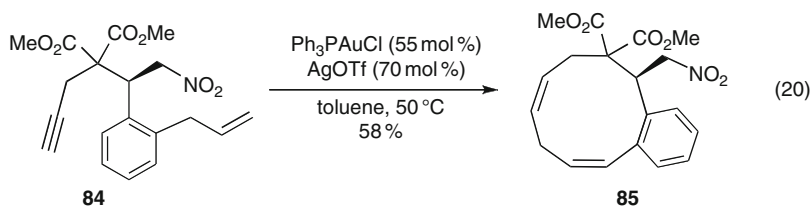
Remarkably, the 10-*endo* cycloisomerization of a 1,9-enyne **84** was described under forcing conditions (Scheme 15), thus demonstrating that carbophilic Lewis acid catalysts can lead to the formation of large ring systems such as **85** [93].

Dake et al. applied this transformation in their total synthesis of (+)-fawcettidine **88** (Scheme 16) [94]. This cycloisomerization once again highlights the functional group tolerance of the platinum-catalyzed methodology as neither the amide nor the thiocarbamate reacted under the reaction conditions. The 1,5-enyne **86** was cleanly transformed to the tricycle **87** in 87% yield in the presence of PtCl<sub>2</sub> in toluene at 90 °C (21).

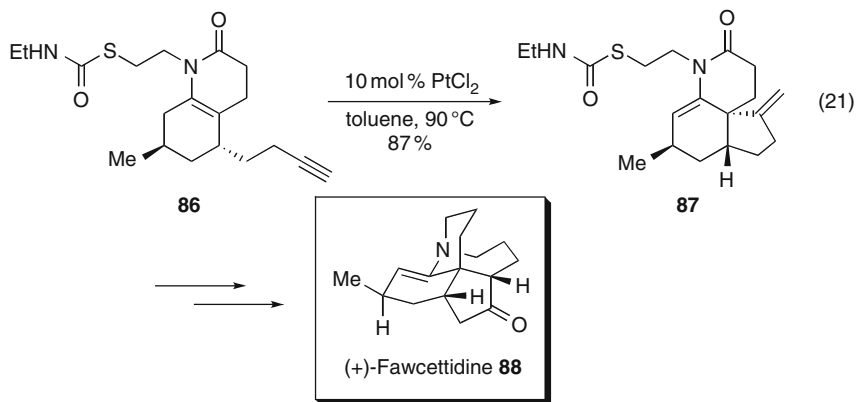
The group of Echavarren has also investigated the possibility of using allylsilane and allylstannanes as alkene partners in the cycloisomerization of 1,6- and 1,7-enynes [95, 96]. In acetone at reflux, a silylated enyne, such as **89**, is transformed in the presence of 5 mol% PtCl<sub>2</sub> to the 1,4-diene **90** in 94% yield (Scheme 17, (22)). The reaction proceeds with an *anti* stereoselectivity, thus indicating a mechanism based on the nucleophilic attack of the allylsilane fragment on a  $\eta^2$ -coordinated alkyne function. The allylstannane-substituted enyne **91** is transformed in the



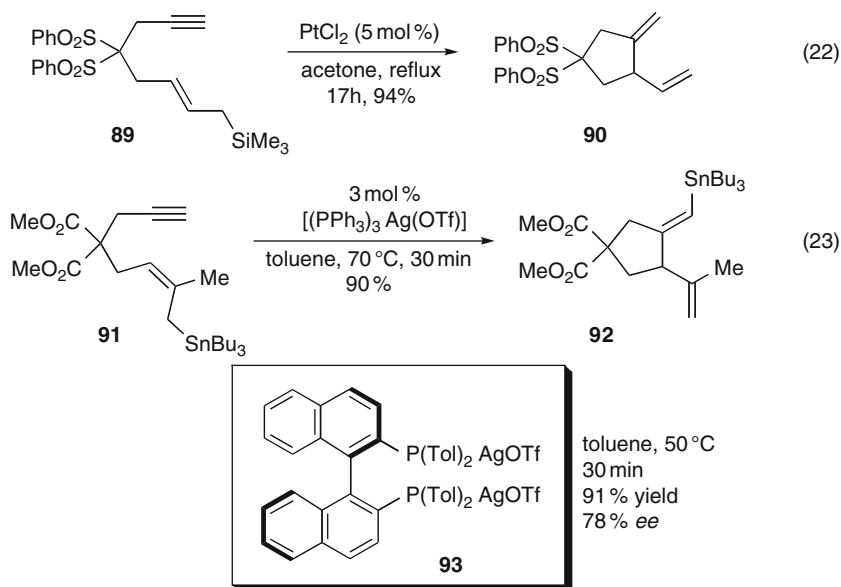
**Scheme 14** Asymmetric examples of cycloisomerization of 1,6-enynes



**Scheme 15** Macrocyclization reaction



**Scheme 16** Cycloisomerization reaction of 1,5-enyne

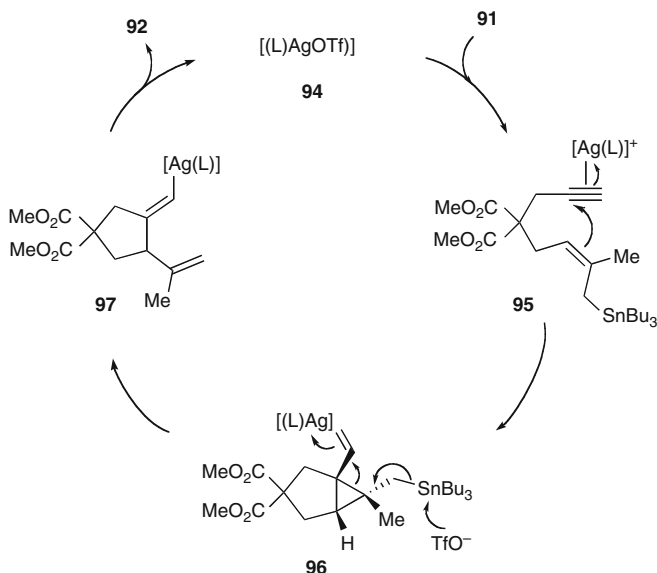


**Scheme 17** Cycloisomerization of allylsilanes and allylstannanes

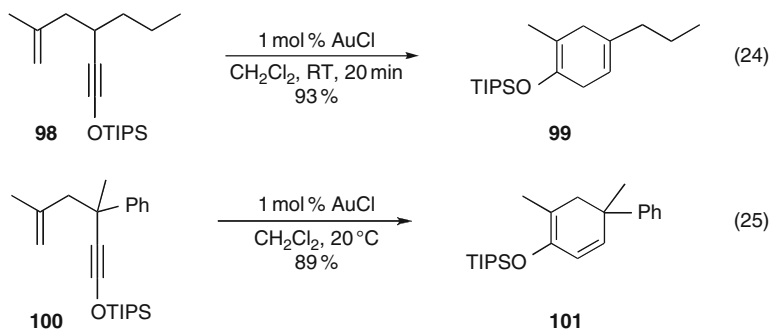
presence of  $[(\text{PPh}_3)_3\text{AgOTf}]$  in a 5-*exo* manner at 70 °C in toluene to the vinylstannane cyclopentane **92** in 90% yield (23) [97]. It is noteworthy that 1,7-enynes are well tolerated and the corresponding stannane is formed following a 6-*exo* cyclization. An enantioselective variant of this transformation has been reported using complex **93**. In toluene at 50 °C, product **92** has been isolated after 30 min in 91% yield and 78% *ee*.

The authors propose a mechanism relying on the initial  $\eta^2$ -coordination of the alkyne moiety by the silver complex, followed by an *anti* nucleophilic attack of the alkene function to form transiently the cyclopropyl carbene **96**. Elimination of the trialkylstannyl cation would release the 1,4-dienyl-silver complex **97**. Stannyl-desilveration completes the catalytic cycle and regenerates the cationic silver complex **94** (Scheme 18).

In 2004, Kozmin and coworkers introduced a general method for the synthesis of 1,4-cyclohexadienes from silyloxy-5-en-1-yne (Schemes 19 and 20) [98]. Substrate **98** reacted at room temperature in the presence of 1 mol% AuCl to give diene **99** as a single isomer in 93% yield (24). The reaction is limited to silyloxyalkynes whereas terminal or trisubstituted alkene functions are well tolerated. Later on, the same group reported the use of  $\text{PtCl}_2$  in the same reaction under forcing conditions (10 mol% catalyst, 80 °C, 66% yield) [99]. It is noteworthy that, when the 3-position of the enyne is fully substituted, elimination occurs to give 1,3-diene **101** via a sequence involving  $\beta$ -hydride abstraction and elimination (25). In this latter case, the substitution pattern of the alkyne is much broader as terminal and alkyl- or aryl-substituted ones are well tolerated.



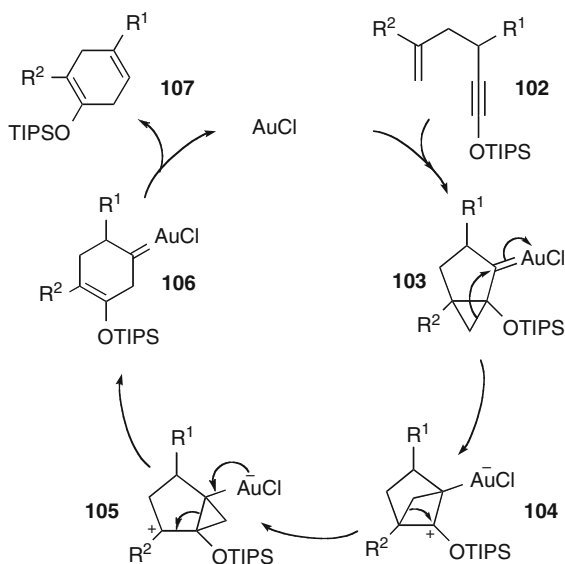
**Scheme 18** Mechanistic rationale



**Scheme 19** Cycloisomerization of 1,5-enynes leading to dienes

The formation of 1,4-diene can be rationalized according to the following mechanism (Scheme 20).

The activation of the alkyne leads to the cyclopropyl carbene **103**, which undergoes a 1,2-alkyl shift (and not a hydride migration), giving the zwitterionic species **104**. Two more 1,2-alkyl shifts then afford the six-membered ring carbene **106**. Depending on the substituents, the elimination step alternatively allowed the formation of 1,3-diene or 1,4-diene **107**.

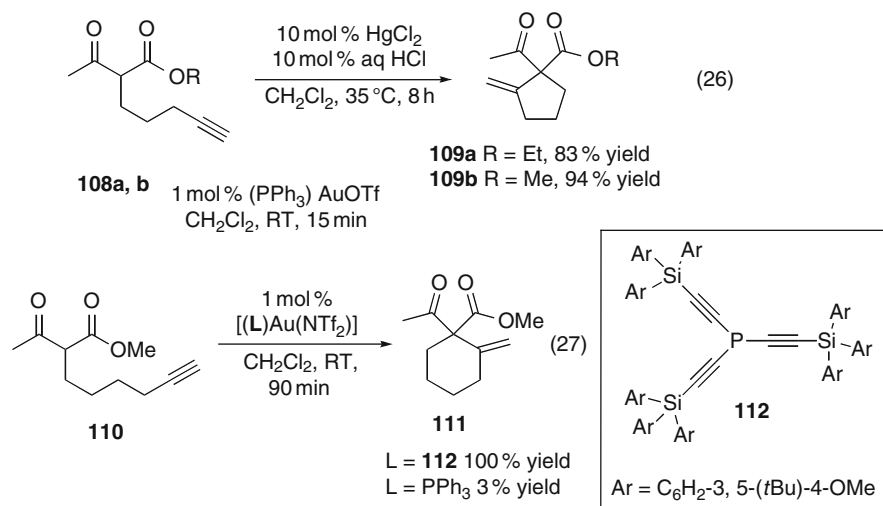


**Scheme 20** Mechanistic rationale

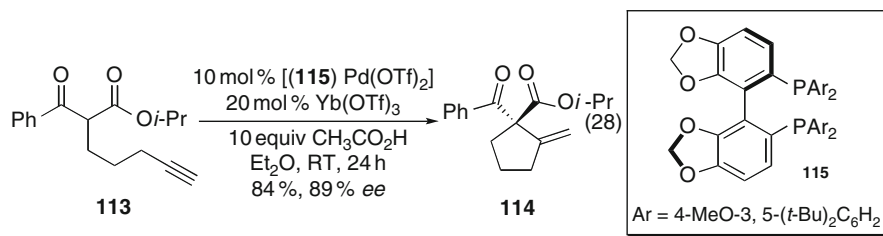
### 3.2 Conia Ene Type Reactions

The first report of the metal-catalyzed addition of an electron rich alkene to an alkyne dates from 1983 when the group of Conia (Scheme 21) [100] reported the cyclization of  $\varepsilon$ -acetylenic carbonyl compounds in the presence of a catalytic amount of HgCl<sub>2</sub> and a Brønsted acid. The combination of the two catalysts is a prerequisite to obtain a high activity. The cycloisomerization occurs in a 5-*exo* mode of cyclization to give methylene cyclopentanes such as **109a** resulting from a C-alkylation of the triple bond (26). The proposed mechanism relies on the addition of the enol form of the carbonyl nucleophile (including ketones, 1,3-diketones, and  $\beta$ -ketoesters) on the alkyne activated towards nucleophilic attack by the mercury metal center. In 2004, Toste and coworkers [101] reported the superior reactivity of Au(I) catalysts. In the presence of 1 mol% (PPh<sub>3</sub>)AuOTf,  $\beta$ -ketoester **108b** is transformed to **109b** in 94% yield at room temperature in 15 min. Deuteration experiments are consistent with a mechanism involving an *anti* nucleophilic attack of the enol on the  $\eta^2$ -coordinated alkyne. The same group [102] subsequently described the 5-*endo* cyclization of the  $\delta$ -acetylenic carbonyl compounds.

The use of bulky triethynyl-based phosphines as superior ligands for the 6-*exo* and 6-*endo* cycloisomerization allowed  $\beta$ -ketoester **110** to be converted to cyclohexane **111** in quantitative yield (27). The use of PPh<sub>3</sub> on the triflimidate gold catalyst instead of ligand **112** allows the formation of **111** in only 3% yield [103, 104]. In an effort to develop an enantioselective variant of the Conia-ene reaction, the introduction of a dual system consisting of a dicationic palladium-(DTBM-SEGPHOS **115**) complex,



**Scheme 21** Cycloisomerization reaction of alkynyl- $\beta$ -ketoesters



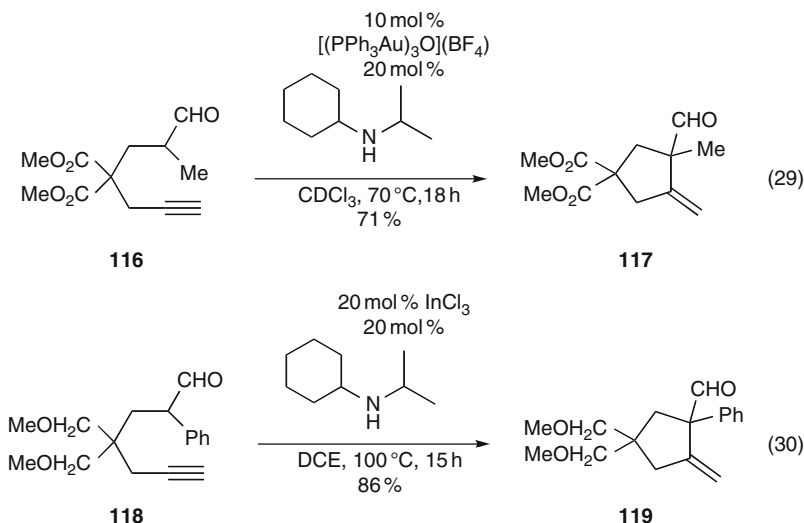
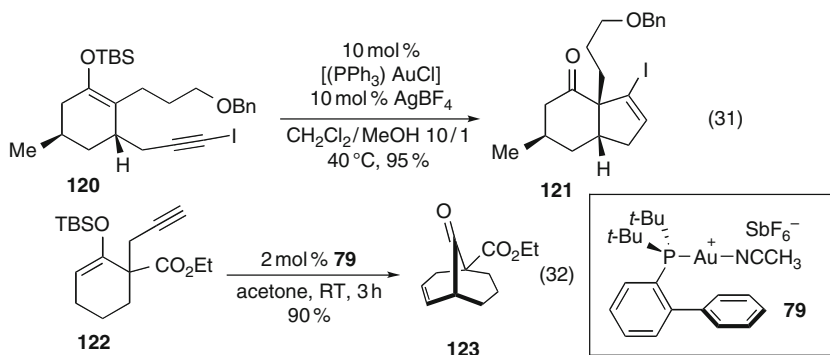
**Scheme 22** Asymmetric version of the cycloisomerization reaction of alkynyl- $\beta$ -ketoesters

ytterbium triflate, and excess acetic acid was particularly efficient and led to the *exo*-methylene cyclopentanes in up to 89% enantiomeric excess (Scheme 22) [105]. The Lewis acid/Brønsted acid couple Yb(OTf)<sub>3</sub>/acetic acid was essential to obtain high yields.

The generation of enamine intermediates, as an alternative to enols, has also been envisioned starting from aldehydes in the presence of a secondary amine (Scheme 23) [106]. A dual catalyst consisting of an Au(I) cationic complex, [(PPh<sub>3</sub>Au)<sub>3</sub>O](BF<sub>4</sub>) and cyclohexyl isopropyl amine, enables the cycloisomerization of substrate **116** to the cyclopentane **117** in 71% yield (29).

The scope of the reaction was broadened in the presence of an indium catalyst instead of gold, which allowed the cyclization of various  $\alpha$ -disubstituted aldehydes such as **118** on alkynes in good to excellent yield (30) [107].

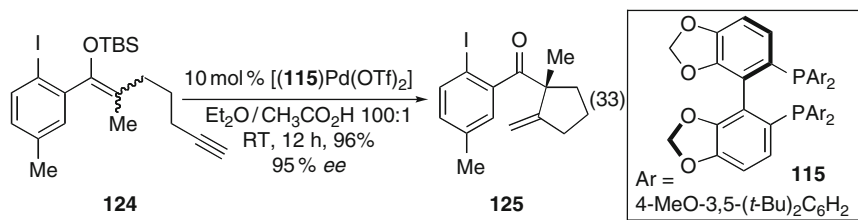
Silyl enol ethers have emerged as excellent nucleophiles that may add to  $\eta^2$ -metal-alkyne intermediate (Scheme 24). The synthesis of carbonyl substituted cyclopentene from silyloxyenynes such as **119** was indeed reported, the 5-*endo*

**Scheme 23** Cycloisomerization of  $\alpha$ -substituted alkynyl aldehydes**Scheme 24** Cycloisomerization of silyloxyenynes

mode of cyclization being selectively observed for the 1,5-enynes (31), whereas the 5-*exo* mode of cyclization is favored for the 1,6-enynes [108]. The presence of a protic oxygen nucleophile (water or methanol) as an additive is a prerequisite for the efficiency of the transformation. Its role is to prodemetalate the vinylaurate intermediate and to trap the trialkylsilyl fragment. This strategy has also been employed to synthesize the bicyclic core of the [n, 3, 1]alkanones such as **121** [109]. Optimal yields are obtained with an Au(I) cationic catalyst possessing a bulky biphenyl-based monodentate ligand (32).

The palladium-(DTBM-SEGPHOS) complex was also successfully employed in the asymmetric Conia ene type reaction involving silyl enol ethers as nucleophile





**Scheme 25** Asymmetric version of the cycloisomerization of silyloxyenynes

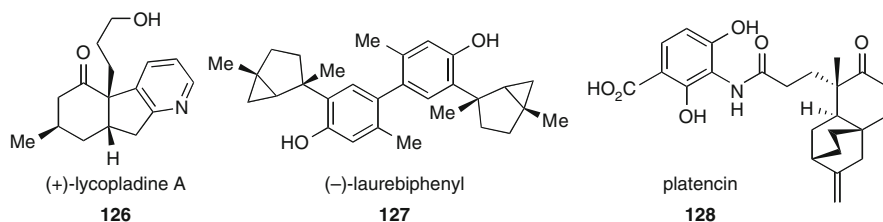


**Fig. 4** Applications in total synthesis

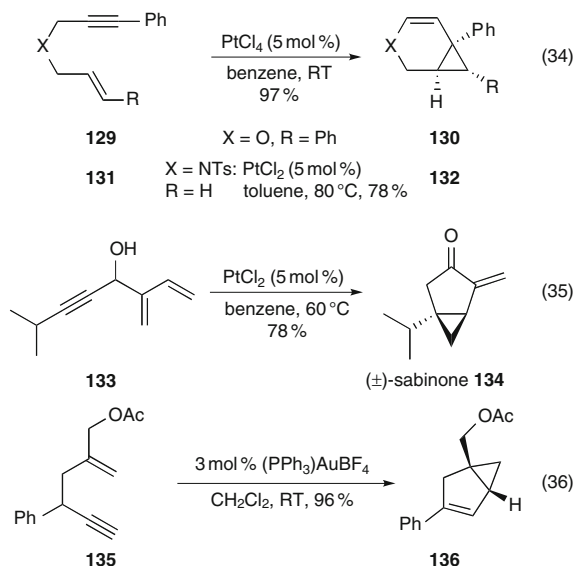
reaction partners (Scheme 25) [110]. It allowed the construction of quaternary carbon centers in 95% enantiomeric excess. The geometry of the alkene and the nature of the trialkylsilyl group have a strong influence on the enantioselectivity of the transformation.

These methodologies have been successfully applied respectively to the diastereoselective and enantioselective total syntheses of (+)-lycopoladine A **126** [108], platencin **128** [111], and (–)-laurebiphenyl **127** [110] (Fig. 4).

### 3.3 Formation of Bicyclic Derivatives Via Cycloisomerization Reactions

#### 3.3.1 Bicyclopropane Formation

In 1995, a seminal contribution was reported by Blum et al. for the synthesis of cyclopropane-annulated dihydropyrans, such as **130**, starting from allyl propargyl ethers, e.g., **129**, in the presence of a catalytic amount of  $\text{PtCl}_4$  (Scheme 26) [112]. Later on, the scope of this transformation was highly expanded using  $\text{PtCl}_2$  at 80 °C in toluene to nitrogen-tethered enynes (which could be converted to the [4,1,0]-bicycloheptenes), and to enol ethers as alkene partners in the cycloisomerization reaction [70, 83, 113, 114]. This methodology was also extended to the case of 1,5-enynes (35, 36). For example, 3-hydroxylated 1,5-enyne **133** participates to the cycloisomerization process and afforded bicyclic ketone such as (±)-sabinone **134**



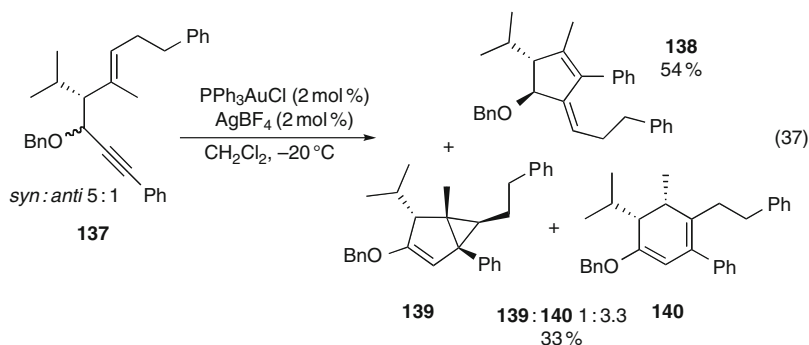
**Scheme 26** Cycloisomerization reactions leading to bicyclopropane derivatives

[115, 116]. The cyclization proceeds nicely in benzene at 60 °C to give the product in 78% yield. Due to their superior carbophilic character, cationic Au(I) complexes indeed catalyze the same reaction under milder conditions (room temperature, 1–3 mol% catalyst, 5 min) [117]. The functionalized substrate **135** is cleanly transformed to the corresponding bicyclo[3.1.0]hexene **136** in 96% yield.

The cycloisomerization reactions are generally substrate-dependent and often lead to a mixture of products resulting from competitive reaction paths. In the case of the enyne **137** [118] (Scheme 27), the formation of three different products is observed when treated at –20 °C in dichloromethane with a combination of 2 mol% (PPh<sub>3</sub>)AuCl and 2 mol% AgBF<sub>4</sub>. The bicyclopropane **139** is obtained as a minor product whereas 1,3-dienes **138** and **140** resulting from skeletal rearrangement (see Sect. 3.1.1) form predominantly.

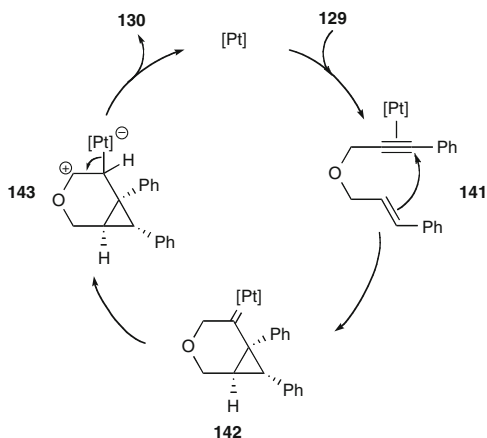
The mechanism of the formation of bicyclo[3.1.0]hexenes and bicyclo[4.1.0]heptenes transformation has been studied by Soriano et al. [119] by using computational methods in the case of 1,6-enynes. The initial postulated step of the catalytic cycle is the  $\eta^2$  coordination of the alkyne moiety to the platinum metallic center. Nucleophilic *anti* attack of the alkene group in a 6-*endo* fashion results in the formation of the cyclopropyl carbene **142** stereospecifically. A 1,2-hydride shift to give the zwitterionic intermediate **143** and elimination complete the catalytic cycle, which was corroborated by some recent DFT calculations [120] (Scheme 28).

In the case of 1,6-enynes, when a carbon atom replaces the heteroatom-tether, the 5-*exo* cycloisomerization process is generally predominant (see the previous Sect. 3.1 on the formation of dienes) and the reaction may be driven towards the

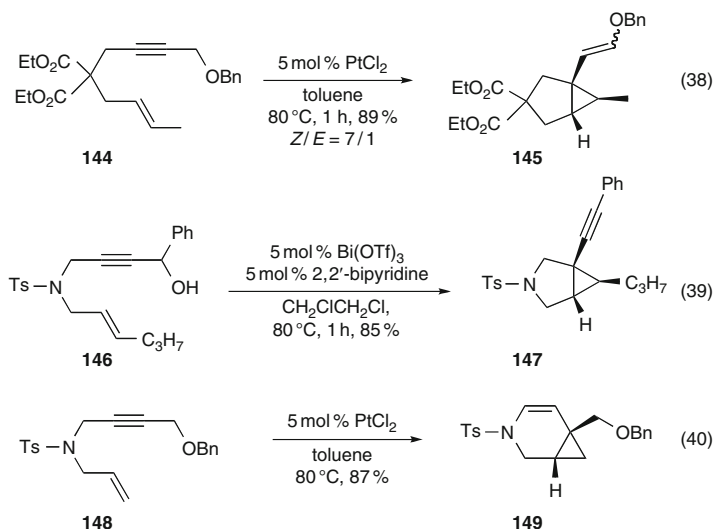


**Scheme 27** Example of substrate-dependency inducing competitive reactions

**Scheme 28** Mechanistic rationale



formation of bicyclic cyclopropanes by modifying the substitution of the enyne. Some interesting rearrangements have indeed been described in the presence of platinum [115, 121], gold [90], or bismuth [122] complexes (Scheme 29). The formation of functionalized bicyclo[4.1.0]hexanes such as **145** has been performed in the presence of 5 mol%  $\text{PtCl}_2$  in toluene at  $80^\circ\text{C}$  and the bicyclic derivative **145** was isolated in 89% yield [121]. Substrate **146** cyclized in 1,2-dichloroethane at  $80^\circ\text{C}$  in 60 min to give the alkynylbicyclohexene **147** in 85% yield in the presence of a combination of 5 mol%  $\text{Bi}(\text{OTf})_3$  and 5 mol% 2,2'-bipyridine (35) [121]. This latter example is particularly impressive as it is a rare example of 5-*exo* cycloisomerization mode with an *N*-tethered 1,6-enyne. Another enyne such as **148**, bearing a heteroatom at the propargylic position, was, for example, classically transformed to bicyclic derivative **149** [121]. The authors propose a dual complexation of bismuth catalyst to the alkyne and the alcohol, which would be followed by the addition of the alkene, a second cyclization, and then deprotonation to give the



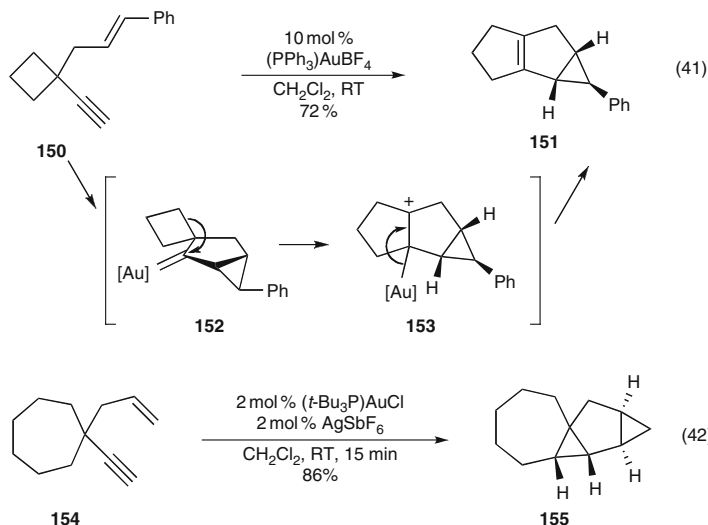
**Scheme 29** Formation of bicyclo[4.1.0]hexanes

alkynyl function. The whole process could be considered as a dehydrative alkynylcyclopropanation.

Metal carbenoid intermediates associated with carbophilic Lewis acid can also induce a variety of alkyl shift rearrangements, one of the first examples being reported for the synthesis of bicyclo[3.1.0]hexanes (Scheme 30) [117].

The transformation of the cyclobutane-containing 1,5-enyne **150** afforded the tricyclic product **151** in 72% yield in the presence of [(PPh<sub>3</sub>)AuBF<sub>4</sub>] catalyst (41). A recent investigation of the factors favoring the 1,2-alkyl shift has been conducted [123] and shows that the spatial proximity between the gold carbenoid (structure **152**) bond and respectively the C–C and C–H bonds present in the enyne is the key parameter governing the selectivity. Whereas spiro-cyclobutane and cyclopentane at the 3-position of the enyne lead to alkyl shift rearrangements, larger rings such as spirocycloheptane and spirocyclooctane **154** induce a C–H insertion reaction (42). Another particularly elegant example of 1,2-alkyl shift during the cycloisomerization process, has been described for the cyclization of 5-en-1-yn-3-ols in the presence of Cu(I) catalysts (Scheme 31) [124–126]. The reaction of an enyne such as **156** in toluene at 70 °C for 4 h with 1 mol % of [Cu(CH<sub>3</sub>CN)<sub>4</sub>](BF<sub>4</sub>) leads to the formation of the tetracyclic ketone **157**. Upon alkynophilic activation by the Cu catalyst, the alkene function attacks to form the cyclopropyl carbene **158**, which upon 1,2-alkyl shift and protodemetalation gives the strained ketone **157**.

The first report of an enantioselective version of the cycloisomerization reaction of 1,6-enynes to form bicyclo[4.1.0]heptenes has been introduced by the group of Shibata [127]. The authors proposed a catalytic system consisting of [{IrCl(cod)}<sub>2</sub>], AgOTf, and Tol-BINAP **162** under an atmosphere of CO. The substrate scope of the reaction is rather limited as only the rearrangements of nitrogen-tethered enynes

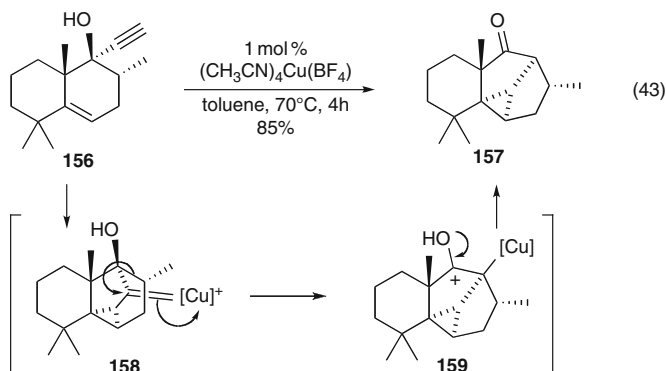
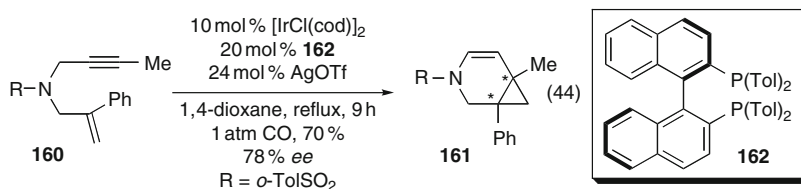
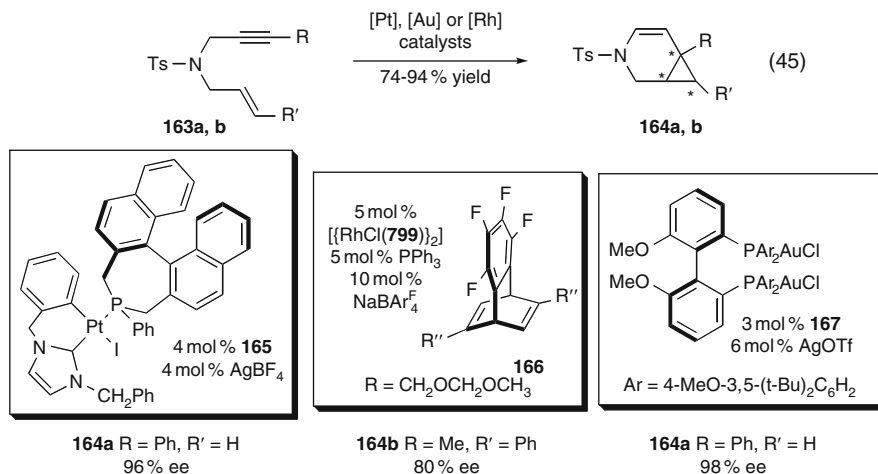


**Scheme 30** Examples of alkyl shift rearrangements leading to bicyclopropane derivatives

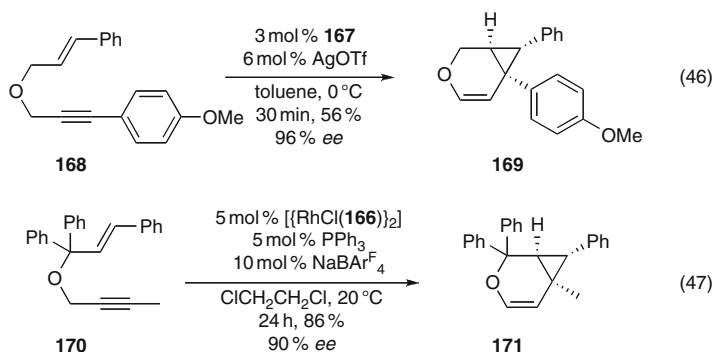
possessing a methyl substituent on the alkyne such as **160** and an internal aryl group on the alkene have been investigated. Good to excellent yields and enantioselectivity excesses between 35% and 78% are reported (Scheme 32).

The past 3 years have seen other catalytic systems appeared, based on platinum [128, 129], gold [130], and rhodium [131] catalysts (Scheme 33). Various nitrogen-tethered 1,6-enynes have been cyclized in the presence of a square-planar dicationic platinum catalysts. Taking advantage of the mechanistic rationale that postulates the involvement of a single coordination site, the authors tailored a chiral environment by combining a bidentate and a monodentate ligand around the complex **165** and showed that the best asymmetric induction is in toluene at 80 °C as bicyclo[4.1.0]heptene **164a** is obtained in 90% yield and 96% *ee* [128]. The groups of Nishimura and Hayashi [131] recently applied this strategy to the rhodium-catalyzed (for a related non-asymmetric rhodium-catalyzed cycloisomerization of 1,6-enynes, see [132]) cycloisomerization of nitrogen-tethered 1,6-enynes (45). In the presence of a combination of a chiral electron-poor diene **166**, an achiral monophosphine such as  $\text{PPh}_3$  and a cationic  $\text{Rh}(\text{I})$  center formed from the corresponding chloride precursor and  $\text{NaBARf}_4$ , the enyne **163b** is cleanly transformed in dichloroethane at 50 °C to the bicyclic product **164b** in 94% yield and 80% *ee*. An asymmetric  $\text{Au}(\text{I})$ -catalyzed synthesis of bicyclo[4.1.0]heptene derivatives has also been developed by Michelet et al. [130] The chiral catalyst formed from the bimetallic complex **167** and  $\text{AgOTf}$  allows the transformation of nitrogen-tethered enyne **163a**, in toluene at 60 °C, both yield and enantioselectivity being remarkably increased with temperature.

It is noteworthy that these asymmetric cycloisomerization reactions could be extended to oxygen-tethered 1,6-enynes in the case of rhodium and gold catalysts

**Scheme 31** Example of 1,2-alkyl shift rearrangements**Scheme 32** Ir-catalyzed asymmetric synthesis of bicyclopropane derivatives**Scheme 33** Pt-, Au-, and Rh-catalyzed asymmetric synthesis of bicyclopropane derivatives

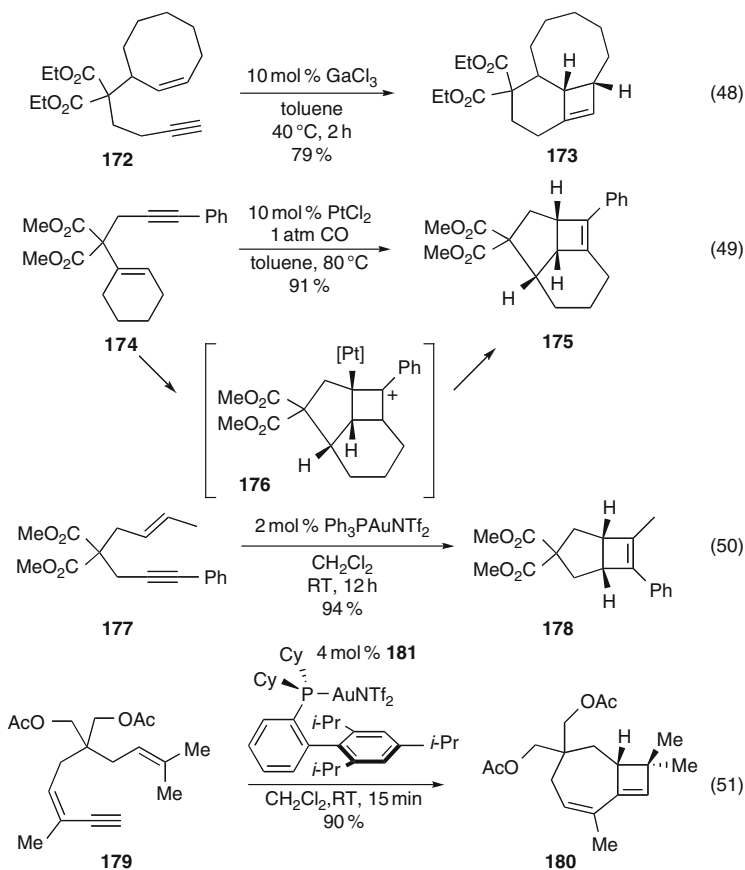
only (Scheme 34). The enyne **168** was for example cleanly transformed to the corresponding bicyclic product **169** in moderate yield and 96% *ee*. The bicyclic derivative **171** was obtained in good yield and enantiomeric excess (47).



**Scheme 34** Au and Rh-catalyzed asymmetric synthesis of bicyclopropane derivatives

### 3.3.2 Bicyclobutene Formation

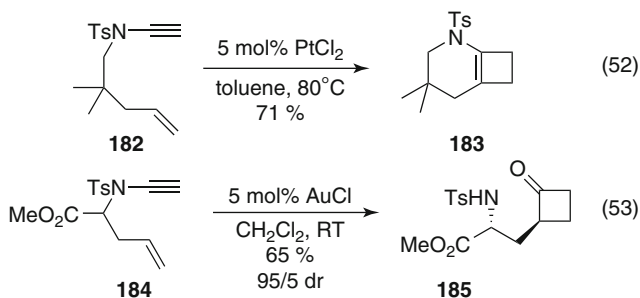
The formation of cyclobutenes has been investigated in the presence of various electrophilic complexes, both in the case of 1,*n*-enynes [70, 133–137], and 1,7-enynamides [138–141] (Scheme 35). This formal [2 + 2]-cycloaddition allowed, for example, the cyclization of enyne **172** to tricyclic alkene **173** in the presence of 10 mol% of gallium chloride [133]. Fürstner et al. [133] presented a study outlining the importance of substituent effects on the selectivity of the reaction. As the transformation was assumed to proceed through the intermediacy of the cationic cyclobutane **176**, incorporation of stabilizing aryl groups at the terminal position of the alkyne function should favor the invoked pathway (49). Furthermore, using  $\text{PtCl}_2$  as a catalyst precursor, the authors identified a strong accelerating effect obtained when the reaction is conducted under an atmosphere of CO. This behavior is explained by the increase of electrophilicity resulting from the coordination of a  $\pi$ -acceptor ligand at the platinum metal center. Under the optimized conditions, enyne **174** was converted to the tricyclic product **175** in 91% yield. A very high activity was once again observed in the presence of cationic gold complexes and the cycloisomerization of enyne **177** afforded the bicyclic derivative **178** in 94% yield [135] (50). The influence of the length of the tether is also crucial for the fate of the cycloisomerization. Whereas bicyclobutene are generally observed as minor by-products in the case of 1,6-enynes, they become the major product in the case of the 1,7- and 1,8-enynes. The bicycle **180** was isolated in 90% yield upon cycloisomerization of the dienyn **179** in the presence of a Au(I)bistriflimidate complex **181** at room temperature (51). It is noteworthy that these cyclobutene products have long been postulated as intermediate in the reaction of formation of 1,3-diene by single or double cleavage pathways (see Sect. 3.1). Computational results predict a rather high activation barrier for the conrotatory opening of the cyclobutene [71]. The isolation of cyclobutene products from reaction along with the formation of skeletal rearrangement products at  $-60^\circ\text{C}$  in the presence of cationic Au(I) catalysts or at higher temperature in the presence of Pt(II) complexes clearly discard such an hypothesis [71].



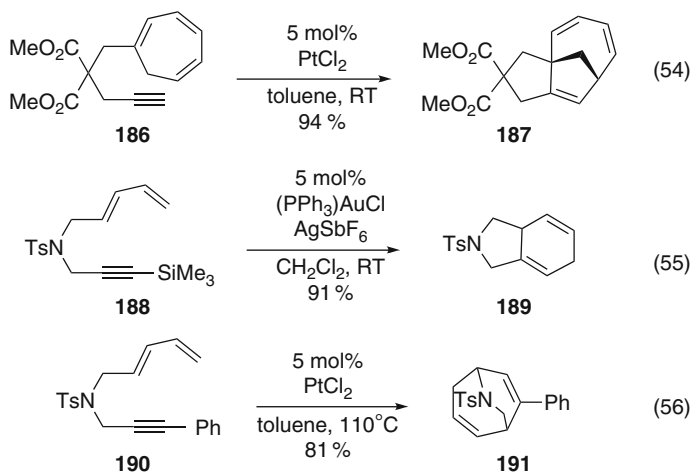
**Scheme 35** Cycloisomerization reactions leading to bicyclobutene derivatives

The case of 1,7-enamides such as **182** was particularly original as their cyclization gave rise to various bicyclic enamines such as **183** in the presence of  $\text{PtCl}_2$  in toluene at 80 °C [138] (Scheme 36). Soriano et al. thoroughly studied the cycloisomerization of 1,6- and 1,7-enamides, providing a unified mechanistic picture and showing the importance of the heteroatom attached to the alkynyl moiety on the polarization of the triple bond and therefore on the outcome of this formal [2 + 2] cycloaddition [142]. This methodology could be extended to the case of 1,6-enamides using Au(I) catalysts, where the reaction proceeded at room temperature and was exploited to synthesize cyclobutanone **185** upon subsequent hydrolysis, due to the ring strain, of the cyclobutene intermediate [140]. Using substrates possessing a substituent either at the 4- or 5-position of the enyne such as **184**, the reaction occurs with good diastereoselectivity and leads to the cyclobutane **185** with 65% yield.





**Scheme 36** Cycloisomerization reactions of 1,7-enynamides



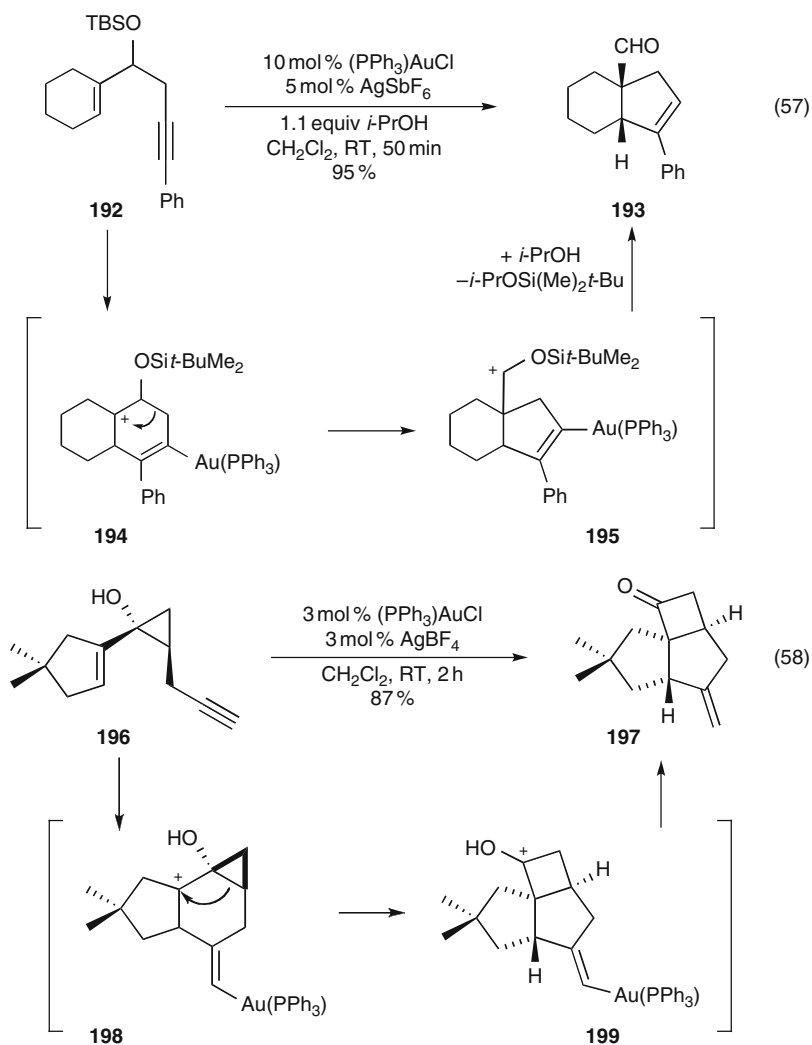
**Scheme 37** Cycloisomerization reactions of trienynes and dienynes

### 3.3.3 Formation of Variable Sized Cycles Via Rearrangements

The cycloaddition of enynes bearing a cyclotriene moiety was recently studied in the presence of electrophilic catalysts [143] (Scheme 37). A formal [6 + 2] cycloaddition was observed in the presence of either  $\text{PtCl}_2$  or  $\text{AuCl}_3$  as catalysts. The cycloisomerization of trienynone **186** led to the selective formation of **187** via presumably an exocyclic cyclization followed by a “concerted” electron redistribution releasing the cyclic triene in 94% yield (54). The synthetic potential of ring systems and their reactivity may also vary for similar substrates. A recent example is the cycloisomerization of dienyne **188**, reacting according to a formal [4 + 2] cycloaddition catalyzed by gold complexes [144]. Changing the substrate slightly

allowed a completely different outcome as substrate **190** was transformed to diene **191** via a cycloisomerization reaction followed by a Cope rearrangement [145] (56). It is noteworthy that similar reactivity was observed in the presence of gold cationic complex despite a lower yield.

The cycloisomerization of 3-silyloxy-1,5-enynes in the presence of Au(I) and Pt (II) complexes could be associated with a domino pinacol rearrangement [146] (Scheme 38). Substrate **192** is reacted in the presence of 10 mol% [(PPh<sub>3</sub>)AuCl], 5 mol% AgSbF<sub>6</sub>, and 1.1 equiv. of *iso*-propyl alcohol to give the formyl-substituted cyclopentene **193** in 95% yield. The mechanism proceeds through an initial 6-*endo*



**Scheme 38** Enyne cycloisomerization reactions involving 1,2-alkyl shift

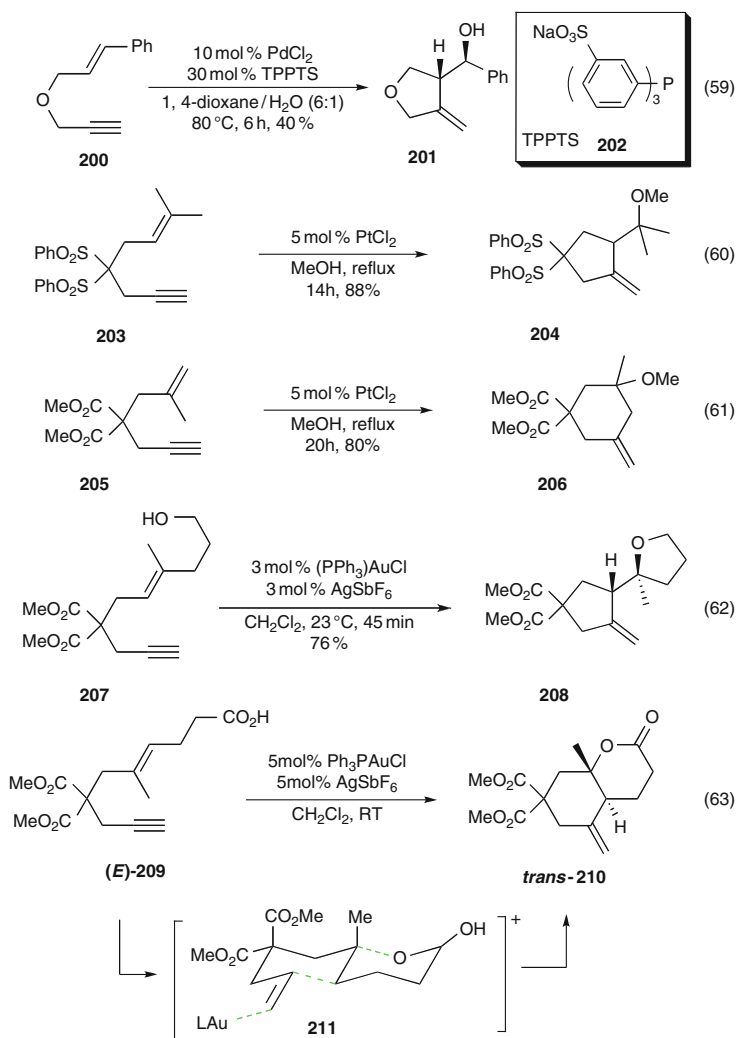
cyclization of the 1,5-enyne to give the vinyl aurate intermediate **194**, followed by a 1,2-alkyl shift migration to give the product upon protodesilylation. This methodology was applied to the total synthesis of ( $\pm$ )-ventricos-7(13)-ene [147]. The cyclopropyl alcohol containing 1,6-enyne **196** is transformed to the tricyclic ketone **197** in 87% yield under very mild conditions (58). The reaction proceeds via a 6-*exo* cyclization to give the vinyl aurate intermediate **198**, followed by a 1,2-alkyl shift and protodemetalation to furnish **197**.

## 4 Domino Enyne Cycloisomerization-Nucleophile Addition Reaction

### 4.1 Oxygen Nucleophiles

The first report [148–150] of the transformation of an enyne in the presence of an oxygen nucleophile dates from 1997, when Genêt and coworkers discovered the hydroxycyclization of allylpropargylethers implying the addition of water at the benzylic position and the cyclization of the enyne (Scheme 39).

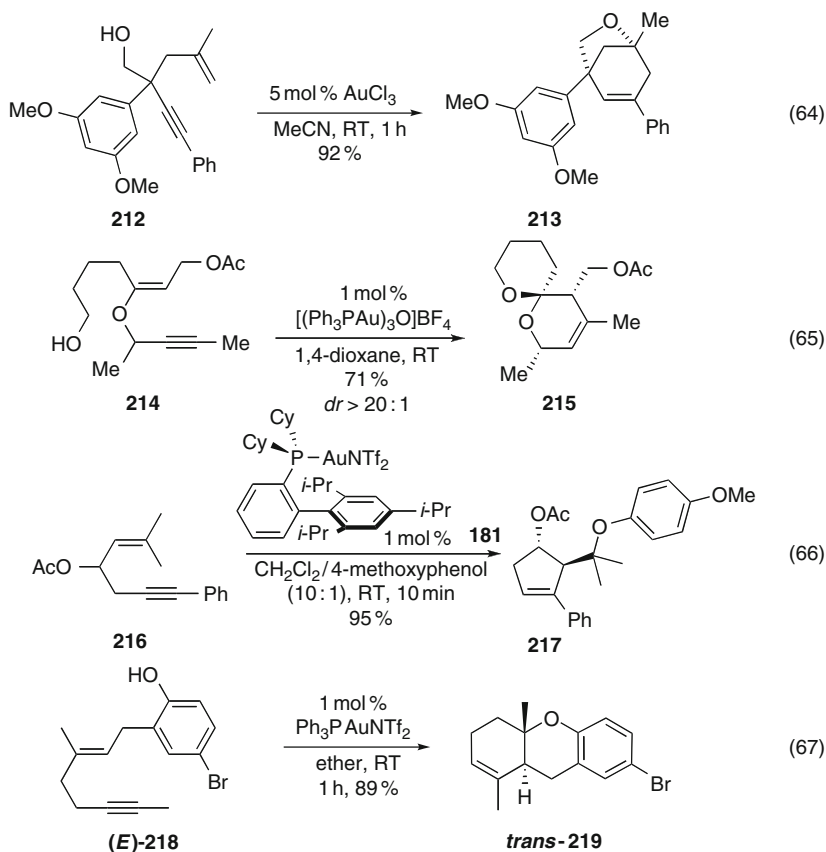
The enyne **200** was transformed into the alcohol **201** in the presence of a system consisting of Pd(OAc)<sub>2</sub> and a water-soluble ligand (TPPTS **202**: sodium salt of triphenylphosphinotrimetasulfonate) in a dioxane/water mixture. This process was shown to be completely diastereospecific and led to various tetrahydrofurans in moderate to good yields. Whereas activities and substrate scope remained limited with Pd catalysts, the group of Echavarren [88, 151] expanded the scope of the reaction using platinum catalysts. A large variety of carbon-, oxygen-, and nitrogen-tethered enynes possessing substituted double bonds have been engaged and were efficiently transformed according to a 5-*exo* mode to the corresponding alcohols, ethers, and esters. For example, enynes **203** and **205** were treated with 5 mol% of PtCl<sub>2</sub> in methanol under reflux to give carbocyclic ethers **204** and **206** in good yields. In the case of gem-disubstituted alkenes such as **205**, a different regioselectivity was observed as six-membered carbocycles such as **206** resulting from a 6-*endo* cyclization are isolated in good to excellent yields (61). The reaction was also extended to enynes bearing an enol ether function as the alkene partner and led to the preparation of functionalized acetals [152]. Since these pioneering studies, these domino processes have been described with a variety of transition metal Lewis acids including Hg [153], Ru [154], but none surpassed the outstanding reactivity obtained with the alkynophilic Au catalysts. The reaction proceeds at room temperature, in the presence of 1–3 mol% of either an Au(I) [63, 64, 66, 155] or Au(III) [88, 156, 157] source. As observed for Pt systems, the weak oxophilicity of these acids allows the reaction to proceed in pure alcohol solvents. It is noteworthy that the reaction can also be performed intramolecularly and the ether **208** was for example obtained in 76% yield (62). Other nucleophiles such as carboxylic acids can be used, the reaction being totally diastereospecific



**Scheme 39** Domino hydroxy-, alkoxy-, and oxycarbonylation/cycloisomerization reactions of enynes

and occurring via a concerted transition state **211** analogous to that involved in carbocation-induced polyene cyclization reactions. The (*E*)-derivative **209** was efficiently cyclized leading to the *trans* bicyclic lactone **210**, whereas the (*Z*)-isomer gave rise to the *cis* isomer [44]. For a recent asymmetric version of polycyclization reactions implying carboxylic acid, phenol and aromatic rings as nucleophile, see [158] (63).

The hydroxy- and alkoxycyclization reactions are not limited to 1,6-enynes, depending on the substitution pattern of the starting 1,5-enyne, 5-*endo*- or 6-*endo*-cyclization is observed for a variety of substrates (Scheme 40). The treatment of

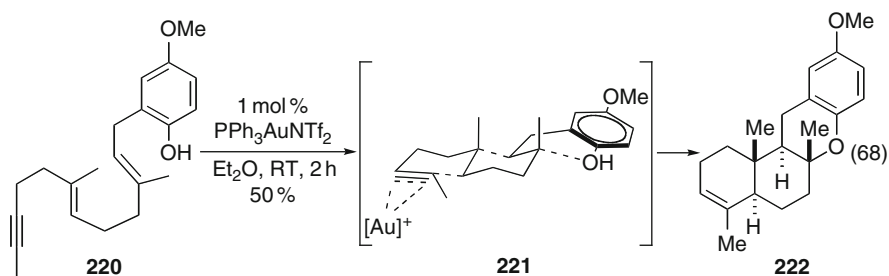


**Scheme 40** Domino alkoxy- and phenoxylation/cycloisomerization reactions of enynes

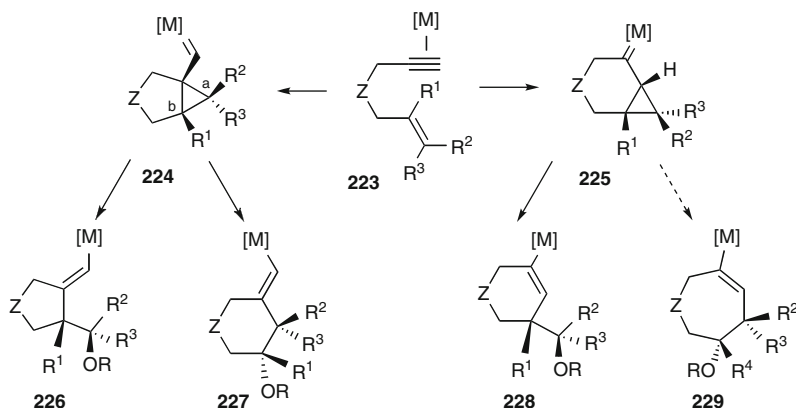
enyne **212** in the presence of 5 mol% of  $\text{AuCl}_3$  in acetonitrile afforded the bicyclic ether **213** in 92% yield [159]. The synthesis of dihydropyrans possessing an acetal or an hemiacetal function such as **215** was particularly original starting from an enol ether as alkene partners (65) [160] and was achieved in a diastereoselective manner in the presence of an Au(I) trimer. The scope of oxygen nucleophile partners in the case of 1,5-enynes has also been extended to secondary alcohols and phenols [161, 162] (66, 67) and to the synthesis of polysubstituted aromatic rings [163]. 1,7-Enynes have also been shown to react in the presence of alcohols and water to give the corresponding adducts [81, 156].

Interestingly, the cycloisomerization of phenol-substituted dienynes was recently investigated and, according to a biomimetic process, allowed the 6-*endo-dig* cyclization of the phenols [162] (Scheme 41). In the presence of 1 mol%  $[(\text{PPh}_3)\text{AuNTf}_2]$ , substrate **220** furnishes the tetracyclic ether **222** as a single isomer in 50% yield.

On the basis of deuterium labeling experiments [164], DFT calculations [30, 64, 71, 88, 119, 152], and mass spectroscopy analysis [165] the authors invoked a



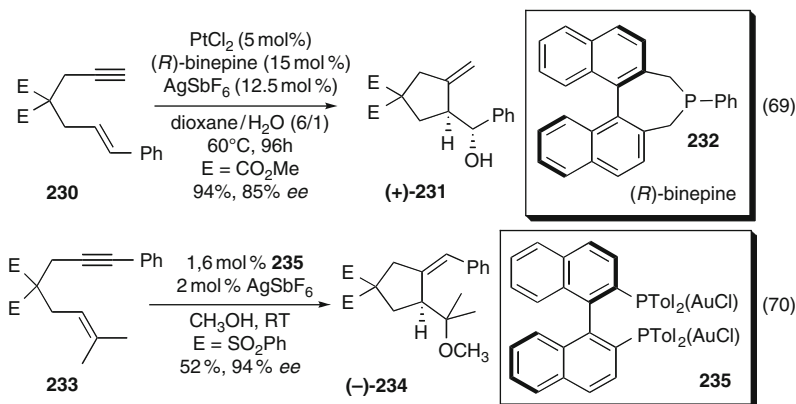
**Scheme 41** Domino intramolecular phenoxylation/cycloisomerization reactions of a 1,5,9-dienyne



**Scheme 42** Regioselectivity in the domino alkoxylation/cycloisomerization reactions of enynes

mechanistic rationale based on the initial formation of an electrophilic  $\pi$ -alkyne-metal complex **223** (Scheme 42). In the case of 1,6-enynes, nucleophilic attack of the alkene moiety can occur by 5-*exo-dig* or 6-*endo-dig* pathways to give respectively cyclopropyl carbenes **224** and **225**. The opening of the cyclopropane ring and rearrangement of the metal complex **224** upon *anti* addition of the oxygen nucleophile can take place at either carbone *a* or *b* to lead selectively to the vinyl metal intermediates **226** and **227**. Whereas an intermediate analogous to **225** has already been invoked in related transformations in the absence of nucleophile (see Sect. 3.3.1), very few reports dealing with the formation of ethers resulting from the 6-*endo*-type cyclization have appeared [152]. Protodemetalation completes the catalytic cycle (for a rare example of characterization of a vinylmetal intermediate, see [166]).

The first highly enantioselective hydroxycyclization of 1,6-enynes was reported in 2004 by Genêt, Gladiali, and Michelet [167] (Scheme 43). A dicationic platinum complex prepared in situ from  $\text{PtCl}_2$ , 3 equiv. of (*R*)-Ph-binepine **232** (for recent reviews, see [168–170]), an electron-rich phosphane of narrow bite angle, and 2.5 equiv. of  $\text{AgSbF}_6$  catalyzes the reaction of enyne **230** to alcohol (+)-**231** in a



**Scheme 43** Asymmetric Pt- and Au-catalyzed domino hydroxy- and alkoxylation/cycloisomerization reactions

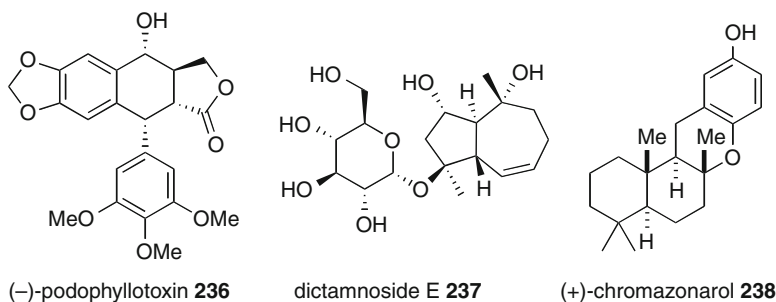
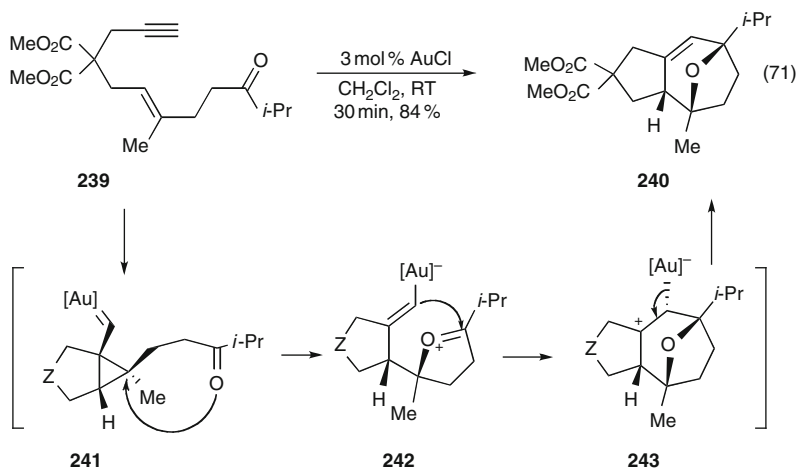


**Fig. 5** Applications in total synthesis

dioxane/H<sub>2</sub>O mixture (6:1), the product being obtained in 94% yield and 85% ee (69). In the case of Au(I) catalysts, a promising enantiomeric excess was obtained in the presence of the (*R*)-Tol-binap-gold chloride complex **235** but the scope was limited to the carbon-bridged derivative **233**. The methoxycyclization product (-)-**234** was isolated in 52% yield and 94% ee [171] (for a recent enantioselective of functionalized indenenes, see [172]). Other approaches involving the in situ preparation of the (phosphine)Au(I) complexes from AuCl<sub>3</sub> [173] or the use of chiral *N*-heterocyclic carbene gold complexes [174] have resulted in moderate enantioselectivities.

The alkoxycyclization reaction has so far received little attention in total synthesis (Fig. 5). Nevertheless, seminal contributions appeared regarding the synthesis of complex synthons of synthetic relevance towards natural products such as podophyllotoxin **236** [150] (and analogs), or dictamnaside E **237** [161]. An original and biomimetic approach to synthesis of hydroquinone-containing sesquiterpenes such as chromazonarol **238** has also been described [162].



**Scheme 44** Domino cycloisomerization/Prins cyclization reactions

Carbonyl derivatives have also been shown to exhibit a good reactivity in enyne cycloisomerization as an oxygen nucleophile, especially in the presence of weakly oxophilic Au(I) Lewis acids (Scheme 44). The formation of the tricyclic ether **240** was disclosed upon submission of the enyne **239** to a catalytic amount of AuCl [175]. The mechanism of this transformation is postulated to involve the nucleophilic attack of the carbonyl oxygen in an *anti* fashion on the cyclopropyl carbene intermediate **241**. The vinylaurate oxonium cation **242** resulting from this initial attack thus reacts via a Prins reaction to give the carbocationic gold–alkyl complex **243**. Elimination regenerates the gold catalyst and releases **240**.

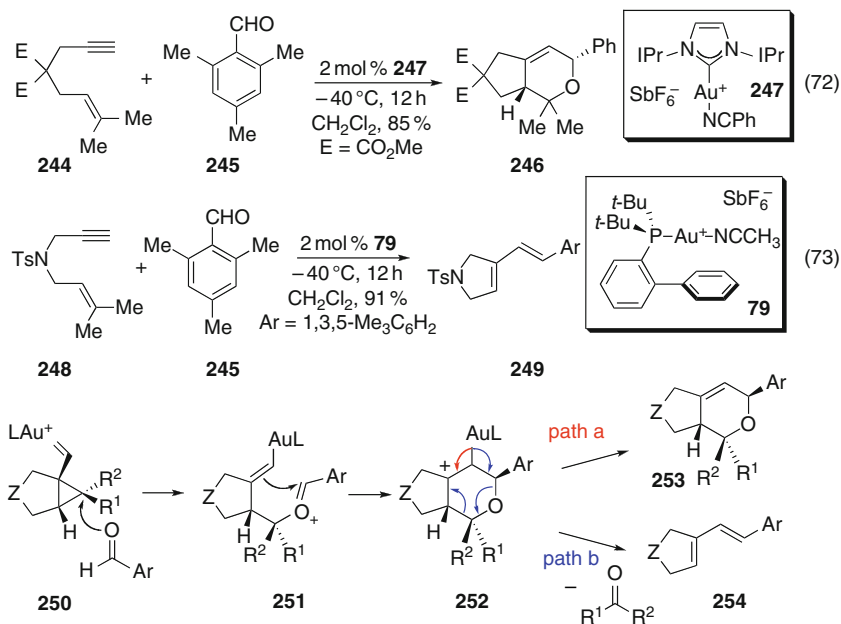
This methodology has been applied intermolecularly and was completely selective in the presence of an Au(I) catalyst with increased steric hindrance **247** [176] (Scheme 45).

When substrate **244** is placed at  $-40\text{ }^{\circ}\text{C}$  in the presence of the cationic Au(I) catalyst **247** and 2 equiv. of the hindered aldehyde **245**, the dihydropyran **246** is formed in 85% yield. The reactivity and product distribution may depend on the catalyst. Indeed, alternatively, when enyne **248** is treated with the gold catalyst **79** in the presence of the same aldehyde (2 equiv.), the diene **249** is selectively obtained in 91% yield (73). The mechanism would imply the formation of the 5-*exo* cyclopropyl carbene **250**, which would be trapped by the aldehyde (Scheme 45). A Prins cyclization would then lead to the cationic intermediate **252**, which upon path a or b would give **253** or **254**.

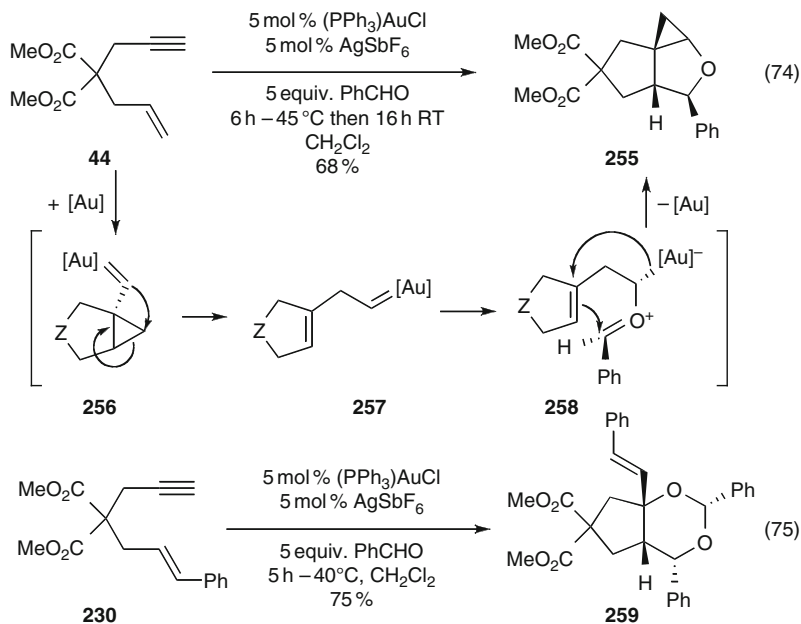
A variety of other behavior has been observed in the case of the intermolecular cycloisomerization of enynes with carbonyl nucleophiles. The reaction between 1,6-enynes with a terminal alkene group and carbonyl compounds in the presence of cationic Au(I) complexes was reported [177] (Scheme 46).

When 5 equiv. of benzaldehyde are used, enyne **44** is cleanly converted to the ether **255** in the presence of a catalyst formed from a combination of  $[(\text{PPh}_3)\text{AuCl}]$





**Scheme 45** Intermolecular domino carbonyl addition/cycloisomerization reactions



**Scheme 46** Intermolecular domino carbonyl addition/cycloisomerization reactions

and  $\text{AgSbF}_6$ . The mechanistic rationale [178] implies the initial formation of the cyclopropyl carbene **256** upon nucleophilic attack of the alkene on the Lewis-coordinated alkyne. Skeletal rearrangement leads to the formation of carbene **257** and is followed by nucleophilic attack of the carbonyl function giving the oxonium **258**. The subsequent attack of the alkene function in an intramolecular fashion then results in the formation of the gold-alkyl complex. Cyclopropanation and elimination of the gold cationic active species complete the catalytic cycle. Under the same conditions, the reactivity of enyne **230** bearing a substituted alkenyl side chain was different [178]. The formation of dioxolane **259** corresponding to an addition of two aldehydes to the enyne **230** was observed, the mechanism not being discussed by the authors (75). The domino cycloisomerization-Prins reactions were recently applied to the enantioselective synthesis of (+)-orientalol **260**, (±)-pubinernoid **261**, and (–)-englerins A **262** and B **263** [179–181] (Fig. 6).

One unique report has described the use of sulfoxides as oxygen nucleophiles in 1,6-enyne cycloisomerization (Scheme 47). In the presence of a combination of  $[\text{IPrAuCl}]$  **264** and  $\text{AgSbF}_6$ , the oxygen tethered enyne **200** reacts with  $\text{Ph}_2\text{SO}$  (2 equiv.) to give the bicyclic aldehyde **265** in 94% yield [182]. It is noteworthy that the cyclopropyl aldehyde had been observed at around 10% yield in the presence of palladium and platinum catalysts under organoaqueous conditions [88, 164]. The proposed mechanism for this transformation implies an initial attack of the sulfoxide on the carbene of a cyclopropyl carbene analog of **224** (Scheme 42). Elimination produces diphenyl sulfide and **265**, via a formal transfer of an oxene fragment, and regenerates the cationic gold catalyst.

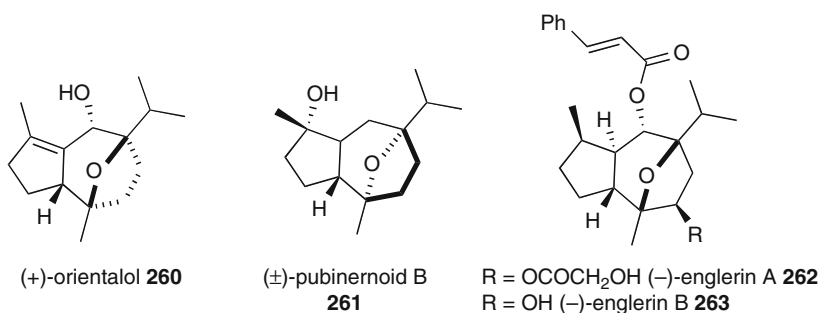
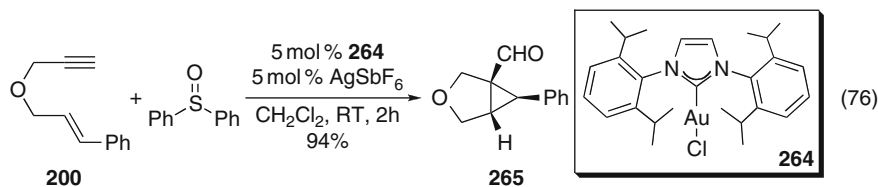


Fig. 6 Applications in total synthesis



Scheme 47 Intermolecular domino cycloisomerization/oxidation reactions

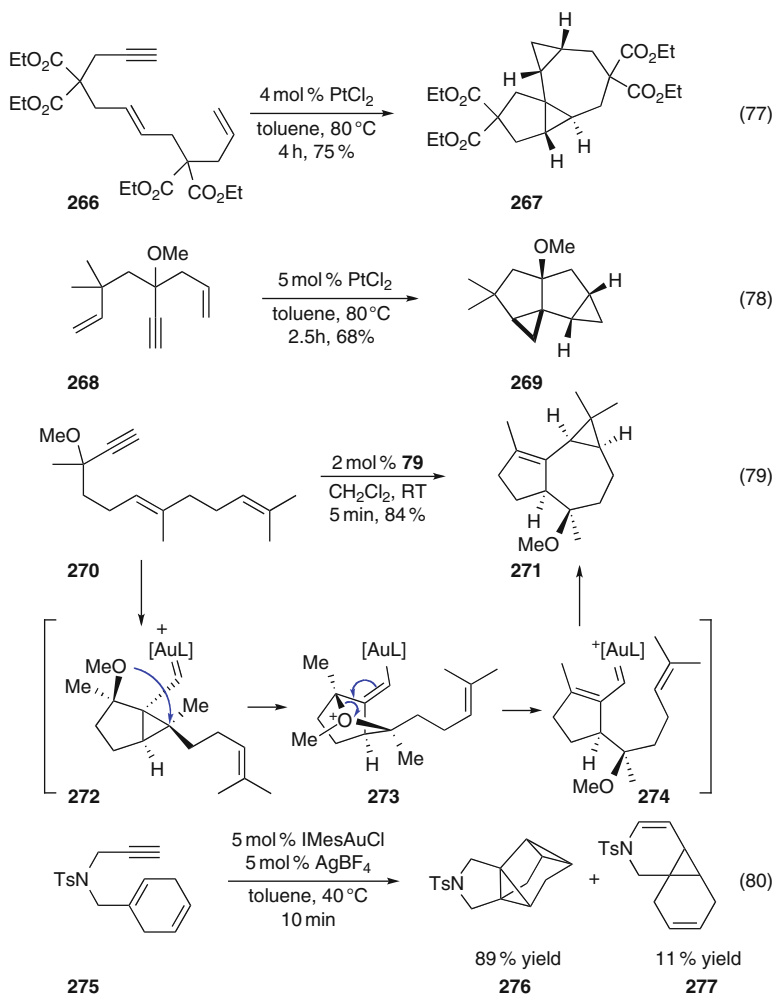
## 4.2 Carbon Nucleophiles

### 4.2.1 Alkene as Nucleophiles

Alkenes can react, either intra- or intermolecularly, with late transition metal carbenoids resulting from the cycloisomerization event, leading to complex polycyclic structures. The first report of trapping of a cyclopropyl carbene intermediate via an intramolecular cyclopropanation dates from 1998 when Murai and coworkers [183] described the formation of the tetracyclic structure **267** upon submission of diyne **266** to a catalytic amount of  $\text{PtCl}_2$  in toluene at 80 °C (Scheme 48).

This type of transformation has led to the synthesis of highly functionalized polycyclic structures in a completely diastereoselective manner. This methodology has been developed with other enynes such as diyne **268**, which upon reaction with  $\text{PtCl}_2$  in toluene at 80 °C afforded polycyclic **269** in 68% yield [184] (78). The mechanism of this transformation has recently been studied using computational tools [72, 185]. The authors demonstrated that the cyclization pathway is favored for polyenyne precursors bearing a hydroxylic or ether group at the propargylic positions by the presence of the remaining alkenyl moiety. The superior reactivity of cationic Au(I) species in these transformations has been demonstrated and quantitative yields are obtained at room temperature for substrates similar to that tested by Murai's group [186]. The specific case of 1,6-enyne **270** is particularly revealing regarding the complexity and difference of reactivity depending on the substrate [187] (Scheme 48, (79)). The cyclopropyl carbene **272**, formed upon *anti* nucleophilic attack of the alkene function on the activated alkyne, reacts intramolecularly by 1,5-migration of the methoxy group on the cyclopropane ring in an *anti* fashion. Skeletal rearrangement then furnishes the carbene **274**, which evolves classically towards the tricyclic ether **271**. Upon submission of diyne **275** to cycloisomerization in the presence of the gold-*N*-heterocyclic carbene complex, the tetracyclic structure **276** is formed in 89% isolated yield [188]. This transformation has recently been shown to proceed efficiently in the presence of Ir catalysts under harsher conditions; see [189] (80). It corresponds to the formal cyclopropanation of the two alkenyl functions at both ends of the alkyne and most probably involves a cyclopropyl carbene resulting from a 5-*exo* mode of cyclization.

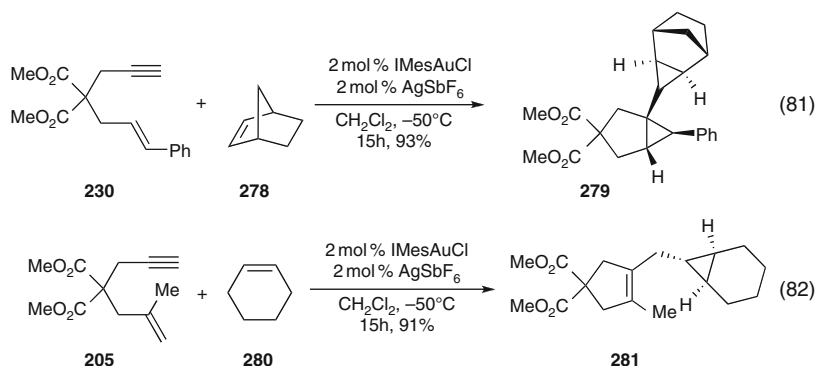
This type of transformation can also be performed in an intermolecular fashion [190] (Scheme 49). In the presence of 5 equiv. of norbornene and catalyst  $\text{Ime-sAuSbF}_6$  at -50 °C, enyne **230** is cleanly transformed to the bicyclopropane **279** in 93% yield. Depending on the substitution pattern of the enyne partner, the carbenoid species can be trapped by the external alkene nucleophile. Cyclopropane **281** is obtained in 91% yield when enyne **205** is reacted with cyclohexene (5 equiv.) in the presence of 2 mol% of the *N*-heterocyclic gold catalyst (82).



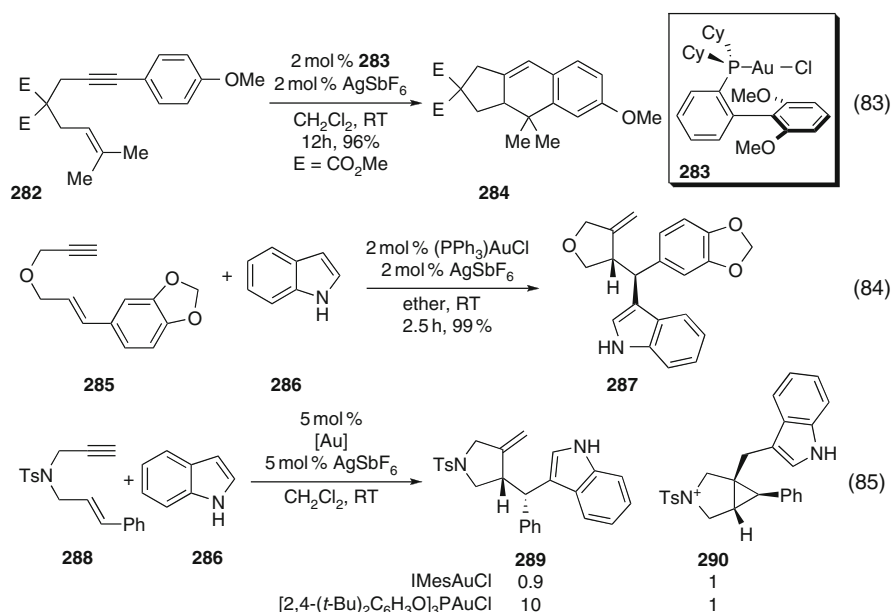
**Scheme 48** Intramolecular domino cycloisomerization/cyclopropanation reactions of dienynes

#### 4.2.2 Aromatic Rings as Nucleophiles

In 2005, the intramolecular domino hydroarylation/cycloisomerization of 1,6-enynes catalyzed by cationic Au(I) species was reported [191] (Scheme 50). Enyne **282**, possessing an aryl substituent on the alkyne, cyclizes to give the tricyclic carbocycle **284** in 86% yield. Whereas this transformation can be viewed as a [4 + 2] cycloaddition, the mechanism has been proposed to proceed via a cyclopropyl carbene. Stabilization of the developing positive charge at the alkene terminal position turns to be a key parameter to achieving a good chemoselectivity in favor of the aromatic ring nucleophilic addition. This methodology has recently

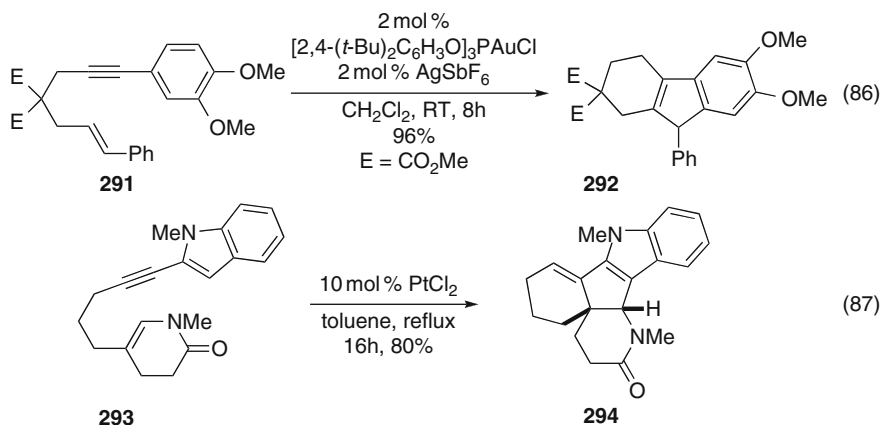


**Scheme 49** Intermolecular domino cycloisomerization/cyclopropanation reactions of enynes



**Scheme 50** Domino hydroarylation/cycloisomerization reactions of enynes

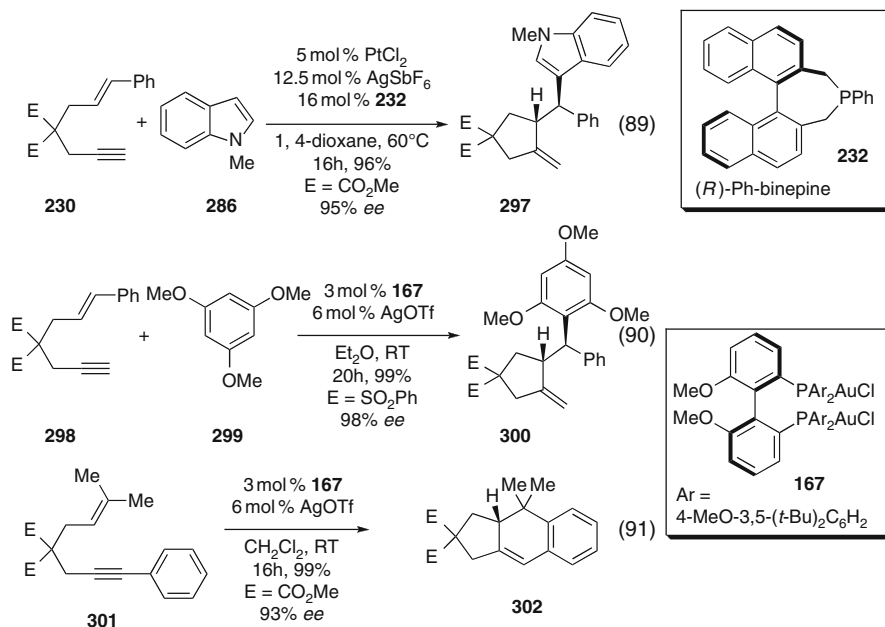
been applied to the cyclizations of 1-aryl-6,8-dien-1-ynes [192]. The intermolecular reaction has then been introduced [193–195], implying a wide range of electron-rich aromatic systems including anisole derivatives or indoles and pyrroles. The presence of cation-stabilizing groups at the terminal position of the alkene is a prerequisite to obtaining good yields. Deuterium labeling experiments as well as the diastereospecificity of the transformation supports a mechanism similar to that operating in the alkoxy cyclization of enynes [196].

**Scheme 51** Intramolecular domino hydroarylation/cycloisomerization reactions of enynes**Scheme 52** Domino hydroarylation/cycloisomerization reactions of dienynes

A strong influence of the stereoelectronic parameters of the ligand coordinated to the gold atom on the course of the reaction was also observed [194, 195]. Whereas the hydroarylation/cycloisomerization proceeds via the *anti* attack on the cyclopropane ring in the presence of a triarylphosphite-based catalyst leading to product **289**, the nucleophile addition takes place at the carbene carbon to give bicyclopropane **290** in the presence of *N*-heterocyclic carbene-based catalyst (85).

The bulky triarylphosphite-based catalyst also induces a reversal of regioselectivity of the cyclization event for some selected substrates [197] (Scheme 51). Enyne **291** is transformed to the cycloadduct **292** in 96% yield at room temperature in 8 h. The product is formed upon initial 6-*endo* cyclization followed by the isomerization of the alkene to the internal position. This reaction was extended to the case of enyne possessing an enamide function as alkene moiety [198, 199] (87). Enynes, such as **293**, having electron-rich aromatic or heteroaromatic ring systems on the alkyne cyclize in the presence of  $\text{PtCl}_2$  in refluxing toluene in a 6-*endo* fashion to give polycycles (e.g., **294**) in good yields.

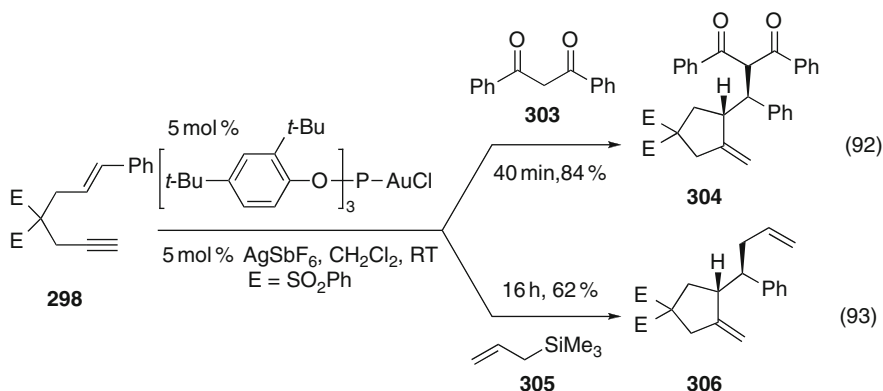
An elegant intramolecular domino hydroarylation/cycloisomerization of 1,5-enynes [200] and 1,5,9-dienynes [201] was described in the presence of a catalytic amount of mercury salts (Scheme 52). The reaction proceeds with diastereospecificity and moderate to excellent yields for, respectively, dienynes and enynes using



**Scheme 53** Asymmetric domino hydroarylation/cycloisomerization reactions of enynes

Hg(OTf)<sub>2</sub> (for a recent account on the applications of Hg(OTf)<sub>2</sub>, see [202]) under very mild conditions.

The first asymmetric version of the hydroarylation/cyclization reaction was described in 2008 by the group of Michelet [203] using dicationic platinum catalysts. As the reaction involves a single coordination site on the catalyst, the authors postulate that a square-planar dicationic complex coordinated by three monodentate phosphine ligands can create an optimum chiral environment around the metal (Scheme 53). The combination of PtCl<sub>2</sub> and AgSbF<sub>6</sub> with 3 equiv. of Ph-binepine **232** gives the best results. In a typical experiment, the reaction of enyne **230** with 3 equiv. of *N*-methyl indole in dioxane at 60 °C with 5 mol% of the catalyst combination leads to cyclopentane product **297** in 96% yield and 95% *ee* (89). Remarkably, the observation that a combination of 1 equiv. of Ph-binepine **232** and 1 equiv. of diphenylphosphinoethane induces a similar level of enantioselection that the system involving 3 equiv. of Ph-binepine (91% vs 95% *ee*) is paving the way for the development of a combinatorial design of Pt-based chiral catalysts. An enantioselective version using Au(I) bimetallic complexes has also been described using a combination of the complex **167** based on a crowded electron-rich atropisomeric chiral diphosphine ligand and silver triflate [204] (90, 91). The domino hydroarylation/cycloisomerization reaction of 1,6-enynes takes place under milder reaction conditions than with the dicationic Pt system due to the higher carbophilicity of Au(I) Lewis acids. The reaction proceeds either



**Scheme 54** Intermolecular domino cycloisomerization/1,3-dicarbonyl and allylsilane addition reactions

intra- or intermolecularly to give cycloadducts in good yields and excellent enantioselectivities. Steric hindrance on the tether plays a pivotal role in obtaining high enantioselectivities.

### 4.2.3 Other Carbon Nucleophiles

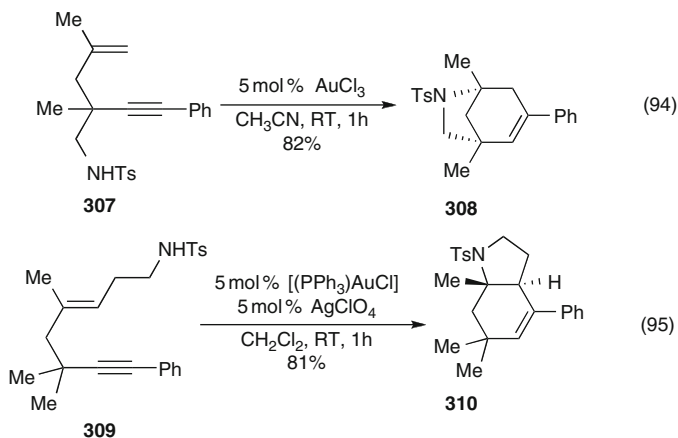
1,3-Dicarbonyl compounds, present mainly in their enol form, can also play the role of carbon nucleophiles at the 2-position [195] (Scheme 54). Dibenzoylmethane reacts with enyne **298** in the presence of Au(I) catalyst via a 5-*exo-dig* cyclization pathway to give the diketone **303** in 84% yield. Allylsilanes such as **305** were also examined as nucleophilic partners: using the same conditions, moderate yields of 1,6-dienes (**306**) were obtained (93).

## 4.3 Nitrogen Nucleophiles

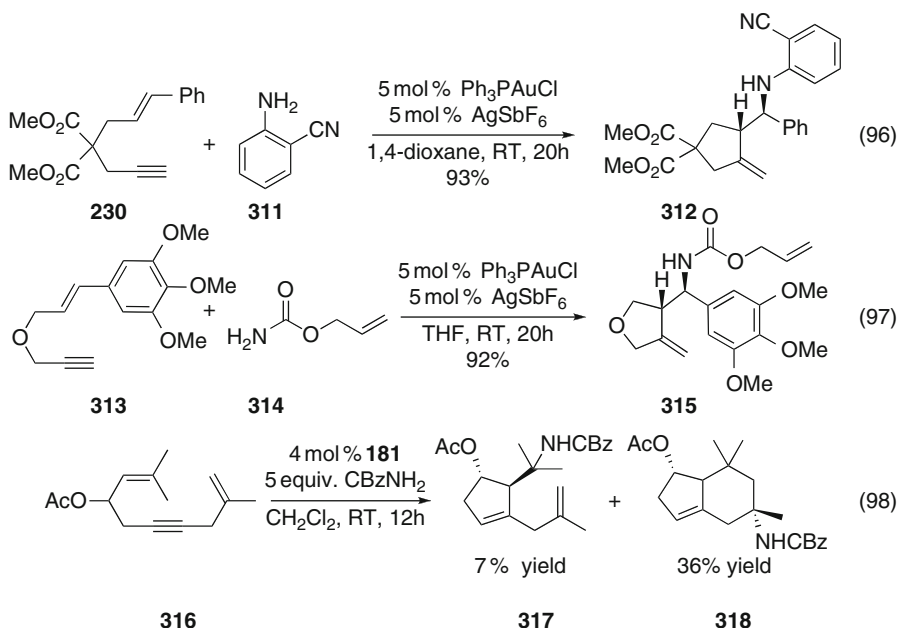
The domino intramolecular hydroamination/cycloisomerization of 1,5-enynes was the first report dealing with nitrogen as nucleophile [159] (Scheme 55). In the presence of either AuCl<sub>3</sub> or a catalytic system consisting of (PPh<sub>3</sub>)AuCl and AgClO<sub>4</sub>, enynes such as **307** or **309** are respectively transformed to the corresponding bicyclic pyrrolidine products **308** and **310** in 82% and 81% yields (94, 95).

The intermolecular version of this reaction was introduced later [205] (Scheme 56). Weakly nucleophilic amines including sulfonamides, carbamates and electron-poor anilines can be introduced with success on a variety of 1,6-enynes. In a typical experiment, substrate **230** is reacted with 3 equiv. of the amine nucleophile **311** in the presence of a combination of PPh<sub>3</sub>PAuCl and





**Scheme 55** Intramolecular domino hydroamination/cycloisomerization reactions of enynes



**Scheme 56** Intermolecular domino hydroamination/cycloisomerization reactions of enynes

$\text{AgSbF}_6$  in dioxane. The cycloisomerization product **315** is obtained as a single diastereoisomer in all enyne/amine combinations tested with an *anti* selectivity. The authors showed a strong influence of the solvent on the chemoselectivity. Bicyclo[4.3.0]nonanes products may also be synthesized starting from 1,5-dienynes and are obtained in moderate yields as a single diastereoisomer [206] (98).

## 5 Conclusion

The carbophilic Lewis acid activation concept has proved to be highly valuable for the rearrangement of enynes within the past 10 years. Various 1,*n*-enynes have been cyclized in the presence of metal complexes such as platinum, gold, indium, gallium, etc., complexes. The general pathway implies the activation of the alkyne moiety followed by the addition of the alkenyl part as a nucleophile. Depending on the substrates, the solvent, and the metal, various functionalized carbo- or heterocycles have been prepared with a high level of diversity and complexity compared to the simplicity of the 1,*n*-enynes. The emergence of theoretical studies has played a crucial role in interpreting the experimental results and moreover in stimulating new transformations. Platinum and gold catalysts have been the “rising stars” for the discovery of novel rearrangements and have opened great opportunities, both for fundamental research and for application in the total synthesis of biologically active or natural products. Of particular note is the extraordinary activity of silver and copper catalysts, which open new perspectives in catalysis. The past few years have seen several breakthroughs coming in asymmetric catalysis: although substantial efforts have been made, it is still essential to develop strategic asymmetric protocols that are general and applicable to various structural types. The success of this later area will probably need some further insights in the implied mechanism and intermediates and may be solved thanks to a complementary experimental/theoretical/analytical teams’ collaborations.

## References

1. Belmont P, Parker E (2009) *Eur J Org Chem* 35:6075
2. Lee SI, Chatani N (2009) *Chem Commun*:371
3. Jimenez-Nunez E, Echavarren AM (2008) *Chem Rev* 108:3326
4. Michelet V, Toullec PY, Genet J-P (2008) *Angew Chem Int Ed* 45:7427
5. Zhang L, Sun J, Kozmin S (2006) *Adv Synth Catal* 348:2271
6. Fairlamb IJS (2004) *Angew Chem Int Ed* 43:1048
7. Lloyd-Jones G (2003) *Org Biomol Chem* 1:215
8. Buisine O, Aubert C, Malacria M (2002) *Chem Rev* 102:813
9. Shapiro ND, Toste FD (2010) *Synlett* 675
10. Das A, Abu Sohel SM, Liu R-S (2010) *Org Biomol Chem* 8:860
11. Abu Sohel SM, Liu R-S (2009) *Chem Soc Rev* 38:2269
12. Furstner A (2009) *Chem Soc Rev* 38:3208
13. Arcadi A (2008) *Chem Rev* 108:3266
14. Patil NT, Yamamoto Y (2008) *Chem Rev* 108:3395
15. Li Z, Brouwer C, He C (2008) *Chem Rev* 108:3239
16. Shen HC (2008) *Tetrahedron* 64:3885
17. Skouta R, Li C-J (2008) *Tetrahedron* 64:4917
18. Hashmi ASK, Rudolph M (2008) *Chem Soc Rev* 37:1766
19. Muzart J (2008) *Tetrahedron* 64:5815
20. Gorin DJ, Sherry BD, Toste FD (2008) *Chem Rev* 108:3351
21. Hashmi ASK (2007) *Chem Rev* 107:3180

22. Fürstner A, Davies PW (2007) *Angew Chem Int Ed* 46:3410
23. Gorin DJ, Toste FD (2007) *Nature* 446:395
24. Hashmi ASK, Hutchings GJ (2006) *Angew Chem Int Ed* 45:7896
25. Jimenez-Nunez E, Echavarren AM (2007) *Chem Commun*:333
26. Chianese AR, Lee SJ, Gagné MR (2007) *Angew Chem Int Ed* 46:4042
27. Ma S, Yu S, Gu Z (2006) *Angew Chem Int Ed* 45:200
28. Hashmi ASK (2005) *Angew Chem Int Ed* 44:6090
29. Höffmann-Röder A, Krause N (2005) *Org Biomol Chem* 23:387
30. Soriano E, Marco-Contelles J (2009) *Acc Chem Res* 42:1026
31. Bongers N, Krause N (2008) *Angew Chem Int Ed* 47:2178
32. Widenhoefer RA (2008) *Chem Eur J*:5382
33. Sengupta S, Shi X (2010) *Chem Cat Chem* 2:609
34. Marion N, Nolan SP (2007) *Angew Chem Int Ed* 46:2750
35. Marco-Contelles J, Soriano E (2007) *Chem Eur J* 13:1350
36. Schmidbaur H, Schier A (2010) *Organometallics* 29:2
37. Yukuda Y, Utimoto K (1991) *J Org Chem* 56:3729
38. Yukuda Y, Utimoto K (1991) *Synthesis*:975
39. Eisenstein O, Hoffmann R (1981) *J Am Chem Soc* 103:4308
40. Shapiro ND, Toste FD (2008) *Proc Natl Acad Sci USA* 105:2779
41. Hooper TN, Green M, Russell CA (2010) *Chem Commun* 46:2313
42. Zuccaccia D, Belpassi L, Rocchigiani L, Tarantelli F, Macchioni A (2010) *Inorg Chem* 49:3080
43. Flügge S, Anoop A, Goddard R, Thiel W, Fürstner A (2009) *Chem Eur J* 15:8558
44. Fürstner A, Morency L (2008) *Angew Chem Int Ed* 47:5030
45. Hashmi ASK (2008) *Angew Chem Int Ed* 47:6754
46. Eschenmoser A, Ruzicka L, Jeger O, Arigoni D (1955) *Helv Chim Acta* 38:1890
47. Eschenmoser A, Arigoni D (2005) *Helv Chim Acta* 88:3011
48. Stork G, Burgstahler AW (1955) *J Am Chem Soc* 77:5068
49. Schubert U, Ackermann K, Aumann R (1982) *Cryst Struct Commun* 11:591
50. Seidel G, Mynott R, Fürstner A (2009) *Angew Chem Int Ed* 48:2510
51. Benitez D, Shapiro ND, Tkatchouk E, Wang Y, Goddard WA, Toste FD (2009) *Nat Chem* 1:482
52. Fedorov A, Moret M-E, Chen P (2008) *J Am Chem Soc* 130:8880
53. Fedorov A, Chen P (2009) *Organometallics* 28:1278
54. Batiste L, Federov A, Chen P (2010) *Chem Commun* 46:3899
55. Trost BM, Chang VM (1993) *Synthesis*:824
56. Chatani N, Morimoto T, Muto T, Murai S (1994) *J Am Chem Soc* 116:6049
57. Chatani N, Furukawa N, Sakurai H, Murai S (1996) *Organometallics* 15:901
58. Fürstner A, Szillat H, Gabor B, Mynott R (1998) *J Am Chem Soc* 120:8305
59. Oi S, Tsukamoto I, Miyano S, Inoue Y (2001) *Organometallics* 20:3704
60. Oh CH, Bang SY, Rhim CY (2003) *Bull Korean Chem Soc* 24:887
61. Ota K, Lee SI, Tang J-M, Takachi M, Nakai H, Morimoto T, Sakurai H, Kataoka K, Chatani N (2009) *J Am Chem Soc* 131:15203
62. Chatani N, Inoue H, Morimoto T, Muto T, Murai S (2001) *J Org Chem* 66:4433
63. Nieto-Oberhuber C, Muñoz MP, López S, Jiménez-Núñez E, Nevado C, Herrero-Gómez E, Raducan M, Echavarren AM (2006) *Chem Eur J* 12:1677
64. Nieto-Oberhuber C, Muñoz MP, Buñuel E, Nevado C, Cárdenas DJ, Echavarren AM (2004) *Angew Chem Int Ed* 43:2402
65. Nieto-Oberhuber C, López S, Muñoz MP, Cárdenas DJ, Buñuel E, Nevado C, Echavarren AM (2005) *Angew Chem Int Ed* 44:6146
66. Mezailles N, Ricard L, Gagosz F (2005) *Org Lett* 7:4133
67. Miyanohana Y, Chatani N (2006) *Org Lett* 8:2155
68. Chatani N, Inoue H, Kotsuma T, Murai S (2002) *J Am Chem Soc* 124:10294

69. Nakai H, Chatani N (2007) *Chem Lett* 36:1494
70. Fürstner A, Stelzer F, Szillat H (2001) *J Am Chem Soc* 123:11863
71. Nieto-Oberhuber C, López S, Jiménez-Núñez E, Echavarren AM (2006) *Chem Eur J* 12:5916
72. Soriano E, Ballesteros P, Marco-Contelles J (2005) *Organometallics* 24:3172
73. Soriano E, Ballesteros P, Marco-Contelles J (2005) *Organometallics* 24:3182
74. García-Mota M, Cabello N, Maseras F, Echavarren AM, Pérez-Ramírez J, López N (2008) *Chem Phys Chem* 9:1624
75. Cabello N, Jiménez-Núñez E, Buñuel E, Cárdenas DJ, Echavarren AM (2007) *Eur J Org Chem*:4217
76. Dankwardt JW (2001) *Tetrahedron Lett* 42:5809
77. Belmont P, Andrez J-C, Allan CSM (2004) *Tetrahedron Lett* 45:2783
78. Shibata T, Ueno Y, Kanda K (2006) *Synlett*:411
79. Grisé CM, Barriault L (2006) *Org Lett* 8:5905
80. Imase H, Noguchi K, Hirano M, Tanaka K (2008) *Org Lett* 10:3563
81. Cabello N, Rodriguez C, Echavarren AM (2007) *Synlett*:1753
82. Bajracharya GB, Nakamura I, Yamamoto Y (2005) *J Org Chem* 70:892
83. Fürstner A, Stelzer F, Szillat H (2000) *J Am Chem Soc* 122:6785
84. Trost BM, Doherty GA (2000) *J Am Chem Soc* 122:3801
85. Simmons EM, Hardin AR, Guo X, Sarpong R (2006) *Angew Chem Int Ed* 47:6650
86. Simmons EM, Sarpong R (2006) *Org Lett* 8:2883
87. de Jesus CJ, Sarpong R (2010) *Org Lett* 12:1428
88. Méndez M, Muñoz MP, Nevado C, Cárdenas DJ, Echavarren AM (2001) *J Am Chem Soc* 123:10511
89. Fang S, Wang Z (2009) *Eur J Org Chem*:5505
90. Harrak Y, Simonneau A, Malacria M, Gandon V, Fensterbank L (2010) *Chem Commun* 46:865
91. Lee SI, Kim SM, Kim SY, Chung YK (2006) *Synlett*:2256
92. Lee SI, Kim SM, Kim SY, Chung YK (2009) *Synlett*:1355
93. Comer E, Rohan E, Deng L, Porco JA (2007) *Org Lett* 9:2123
94. Kozak JA, Dake GR (2008) *Angew Chem Int Ed* 47:4221
95. Fernandez-Rivas C, Méndez M, Echavarren AM (2000) *J Am Chem Soc* 122:1221
96. Fernandez-Rivas C, Méndez M, Nieto-Oberhuber C, Echavarren AM (2002) *J Org Chem* 67:5197
97. Porcel S, Echavarren AM (2007) *Angew Chem Int Ed* 47:2672
98. Sun J, Conley MP, Zhang L, Kozmin SA (2006) *J Am Chem Soc* 128:9705
99. Zhang L, Kozmin SA (2004) *J Am Chem Soc* 126:11806
100. Boaventura MA, Drouin J, Conia JM (1983) *Synthesis*:801
101. Kennedy-Smith JJ, Staben ST, Toste FD (2004) *J Am Chem Soc* 126:4526
102. Staben ST, Kennedy-Smith JJ, Toste FD (2004) *Angew Chem Int Ed* 43:5350
103. Ochida A, Ito H, Sawamura M (2006) *J Am Chem Soc* 128:16486
104. Ito H, Makida Y, Ochida A, Ohmiya H, Sawamura M (2008) *Org Lett* 10:5051
105. Corkey BK, Toste FD (2005) *J Am Chem Soc* 127:17168
106. Binder JT, Crone B, Haug TT, Menz H, Kirsch SF (2008) *Org Lett* 10:1025
107. Montaignac B, Vitale MR, Michelet V, Ratovelomanana-Vidal V (2010) *Org Lett* 12:2582
108. Staben ST, Kennedy-Smith JJ, Huang D, Corkey BK, LaLonde RL, Toste FD (2006) *Angew Chem Int Ed* 45:5991
109. Barabé F, Bétournay G, Bellavance G, Barriault L (2009) *Org Lett* 11:4236
110. Corkey BK, Toste FD (2005) *J Am Chem Soc* 129:2764
111. Nicolaou KC, Tria GS, Edmonds DJ (2008) *Angew Chem Int Ed* 47:1783
112. Blum J, Beer-Krafts H, Badrieh Y (1995) *J Org Chem* 60:5567
113. Nevado C, Ferrer C, Echavarren AM (2004) *Org Lett* 6:3191
114. Ferrer C, Raducan M, Nevado C, Claverie CK, Echavarren AM (2007) *Tetrahedron* 63:6306
115. Mamane V, Gress T, Krause H, Fürstner A (2004) *J Am Chem Soc* 126:8654

116. Harrak Y, Blazyskowski C, Bernard M, Cariou K, Mainetti E, Mouriès V, Dhimane AL, Fensterbank L, Malacria M (2004) *J Am Chem Soc* 126:8656
117. Luzung MR, Markham JP, Toste FD (2004) *J Am Chem Soc* 126:10858
118. Freytag M, Ito S, Yoshifuji M (2006) *Chem Asian J* 1:693
119. Soriano E, Ballesteros P, Marco-Contelles J (2004) *J Org Chem* 69:8018
120. He R-X, Li M, Li X-Y (2005) *J Mol Struct THEOCHEM* 717:21
121. Ye L, Chen Q, Zhang J, Michelet V (2009) *J Org Chem* 74:9550
122. Komeyama K, Saigo N, Myiagi M, Takaki K (2009) *Angew Chem Int Ed* 48:9875
123. Horino Y, Yamamoto T, Ueda K, Kuroda S, Toste FD (2009) *J Am Chem Soc* 131:2809
124. Fehr C, Farris I, Sommer H (2006) *Org Lett* 8:1839
125. Fehr C, Winter B, Magpantay I (2009) *Chem Eur J* 15:9773
126. Fehr C, Magpantay I, Arpagaus J, Marquet X, Vuagnoux M (2009) *Angew Chem Int Ed* 48:7221
127. Shibata T, Kobayashi Y, Maekawa S, Toshida N, Takagi K (2005) *Tetrahedron* 61:9018
128. Brissy D, Skander M, Retailleau P, Marinetti A (2007) *Organometallics* 26:5782
129. Brissy D, Skander M, Jullien H, Retailleau P, Marinetti A (2009) *Org Lett* 11:2137
130. Chao C-M, Beltrami D, Toullec PY, Michelet V (2009) *Chem Commun*:6988
131. Nishimura T, Kawamoto T, Nagaosa M, Kumamoto H, Hayashi T (2010) *Angew Chem Int Ed* 49:1638
132. Kim SY, Chung YK (2010) *J Org Chem* 75:1280
133. Chatani N, Inoue H, Kotsuma T, Murai S (2002) *J Am Chem Soc* 124:10295
134. Fürstner A, Davies PW, Gress T (2005) *J Am Chem Soc* 127:8244
135. Nieto-Oberhuber C, Pérez-Galán P, Herrero-Gómez E, Lauterbach T, Rodriguez C, López S, Bour C, Rosellón A, Cárdenas DJ, Echavarren AM (2008) *J Am Chem Soc* 130:269
136. Odabachian Y, Gagosz F (2009) *Adv Synth Catal* 351:379
137. Lee YT, Kang YK, Chung YK (2009) *J Org Chem* 74:7922
138. Marion F, Coulomb C, Courillon C, Fensterbank L, Malacria M (2004) *Org Lett* 6:1509
139. Marion F, Coulomb J, Servais A, Courillon C, Fensterbank L, Malacria M (2006) *Tetrahedron* 62:3856
140. Couty S, Meyer C, Cossy J (2006) *Angew Chem Int Ed* 45:6726
141. Couty S, Meyer C, Cossy J (2009) *Tetrahedron* 65:1809
142. Soriano E, Marco-Contelles J (2005) *J Org Chem* 70:9345
143. Tenaglia A, Gaillard S (2008) *Angew Chem Int Ed* 47:2454
144. Fürstner A, Stimson CC (2007) *Angew Chem Int Ed* 46:8845
145. Kim SY, Park Y, Chung YK (2010) *Angew Chem Int Ed* 49:415
146. Kirsch SF, Binder JT, Crone B, Duschek A, Haug TT, Liébert C, Menz H (2007) *Angew Chem Int Ed* 46:2310
147. Sethofer SG, Staben ST, Hung OY, Toste FD (2008) *Org Lett* 10:4315
148. Galland JC, Savignac M, Genêt JP (1997) *Tetrahedron Lett* 38:8695
149. Galland JC, Dias S, Savignac M, Genêt JP (2001) *Tetrahedron* 57:5137
150. Charruault L, Michelet V, Genêt JP (2002) *Tetrahedron Lett* 43:4757
151. Méndez M, Muñoz MP, Echavarren AM (2000) *J Am Chem Soc* 122:11549
152. Nevado C, Cárdenas DJ, Echavarren AM (2003) *Chem Eur J* 9:2627
153. Nishizawa M, Yadav VK, Skwarczynski M, Takao H, Imagawa H, Sugihara T (2003) *Org Lett* 5:1609
154. Faller JW, Fontaine PP (2006) *J Organomet Chem* 691:1912
155. Nieto-Oberhuber C, Paz Muñoz M, Bunuel E, Nevado C, Cardenas DJ, Echavarren AM (2005) *Angew Chem Int Ed* 44:6146
156. Genin E, Leseurre, Toullec PY, Genêt J-P, Michelet V (2007) *Synlett*:1780
157. Chao C-M, Toullec PY, Michelet V (2009) *Tetrahedron Lett* 50:3719
158. Sethofer SG, Mayer T, Toste FD (2010) *J Am Chem Soc* 132:8276
159. Zhang L, Kozmin SA (2005) *J Am Chem Soc* 127:6962
160. Sherry BD, Maus L, Laforzeta BN, Toste FD (2006) *J Am Chem Soc* 128:8132

161. Buzas AK, Istrate FM, Gagosz F (2007) *Angew Chem Int Ed* 46:1141
162. Toullec PY, Blarre T, Michelet V (2009) *Org Lett* 11:2888
163. Li G, Liu Y (2010) *J Org Chem* 75:2903
164. Nevado C, Charuault L, Michelet V, Nieto-Oberhuber C, Muñoz MP, Méndez M, Rager M-N, Genêt J-P, Echavarren AM (2003) *Eur J Org Chem*:706
165. Baumgarten S, Lesage D, Gandon V, Goddard J-P, Malacria M, Tabet J-C, Gimbert Y, Fensterbank L (2010) *Chem Cat Chem* 1:138
166. Nelsen DL, Gagné MR (2009) *Organometallics* 28:950
167. Charruault L, Michelet V, Taras R, Gladiali S, Genêt JP (2004) *Chem Commun*:850
168. Gladiali S, Alberico E (2008) In: Börner A (ed) *Trivalent phosphorus compounds in asymmetric catalysis: synthesis and applications*, vol 2. Wiley-VCH, Weinheim, p 177
169. Toullec PY, Michelet V (2010) *Curr Org Chem* 14:1245
170. Gladiali S, Toullec PY, Genêt J-P, Michelet V (2011) *Electronic encyclopedia of reagents for organic synthesis*. Wiley, New York
171. Muñoz MP, Adrio J, Carretero JC, Echavarren AM (2005) *Organometallics* 24:1293
172. Martinez A, Garcia-Garcia P, Fernandez-Rodriguez MA, Rodriguez F, Sanz R (2010) *Angew Chem Int Ed* 49:4633
173. Chao C-M, Genin E, Toullec PY, Genêt JP, Michelet V (2009) *J Organomet Chem* 694:538
174. Matsumoto Y, Selim KB, Nakanishi H, Yamada K-I, Yamamoto Y, Tomioka K (2010) *Tetrahedron Lett* 51:404
175. Jiménez-Núñez E, Claverie CK, Nieto-Oberhuber C, Echavarren AM (2006) *Angew Chem Int Ed* 45:5452
176. Escribano-Cuesta A, López-Carillo V, Janssen D, Echavarren AM (2009) *Chem Eur J* 15:5646
177. Schelwies M, Dempwolff AL, Rominger F, Helmchen G (2007) *Angew Chem Int Ed* 46:5598
178. Schelwies M, Moser R, Dempwolff AL, Rominger F, Helmchen G (2009) *Chem Eur J* 15:10888
179. Jiménez-Núñez E, Molawi K, Echavarren AM (2009) *Chem Commun*:7327
180. Molawi K, Delpont N, Echavarren AM (2010) *Angew Chem Int Ed* 49:3517
181. Zhou Q, Chen X, Ma D (2010) *Angew Chem Int Ed* 49:3513
182. Witham CA, Mauleón P, Shapiro ND, Sherry BD, Toste FD (2007) *J Am Chem Soc* 129:5838
183. Chatani N, Kataoka K, Murai S, Furukawa N, Seki Y (1998) *J Am Chem Soc* 120:9104
184. Mainetti E, Mouries V, Fensterbank L, Malacria M, Marco-Contelles J (2002) *Angew Chem Int Ed* 41:2132
185. Marco-Contelles J, Soriano E (2006) *J Mol Struct THEOCHEM* 761:45
186. Nieto-Oberhuber C, López S, Muñoz MP, Jiménez-Núñez E, Buñuel E, Cárdenas DJ, Echavarren AM (2006) *Chem Eur J* 12:1694
187. Jiménez-Núñez E, Raducan M, Lauterbach T, Molawi K, Solorio CR, Echavarren AM (2009) *Angew Chem Int Ed* 48:6152
188. Kim SM, Park JH, Choi SY, Chung YK (2007) *Angew Chem Int Ed* 46:6172
189. Sim SH, Lee SI, Park JH, Chung YK (2010) *Adv Synth Catal* 352:317
190. López S, Herrero-Gómez E, Pérez-Galán P, Nieto-Oberhuber C, Echavarren AM (2006) *Angew Chem Int Ed* 45:6029
191. Nieto-Oberhuber C, López S, Echavarren AM (2005) *J Am Chem Soc* 127:6178
192. Yeh M-CP, Tsao W-C, Lee B-J, Lin T-L (2008) *Organometallics* 27:5326
193. Toullec PY, Genin E, Leseurre E, Genêt JP, Michelet V (2006) *Angew Chem Int Ed* 45:7427
194. Amijs CHM, Ferrer C, Echavarren AM (2007) *Chem Commun*:698
195. Amijs CHM, López-Carrillo V, Raducan M, Pérez-Galán P, Ferrer C, Echavarren AM (2008) *J Org Chem* 73:7721
196. Leseurre L, Chao C-M, Seki T, Genin E, Toullec PY, Genet J-P, Michelet V (2009) *Tetrahedron* 65:1911

197. Nieto-Oberhuber C, Pérez-Galán P, Herrero-Gómez E, Lauterbach T, Rodríguez C, López S, Bour C, Rosellón A, Cárdenas DJ, Echavarren AM (2008) *J Am Chem Soc* 130:269
198. Harrison TJ, Patrick BO, Dake GR (2007) *Org Lett* 9:367
199. Kozak JA, Dodd JM, Harrison TJ, Jardine KJ, Patrick BO, Dake GR (2009) *J Org Chem* 74:6929
200. Imagawa H, Iyenaga T, Nishizawa M (2005) *Org Lett* 7:451
201. Imagawa H, Iyenaga T, Nishizawa M (2005) *Synlett*:703
202. Nishizawa N, Imagawa H, Yamamoto H (2010) *Org Biomol Chem* 8:511
203. Toullec PY, Chao C-M, Chen Q, Gladiali S, Genêt J-P, Michelet V (2008) *Adv Synth Catal* 350:2401
204. Chao C-M, Vitale MR, Toullec PY, Genêt J-P, Michelet V (2009) *Chem Eur J* 15:1319
205. Leseurre L, Toullec PY, Genêt J-P, Michelet V (2007) *Org Lett* 9:4049
206. Böhringer S, Gagosz F (2008) *Adv Synth Catal* 350:2617

# DFT-Based Mechanistic Insights into Noble Metal-Catalyzed Rearrangement of Propargylic Derivatives: Chirality Transfer Processes

Olalla Nieto Faza and Angel R. de Lera

**Abstract** Cascade transformations of enynes and propargylic acyl derivatives triggered by the  $\pi$ -acid activation of the alkyne by gold or platinum catalysts can afford diverse and complex molecular skeletons under mild conditions in an atom-economical manner. Often the rearrangements benefit from additional roles of the metal, either activating other functional groups and/or organizing the intermediates for further reactions. Mechanistic insights gleaned from kinetic and labeling studies have been complemented by quantum chemical calculations for different substrates and reaction types, which show some common features that can be traced back to the combination of the propargylic system and the noble metal catalyst. Among other results, theoretical studies of the reactivity of some systems revealed the prevalence of very low barriers for the bond-forming/bond-breaking processes along complex multistep mechanistic manifolds. As a consequence, the barriers corresponding to conformational changes (single bond rotations, helix inversions...) of the intermediates acquire unexpected importance. Thus, memory of chirality in reactions of enantiopure substrates is preserved, in some cases, in formally planar intermediates that however do not undergo conformational scrambling. In this chapter we will review how computational chemistry continues to play a key role in our understanding and interpretation of the catalytic cycles of complex transformations catalyzed by gold and platinum, in particular those involving transfer of chirality.

**Keywords** Computational studies · Memory of chirality · Noble metals · Propargylic substrates · Rearrangements

---

O.N. Faza (✉) and A.R. de Lera (✉)  
Departamento de Química Orgánica, Universidade de Vigo, As Lagoas/Marcosende, 36310 Vigo, Spain  
e-mail: faza@uvigo.es, qolera@uvigo.es



## Contents

1	Introduction .....	82
2	Reactivity of Propargylic Systems in the Presence of Noble Metals .....	83
2.1	Metal-Alkyne Bonding: Metal as a Lewis Acid .....	83
2.2	Start of the Catalytic Cycle: Gold-Alkyne Complexes .....	85
2.3	Propargylic Esters and Enynes .....	85
2.4	Mechanistic Considerations: Carbene–Carbocation Continuum .....	88
2.5	Synthetic Relevance – Domino Processes: Generation of Complexity .....	90
2.6	Computational Studies: Technical Aspects and Relevance .....	90
2.7	Opportunities and Challenges of Chirality Transfer .....	91
3	General Mechanisms .....	93
4	Cyclopropanation Reactions .....	95
5	Configurational Stability of Allenes .....	100
6	Nucleophilic Additions .....	102
7	Pericyclic Reactions .....	104
8	Complex Reaction Cascades .....	118
9	Conclusions .....	125
	References .....	127

## 1 Introduction

In this work we provide an account of recent developments in the understanding of the mechanisms of gold- and platinum-catalyzed rearrangements of propargylic derivatives. Although intermolecular reactions are also described in some instances, we will focus on intramolecular rearrangements as the gate to the stereoselective generation of complexity. The use of molecular modeling techniques, especially density functional theory (DFT), has provided an invaluable tool to help in the elucidation of these mechanisms and afforded otherwise difficult to gather structural and energetic information about the main intermediates involved in these reaction paths, a knowledge that is more needed than ever, as the scope of  $\pi$ -acid catalysis is daily expanding, as is the need to design new catalysts for new, more controlled processes.

Accordingly, this review is divided into four main sections. The starting point is a general introduction on the scope of noble metal-catalyzed rearrangements and the general trends that have already been established, focusing on why gold and platinum display their characteristic reactivity towards alkynes and the systematic ways to exploit this in synthesis. Subsections are included to summarize the DFT techniques more extended for this kind of mechanistic studies and the three main strategies that can be used to generate selectivity. Then follows the core of the review, with the description of different mechanisms taken from the recent literature in which stereoselectivity, with special focus on chirality transfer and memory of chirality phenomena, is achieved. When possible, examples where DFT has played an important role in the characterization of mechanisms are given preferential attention, since they represent light points that help guide us in the sometimes confusing open reaction manifolds and a powerful tool in the systematization of

knowledge. The presentation has been organized using a bottom-up approach, starting with reactions involving simpler rearrangements (although some of this simplicity is lost upon a closer look at many of them) and adding steps until we reach the more complex reaction cascades with very functionalized substrates that interact with the metal catalysts in many different ways along the reaction paths. A short conclusion section is added at the end to summarize the main points arising from this description and hopefully provide some new insights that could guide further discussion.

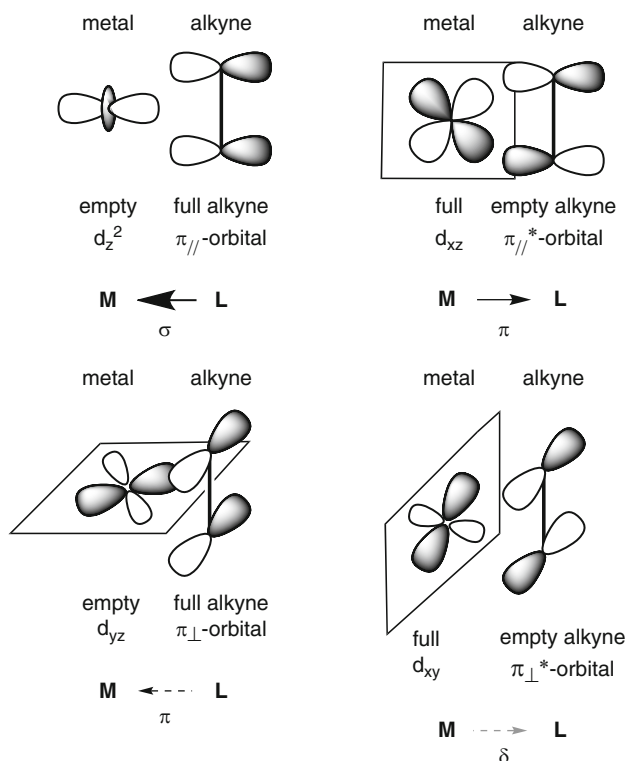
More recently, many comprehensive reviews have appeared on different aspects of noble metal catalysis and its use in the generation of complexity. The reader is directed to them to get a more complete view on the subject (for recent reviews, see [1–11]).

## 2 Reactivity of Propargylic Systems in the Presence of Noble Metals

### 2.1 *Metal-Alkyne Bonding: Metal as a Lewis Acid*

Alkynes are among the most popular substrates in homogeneous gold and platinum catalysis. The C–C triple bond functional group is characterized by two orthogonal  $\pi$ -bonds, high in energy, that easily interact with the  $d$  orbitals in transition metals (electrophiles). At the same time, the LUMO in alkynes is low in energy, which allows the attack of strong nucleophiles. If the alkyne is activated by coordination to the electrophilic metal complex, it becomes susceptible to attack by weaker nucleophiles, opening the door to a very rich reactivity involving the formation of new C–C, C–O, C–N, or C–S bonds. Thus, among the variety of catalytic transformations in which alkynes are involved – cycloadditions and cyclooligomerizations with compounds with  $\pi$ -systems ( $\text{CO}_2$ , CO, alkenes, alkynes, allenes, aldehydes and ketones, imines...), carbonylations or coupling with different carbon or heteroatom fragments, etc., – one of the most rapidly developing fields in catalysis research is the electrophilic activation of  $\pi$  systems using noble metals complexes. Gold and platinum (the main interests of this review chapter) have jumped into the spotlight during the last decade as activators of carbon–carbon  $\pi$ -bonds functioning as soft, carbophilic Lewis acids in reactions that achieve large increases in molecular complexity under mild conditions, compatible with a wide range of functional groups.

These properties that set apart gold and platinum from other transition metals are the consequence of relativistic effects, which lead to contraction of the  $6s$  orbitals and expansion of the  $d$  and  $f$  orbitals due to the resultant increased shielding of the contracted core. The former causes higher ionization potentials, stronger metal–ligand bonds, and high acidity (contraction of the valence  $s$  and  $p$  orbitals is associated to a relatively low-lying LUMO) and the latter a decreased electron–electron repulsion on the  $d$  orbitals which leads to softness and less nucleophilic



**Scheme 1** Qualitative orbital diagram of the interactions between a generic alkyne and a transition metal. The relative strength of the interactions is proportional to the *arrow* width

metal species for which neither oxidative addition nor reductive elimination (key steps in classical organometallic catalytic cycles) are very common [12].

Computational studies of the bonding in noble metal-alkyne complexes have been carried out, the results of which can be crudely summarized in the general picture in Scheme 1.

Bond decomposition analysis attributes roughly equal contributions to electrostatic and covalent bonding interactions (slightly higher electrostatic terms [13–16] and references therein). Alkynes bond with gold and platinum through the  $\sigma$  overlap of a  $\pi$  orbital with an empty  $d$  orbital on the metal with the appropriate symmetry, but also through back donation of a filled orbital on the metal to the corresponding alkyne in plane  $\pi_{//}^*$ . Other contributions to the bonding can involve the orthogonal  $\pi_{\perp}$  and  $\pi_{\perp}^*$  orbitals donating charge ( $\pi$  symmetry) and accepting it ( $\delta$  symmetry, very weak due to low overlap) from orbitals at the metal center, respectively. Usually, the  $\sigma$  interaction makes the largest contribution to bonding, followed by the in plane  $\pi_{//}$  back donation, a much smaller  $\pi_{\perp}$ -ligand donation to the metal, and a negligible metal- $\pi_{\perp}^*$  back donation, making alkynes in gold(I) and platinum(II) complexes good  $\sigma$  donors and only weak  $\pi$  acceptors.

Usually Pt(II) catalyzed transformations are carried out at higher temperatures than their Au(I) catalyzed counterparts; sometimes they lead to different products [17–19] and sometimes they afford the same products following different mechanisms [20, 21].

A recent relativistic *ab initio* study of model gold and platinum–alkyne complexes ascribes the difference in their reactivity (gold usually more reactive than platinum) to very different metal *d* populations in the outer valence space, resulting in large structural changes in the LUMOs. Gold complexes display high LUMO density on carbon and low LUMO energies, both favoring nucleophilic attack, while platinum complexes have higher energy LUMOs and no LUMO density on carbon, leading to a less favorable overlap with a nucleophilic frontier orbital [22].

The differences in mechanism usually obey the difference in electrophilicity of the catalytic species. Gold complexes being more electrophilic, they tend to displace the system in the carbene–carbocation continuum towards more cationic species, resulting preferentially in cation cyclizations and cationic rearrangements over the C–H insertions and cyclopropanations (carbenoid derived products) favored by platinum [20, 21].

## 2.2 *Start of the Catalytic Cycle: Gold-Alkyne Complexes*

Despite the activity and vitality of this field, and the wealth of experimental and theoretical results available on reactivity, not many gold or platinum alkyne complexes have been isolated in pure form. Computational and experimental studies on these complexes, however, suggest that the electronic properties of the ligands attached to the metal can modulate its effect on the structure of the coordinated alkyne [16, 23, 24].

It is noteworthy that, in the presence of several unsaturations in the substrate, the metal preferentially activates alkynes over alkenes. Since studies on Au<sup>+</sup>–ethylene and Au<sup>+</sup>–ethyne bonding estimate at around 10 kcal/mol the stabilization of the former compared with the latter, preferential coordination of the metal to alkynes cannot be invoked to explain this alkynophilicity of gold and platinum [15, 25] which is expected to have a kinetic origin. This kinetic origin can be explained by a better overlap of the nucleophile with the lower energy LUMO in alkyne complexes which makes the alkyne complexes more reactive.

## 2.3 *Propargylic Esters and Enynes*

One of the main advantages of the reactivity of the metals under study is the compatibility with a wide range of functional groups and the diversity of reaction

paths available for the rearrangement of different substrates. However, this wide applicability and the remarkable increase in complexity that these mechanisms provide somewhat complicate the systematic description of the catalytic cycles initiated by gold or platinum  $\pi$ -acid activation of alkynes, for the product is heavily dependent on the backbone and the functionalization of the substrate. The fact that an activated alkyne presents two activated carbon positions that can be non-symmetric only adds to the diversity of the products.

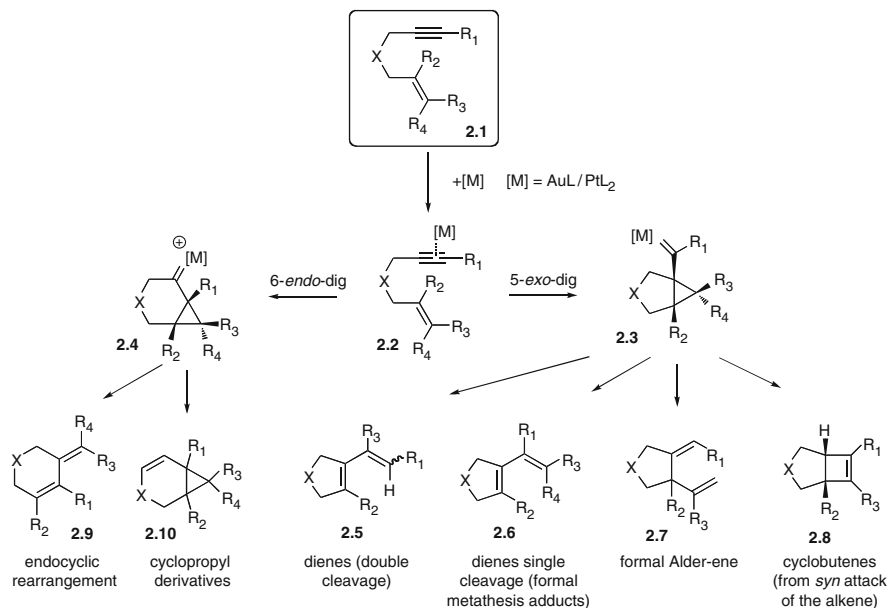
But even if systematization is difficult when looking at the products of these transformations, synergy between experimental and computational work has provided very useful compilations of reactivity patterns, among which those for propargylic esters and enynes are the most widely used. These mechanisms rely on the increased electron delocalization provided by the expanded  $5d$  orbitals (this reactivity goes beyond that promoted by simple acid catalysis) that results in the generation of a series of cationic or carbenoid derivatives at the start of complex reaction cascades and rearrangements.

Enynes are interesting substrates for gold and platinum-catalyzed rearrangements, since they provide at the same time the alkyne to be activated and the nucleophilic alkene that is going to attack it. The intramolecular nature of this reaction allows the facile production of complex cyclic building blocks, and functionalization on the backbone can lead to further reactivity and added complexity on the product [3, 6].

Scheme 2 displays an outline of the main reaction paths available for a general 1,6-enyne. After metal coordination to the alkyne **2.1**, nucleophilic attack of the neighboring alkene can proceed through *exo-dig* or *endo-dig* paths to afford cyclopropyl carbenoid intermediates (**2.3** and **2.4**). Theoretical calculations, together with trapping experiments and the experimental product distributions, support this step as entry to the mechanism [6]. In absence of other nucleophiles, the skeletal rearrangement of these intermediates is the default mechanism. This rearrangement, however, can follow different paths, depending on substitution, on the presence of heteroatoms on the main chain and on the metal used.

When Pt(II) is used (the same products can be obtained with gold catalysts), the most common mechanism is the *5-exo-dig* cyclization, followed by ring expansion to yield a metal-coordinated cyclobutene ring (**2.8**). Conrotatory ring opening of this cyclobutene intermediate results in a diene that could be thought of as the result of a metathesis reaction. Another path that could lead to a diene involves the ring opening of the cyclobutene concerted with a C–H insertion and followed by a [1,2]-hydrogen shift [21].

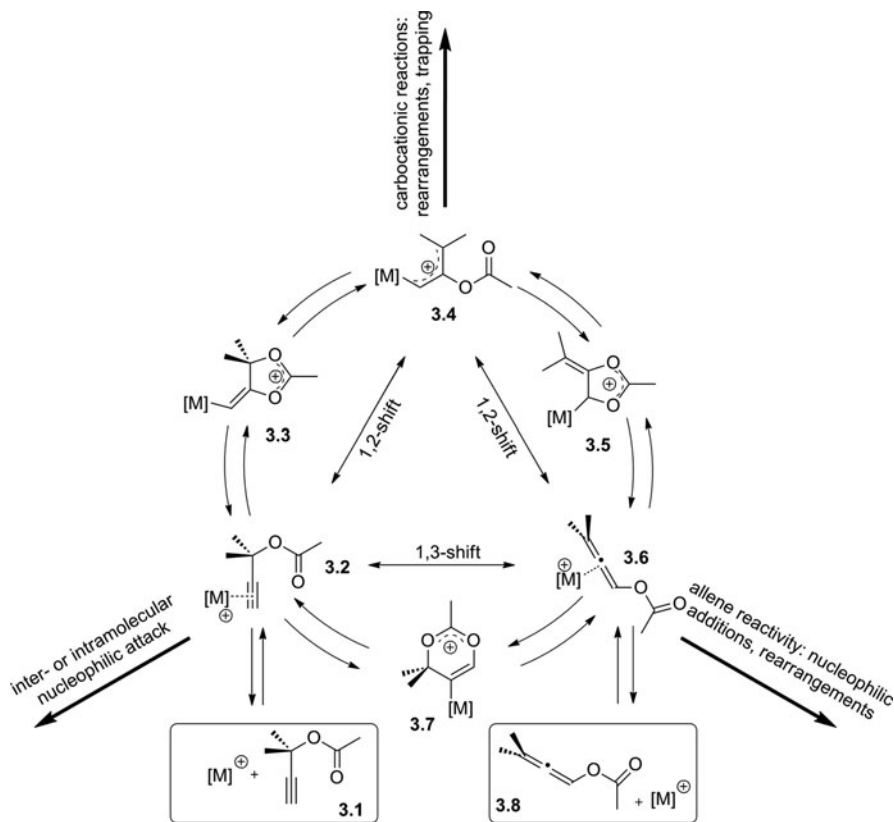
With Au(I), the formation of dienes, however, has been shown through computational studies to proceed via a [1,2]-alkyl shift (before the formation of the cyclobutene) resulting in a carbocation that then evolves into the diene after metal elimination (single cleavage to **2.5**). Another mechanistic possibility involves a dyotropic rearrangement to a new carbene which then loses an  $\alpha$ -hydrogen and protodemetalates to the diene (double cleavage, **2.6**).



**Scheme 2** Reaction paths open to a generic enyne under  $\pi$ -acid activation by gold or platinum

The formation of the Alder-ene product (**2.7**) is explained by the opening of the cyclopropyl ring and deprotonation of the resultant carbocation.

Propargylic esters are readily available synthetic scaffolds that can be easily bedecked with additional functional groups on the core structure. This versatility allows them to participate in a wide variety of intramolecular rearrangements that afford highly functionalized products through different manifolds. Many papers have reviewed the reactivity of these systems when submitted to gold catalytic conditions ([11, 26, 27] and references therein), and their results can be elegantly summarized in the “golden carousel” proposed by Correa et al. (Scheme 3) [26]. This scheme displays a series of structures close in energy (in a bracket of 10 kcal/mol) that can be interconverted through low-energy reaction barriers (the highest value calculated for the model system is about 7 kcal/mol). From initial gold  $\pi$ -coordination to the alkyne (**3.2**), the system can suffer either a 1,2- or a 1,3-carboxyl migration that result in a gold carbenoid/carbocation (**3.4**) or a gold-coordinated allene (**3.6**), respectively. Subsequent 1,2- or 1,3-shifts would close the circle connecting the carbene/carbocation with the allene or the latter with the original alkyne (**3.2**). Thus, three different reactivity paradigms are available for propargylic esters in these catalytic conditions: direct nucleophilic attack on the activated unsaturation in **3.2**, cationic processes starting from **3.4**, or allene chemistry starting from **3.6**. The choice of an exit of this cycle or another depends on the structure of the substrate and the functional groups present.



**Scheme 3** The “golden carousel” [26], a summary of the different intermediates involved in the metal-catalyzed reactivity of propargyl esters and the mechanisms that allow their interconversion. This catalytic cycle is accessible to both alkynes or allenes and can be exited through three reactivity paradigms that correspond to formal activated alkynes, activated allenes, and metal-stabilized carbocationic/carbenoid species

## 2.4 Mechanistic Considerations: Carbene–Carbocation Continuum

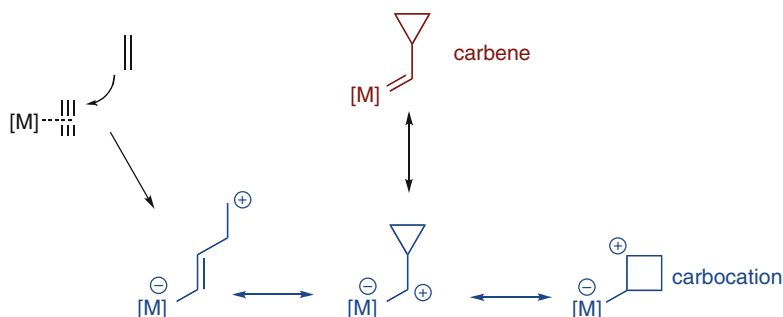
On the basis of these and other reactivity patterns, both gold carbenes and gold-stabilized carbocations have been proposed as intermediates in gold-catalyzed mechanisms.

As an example, in studies about gold-catalyzed enyne cycloisomerizations, the cyclopropyl structure of some of the products, accompanied by mechanistic studies using deuterium labeling, strongly suggests the intermediacy of gold carbene species [28–30]. The recent report of an enyne cycloisomerization terminated by  $sp^3$  C–H bond insertion strongly points toward carbene intermediates as well [31].

Other examples, however, support the description of these key intermediates as nonclassical carbocations based on substituent effects on regioselectivity, trapping experiments, or NMR studies of model systems [32–34].

The products of many gold-catalyzed reactions are compatible with mechanisms that involve either carbene or carbocationic intermediates, as in the example of the gold(I)-catalyzed tandem reactions initiated by 1,2-indole migration described by Sanz et al. (see below) [35], where the cyclization step after the indole migration can be thought of as the electrocyclicization of a gold–pentadienyl cation system or the insertion of a carbene into a C–H bond. Thus, besides labeling experiments, in situ spectroscopic techniques, identification of secondary products, and trapping of intermediates, computational chemistry remains an invaluable tool for the characterization of the electronic structure of these key highly reactive intermediates. Beyond a mere academic exercise, these kinds of mechanistic insights can provide the knowledge base needed to tailor both substrates and catalysts to favor the desired outcome in complex synthesis, further refining the already impressive existent set of reactions.

Relying heavily on computation to help rationalize experimental findings, Benitez et al. [36] have recently published a paper that somehow lays this controversy to rest. Studying barriers to bond rotation in carbenoid/carbocationic species and activation barriers for cyclopropanation reactions, they propose that the carbon–gold bond in these species can be described as a point in a continuum ranging from a gold-stabilized singlet carbene to a metal-coordinated carbocation. This point can be displaced on the scale by the substituents on the substrate and the ligand on the metal, and is reflected on the susceptibility of the system to different reactivity models (Scheme 4).



**Scheme 4** Mesomeric forms of the product of the attack of an alkene to an activated alkyne. The resultant species can be thought of as either a carbocation or a carbene. The different limit structures proposed for the carbocation can be used to explain many of the rearrangements of these intermediates



## 2.5 *Synthetic Relevance – Domino Processes: Generation of Complexity*

As stated above, gold and platinum catalysis on propargylic systems is often the starting point for complex domino processes that result in large increases in complexity in simple one-pot conditions. Some of these syntheses have been developed ad hoc in routes to natural products, other have been explored to provide synthetic scaffolds for more general uses. Besides the manifolds already described, a wealth of new transformations are available where different intra- and intermolecular nucleophiles are used to attack the activated alkyne. An interesting strategy in the design of tandem reactions is to use a metal-catalyzed reaction that generates new functional groups that can be subject to a second or third metal-catalyzed step [1, 7, 10, 37]. Although essentially carbophilic in nature, gold and platinum complexes have a non-negligible affinity towards heteroatoms, that has also been the object of recent interesting developments [38–40].

This dual character can lead to reactivity patterns where sequential gold  $\pi$ -coordination to unsaturations and  $\sigma$ -coordination to heteroatoms are involved in more complex transformations [41, 42].

## 2.6 *Computational Studies: Technical Aspects and Relevance*

In the reviews by Pyykkö, covering the computational chemistry of gold much information can be garnered about state of the art computational approaches used to account for different properties of this metal and its compounds [43–45]. The work by Pernpointner et al. [22] also points towards the need to use relativistic calculations in gold and platinum complexes to account for their electronic structure, whose special features stem, as stated above, from relativistic effects. However, even if some of the conclusions of most of the general reviews on the modeling of transition metal-catalyzed reaction mechanisms can be extrapolated [46–48], there is a dearth of information on the best computational treatment for gold and platinum homogeneous catalytic cycles, specially taking into account the relevance of relativistic effects to their chemistry.

In most of the literature surveyed, the computational method of choice is DFT [49], allaying some account of electron correlation with a reasonable computational cost. The most popular functional is, by far B3LYP [50, 51], and the choice of basis sets is usually 6-31G(d) for main group atoms, and an electron core potential (ECP) with its associated basis set for the heavy metals. Among the ECPs used (in order to reduce the computational cost associated with the high number of core electrons in late transition metals and to incorporate in a parametric way some relativistic effects), LANL2DZ [52] is the most common, with some instances of SDD [53], and BP86 [50, 54] with the LACVP family of basis sets (a combination of Pople's with LANL2DZ effective core basis sets) is also common among the users of Jaguar.

In most recent papers, the need for more accurate results has led to larger basis sets being used, at least in single point energy corrections (triple zeta basis with generous inclusion of diffuse and polarization functions), but also for geometry optimizations, and it is expected that the success of the new generation of hybrid functionals, such as M06 [55] and further development of basis sets and ECPs [56], will also extend their application in this field.

The choice of this level of theory is usually supported by some general benchmark calculations on sample systems and by the good agreement between the conclusions and predictions from computational studies and the experimental findings at the bench. However, many authors seem to rely just on the “*everyone else is doing it*” argument and use these computational methodologies as established protocols without a second thought.

As an example of not so common benchmarking, MP2 and B3LYP calculations with the same basis set and ECP have been carried out by Soriano et al. for the *exo* and *endo* addition of ethene to PtCl<sub>2</sub>-activated propyne. The variations in the geometries of minima and transition states are not large, even if DFT yields longer forming bonds (~0.1 Å) and shorter C–Pt distances in the carbene structures (~0.06 Å) [57]. Even if the activation energies are somewhat higher for MP2 (~3 kcal/mol), the reaction energy and the relative barriers for the two alternative paths don't change with the two approaches, thus not altering the qualitative mechanistic picture obtained with the less costly method. This semiquantitative level of accuracy in the computed energies is enough for the most general mechanistic discussions, but this approach has to be taken with care when subtle differences come into play, such as in dealing with substituent effects or competing reaction paths that are close in energy.

In their description of the bonding model in gold carbenes, for example, Benitez et al. show that M06 (with Hay Wadt pseudopotential and LACV3P++\*\* (2f)//LACVD\*\* for gold, and 6-311++G\*\*//6-31G\*\* for main group atoms) is able to reproduce correctly the effect of the different electron donating properties of gold ligands on the experimental bond rotation barriers of gold carbenoid species, while B3LYP and BP86 fail at this task [36].

Thus, although the correspondence of calculated data with the available experimental evidence gives us confidence in the common methodologies used, they should be applied with care when dealing with new phenomena or when an accurate description of bonding or subtle interactions is required.

## 2.7 Opportunities and Challenges of Chirality Transfer

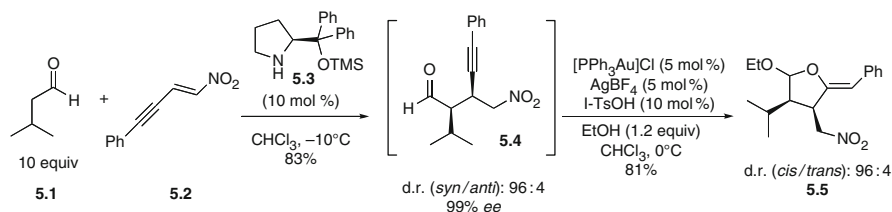
Because of this veritable explosion of results describing new reactions through homogeneous gold and platinum catalysis, it was easy to forget the earlier initial success of some enantioselective reactions [58] and the development of stereoselective versions seemed to lag behind for some time.

However, the fact that these reactions often proceed with very good selectivities, resulting in complex structures of controlled stereochemistry, is receiving more and more attention. The field has revived and novel examples of stereoselective gold-catalyzed reactions are frequently described in the literature [59, 60].

Diastereo and enantioselective homogeneous gold and platinum-catalyzed reactions can be achieved through three different strategies:

1. Chiral ligands on the metal center [4, 61]. Ito et al. [58] started the homogeneous catalytic gold rush with their description of the first asymmetric aldol reaction using a gold(I) complex. For a long time after this first example, however, the use of chiral ligands on gold complexes was not fully explored, under the belief that, due to the linear geometry at the metal center, which places the stereogenic elements far from the reaction site, it would not be the most efficient strategy. Nevertheless, plenty of examples are being developed where this is not an impediment as in the enantioselective hydroalkoxylation of allenes [62, 63], hydrogenation of alkenes [64], cycloadditions [65], olefin cyclopropanation [66], enyne cycloisomerization [67], etc.
2. Chiral counter-ions. Through ion-pair formation in the hydroalkoxylation of allenes, Toste et al. have developed the concept of using a chiral counter-ion, not directly attached to the metal, to achieve stereocontrol in gold catalysis [68], but, although very promising [69, 70], especially when chiral ligands and chiral anions are combined in a synergistic strategy, the scope of the method has not yet been completely explored. Among recent advances are the work of Zuccaccia et al., who have shown (combining NMR spectroscopy and DFT calculations) that the relative orientation of the counterion in cationic gold complexes can be tuned by the choice of the ligand, opening another way of control on the properties and activity of this kind of catalysts, ( $\text{BF}_4^-$  locates to the side of the styrene moiety in  $[(\text{PPh}_3)\text{Au}(4\text{-Me-styrene})]\text{BF}_4$ , while it prefers the vicinity of NHC (1,3-bis(di-iso-propylphenyl)-imidazol-2-ylidene) when it is used as the gold ligand in  $[(\text{NHC})\text{Au}(4\text{-Me-styrene})]\text{BF}_4$ ) [71].
3. Transfer of chiral information from the substrate to products. The transfer of chiral information between a stereogenic center or axis in the substrate and a center in the product remains the most widely reported strategy for performing stereoselective gold-catalyzed reactions. Allenes are common chiral groups involved in chirality transfer, as exemplified in the transformation of  $\beta$ -hydroxy- or amino-allenes into dihydropyrans and tetrahydropyridines [72] or of  $\alpha$ -hydroxy allenes into dihydrofurans [73]. However, many examples are being developed where the configuration of an alcohol, ester, or ether function, or even an epoxide, determines the configuration of a new center created in the reaction, such as the enantioselective propargyl Claisen rearrangement [74], the tandem Claisen rearrangement–heterocyclization used in the synthesis of dihydropyrans [75], the synthesis of spiropyranones from epoxyalkynes [76], or the Rautenstrauch reaction [17].

These possibilities, together with the compatibility of  $\pi$ -acid catalysis with different functional groups and reaction conditions, allow for very interesting



**Scheme 5** One-pot organocatalysis/gold-catalysis sequence [77]

developments in the design of efficient catalytic transformations. The work by Belot et al. [77] on the synthesis of tetrahydrofurans (see Scheme 5) elegantly combines organocatalysis with gold catalysis in a tandem one-pot process. In a first step, an enantiopure pyrrolidine derivative (**5.3**) catalyzes the asymmetric conjugated addition of the enol form of an aldehyde (**5.1**) to a nitroolefin (**5.2**), while the resultant adduct (**5.4**) undergoes a gold-catalyzed acetalization/cyclization through activation of the alkyne. In the first step two stereocenters are generated and the chiral information is preserved in the second. A similar strategy is developed in the highlights on binary catalytic systems by Hashmi and Hubbert [78].

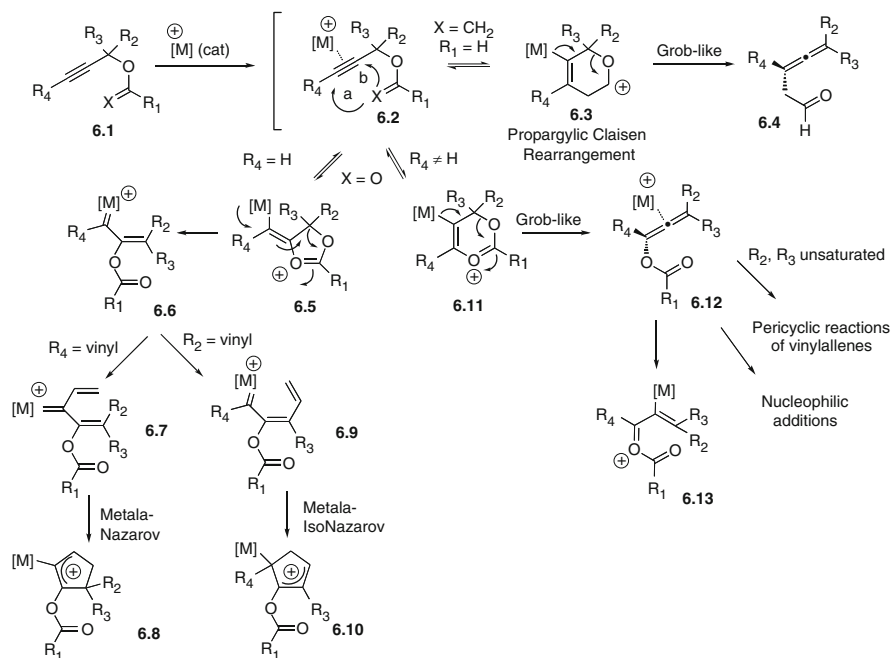
### 3 General Mechanisms

In this review we will focus on chirality transfer processes in gold- and platinum-catalyzed rearrangements of propargylic derivatives, and on how DFT calculations can provide insight into the mechanisms that lead to stereoselection. The aim is to provide an overview of the most common reactivity paradigms with detailed description of selected examples that will allow systematization of the general principles underlying these phenomena and the harnessing of the available knowledge to design better catalytic systems with the desired properties.

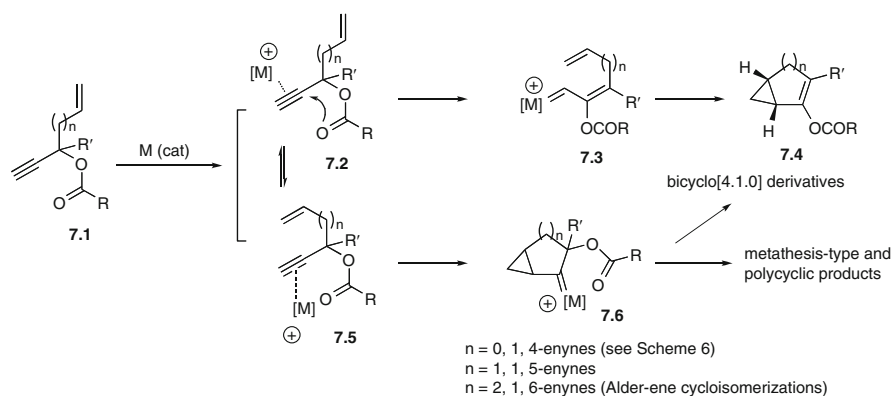
Thus we will deal with the stereoselective versions of the reactions depicted in Schemes 6 and 7.

Scheme 6 represents the reaction paths available for a propargylic enol ether or ester (**6.1**) under noble metal catalysis that will be discussed. Some of these transformations can be integrated into the general scheme for propargyl esters discussed in the Introduction (see Scheme 3), while others are more specific for certain substrates.

After the first coordination step, a different path opens for enoethers or esters (**6.2**): the former can experience a propargylic Claisen rearrangement followed by a Grob-like fragmentation leading to 3,4-pentadienal (**6.4**), whereas the latter can evolve through nucleophilic attack of a lone pair of the oxygen in the carboxylate to the activated alkyne. Depending on the alkyne position attacked, a five- (**6.5**) or six-membered (**6.11**) ring intermediate is formed that can afterwards rearrange to either a carbocation/carbenoid species (**6.6**) or to an acetoxallene (**6.12**), again through



**Scheme 6** Model reactions with propargyl esters or enol ethers as starting points



**Scheme 7** Model reactions for propargylic acetate 1,*n*-enynes

a Grob-like transformation. These intermediate species, starting from 1,2- or 1,3-carboxylate migration, can experience further transformations, depending on their base structure and the nature of  $R_1$ ,  $R_2$ ,  $R_3$ , and  $R_4$  groups: metal-(iso)-Nazarov reactions when one of the substituents is a vinyl group, other pericyclic reactions of polyenes or vinylallenes, or simple nucleophilic additions.

Scheme 7 shows the reaction paths that can be followed by propargyl 1,4-, 1,5-, and 1,6-enyne esters. After metal activation, the alkyne can suffer the nucleophilic attack of either the carbonyl oxygen (**7.3**) or the neighboring unsaturation (**7.6**). The result is a carbenoid species whose evolution will be determined by the molecular skeleton and the substituents it supports. In the upper part of the scheme, the nucleophilic attack of the oxygen is followed by 1,2-carboxyl migration and subsequent insertion of the resultant carbenoid in the unsaturated C–C bond to afford bicyclo[4.1.0] derivatives (**7.4**). This same scaffold can be obtained by direct cyclopropanation on the alkene and further migration of the carboxyl group on the carbenoid structure. From this last intermediate, other metathesis-type and polycyclic products can also be obtained.

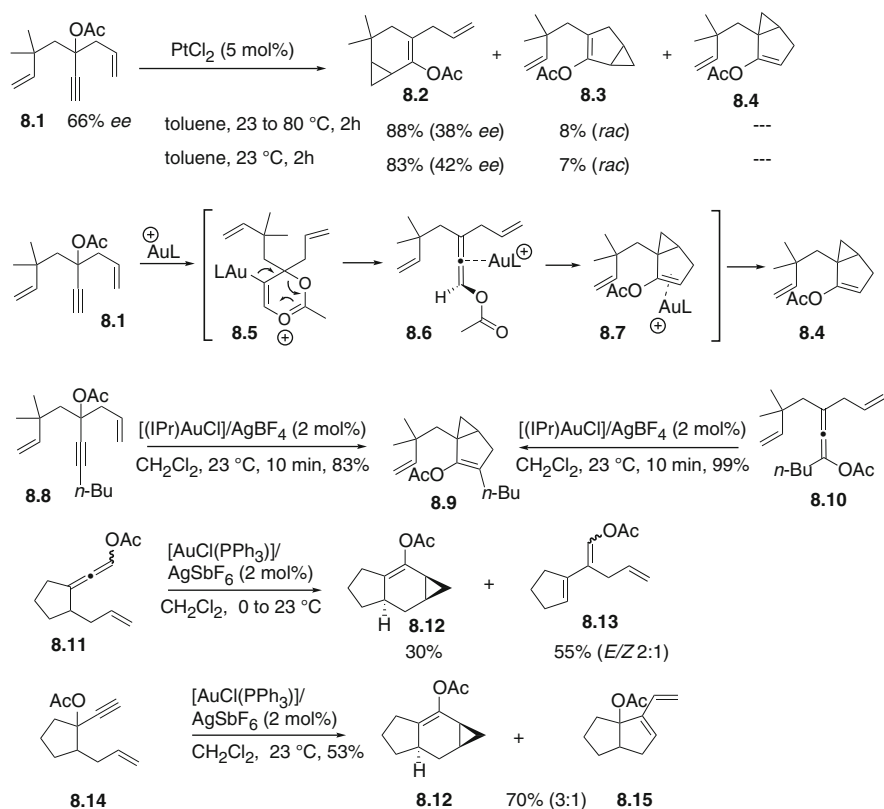
## 4 Cyclopropanation Reactions

We will start our discussion of stereoselective gold and platinum-catalyzed reactions of propargyl systems in a radial approach, starting from the first step in the catalytic cycles, and gradually adding circles of complexity.

The first step in many of the noble metal-catalyzed reactions of polyunsaturated systems, and the only available when there are no other external or internal nucleophiles, is the intramolecular cyclopropanation. This skeletal rearrangement is very common, both as the key step in transformations affording bicyclo[4.1.0]heptene derivatives and as the entry point to a metal carbenoid/carbocation manifold.

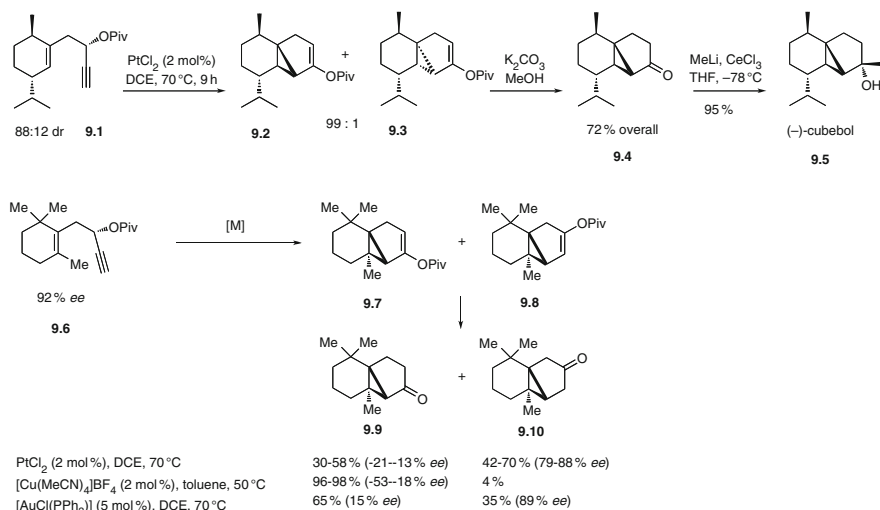
One of the first reports of this kind of reactivity accompanied by computational studies is the work by Marion et al. on the gold and platinum-catalyzed rearrangement of enynyl esters [28, 79]. In these papers the authors describe the catalyzed cycloisomerization of a dienyne with an acetate group on the propargylic position (**8.1**). The key to the interesting reactivity of this system is its double character as a 1,5- and 1,6-enyne, which leads to mixtures of bicyclic compounds **8.2**, **8.3**, and **8.4** (see Scheme 8). The most puzzling data obtained from studies on the reactivity of this precursor (**8.1**) are the fact that, with platinum, bicyclo[4.1.0]heptene **8.2** is obtained as the main product, with **8.3** as a byproduct, and some erosion in the enantiomeric excess with respect to the *ee* of the reactant when an enantioenriched mixture of **8.1** is used (38–42% *ee* in the product vs 66% in the reactant). When gold is used as catalyst, although the formation of **8.2** and **8.3** is still observed, the new bicyclo[3.1.0]hexene **8.4** is the major product. Although no chirality transfer can be found in the reported transformations, we decided to include the studies on this system here as both an example of the structural variability to be found in this kind of rearrangements and as a reminder of the power of interpretation that only the combined use of laboratory experiments and molecular modeling can afford.

The catalytic cycle starts with coordination of **8.1** to the metal and subsequent nucleophilic attack of the C6–C7 alkene to the terminal carbon on the activated alkyne. From this point there are several paths available that could lead to the formation of the observed products. Many of the relevant steps can be traced back



**Scheme 8** Rearrangement of enynyl esters to bicyclic cyclopropane skeletons [28]

to the “golden carousel” in Scheme 3. DFT calculations show that, from the two reaction paths that could lead to **8.2**, the [1, 2]-acetate shift on **8.1**, followed by cyclopropanation of the resultant carbenoid, is preferred by 14 kJ/mol over the reverse sequence of nucleophilic attack of the C6–C7 alkene to the terminal position of the activated alkyne and [1,2]-acyl migration on the resultant bicyclic intermediate. The formation of **8.3** follows a similar path involving the alternative instead. Again, the preferred path is [1,2]-migration followed by cyclopropanation, now with an 18 kJ/mol difference between the competing rate-limiting steps in the two paths. The formation of **8.4** is not so straightforward, and at least three paths can be proposed for it. The intervention of allene **8.6**, however, is needed in the three of them. The calculations show that the preferred path for this transformation involves the formation of the allenyl ester **8.6** through [1,3]-migration on **8.1**, and subsequent cyclization between the allene and the alkene part of the 1-acetoxy-1,2,5-triene branch. Rearrangement of structures such as **8.11** or **8.14** and the resultant product distributions support the predictions of DFT. Worthy of note is the fact that the competition between acetate and alkene migration in these processes is very



**Scheme 9** Representation of the synthetic route to (–)-cubebol starting from propargylic-1,5-enyne esters [80–82]

dependent on the choice of metal ligand, a point not always properly treated in simulations.

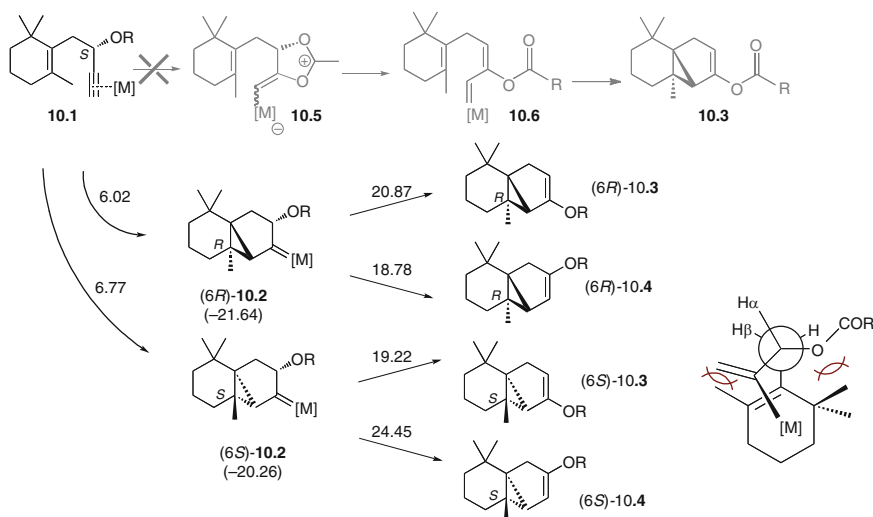
Another example of cyclopropanation rearrangements in 1,5-enynes can be found in the use of the Rautenstrauch cyclopropanation reaction in the synthesis of cubebol by Fehr et al. [80, 81] and Fürstner et al. [82]. The stereoselectivity of this process is a clear example of chirality transfer where the chiral information of the stereogenic center at C<sub>3</sub> in the reactant is passed onto the configuration of the new stereocenters in the product.

From the experimental data in Scheme 9, it can be seen that this chirality transfer is not complete, since there is some erosion of the enantiomeric excess in the products. However, racemization is not involved in this loss of *ee*, since the enantiomeric excesses of the products remain constant during the reaction, and can only be attributed to deficiencies in the stereocontrol mechanism.

Prior to this work it was considered that the mechanism for the gold or platinum-catalyzed cycloisomerizations of secondary enynol esters involved an initial [1,2]-acyl shift followed by cyclopropanation of the resultant carbene. But the selectivity of this reaction is not compatible with such a reaction path, because a vinyl carbene intermediate would imply planarization of the stereocenter in the substrate before the stereocenters in the cyclopropyl fragment are generated, denying the possibility of chirality transfer in this system.

The results from the experiments carried out by Fehr et al. [80, 81] and Fürstner et al. [82] strongly suggested that the correct sequence is the nucleophilic attack of the alkene to the activated alkyne to afford an electrophilic cyclopropyl carbene, which subsequently reacts with the acetate moiety to generate the product. But it



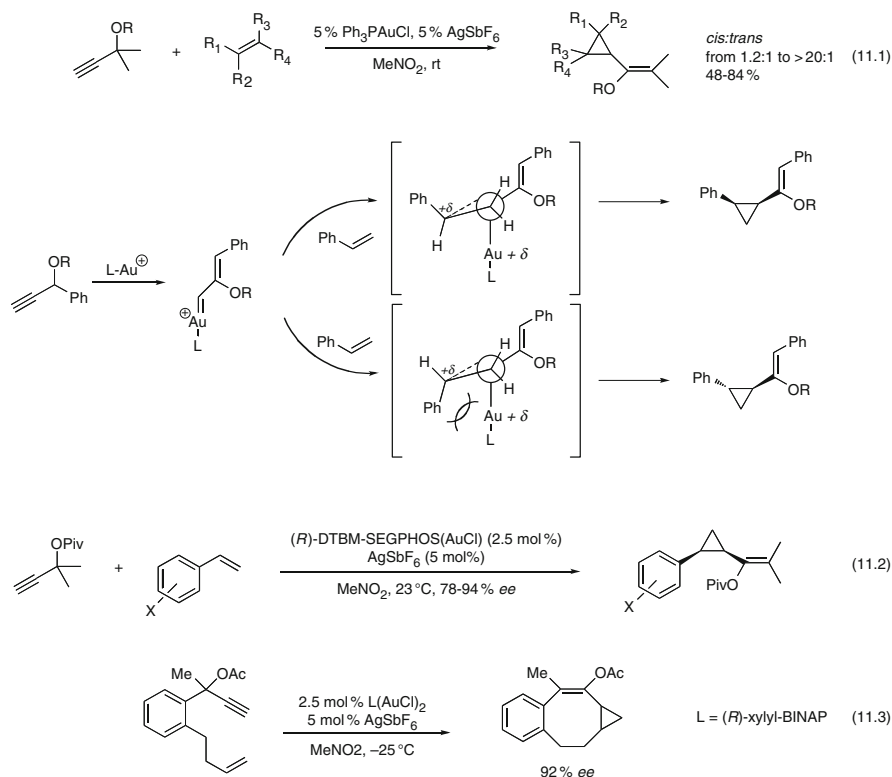


**Scheme 10** Mechanisms proposed for the reaction in Scheme 9, with [M] = PtCl<sub>2</sub>. Since it is not compatible with the experimental stereoselectivities, the path in gray is not considered. The numbers on the arrows represent activation barriers (kcal/mol) and those between parenthesis free energy differences with respect to the reactant (B3LYP/6-31G\*, LANL2DZ, with CPCM) [83]. On the right the transition structure for the transition state corresponding to the cyclopropanation step for (S)-10.1 is represented as a Newman projection

was the computational DFT study of the reaction mechanism for this transformation performed by Soriano et al. [83] that confirmed these hypotheses (see Scheme 10).

The calculations show that the cycloisomerization of **10.1** proceeds preferentially from the “top face,” albeit with a very small difference with respect to the activation barrier of the alternative “bottom face” attack, which explains the formation of both (6*R*)-**10.2** and (6*S*)-**10.2**.

It is in the following step that the transfer of chiral information takes place. There are two different paths available for the evolution of **10.2**: [1,2]-acyl shift or [1,2]-H shift that will result in the formation of **10.3** and **10.4**, respectively. For (6*R*)-**10.2** the most favorable process now is a [1,2]-H shift (18.78 vs 20.87 kcal/mol) while for (6*S*)-**10.2** the acyl shift is preferred (19.22 vs 24.45 kcal/mol). The product ratios calculated from these values match well those found in the experimental setups. The calculations predict that the degree of stereoselectivity depends on the structure of the substrate, that the diastereoselectivity of the cyclopropanation step depends on subtle intramolecular steric interactions, and that the efficiency of the chirality transfer depends on the different susceptibilities of (6*R*)-**10.2** and (6*S*)-**10.2** to [1,2]-H and [1,2]-acyl migration. On this line, the linear structure of the gold(I) catalyst can be expected to result in less steric hindrance for the acyl migration (from both faces), making this process more competitive than with the T-shaped PtCl<sub>2</sub> catalyst, supporting the experimental findings.



**Scheme 11** Inter- and intramolecular olefin cyclopropanation reactions. The first was used to optimize the reaction, the latter to build on these results to provide enantioselective versions of this transformation through the use of chiral gold ligands [66, 84]

In the paper by Fürstner et al. [82], the authors use these findings about the reactions involved in the synthesis of (–)-cubebol to address the making of the skeleton of another natural product (2-sesquicarene) and explore new aspects of the stereoselectivity of these rearrangements.

To close this section we will include two examples of ligand-induced stereoselectivity in enyne cycloisomerizations, transformations that are useful but not very common [63].

The simplest of them is the intermolecular gold(I)-catalyzed stereoselective olefin cyclopropanation developed by Johansson et al. [66]. Already the nonstereoselective version of this reaction is interesting (see Scheme 11, (11.1)), since gold-catalyzed intermolecular cyclopropanation reactions are not so common. The steric model to explain the *cis* preference for the cyclization is also applicable to the equivalent intramolecular processes. Once this reaction was well optimized, the authors proceeded to develop its enantioselective version, which they achieved by testing different chiral phosphine ligands (see Scheme 11, (11.2)). The results are

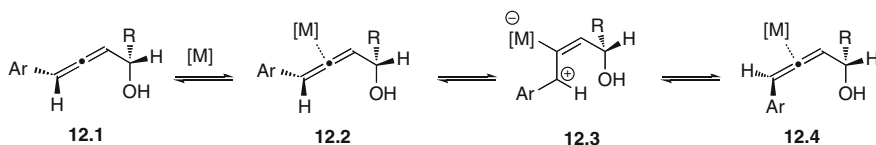
satisfactory, although there is ample room for improvement, with better results for the bulkier aromatic groups, as expected from the chirality induction strategy used.

The enantioselective cycloisomerization of chiral, racemic propargylic esters by Watson et al. [84], an intramolecular version of the former (see Scheme 11, (11.3)), uses chiral ligands on gold to achieve moderate to good enantiomeric excesses depending on ligand and solvent (from 20% to 90% with xylyl-BINAP). This transformation occurs through a different sequence of steps from that of the Rautenstrauch cyclopropanation: initial formation of a carbenoid through [1,2]-acyl migration, followed by cyclopropanation on the alkene. Since the substrates used are 1,7- or 1,8-enynes, this reaction represents a good synthetic tool for obtaining functionalized medium-sized rings, which are often challenging to build.

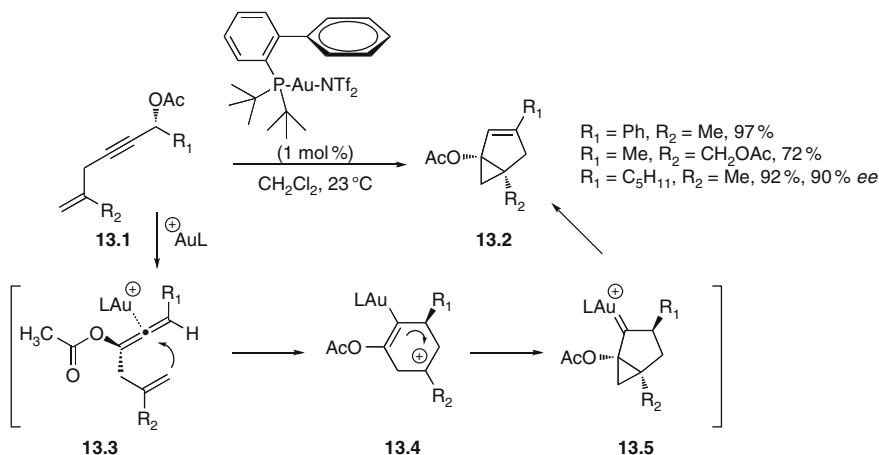
## 5 Configurational Stability of Allenes

A common intermediate in many chirality transfer processes starting from propargylic esters are allenes, usually the product of a [1,3]-acyl migration. The transfer of chiral information would then travel from the stereogenic center in the reactant to the axial configuration of the allene and from there to one or more stereogenic centers with controlled configuration in the product, a center-to-axis-to-center chirality transfer. For this transfer to be efficient, these allene intermediates must present certain configurational stability, something that is not always achieved due to the many existing exit points from this species in the catalytic manifold considered, some of which involve planarized carbocation or carbene intermediates. An example of how to limit allene epimerization to ensure high levels of axis-to-center chirality transfer is described in the study on the gold-catalyzed cycloisomerization of  $\alpha$ -hydroxyallenes to 2,5-dihydrofurans by Deutsch et al. [85], where the authors try to reduce the Lewis acidity of the gold catalyst, changing the solvent, and using different additives so that the zwitterionic intermediates (**12.3**) are disfavored (Scheme 12).

When the propargylic carboxylate is at the end of the conjugated chain of an enyne, instead of between the reactive unsaturations, it allows the usual cyclopropanation to proceed through a slightly different mechanism belonging to the same manifold as the reactions in the previous section. In the reaction described by Buzas et al. [86] for the cycloisomerization of 5-en-2-yn-1-yl acetates **13.1** to afford



**Scheme 12** General metal-catalyzed allene epimerization through a carbocationic intermediate. Other more complex mechanisms can also be responsible for this loss of configurational stability

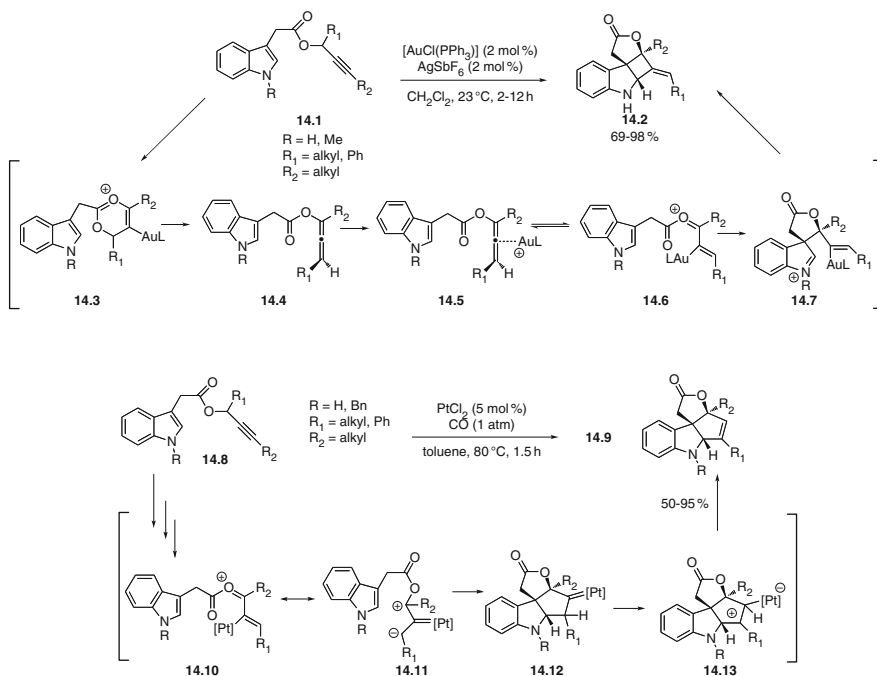


**Scheme 13** Enantioselective cycloisomerization of a propargyl enyne proceeding through an allene intermediate [86]

bicyclo[3.1.0]hexenes **13.2** and eventually 2-cycloalken-1-ones, the catalytic cycle (see Scheme 13) starts with gold coordination to the alkyne, followed by the formation of a gold-activated allene (**13.3**) through a [3,3]-sigmatropic shift ([1,3]-acyl migration). This allene is then attacked by the alkene, resulting in the formation of a cationic vinyl gold species (**13.4**) embedded in a six-membered ring that then collapses to the cyclopropyl carbene (**13.5**). The reaction ends when bicyclo[3.1.0] hexene (**13.2**) is produced after a [1,2]-hydride shift that regenerates the catalyst. The uses of such a transformation rely on the complex bicyclic structure generated and the acetoxyl functionality at the ring junction, which can be precursor to further transformations. In the case of enantioenriched substrates (see Scheme 13), there is a faithful transfer of chiral information from the substrate (99% *ee*) to the product (90% *ee*) through the configuration of the allene intermediate in what could be considered a good example of center-to-axis-to-center chirality transfer.

Other examples of allene-mediated chirality transfer from propargylic esters are rather impressive in the complexity of the polycyclic structures generated. Among these examples we have highlighted the gold-catalyzed synthesis of 2,3-indoline-fused cyclobutanes [87], and the platinum-catalyzed 2,3-indoline-fused cyclopentenones [88] depicted in Scheme 14. The mechanism postulated for the first transformation starts with the alkyne activation by gold on **14.1** followed by a [3,3]-rearrangement of the acetoxyl group that leads to the allenyl ester **14.4**. This allene intermediate can, in its turn, be activated by gold producing oxonium ion **14.6** with gold *S-trans* to  $R_2$  in order to minimize allylic strain. Cyclization of this oxonium ion and subsequent trapping of the iminium ion with the alkenylgold affords alkylidenecyclobutane **14.2** stereoselectively.

When the gold catalyst is replaced by platinum, the mechanism changes and a cyclopentene is produced instead, in an uncommon display of divergent reactivity



**Scheme 14** Different reactivity for gold and platinum complexes upon allenyl ester activation. Platinum(II) reacts at the  $\beta$ -position through a carbenoid intermediate while gold(I) acts through the nucleophilicity at the  $\alpha$ -position [87, 88]

between cationic gold(I) and  $\text{PtCl}_2$ . The first steps of the mechanism do not change with respect to the gold version, until oxonium **14.10** (equivalent to **14.6**) is formed. Instead of undergoing a cyclization to an alkylidenecyclobutane, this intermediate proceeds through a 5-*exo* cyclization to the Pt-carbenoid **14.12** that could be interpreted as a 1,3-dipolar cycloaddition. Hydride migration and demetalation afford the cyclopentene product **14.9**.

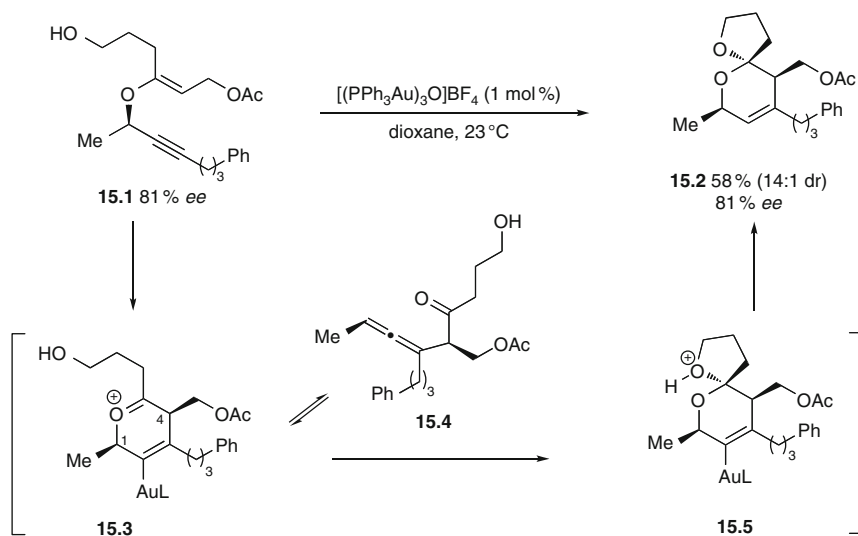
## 6 Nucleophilic Additions

In this section we will address another entry point for gold- or platinum-catalyzed mechanisms: direct attack of a heteroatom nucleophile on the metal-activated alkyne.

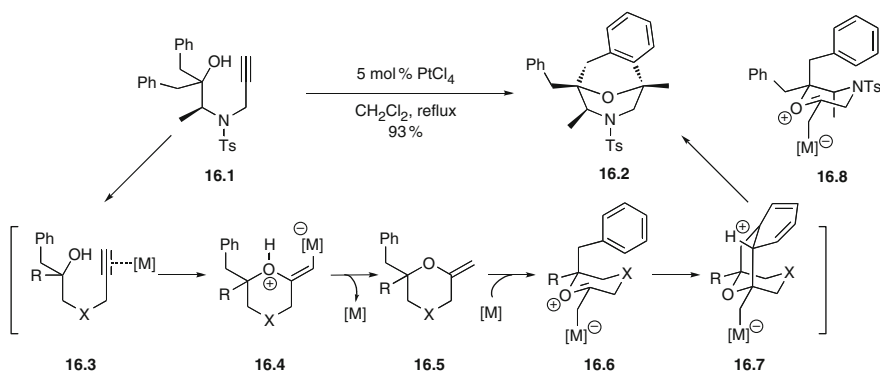
There are plenty of versions of these kinds of processes that proceed in either intra- or intermolecular fashion. In the following lines we will focus on some keynote stereoselective examples that highlight relevant mechanistic issues that can determine their outcome and/or be elevated to the status of general rules or trends.

One of the most popular reactions in this family is the use of metal catalysis to activate alkynes towards the nucleophilic attack of a tethered heteroatom to afford heterocycles in much milder conditions than most alternatives [89, 90]. The nucleophile can be the oxygen of alcohols, carbonyls, carboxylic acids, amides, etc., a nitrogen in amines and amides, a sulfur, etc. Although the field is very active and new reactions still appear every day, methodology has reached maturity, and is of wide applicability nowadays in the synthesis of furans, pyrroles, and thiophenes from heteroatom-substituted propargylic alcohols [91], oxazoles and oxazines from *N*-propargyl carboxamides, [92], pyrazolidines, isoxazolidines and tetrahydrooxazines from hydrazine and hydroxylamine nucleophiles [69], lactones from carboxylic acids [93], oxazolidinones from alkynylamines [94], sulfur heterocycles from sulfoxide-tethered enynes [95], etc.

After the discovery of a gold(I)-catalyzed Claisen rearrangement (6.2–6.3 in Scheme 6), nucleophilic addition to the resultant oxocarbenium intermediate (15.3 in Scheme 15) was proposed as a strategy for the synthesis of dihydropyrans from enol ethers by Serry et al. [75]. However, the capture of this intermediate can be competitive with the rearrangement to the allene 15.4, which would then favor the 5-*exo-dig* cyclization, instead of regenerating 15.3. When the nucleophile used to trap 15.3 is a tethered alcohol, this reaction stereoselectively produces spiroketals (15.2) with complete chirality transfer. This high diastereoselectivity (14:1 d.r.) and complete enantioselectivity can be explained by resorting to two competing mechanisms where the initial Claisen rearrangement determines the relative configuration of C1 and C4 in intermediate 15.3 (see Scheme 15), which, in turn, control either the configuration of allene 15.4 (which then reverts to 15.3 through a Grob-like fragmentation) or that of the final product.



**Scheme 15** Substrate-induced diastereoselective cyclization to dihydropyrans [75]



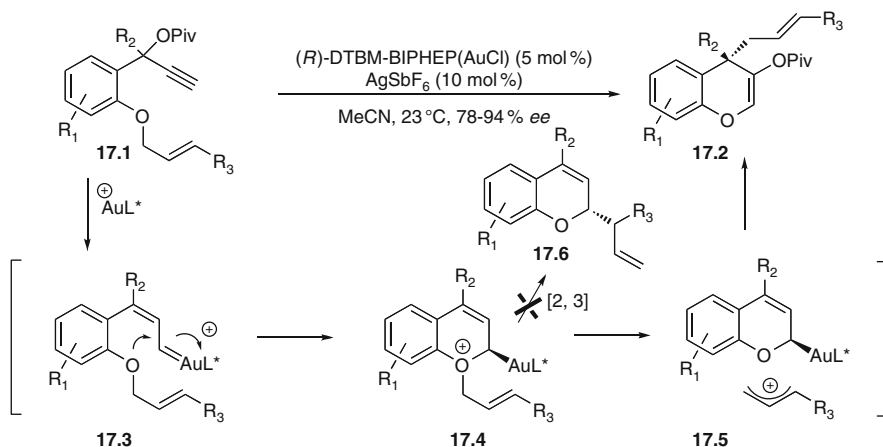
**Scheme 16** Proposed mechanism for the enantioselective gold- or platinum-catalyzed intramolecular hydroalkoxylation–hydroarylation of propargylic sulfonamides [96]

Another example of chirality transfer in more or less straightforward nucleophilic attacks to the activated alkyne is provided by Barluenga et al. in their enantioselective gold- and platinum-catalyzed tandem intramolecular hydroalkoxylation–hydroarylation reactions [96] and the related gold- or platinum-catalyzed tandem hydroalkoxylation–Prins cyclization transformations [97]. When chiral alkynols such as **16.1** (Scheme 16) are used as substrates, the reaction affords in very high yields enantiopure bicyclo[3.3.1]nonanes. The mechanism proposed in Scheme 16 explains the formation of the two new rings through an initial 6-*exo*-cycloisomerization where the nucleophilic alcohol attacks the metal-activated alkyne. Protodemetalation of **16.4** affords the enol ether **16.5**, which upon metal coordination to the C–C double bond is subjected to another nucleophilic attack of the phenyl group. It is in this last step (the formation of **16.7**) that the new stereocenters are generated, with configurations that are determined by the axial disposition of the aryl group needed for the cyclization. Intermediate **16.8** (analogous to **16.6**), with a methyl group in a pseudoaxial position, is the key to this faithful chirality transfer from the stereogenic center in **16.1** to the new centers in **16.2**. DFT calculations show that this intermediate is lower in energy than other conformers with the methyl group in pseudo-equatorial position.

As described for other families of metal-catalyzed reactions, some of these transformations, such as the gold-catalyzed synthesis of pyrazolidines, isoxazolidines, and tetrahydrooxazines by attack of a hydrazine or hydroxylamine nucleophile to an allene, can be made enantioselective by the use of a chiral ligand [69].

## 7 Pericyclic Reactions

Although “pericyclic” is far from the first adjective that comes to mind when referring to transition metal-catalyzed processes, the polyunsaturated compounds that are often used as substrates with gold and platinum complexes generate charged



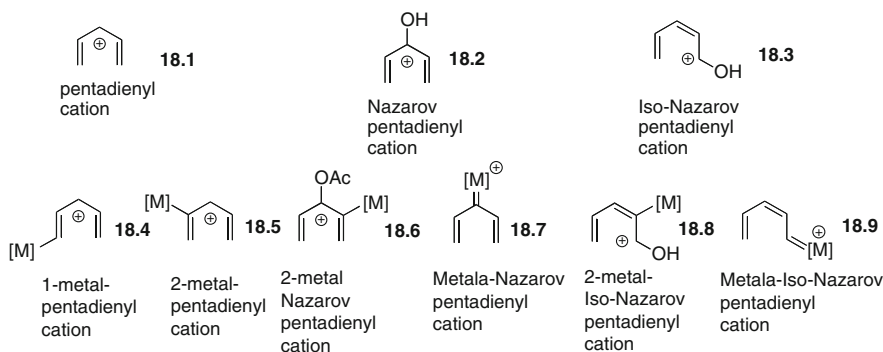
**Scheme 17** Synthesis of enantioenriched benzopyrans by ligand-induced enantioselective  $\text{S}_{\text{E}}2'$  reaction of chiral allylgold(I) intermediates and allyl cations [104]

intermediates that can be assimilated to derivatives of pentadienyl or heptatrienyl cations, vinylallenes, etc. As a result the reactions starting from these intermediates can, in many cases, be considered (at least formally) as pericyclic. Gold activation has revived the already explored rich thermal reactivity of vinylallenes and larger conjugated systems which are both reactants and intermediates in these processes [98, 99]. Several gold versions of pericyclic reactions that start with the activation of enynes [100], diene allenes [101], ene allenes [102], as well as yne allenes [103], have already been described.

An enantiopure phosphine ligand induces the generation of enantioenriched benzopyrans **17.2** containing quaternary stereocenters by carboalkoxylation of propargyl esters **17.1** (Scheme 17). A tandem [2,3]/[3,3]-rearrangement through **17.6** was considered among other mechanisms to explain the rearrangement of the allylic oxonium intermediate **17.4**. This proposal was discarded for not being compatible with the observed reaction of benzylic systems and for the lack of reactivity of unsubstituted allyl ethers. A direct formal [1,4]-sigmatropic rearrangement was also unlikely since substituted systems underwent inversion of the allyl moiety. Therefore, a mechanistic proposal that includes the addition of the nucleophilic allyl ethers toward the electrophilic gold(I)-carbenoid intermediate **17.3** and the reaction of an allyl carbocation with a chiral allylgold(I) intermediate **17.5**, generated from a gold(I)-stabilized vinylcarbenoid, was considered as more likely for this cascade process [104].

The electrocyclic reactions of propargyl-activated systems by noble metal catalysis will be encountered as elementary steps following the formation of conjugated cationic species. Although other variants are possible, the examples described thus far belong to the class of  $4\pi e^-$  electrocyclization reactions of pentadienyl cations and analogous systems (Scheme 18). Depending upon their precursors and method of generation, these systems might contain noble metals in the periphery of the





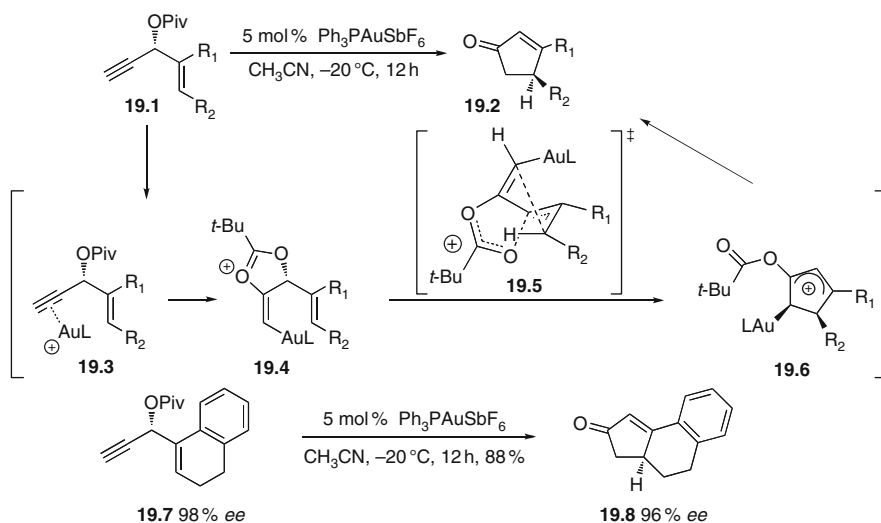
**Scheme 18** Diversity of pentadienyl cations

cyclic array and in these cases the metals stabilize the positive charge either in the pentadienyl cation or in the allyl cation after cyclization. For the discussion that follows, it is convenient to illustrate the structural diversity of the cyclizing species, including the special designation when the noble metal is present at particular locations. Scheme 18 describes the three main variants (resonance forms are not indicated) grouped according to the analogy to the parent pentadienyl cations **18.1**, Nazarov **18.2**, or iso-Nazarov analogs **18.3** [105–109]. The systems differ by the presence of the metal at the termini of the allyl/pentadienyl cation (odd) or at the internal (even) positions. We have already reported computational studies of pentadienyl cation cyclizations [110, 111], as well as metal variants of the Nazarov and iso-Nazarov reactions [18].

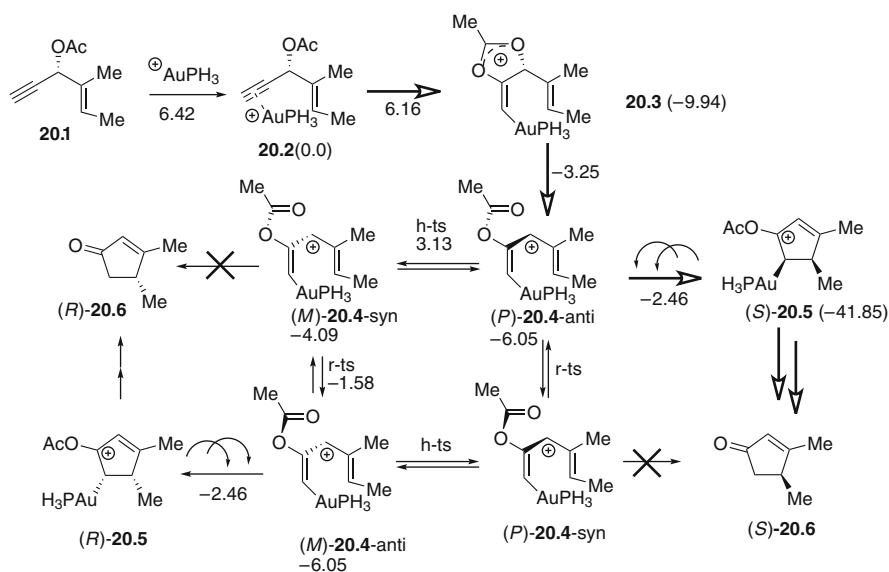
Moreover, since the product of the electrocyclic reaction is another charged system (an allyl/benzyl cation) the cyclopentannulation is usually accompanied by cascade reactions that follow patterns of reactivity typical of (oxo)carbenium ions [112].

The gold version [17] of the Rautenstrauch rearrangement [113] provides a more convenient access to cyclopentenones **19.2** from 1-ethynyl-2-propenyl acetates (pivaloates) **19.1** than the parent Pd-mediated process [113], since the milder condition of the former are compatible with substitutions at the acetylenic and olefinic positions (Scheme 19). Experiments with diastereomerically-enriched substrates already suggested that the stereochemistry of the starting ester influenced that of the product. Moreover, the rearrangement of enantioenriched substrates such as **19.7** (98% *ee*) afforded compounds with preservation of the enantiomeric purity (**19.8**, 96% *ee*). To explain the Au(I)-catalyzed chirality transfer of enantioenriched propargyl pivaloates, it was proposed that the 1,2-acyl migration followed by a C–C bond-forming process takes place either before or in concert with the cleavage of the stereogenic C–O bond as shown in transition state **19.5** in order to avoid the formation of discrete pentadienyl cations [17].

We have computationally examined (Scheme 20) the mechanistic issues of the gold variant of the Rautenstrauch rearrangement [18]. Our results confirm as most likely the formation of a discrete vinylgold intermediate **20.4** upon complete transfer



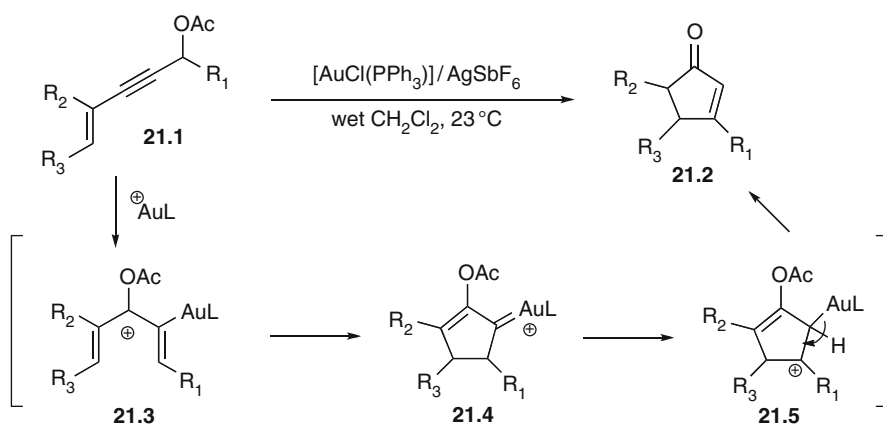
**Scheme 19** Chirality transfer in the gold variant of the Rautenstrauch reaction, showing the proposed involvement of a helical transition state (**19.5**) [17]



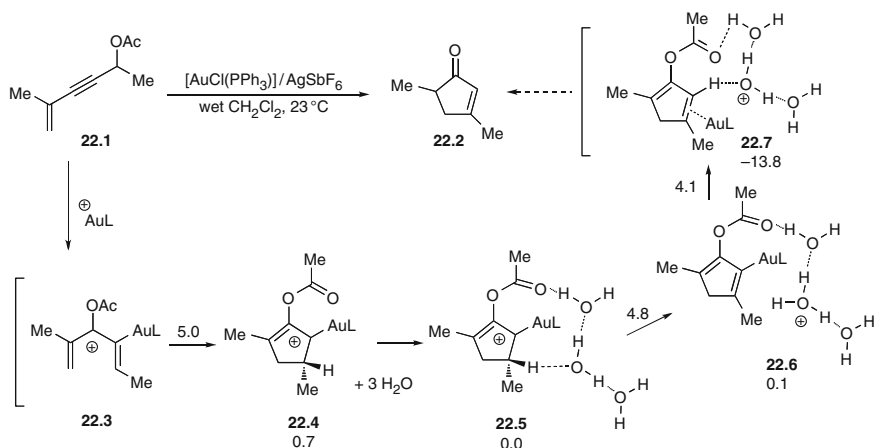
**Scheme 20** Energies (kcal/mol) for the species involved in the center-to-center chirality transfer via enantioenriched (nonracemized) helical pentadienyl cations in the gold variant of the Rautenstrauch reaction [18]

of the acetate (pivaloate) group to the gold-activated alkyne **20.2** by *anti* addition. Since the C–C bond formation event *follows* the Au(I)-induced pivaloyl transfer to the vicinal Csp atom, the chiral information must be preserved on the helicity of the formal 1-aura-2-acetoxypentadienyl cation intermediate **20.4**. This center-to-helix-to-center chirality transfer requires that both the helix interconversion and the pivaloyl rotation should be disfavored relative to cyclization. The calculations are consistent with this scenario: the cyclization of the pentadienyl cation intermediate (*P*)-**20.4**-anti to (*S*)-**20.5** is of lower energy than the conformational changes that can either invert the helicity (**h-ts**) or switch the orientation of the acetate (**r-ts**) from *anti* to *syn*, leading eventually to the cyclopentenone (*R*)-**20.6**, the enantiomer of the experimentally observed product (Scheme 20). Thus, the chiral information present in the original enyne is conveyed through **20.3** to the pentadienyl cation (*P*)-**20.4**-anti, where it is stored in the helicity of the main carbon chain. The concurrent existence of a barrier to cyclization lower than that corresponding to the inversion of the helix (**h-ts**) ensures the faithful transfer of this information to the final product (*S*)-**20.6** (Scheme 20).

The role of AuCl(PPh<sub>3</sub>)/AgSbF<sub>6</sub> as dual alkyne and allene activators allows the preparation of 2-aura-pentadienyl cations **21.3** via Au(I)-catalyzed tandem [3,3]-rearrangement of enynyl acetates **21.1** and the in situ generated allenyl acetate (Scheme 21). Electrocyclic ring closure of **21.3** forms the gold-stabilized cyclopentenyl cation **21.4**, or its Au carbenoid form, which undergoes regioselective [1,2]-hydride shift or E1-type elimination assisted by H<sub>2</sub>O, and deauration/protonation of the alkenylgold intermediate **21.5**. The sequence allows the preparation of cyclopentenones **21.2** from enynyl acetates **21.1** via tandem Au(I)-catalyzed [3,3]-rearrangement and 2-aura-Nazarov reaction. Moreover, the presence of the noble metal drives the position-controlled synthesis of cyclopentenones due to the stabilization of the intermediate allyl cation, thus solving one of the main limitations of the Nazarov cyclization [114].



**Scheme 21** Synthesis of cyclopentenones from enynylacetates by 2-aura-Nazarov cyclization reaction [114]

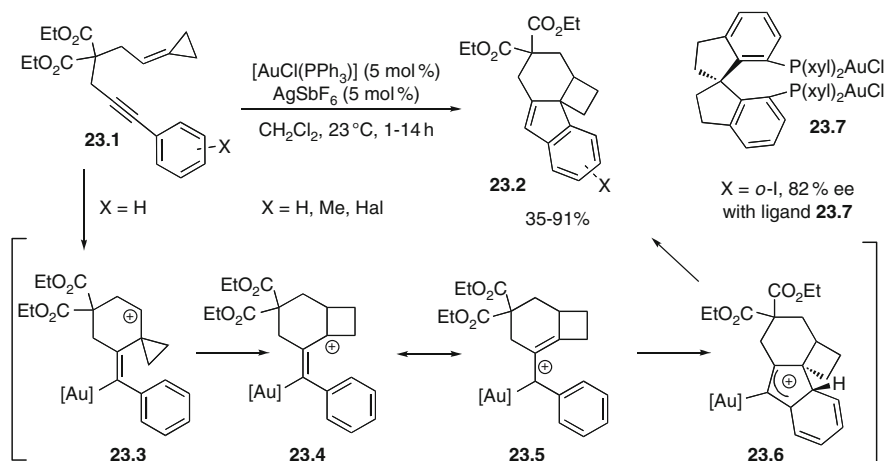


**Scheme 22** Computationally-based proposal for the effect of water cluster in the [1, 2]-H shift of the gold-carbenoid intermediate (energies in kcal/mol) [116]

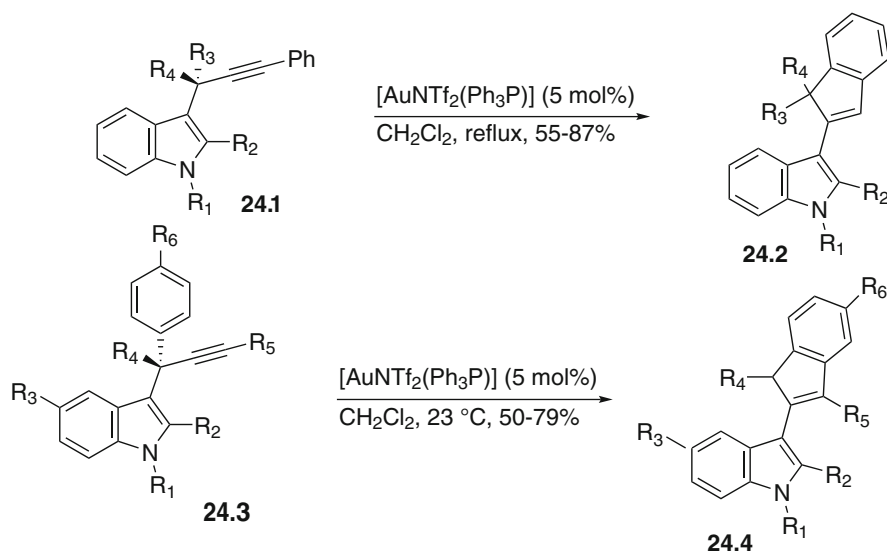
DFT calculations (Scheme 22) confirmed the general mechanism proposed and helped clarify the intriguing role of water in this process, which has also been documented in other gold-catalyzed rearrangements [115]. In addition to showing that the [3,3]-rearrangement can occur stepwise with activation free energies below 10 kcal/mol for each step, the calculations predict an energy of activation for the water-mediated 2-aura-Nazarov electrocyclic ring-closure reaction of only 3.2 kcal/mol in  $\text{CH}_2\text{Cl}_2$  (5.5 kcal/mol in gas phase). The [1,2]-hydride shift becomes then the rate-limiting step, with a computed activation free energy of 20.2 kcal/mol in anhydrous  $\text{CH}_2\text{Cl}_2$ , 16.4 kcal/mol when water is present and 13.0 kcal/mol with a three-water cluster as the catalyst. Water was proposed to mediate an enzyme-like proton shuttle occurring in a two-step deprotonation/protonation process (via **22.5** and **22.6**), with the acetoxy group in the substrate acting as either a proton acceptor when one water molecule is involved or a proton relay stabilizer with a water cluster [116].

The aura-Nazarov cyclization has been proposed as key step in the rearrangement with ring expansion promoted by gold(I)/silver(I) catalysts of aryl ynylidene-cyclopropanes **23.1** [117]. In this occasion, the 6-*exo*-dig cyclization of the activated alkyne by addition of the alkylidenecyclopropane affords the cyclopropylcarbiny cation **23.3**, possibly stabilized through back-bonding from gold. The ring expansion generates the bridgehead carbocation **23.4**, which exhibits the electronic features of a substrate for the gold version of the Nazarov reaction (Scheme 23). Tetracycles **23.2** are obtained in good to excellent yields as single diastereomers, and enantioenriched when a chiral nonracemic gold catalyst (*R*)-xylSDP( $\text{AuCl}$ ) $_2$ /AgSbF $_6$  **23.7** is used.

In certain substrates, the noble metal variants of the  $4\pi\text{-e}^-$  electrocyclic reactions can enter into competition. Sanz et al. found that upon treatment with the bis(trifluoromethanesulfonyl)imide triphenylphosphine gold complex  $[\text{AuNTf}_2(\text{Ph}_3\text{P})]$ , a propargylic



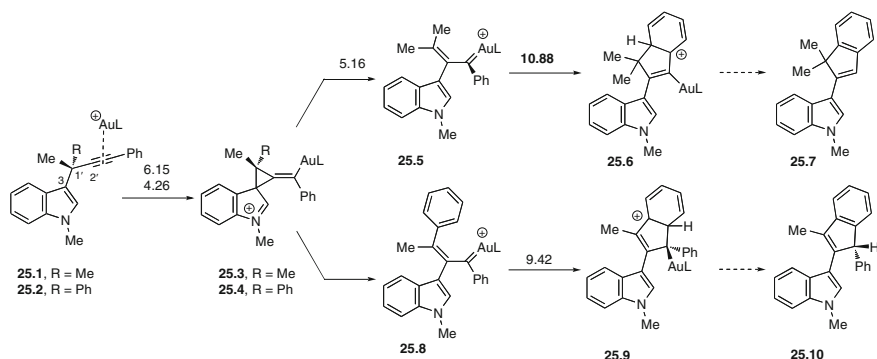
**Scheme 23** Involvement of alkylidenecyclopropanes in the capture of gold-activated alkynes and aura-Nazarov cyclization [117]



**Scheme 24** Gold-induced migration of indole rings in propargylic systems [35]

indole group could undergo a [1,2]-migration reaction similar to that of propargylic carboxylates or propargylic sulfides. Depending upon the presence of an aryl or an alkyl group at the propargylic position, 3-(1*H*-inden-2-yl)-1*H*-indole **24.4** or 3-(inden-2-yl)indole **24.2** were selectively obtained (Scheme 24) [35].

Our computational studies with model systems confirmed the proposed overall mechanistic picture, summarized in Scheme 25. It comprises three major steps: (1)



**Scheme 25** Computational support (energies in kcal/mol) for the gold-induced migration of indole rings in propargylic systems [118]

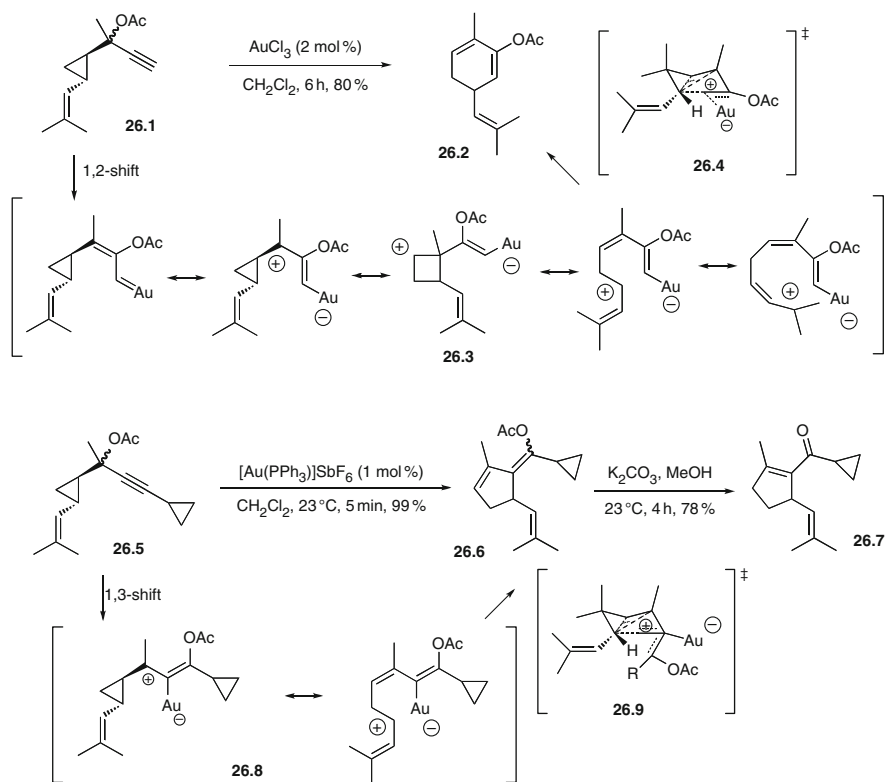
the electrophilic addition of the gold-activated alkyne to the indole ring with formation of an alkylidenecyclopropane intermediate, (2) its further evolution by torquoselective ring opening to a gold carbocation/carbenoid, and (3) the  $4\pi e^-$ -electrocyclic ring closure of the gold-stabilized carbocation species following alternatively the gold variants of the Nazarov or iso-Nazarov reactions [118].

Starting from **25.1** and **25.2**, the cascade process starts with capture at C2' of the gold-activated alkyne by nucleophilic attack of the indole C3 position, resulting in the formation of a new C—C bond through an early transition state of low-energy (4.26 kcal/mol for **ts25.1** and 6.15 kcal/mol for **ts25.2**). The alkylidenecyclopropane intermediate **25.4** (featuring an elongated C3—C1' bond length of 1.62 Å), which could be characterized for the model system with alkyl substituents, rapidly undergoes C3—C1' scission. Intermediate **25.4** is then connected to the aura-“carbenoid” **25.5** through **ts25.4** in the rate-limiting step of the tandem rearrangement. In this transition state the alkylidene group on the cyclopropane ring smoothly rotates to avoid the steric interaction between the phenyl and the indole rings in **25.5**. This rotation of the C1'—C2'—C3'—Ph dihedral is coupled with the ring opening in **25.4** and this rearrangement determines both the helicity (*P* from the arbitrary configuration of **25.2**) and the *Z* geometry of the olefin in the gold-containing pentadienyl cation. The aura-Nazarov process from **25.5** to **25.6** benefits from the proximity of the C1'—C2' olefin and the terminal phenyl group in the conformation adopted by **25.5** after the indole migration is complete and occurs with a 10.88 kcal/mol reaction barrier.

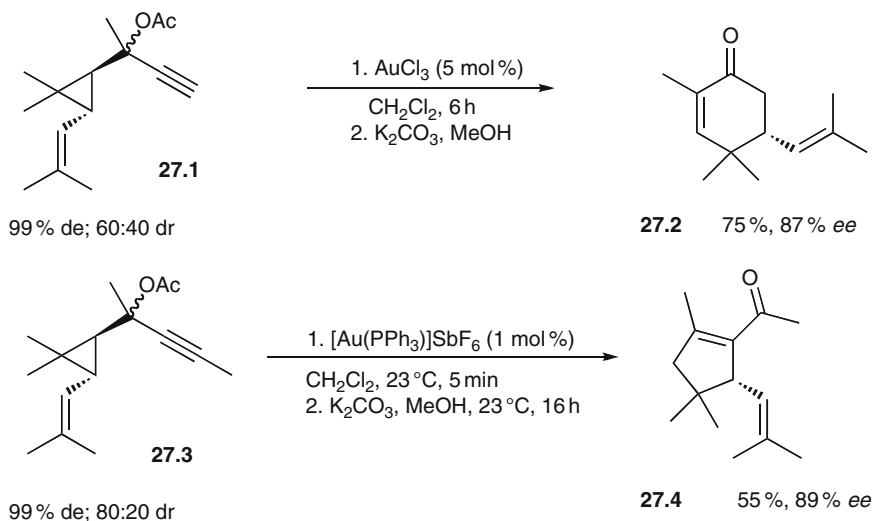
The evolution of **25.8** takes place by aura-iso-Nazarov cyclization, the alternative electrocyclic ring closure involving the phenyl ring *cis* to the gold-containing carbon atom within the gold-stabilized  $\alpha,\beta$ -unsaturated pentadienyl cation. This intermediate features a *Z* double bond and an *s-cis* conformation of the adjacent bond due to the torquoselective outwards rotation of the bulky phenyl group on C1' in the 4-electron ring opening of **25.4**. This rotation of the bulky phenyl group away from the indole, after the initial anti- $\pi$  gold alkyne coordination, can easily be ascribed to

steric effects. The computed energy values for these transition states confirm that the *aura*-iso-Nazarov is favored over the alternative *aura*-Nazarov reaction channel available from the twisted *s-cis* conformation of **25.8**. The energy barrier for the favored cyclization of **25.8**, 9.42 kcal/mol, is 2.29 kcal/mol lower than the alternative ring closure that would involve the external Ph group (11.71 kcal/mol). Moreover, it is 3.67 kcal/mol more favorable than yet another *aura*-iso-Nazarov reaction available from the initial *syn* coordination of gold to the alkyne.

In order to expand the range of applications of the Rautenstrauch reaction and obtain five-, six-, and also seven-membered-ring vinyl acetates, the homologous Au-catalyzed rearrangement of 1-cyclopropyl tertiary propargylic esters was studied by Nevado et al. [119, 120]. At the outset the presence of a cyclopropyl ring could stabilize nonclassical carbonium ions as intermediates (see resonance structures **26.3** and **26.8**) and therefore provide ring systems from 5 to 8 atoms (Scheme 26). However, the process is selective and provides cyclohexadienyl acetates **26.2** from terminal propargylic acetates **26.1** and acetoxy-alkylidene cyclopentenes **26.6** from the internal counterparts **26.5** [119, 120].



**Scheme 26** Divergent homo-Rautenstrauch reactions [119]

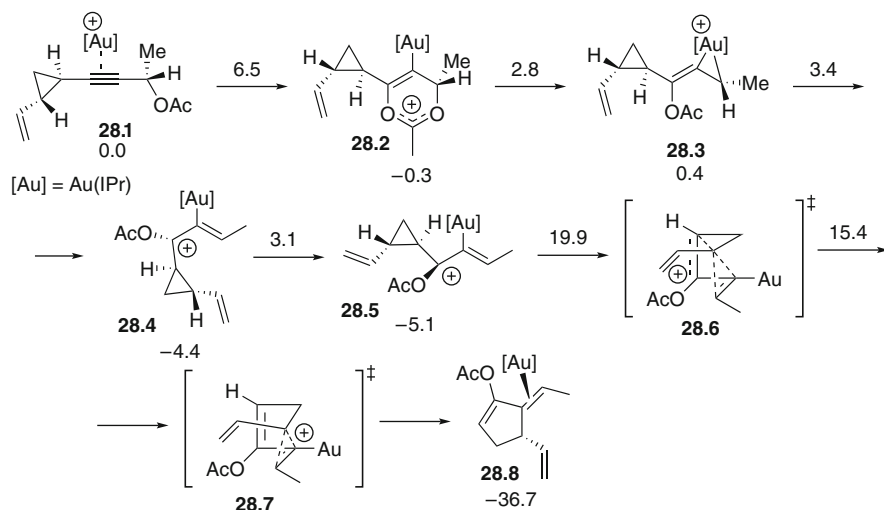


**Scheme 27** Enantioselective and divergent homo-Rautenstrauch reactions [119]

Moreover, optically active substrates **27.1** and **27.3** (99% ee) underwent cycloisomerization using  $\text{AuCl}_3$  or  $[\text{Au}(\text{PPh}_3)]\text{SbF}_6$ , respectively, as the catalyst to provide after methanolysis (*R*)-**27.2** (87% ee) and acetylcyclopentenone (*R*)-**27.4** (89% ee) with good chirality transfer. The authors disfavor mechanisms of chirality transfer under the control of the stereogenic propargyl ester unit as reported for the systems above [18], since other stereocenters present in the substrates might impact on the stereochemical outcome. Alternatively, the participation of species (carbene, nonclassical carbonium ion complex or vinyl/gold unit species as the intermediate) that display a certain configurational stability and store the stereochemical information throughout the reaction before transfer to the product upon cyclization, was proposed (Scheme 27).

Based on these precedents, the gold-induced rearrangement of the related 3-cyclopropyl propargylic carboxylates **28.1** (Scheme 28) provided 5-(*E*)-alkylidene cyclopentenyl acetates in a highly stereocontrolled manner [120]. The selection of substituents at the cyclopropyl ring provided the handle to favor the cyclopentannulation over the formation of  $\alpha$ -ylidene- $\beta$ -diketones following acetate fission, first reported by Zhang et al. [121]. DFT calculations support the intermediacy of gold-stabilized “nonclassical carbocationic” (carbonium ion) species and revealed the intrinsic stereospecific nature of these processes (Scheme 28). According to the calculations presented in Scheme 28, the formation of an “allene” structure with gold coordinated to the more external double bond and the four allenyl substituents disposed perpendicularly, and its isomerization to the internally-activated position with gold coordinated to the central carbon atom of the allene are easily affordable for secondary propargylic acetates **28.1**. The cyclization to the alkylidene cyclopentenyl acetate from **28.5** involves two adjacent transition





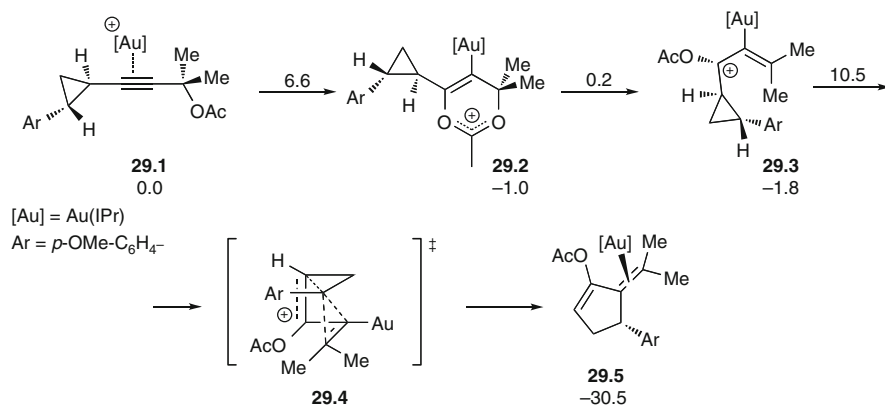
**Scheme 28** Computational proposal (energies in kcal/mol) for the mechanism of the homo-Rautenstrauch reaction of secondary propargylic acetates [120]

states without any discrete intermediate in the reaction profile. The first transition state, which is higher in energy (19.9 kcal/mol) leads to species **28.7** that can be described as a gold-stabilized nonclassical carbocation. Furthermore, the geometry of the alkylidene olefin is under kinetic control. Computations on the alternative diastereomeric transition states confirmed this outcome, although the *E* product (**28.8**) is also thermodynamically more stable.

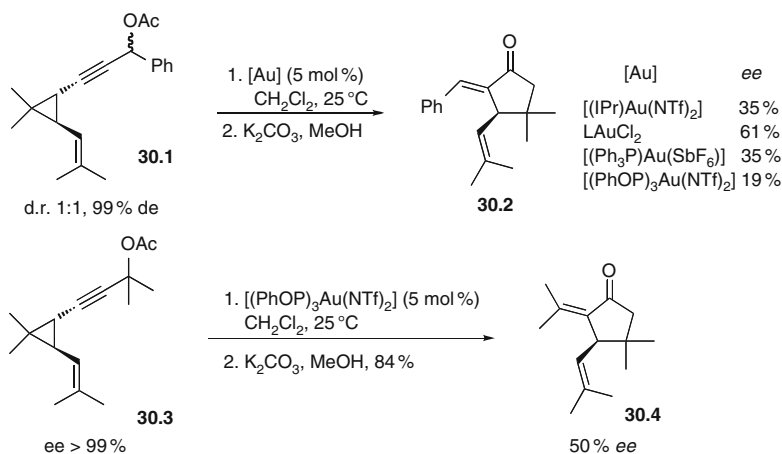
For the tertiary acetate **29.1** the steric hindrance caused by the presence of two methyl groups at the propargylic position makes competitive the mechanisms along the 1,3- and 1,2-migration paths (Scheme 29).

In principle the reaction should be stereospecific since the ring opening of the cyclopropyl ring via gold-stabilized carbocations takes place with retention of configuration. However, in contrast with the results of the 1-cyclopropyl propargyl acetates positional isomers (Scheme 27), the cycloisomerization of enantioenriched secondary and tertiary substrates **30.1** and **30.3** (d.r. 1:1, 99% *de*) with a variety of gold complexes afforded, after methanolysis, alkylidenecyclopentanones **30.2** and **30.4**, respectively, in 61% *ee* in the best case (Scheme 30). The failure to achieve complete chirality transfer starting from enantiopure substrates was ascribed to a competing gold-triggered cyclopropyl ring opening/ring closure prior to the cyclization event. Mauleón et al. also showed that scrambling in the *cis*-1-cyclopropyl propargyl acetates (but not in the *trans* isomers) at both propargyl and cyclopropyl positions takes place before the cyclization is complete [122].

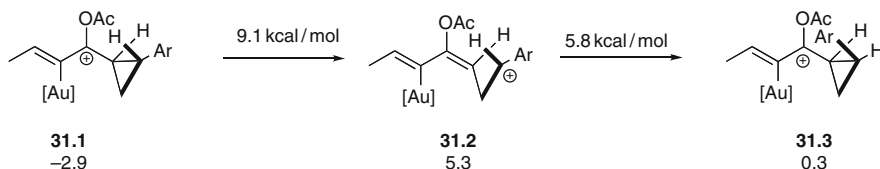
A computational study shed some light onto the configurational instability of the intermediates. Cyclopropyl ring opening provides the high-energy intermediate **31.2**, which, upon C–C rotation, generates the *cis* isomer with activation barriers comparable to those of the cyclopentannulation process (Scheme 31). Therefore,



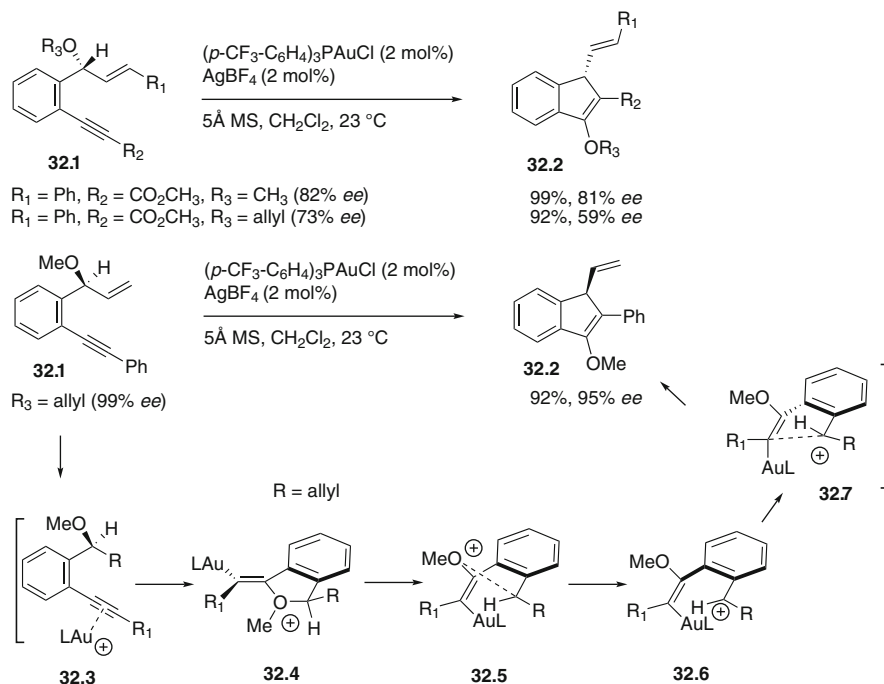
**Scheme 29** Computational proposal (energies in kcal/mol) for the mechanism for the homo-Rautenstrauch reaction of tertiary propargylic acetates [120]



**Scheme 30** Incomplete transfer of chirality for the homo-Rautenstrauch reaction of propargylic acetates [120]



**Scheme 31** Computational proposal (energies in kcal/mol) for the Incomplete transfer of chirality in the homo-Rautenstrauch reaction of propargylic acetates [120]

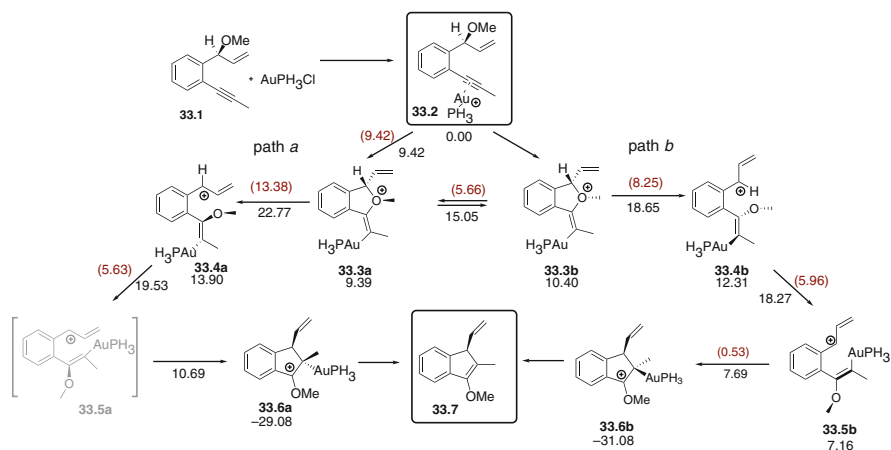


**Scheme 32** Intramolecular carboxyalkoxylation of alkynyl ethers, with memory of chirality, to indenylethers [123]

although the cycloisomerization is an intrinsically stereospecific process, a competitive epimerization at the cyclopropyl moiety via species such as **31.2** can erode the chirality transfer of these transformations.

Toste et al. described an intramolecular carboalkoxylation of alkynyl ethers (**32.1**) by trapping with a benzyl alcohol the activated alkyne to afford a vinylgold intermediate and providing an entry into functionalized indenyl ethers from benzylic ethers, thus avoiding other less-productive pathways such as protonation (Scheme 32). Interestingly, enantioenriched indenyl ethers were obtained by memory of chirality of the stereogenic benzyl center. The cyclization of a helical gold allyl benzyl cation **32.7** was proposed to explain the stereoselective rearrangement [123].

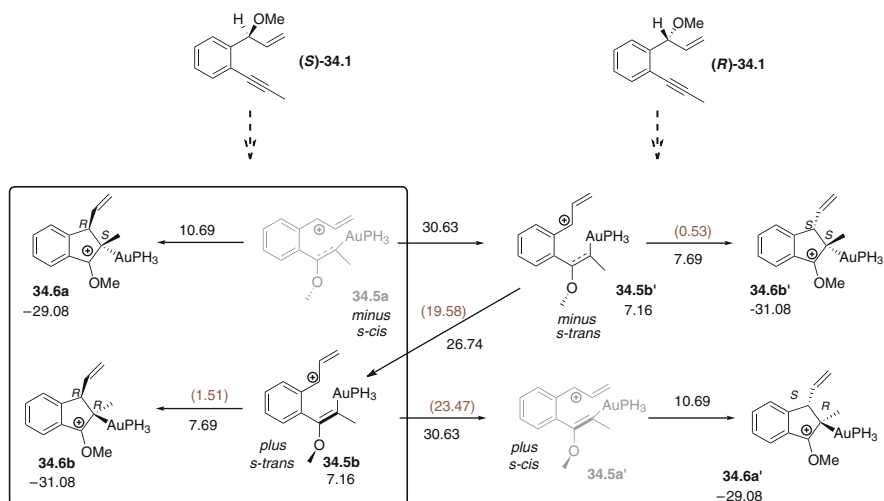
Our computational analysis of the reaction mechanism revealed unexpected avenues (Scheme 33) [124]. The Z cationic gold-alkylideneisobenzofuran intermediate **33.3** is formed first by addition of the alkoxy oxygen in **33.2** to the *syn*-coordinated gold-activated alkyne. This intermediate advances in the cycle through the *b* branch in Scheme 33, since the combined barriers for the interconversion of the two conformers (**ts33.3a**–**33.3b**) and for the C<sub>3</sub>–O bond cleavage on **33.3b** (**ts33.3b**–**33.4b**) are 4.12 kcal/mol lower than the barrier for the corresponding bond cleavage in **3a** (**ts33.3**–**33.4a**). Thus pentadienyl cation **33.4b** with the *minus* helix and *out* vinyl group arises by bond rotations upon the opening of intermediate



**Scheme 33** Memory of chirality in the carboalkoxylation of alkynyl ethers mediated by gold(I) catalyst showing the key conformational and helical stereogenic elements [124]. Relative energies and activation energies (the letter in parenthesis) are noted in kcal/mol

**33.3b** in the rate-limiting step in the mechanism (low barrier of 8.25 kcal/mol). The preferred clockwise rotation (about 110°) of the C<sub>5</sub>–C<sub>6</sub> bond of **33.4b** results in a formal inversion of the helix (now the methoxy group is replaced by the vinyl gold as part of the helix, and **33.5b** sports a *plus* helicity) and leaves the *in*  $\sigma$ -gold-coordinated alkene in the appropriate conformation for subsequent bond formation. A conrotatory four-electron electrocyclozation or the nucleophilic attack of an electron-rich alkene on an allyl–benzyl cation, both favored by the helical conformation of **33.5b**, are feasible mechanisms for an almost barrierless cyclization (0.53 kcal/mol for **ts33.5b–33.6b**). Our previous results on the effect of a donor substituent on C<sub>6</sub> (OMe) and an alkene on Nazarov-like reactions are consistent with these findings [110, 111]. Likewise, previous computations on the iso-Nazarov cyclization in hydroxyheptatrienyl cations justify the torquoselectivity (preference for **ts33.5b–33.6b** over **ts33.5a–33.6a**) as a result of the destabilizing effect of an *inwards* vinyl substituent on one terminus of the cyclizing pentadienyl cation [110].

This system of chirality transfer is robust, and relies on the interplay between both the helicity of the pentadienyl cation intermediate and the *s-cis* or *s-trans* conformation of the allyl substituent. The *plus* helix in **34.5b**, which is a result of the *minus* helix in **34.4b**, which stems in its turn from the puckering of the alkylideneisobenzofuran ring in **34.3b**, determines the rotation taking place at the cyclizing termini and the *R* configuration of C<sub>7</sub> in **34.6b** as a result (Scheme 34). For a given rotation (that is, for a given helix), the configuration of C<sub>3</sub> will depend on the conformation of the allyl group, with *s-trans* and a *plus* helix leading to *R* configuration at C<sub>3</sub>. The opposite configuration of both elements results in the same enantiomer after the release of gold. However, the inversion of only one of the elements, namely a rotation of the C<sub>2</sub>–C<sub>3</sub>–C<sub>4</sub>–C<sub>5</sub> dihedral (switch from *s-cis* to *s-trans*) or an inversion of the pentadienyl cation helicity through a planar transition



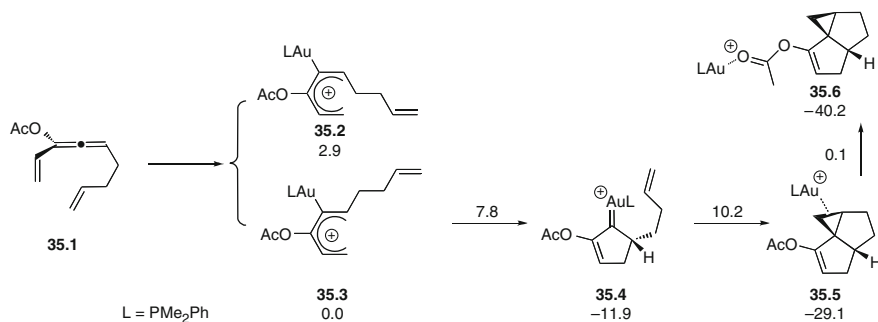
**Scheme 34** Key energy barriers (in parenthesis) and relative energies (in kcal/mol) for helix inversion and conformational change that guarantee the memory of chirality in the carboalkoxylation of alkynyl ethers mediated by gold(I) [124]

state on **34.4** or **34.5**, would result in the loss of optical purity of the reactants. The high activation energies of these two processes ensure the fidelity of the chiral information flow from **34.1** to **33.7** via **34.6b** [124].

## 8 Complex Reaction Cascades

Malacria et al. developed a new synthesis of polycyclic compounds from propargyl acetates and vinyl allenes involving up to three Au(I)-catalyzed elemental steps: [3,3]-rearrangement, 2-aura-Nazarov reaction, and electrophilic cyclopropanation (Scheme 35). The mechanistic rationale, supported by DFT computations, starts with the isomerization of propargyl acetates to 3-acetoxy 1,2,4-trienes followed by coordination of gold to the allene to give the substrate for the 2-aura-Nazarov as a mixture of diastereomers (**35.2** and **35.3**), with the alkyl-out isomer more stable by 2.9 kcal/mol than the in counterpart. The acetoxy 2-aura-Nazarov cyclization leads to a gold-carbenoid **35.4** via a transition state that is located 7.8 kcal/mol above the starting pentadienyl cation **35.3**. The concerted electrophilic cyclopropanation requires 10.2 kcal/mol and affords stereoselectively compound **35.5**. Migration of gold to the acetoxy group is barrierless, and the sequence is completed by decomplexation from **35.6** to recycle the catalyst [125].

The structure of these gold-activated allene complexes has been much debated, and their consideration as allyl cations (pentadienyl cations for vinylallenes), bent allenes, or other resonance forms has been proposed [125, 126]. DFT computations



**Scheme 35** Computed energy values (in kcal/mol) for the 2-aura-Nazarov and cyclopropanation reactions of ene acetoxo-vinylallenes [125]

predict that the 2-aura-Nazarov cyclizations connect the gold carbenoid to a nonplanar species complexed at C2 [126]. Moreover, the rate of racemization of the allene through inversion of configuration occurs via planar transition states that are more difficult to reach when the allenes are more substituted [126]. Allylic interactions disfavor planar conformations for these species so the chiral information should be preserved in the chiral axis of the vinylallene intermediates.

These studies also revealed that only two (out of the four possible) diastereomeric bent allene structures with *anti* orientation of the vinyl group relative to gold are competent in the 2-aura-Nazarov cyclization and lead to the same enantiomer via torquoselective ring closure in opposite directions. Therefore, enantioenriched ene vinylallenes appropriately substituted can afford tetracyclic products with good transfer of chirality. Likewise, the precursor propargylic substrates also undergo enantioselective cycloisomerizations (Scheme 36) [126].

Additional computational studies revealed the structural factors affecting the mechanistic dichotomies in these ene vinylallenes (Scheme 37). The coordination of gold to vinyl allenes may give rise to two types of reactive complexes, **37.6** and **37.2**, which will enter into competition to follow an electrocyclic reaction (and hence cyclopropanation and  $\beta$ -hydride elimination) or a [4 + 2] cyclization, respectively [127]. Cycloaddition of the tetrasubstituted allenes with monosubstituted olefins generates bicyclic compounds **37.3** via concerted asynchronous gold-catalyzed processes. For the pentadienyl cations, the formation of a cyclopentenylidene gold species is followed by diastereoselective intramolecular cyclopropanation giving **37.9** with a short tether, but may also give rise to compounds of type **37.8** via  $\beta$ -elimination with a longer alkyl chain.

Relative energy values for the unsubstituted model system are shown in Scheme 37. Computations predict that the 2-aura-Nazarov reaction is rather insensitive to the length of the tether, but it is favored with a substituent at the enyne. The stability of the gold-activated allene that reacts via [4 + 2]-cycloaddition also depends upon the substitution pattern and increases for R<sub>2</sub> = Me. The transition states for the 2-aura-Nazarov reaction are much lower in energy than those of the intramolecular Diels–Alder cycloaddition, which is consistent with the failure to

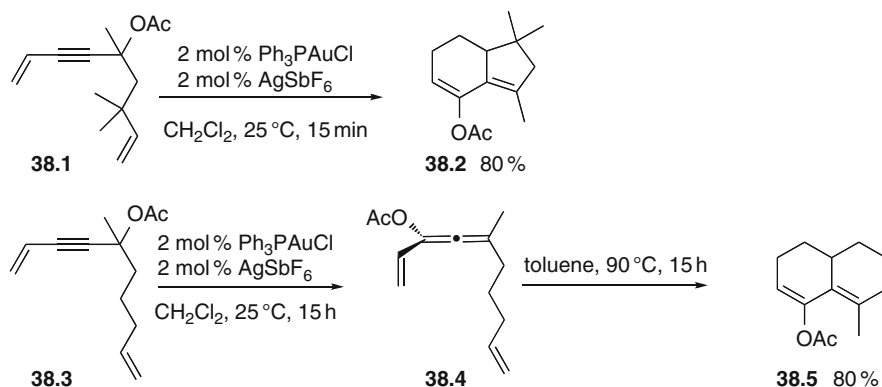


carbon in the tether and no *gem*-dimethyl substitution, to cyclize under the gold-catalyzed conditions (Scheme 38). Heating the acetoxyvinylallene **38.4** in toluene to obtain **38.5** provided an indirect evidence of its mediation in the formation of the bicyclic product [127].

Computations provided quite similar barrier heights of  $\sim 23$  kcal/mol for several  $[4 + 2]$ -cycloaddition processes irrespective of the length of the tether ( $n = 1$  or 2) or the substitution at the allene ( $R_1$ ) or at the internal carbon of the 1,3-diene ( $R_2$ ) by methyl groups. The transition states (**ts37.6**, Scheme 37), where gold is coordinated at the terminal double bond of the 1,3-diene, revealed an almost concerted asynchronous cyclization with formation of the bond between the external carbons of the substrate preceding the one at the internal allene carbon.

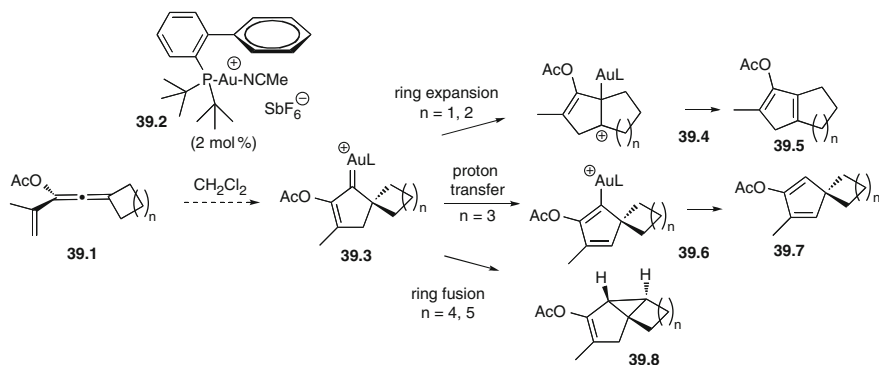
Other competing reactions were discovered upon activation of ene vinylallenes with gold catalysts [127]. The ring expansion to **39.5** by carbocation 1,2-rearrangement and the ring fusion to **39.8** are also available to the same cyclopentenylidenes intermediates **39.3** and their occurrence depends upon the ring size (Scheme 39). Ring expansion by 1,2-rearrangement of the carbenium ion is favored with small rings ( $n = 1$  or 2), as also reported by Toste and coworkers [128]. With larger rings ( $n = 4$  or 5), ring fusion by unusual 1,3-C–H insertion to give **39.8** is observed. Lastly, with a six-membered ring ( $n = 3$ ), a proton transfer gives rise to a spiro-cyclopentadiene **39.7**. DFT computations for the ring fusion and ring expansion agree well with the findings. For model systems using  $\text{Au}(\text{PMe}_3)^+$  as activator the transition state energy for the ring fusion path increases from 16.4 to 29.6 kcal/mol whereas those corresponding to ring expansions decrease from 26.0 to 11.9 kcal/mol as the ring size decreases. For large systems ( $n = 3$ ), the activation energies are similarly high (above 22 kcal/mol), thus allowing the alternative protodeauration to occur [127].

Sarpong et al. developed an efficient synthesis of cyclopentenones **40.2** containing a tertiary stereocenter from epoxide propargylic esters **40.1** using  $\text{PtCl}_2$ .

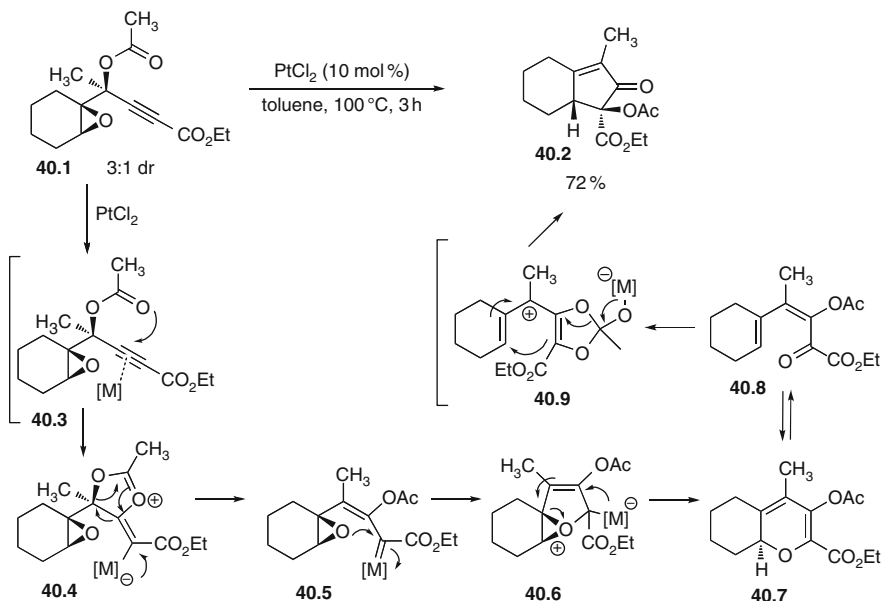


**Scheme 38** Selective intramolecular Diels–Alder cycloaddition of tertiary propargylic acetates and isolation of the ene acetoxy-vinylallenes intermediate [127]





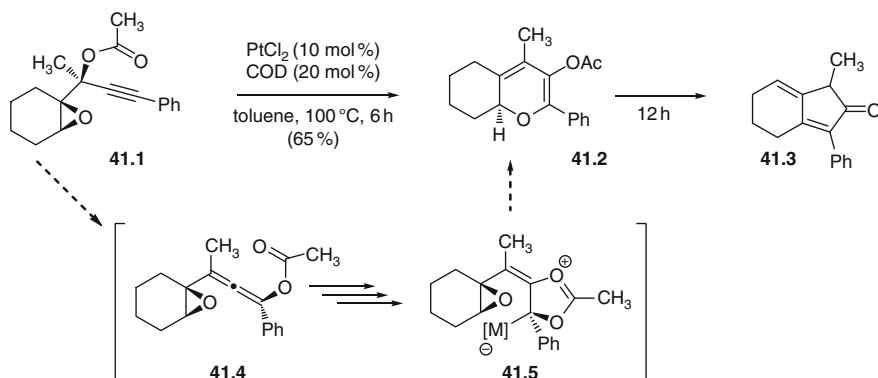
**Scheme 39** Competing reactions of acetoxy-vinylallenes upon gold(I) activation [127]



**Scheme 40** Platinum(II)-catalyzed rearrangement of epoxide propargyl acetates to cyclopentenones [129]

This unprecedented pentannulation (Scheme 40) was conceived to result from a Pt-catalyzed 5-*exo*-dig cyclization to afford zwitterion **40.4** or metallocarbenoid **40.5**, which is then captured by the epoxide affording the strained intermediate **40.6** which rapidly evolves to 2*H*-pyran **40.7**, in equilibrium with the ring-opened tautomer **40.8** via an oxa-6 $\pi$  electrocyclization [129].

In fact, intermediate 2*H*-pyran **41.2** was isolated in one case (Scheme 41), thus lending support to the proposed mechanism up to this point. The subsequent

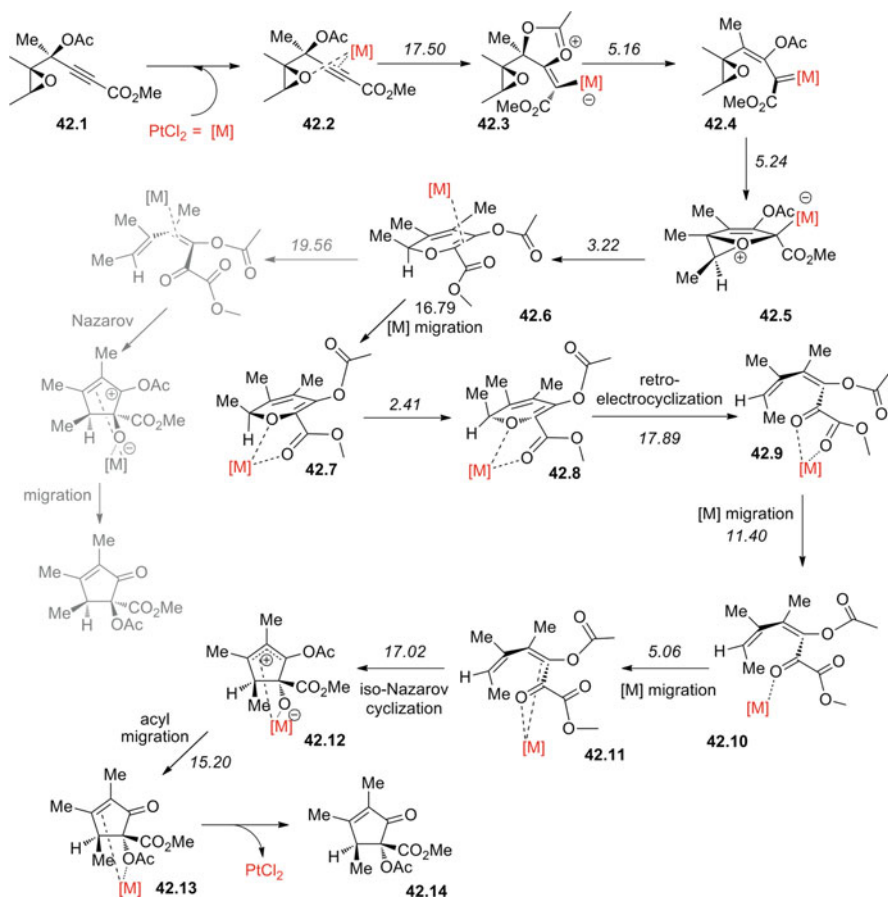


**Scheme 41** Involvement of 2*H*-pyran intermediates in the platinum(II)-catalyzed rearrangement of epoxide propargyl acetates to cyclopentenones [129]

cyclization of the acetoxy dienone **40.8** to the pentannulated product **40.2** was considered as a variant of a stereoselective conrotatory  $4\pi e^-$  electrocyclic ring closure with concomitant acyl shift via the presumed intermediate **40.9** (Scheme 40) [129].

Our examination of the mechanism of this reaction confirmed the overall picture proposed by Sarpong, and moreover revealed other subtle factors that impinge on the stereoselectivity of the transformation and the potential transfer of chirality (Scheme 42). The cascade reaction starts with the formation of a  $\pi$  complex between PtCl<sub>2</sub> and **42.1**, a species **42.2** with the metal coordinated simultaneously to the alkyne and to the oxirane oxygen. Acyloxy 1,2-migration provides platinum carbenoid species **42.4**. The intramolecular nucleophilic attack of the oxirane leads to the bicyclic oxonium ion **42.5** that undergoes a facile ring expansion to 2*H*-pyran **42.6** [130].

Of particular interest in our proposal is the occurrence of a series of conformational changes and metal migrations with non-negligible barriers, which are critical for the stereochemical analysis. The chiral information in the two stereogenic carbons of the oxirane in **42.1** determines both the configuration of the stereocenter in **42.6** and the coordination of platinum on the  $\beta$  side of the flat dihydropyran ring. A direct retro-electrocyclization reaction on **42.6**, that could be followed by a Nazarov-like ring-closing of the resultant pentadienone, would involve a reaction barrier of 19.56 kcal/mol (or 19.71 kcal/mol if there is no coordination to platinum) and afford a diastereomer of the reaction product (path shown in light gray in Scheme 42). At this point of the mechanism, two factors arise that suggest an alternative pathway: the most stable conformation for the 2*H*-pyran ring is **42.8**, with PtCl<sub>2</sub> coordinated to the 2*H*-pyran and carboxyl oxygens (instead of one of the unsaturations), and this coordination also leads to the lowest barrier for the retroelectrocyclization. This coordination of the metal makes **42.8** deviate from planarity with a 2*H*-pyran oxygen with larger  $sp^3$  character that induces a ring puckering that places the methyl substituent on the stereogenic center in a pseudoaxial conformation. This axial conformation of the methyl group minimizes the



**Scheme 42** Complexity in number of steps and noble metal multiple roles in the platinum(II)-catalyzed rearrangement of epoxide propargyl acetates to cyclopentenones [130]

1,2-allylic strain found in planar **42.6** and is the key element in the memory of chirality in the overall transformation. Thus, the configuration of this stereogenic center, together with the associated “downwards” ring-puckering, result in the inwards rotation of the methyl group upon ring-opening and a *plus* helix in the dienone **42.9**. This helicity of a formally planar intermediate is then preserved in a series of metal migrations on the dienone scaffold from **42.9** up to **42.11** (since the steric strain of the corresponding planar transition structures precludes its inversion) and determines the preferred platinum-assisted iso-Nazarov conrotation of **42.11** to afford the heavily substituted cyclopentenyl cation **42.12** with a determined relative configuration of its two stereocenters.

Product **42.14** is then obtained after acetyl migration and demetalation on **42.12**. Besides the generation of a key C–C bond, the iso-Nazarov reaction determines the configuration of the stereogenic centers in the product. A single diastereomer of

**42.12** is formed from the helicity of **42.11** and the adherence to the conrotatory paths for a four-electron process predicted by the Woodward–Hoffmann rules.

Of special relevance is the persistence of this helical conformation through all the changes between **42.9** and **42.11**, which can be traced back to the configuration of the starting oxirane **42.1**. Thus, the chiral information in **42.1**, apparently lost upon the nucleophilic attack in **ts42.5–42.6**, is preserved in the preferred conformation of **42.8**, which, in its turn, results in torquoselectivity on the retroelectrocyclization in **ts42.8–42.9**, with the preferred disrotation leading to both the *Z* alkene and a *P* configuration of the resultant helical pentadienyl frame and thence to the configuration of the cyclopentenone product of a metal-assisted iso-Nazarov process [130].

## 9 Conclusions

When working with enyne or propargylic acyl derivatives as precursors in gold and platinum-catalyzed transformations, the diversity and complexity of the reorganizations and further reactions that can take place can be at the same time extremely interesting and overwhelming.

The first, in terms of the sheer diversity of accessible structural motifs and rich functionalization that can be achieved under mild reaction conditions, the second in terms of the heavy dependence of the final outcome on the structure of the substrate which, in some cases, can render predictions very difficult. That is why mechanistic insights into the reaction paths followed during these transformations are essential for the systematization, and predictability needed for the optimization of these reactions and their inclusion in the common set of synthetic methods for organic synthesis. The transient nature of many of the intermediates makes their characterization difficult, and the many bifurcations of some complex reaction paths make problematic the accurate analysis of the experimental data that can be collected.

DFT calculations or other molecular modeling techniques are extremely useful in discerning between competing mechanisms, describing intermediates or, in general, simply providing a step-by-step account of the structural and energetic changes along the reaction coordinate. The synergy between theory and experiment in this kind of reaction has already fostered large leaps in understanding and is expected to continue to do so, as the models, algorithms, and available computing power evolve.

From the research presented in this review, we can extract some general conclusions that seem to pervade all the mechanistic discussions considered thus far. The first is the key importance of charge in synthetic design. This is not a new concept, already elaborated by Overman in 1992 [112]; introduction of a charged atom into a molecular skeleton undergoing bond reorganization usually lowers the activation energy of the process, which leads to milder reaction conditions and greater selectivities. Even if the controversy between carbene and carbocationic structures is not settled (with evidence regularly coming out favoring one or the other extreme of the continuum), the  $\pi$ -acid activation of the alkyne as a starting

point for the catalytic cycles and the positive charge on the reorganizing chain at least in some of the limit forms corresponding to a Lewis description of the intermediates make it not too risky to affirm that charge is an important driving force behind these transformations. The fact that gold sometimes shows higher reactivity than platinum in analogous transformations could also be attributed to the displacement towards the carbene end of the scale of the platinum-stabilized intermediates, reinforcing the cationic character of much of the reactivity reported here.

A second important point is the effect of the noble metals on the transition state energies. It is generally accepted that platinum and gold act as soft carbophilic Lewis acids and, as such, activate alkynes to all sorts of nucleophilic attacks. However, from the reactions reviewed, it is made clear that their function in some systems goes well beyond that of a generic Lewis acid (in others actually it does not, and some of them can also proceed through general acid catalysis or with other transition metals, such as copper). In some of the cascade reactions we have studied, the metal is needed at various points of the reaction, either sequentially activating different functional groups [42] or providing through coordination the structural framework [130] needed to hold in place and direct towards reaction the desired functional groups. In this last case, the metal could even increase some of the reaction barriers along the path with respect to the noncatalyzed version [130], balancing this with the inherently catalyzed nature of the process and the lowering of other barriers further along the reaction path, where this transition state organization is key.

In pericyclic reactions, transition metals can affect the barriers in the same way as other substituents with similar electronic demands. In electrocyclizations the metal, besides being key to the generation of conjugation and charge, is going to determine where this charge is located on the chain and lower the barriers to cyclization accordingly, in the same way as an oxygen atom would do in a Nazarov reaction.

We would like to include a cautionary note regarding the interpretation of reactivity patterns inferred from the results of DFT calculations. In most cases, just to calculate the stationary points along a determined reaction path is not overly challenging, but there are several pitfalls along the way. The first, as stated at the beginning of this chapter, is using a model that is not appropriate for the description of the phenomena under study. Another problem is taking into account all potentially competitive paths, something that requires at the same time some experience with the usual complex manifolds for these systems and also the ability to go beyond them. In some occasions, just the neglect of a conformational change or an equivalent assumption about a process with a low-energy barrier that would be completely safe in more conventional systems, can here dramatically alter the conclusions of a study. And then there is the difficulty inherent in the accurate description of the elementary reactions involved in a mechanism, for which some advanced techniques are usually needed. One example of such a problem would be the characterization of the key cyclization steps in some gold-catalyzed reactions [18, 118, 124] as ionic or pericyclic processes.

In the Rautenstrauch reaction (Scheme 20) [18], examination of electronic and aromaticity properties of the cyclizing systems indicate that this reaction would be best classified as the intramolecular attack of a nucleophile (an enol acetate with some

additional charge donation from the gold complex) to an allyl cation, although it keeps some features of purely pericyclic reactions, such as a NICS [131] of  $-8$  ppm [18]. In the carboalkoxylation of alkynyl ethers (Scheme 33) [124], however, the maximum NICS value of **ts33.5b–33.6b** is considerably lower ( $-6$  ppm compared to  $-8$  ppm), and much lower than the NICS values found for purely pericyclic processes ( $-11$  ppm) [131]. This can be explained through both the polarization induced by the methoxy group and by the Au–C bond and through the reluctance of the benzene ring to compromise its aromaticity if too involved in the charge delocalization over the pentadienyl system. Analysis of the anisotropy of the induced charge density (ACID) also points towards a borderline mechanism, with the presence of a small ring current (with a low critical isosurface value of 0.030). The analysis of the aromaticity of the transition structures for the cyclizations in the *aura*-Nazarov and *iso-aura*-Nazarov reactions reported by Sanz et al. [35] after the indole migration is consistent with the consideration of the processes as pericyclic reactions. The NICS at the ring center of **ts25.5–25.6** ( $-10.4$  ppm) and at the ring center of **ts25.8–25.9** ( $-9.2$  ppm) indicates their aromatic character and therefore the rearrangements can be considered as  $4\pi e^-$ -electrocyclic processes (Scheme 25) [118].

Already mentioned is also the unprecedented importance of the barriers corresponding to conformational changes (single bond rotations, helix inversions...) on the intermediates for transfer of stereochemical information/memory of chirality. Since these reactions are characterized by having very low barriers for the chemical (bond-forming/bond-breaking) steps in the mechanism, occasionally chiral information is preserved in a formally planar intermediate that is not long-lived enough to undergo conformational scrambling. This results in stepwise reactions sometimes confused with concerted processes, and wrong assumptions being made about the reaction mechanism if only information from the products is obtained.

As reports of unprecedented gold- and platinum-catalyzed transformations and also of traditional reactions that are made more efficient, more versatile, and more selective by the use of these metals are being constantly received, there are three ideas that can summarize the messages of this review chapter:  $\pi$ -acid catalysis leads to diversity in atom-economic reactions under mild reaction conditions; stereoselectivity is desired and when carefully sought using catalyst or reactant engineering is often achieved; these advances are not made by chance, and the designing of new, more efficient processes is rooted in a deep knowledge of mechanism, for which the information provided by calculations is invaluable.

**Acknowledgments** We thank Centro de Supercomputación de Galicia (CESGA) for the allocation of computer time.

## References

1. Jiménez-Núñez E, Echavarren AM (2007) *Chem Commun*:333
2. Michelet V, Toullec PY, Genêt J-P (2008) *Angew Chem Int Ed* 47:4268
3. Jiménez-Núñez E, Echavarren AM (2008) *Chem Rev* 108:3326

4. Gorin DJ, Sherry BD, Toste FD (2008) *Chem Rev* 108:3351
5. Hashmi ASK (2007) *Chem Rev* 107:3180
6. Soriano E, Marco-Contelles JA (2009) *Acc Chem Res* 42:1026
7. Furstner A (2009) *Chem Soc Rev* 38:3208
8. Lee SI, Chatani N (2009) *Chem Commun*:371
9. Das A, Sohel SMA, Liu R-S (2010) *Org Biomol Chem* 8:960
10. Shapiro ND, Toste FD (2010) *Synlett*:675
11. Wang S, Zhang G, Zhang L (2010) *Synlett*:692
12. Gorin DJ, Toste FD (2007) *Nature* 446:395
13. Frenking G, Fröhlich N (2000) *Chem Rev* 100:717
14. Dedieu A (2000) *Chem Rev* 100:8372
15. Hertwig R, Koch W, Schröer D, Schwarz H, Hrušák J, Schwerdtfeger P (1996) *J Phys Chem* 100:12253
16. Schmidbaur H, Schier A (2010) *Organometallics* 29:2
17. Shi X, Gorin DJ, Toste FD (2005) *J Am Chem Soc* 127:5802
18. Nieto-Faza O, Silva-López C, Álvarez R, de Lera AR (2006) *J Am Chem Soc* 128:2434
19. Soriano E, Marco-Contelles JL (2007) *J Org Chem* 72:1443
20. Nieto-Oberhuber C, López S, Jiménez-Núñez E, Echavarren AM (2006) *Chem Eur J* 12:5916
21. Soriano E, Ballesteros P, Marco-Contelles JL (2005) *Organometallics* 24:3172
22. Perpointner M, Hashmi ASK (2009) *J Chem Theory Comput* 5:2717
23. Flügge S, Anoop A, Goddard R, Thiel W, Fürstner A (2009) *Chem Eur J* 15:8558
24. Shapiro N, Toste FD (2008) *Proc Natl Acad Sci USA* 105:2779
25. Nechaev M, Rayon V, Frenking G (2004) *J Phys Chem A* 108:3134
26. Correa A, Marion N, Fensterbank L, Malacria M, Nolan SP, Cavallo L (2008) *Angew Chem Int Ed* 47:718
27. Marion N, Nolan SP (2007) *Angew Chem Int Ed* 46:2750
28. Marion N, Lemiére G, Correa A, Costabile C, Ramón RS, Moreau X, de Frémont P, Dahmane R, Hours A, Lesage D, Tabet J-C, Goddard J-P, Gandon V, Cavallo L, Fensterbank L, Malacria M, Nolan SP (2009) *Chem Eur J* 15:3243
29. Mamane V, Gress T, Krause H, Furstner A (2004) *J Am Chem Soc* 126:8654
30. Kleinbeck F, Toste FD (2009) *J Am Chem Soc* 131:9178
31. Horino Y, Yamamoto T, Ueda K, Kuroda S, Toste FD (2009) *J Am Chem Soc* 131:2809
32. Seidel G, Mynott R, Fürstner A (2009) *Angew Chem Int Ed* 48:2510
33. Fürstner A, Morency L (2008) *Angew Chem Int Ed* 47:5030
34. Hashmi ASK (2008) *Angew Chem Int Ed* 47:6754
35. Sanz R, Miguel D, Rodríguez F (2008) *Angew Chem Int Ed* 47:7354
36. Benitez D, Shapiro ND, Tkatchouk E, Wang Y, Goddard WA, Toste FD (2009) *Nat Chem* 1:482
37. Fürstner A, Davies PW (2007) *Angew Chem Int Ed* 46:3410
38. Aponick A, Li C-Y, Biannic B (2008) *Org Lett* 10:669
39. Marion N, Carlqvist P, Gealageas R, de Frémont P, Maseras F, Nolan SP (2007) *Chem Eur J* 13:6437
40. Sromek AW, Rubina M, Gevorgyan V (2005) *J Am Chem Soc* 127:10500
41. Cordonnier M-C, Blanc A, Pale P (2008) *Org Lett* 10:1569
42. González Pérez A, Silva López C, Marco-Contelles J, Nieto Faza O, Soriano E, de Lera AR (2009) *J Org Chem* 74:2982
43. Pyykkö P (2004) *Angew Chem Int Ed* 43:4412
44. Pyykkö P (2005) *Inorg Chem Acta* 358:4113
45. Pyykkö P (2008) *Chem Soc Rev* 37:1967
46. Cramer C, Truhlar D (2009) *Phys Chem Chem Phys* 11:10757
47. Niu S, Hall M (2000) *Chem Rev* 100:353
48. Harvey JN (2006) *Annu Rep Prog Chem Sect C* 102:203
49. Parr RG, Yang W (1989) *Density functional theory of atoms and molecules*. Oxford University Press, Oxford

50. Becke AD (1993) *J Chem Phys* 98:5648
51. Lee C, Yang W, Parr RG (1988) *Phys Rev B* 37:785
52. Hay PJ, Wadt WR (1985) *J Chem Phys* 82:270
53. Andrae D, Häussermann U, Dolg M, Stoll H, Preuss H (1990) *Theor Chim Acta* 77:123
54. Perdew JP (1986) *Phys Rev B* 33:8822
55. Zhao Y, Truhlar D (2008) *Acc Chem Res* 41:157
56. Pantazis D, Chen X-Y, Landis C, Neese F (2008) *J Chem Theory Comput* 4:908
57. Soriano E, Marco-Contelles JL (2005) *J Org Chem* 70:9345
58. Ito Y, Sawamura M, Hayashi T (1996) *J Am Chem Soc* 108:6405
59. Bongers N, Krause N (2008) *Angew Chem Int Ed* 47:2178
60. Hashmi ASK, Hamzić M, Rominger F, Bats J (2009) *Chem Eur J* 15:13318
61. Widenhoefer RA (2008) *Chem Eur J* 14:5382
62. Zhang Z, Widenhoefer RA (2007) *Angew Chem Int Ed* 46:283
63. Muñoz MP, Adrio J, Carretero JC, Echavarren AM (2005) *Organometallics* 24:1293
64. González-Arellano C, Corma A, Iglesias M, Sánchez F (2005) *Chem Commun*:3451
65. Teller H, Flügge S, Goddard R, Fürstner A (2010) *Angew Chem Int Ed* 49:1949
66. Johansson MJ, Gorin DJ, Staben ST, Toste FD (2005) *J Am Chem Soc* 127:18002
67. Chao C-M, Beltrami D, Toullec PY, Michelet V (2009) *Chem Commun*:6988
68. Hamilton G, Eun J, Mba M, Toste FD (2007) *Science* 317:496
69. Lalonde R, Wang Z, Mba M, Lackner A, Toste FD (2010) *Angew Chem Int Ed* 49:598
70. Lacour J, Moraleda D (2009) *Chem Commun*:7073
71. Zuccaccia D, Belpassi L, Tarantelli F, Macchioni A (2009) *J Am Chem Soc* 131:3170
72. Gockel B, Krause N (2006) *Org Lett* 8:4485
73. Hoffmann-Röder A, Krause N (2001) *Org Lett* 3:2537
74. Sherry B, Toste FD (2004) *J Am Chem Soc* 126:15978
75. Sherry BD, Maus L, Laforteza BN, Toste FD (2006) *J Am Chem Soc* 128:8132
76. Shu X-Z, Liu X-Y, Ji K-G, Xiao H-Q, Liang Y-M (2008) *Chem Eur J* 14:5282
77. Belot S, Vogt K, Besnard C, Krause N, Alexakis A (2009) *Angew Chem Int Ed* 48:8923
78. Hashmi ASK, Hubbert C (2010) *Angew Chem Int Ed* 49:1010
79. Marion N, Fremont Pd, Lemiere G, Stevens ED, Fensterbank L, Malacria M, Nolan SP (2006) *Chem Commun*:2048
80. Fehr C, Galindo J (2006) *Angew Chem Int Ed* 45:2901
81. Fehr C, Winter B, Magpantay I (2009) *Chem Eur J* 15:9773
82. Fürstner A, Hannen P (2006) *Chem Eur J* 12:3006
83. Soriano E, Marco-Contelles JL (2007) *J Org Chem* 72:2651
84. Watson IDG, Ritter S, Toste FD (2009) *J Am Chem Soc* 131:2056
85. Deutsch C, Gockel B, Hoffmann-Röder A, Krause N (2007) *Synlett*:1790
86. Buzas A, Gagosz F (2006) *J Am Chem Soc* 128:12614
87. Zhang L (2005) *J Am Chem Soc* 127:16804
88. Zhang G, Catalano VJ, Zhang L (2007) *J Am Chem Soc* 129:11358
89. Kirsch SF (2008) *Synthesis*:3183
90. Majumdar K, Debnath P, Roy B (2009) *Heterocycles* 78:2661
91. Aponick A, Li C-Y, Malinge J, Marques E (2009) *Org Lett* 11:4624
92. Hashmi SAK (2010) *Pure Appl Chem* 82:657
93. Genin E, Toullec PY, Antoniotti S, Brancour C, Genet J-P, Michelet V (2006) *J Am Chem Soc* 128:3112
94. Robles-Machín R, Adrio J, Carretero JC (2006) *J Org Chem* 71:5023
95. Davies P, Albrecht S-C (2009) *Angew Chem Int Ed* 48:8372
96. Barluenga J, Fernández A, Satrástegui A, Diéguez A, Rodríguez F, Fañanás F (2008) *Chem Eur J* 14:4153
97. Barluenga J, Fernández A, Diéguez A, Rodríguez F, Fañanás F (2009) *Chem Eur J* 15:11660
98. Okamura WH (1983) *Acc Chem Res* 16:81
99. Okamura WH, Curtin ML (1990) *Synlett*:1



100. Nieto-Oberhuber C, Pérez-Galán P, Herrero-Gomez E, Lauterbach T, Rodríguez C, López S, Bour C, Rosellón A, Cárdenas DJ, Echavarren AM (2008) *J Am Chem Soc* 130:269
101. González AZ, Toste FD (2010) *Org Lett* 12:200
102. Luzung MR, Mauleon P, Toste FD (2007) *J Am Chem Soc* 129:12402
103. Cheong PH-Y, Morganelli P, Luzung MR, Houk KN, Toste FD (2008) *J Am Chem Soc* 130:4517
104. Uemura M, Watson IDG, Katsukawa M, Toste FD (2009) *J Am Chem Soc* 131:3464
105. Habermas KL, Denmark SE, Jones TK (1994) *Org React* 45:1
106. Frontier AJ, Collision C (2005) *Tetrahedron* 61:7577
107. Tius MA (2005) *Eur J Org Chem*:2193
108. Pellisier H (2005) *Tetrahedron* 61:6479
109. Grant TN, Rieder CJ, West FG (2009) *Chem Commun*:5676
110. Nieto Faza O, Silva López C, Álvarez R, de Lera AR (2004) *Chem Eur J* 10:4324
111. Nieto Faza O, Silva López C, Alvarez R, de Lera AR (2009) *Chem Eur J* 15:1944
112. Overman LE (1992) *Acc Chem Res* 25:352
113. Rautenstrauch V (1984) *J Org Chem* 49:950
114. Zhang L, Wang S (2006) *J Am Chem Soc* 128:1442
115. Xia Y, Dudnik AS, Gevorgyan V, Li Y (2008) *J Am Chem Soc* 130:6940
116. Shi F-Q, Li X, Xia Y, Zhang L, Yu Z-X (2007) *J Am Chem Soc* 129:15503
117. Sethofer SG, Staben ST, Hung OY, Toste FD (2008) *Org Lett* 10:4315
118. Sanz R, Miguel D, Gohain M, García-García P, Fernández Rodríguez MA, González-Pérez A, Nieto-Faza O, de Lera AR, Rodríguez F (2010) *Chem Eur J* 16:9818
119. Zou Y, Garayalde D, Wang Q, Nevado C, Goeke A (2008) *Angew Chem Int Ed* 47:10110
120. Garayalde D, Gómez-Bengoia E, Huang X, Goeke A, Nevado C (2010) *J Am Chem Soc* 132:4720
121. Wang S, Zhang L (2006) *J Am Chem Soc* 128:8414
122. Mauleón P, Krinsky JL, Toste FD (2009) *J Am Chem Soc* 131:4513
123. Dubé P, Toste FD (2006) *J Am Chem Soc* 128:12062
124. Nieto Faza O, Silva López C, de Lera AR (2011) Submitted
125. Lemiére G, Gandon V, Cariou K, Fukuyama T, Dhimané A-L, Fensterbank L, Malacria M (2007) *Org Lett* 9:2207
126. Gandon V, Lemiére G, Hours A, Fensterbank L, Malacria M (2008) *Angew Chem Int Ed* 47:7534
127. Lemiére G, Gandon V, Cariou K, Hours A, Fukuyama T, Dhimané A-L, Fensterbank L, Malacria M (2009) *J Am Chem Soc* 131:2993
128. Lee JH, Toste FD (2007) *Angew Chem Int Ed* 46:912
129. Pujanauski BG, Bhanu Prasad BA, Sarpong R (2006) *J Am Chem Soc* 128:6786
130. González Pérez A, Nieto Faza O, de Lera AR (2011) Submitted
131. PvR S, Maerker C, Dransfeld A, Jiao H, NJRvE H (1996) *J Am Chem Soc* 118:6317

# ***N*-Heterocyclic Carbene Complexes of Au, Pd, and Pt as Effective Catalysts in Organic Synthesis**

**Andrea Correa, Steven P. Nolan, and Luigi Cavallo**

**Abstract** *N*-Heterocyclic carbenes (NHC) have been developed in the last 20 years as effective alternatives to classical tertiary phosphines in transition metal-catalyzed transformations. The rapid development of this area is a result of synergistic interactions between experimental and computational chemists. Indeed, computer modeling has proven extremely useful in rationalizing large amount of experimental data, and thus has permitted to accelerate the pace at which this chemistry has been developed. In this review, we will discuss catalytic transformations involving NHC-containing gold, platinum, and palladium complexes. Particular attention is drawn to the fundamental insights that computational chemistry provided to rationalize mechanistic aspects of these processes.

**Keywords** Computational chemistry · Homogeneous catalysis · *N*-Heterocyclic carbenes · Reaction pathways · Transition metal catalysis

## **Contents**

1	Introduction .....	132
2	Gold .....	132
2.1	Reactivity of Propargylic Esters and Related Reactions: The “Golden Carousel” .....	133
2.2	Alkenes and Allenes Reactivity .....	136
2.3	Ion Paring in Gold Complexes .....	139
3	Palladium .....	140
3.1	Pd-Catalyzed Aerobic Oxidations .....	141
3.2	Pd-Catalyzed Cross Coupling Reactions .....	145
3.3	Reactivity Involving the Pd–NHC Bond .....	147
4	Platinum .....	149
5	Conclusions .....	152
	References .....	152

---

A. Correa and L. Cavallo (✉)

Department of Chemistry, University of Salerno, via Ponte don Melillo, Fisciano 84084, Italy  
e-mail: lcavallo@unisa.it

S.P. Nolan

EaStCHEM School of Chemistry, University of St Andrews, St Andrews KY16 9ST, UK

## 1 Introduction

It is difficult not to overemphasize the impact that *N*-heterocyclic carbene ligands (NHC) have had in organic and organometallic chemistry. Less than 20 years have passed since the seminal report of Arduengo and co-workers of a stable crystalline carbene in 1991 [1], and already catalysts containing them can be purchased on an industrial scale for a number of rather different chemical transformations.

The discovery of stable NHCs, of course, opened the route to an explosion of studies devoted to the synthesis of new NHCs, to their characterization, and to their use as ligands in transition metal complexes [2–10]. The unexpected surprise was that NHCs ligands could easily replace tertiary phosphines, and that NHC-based catalysts were very stable under many catalytic conditions, although they present a carbene functionality. This ability initiated impressive academic and industrial efforts, and as a result a great number of effective NHC-bearing catalysts, with very different structures, have been designed. In many cases these catalysts exhibited better activity than the corresponding phosphine-based catalysts, the most notable examples being in the field of Ru-catalyzed olefins metathesis [11–17], Ir-catalyzed hydrogenation [18, 19], Pd-catalyzed cross-coupling reactions [20–22], and Au-catalyzed reactions [23–25]. Furthermore, the existence of H atoms in the 4 and 5 positions of the saturated imidazolin-2-ylidene ring is a key structural feature for the introduction of asymmetry in the NHC ring, which opens the possibility of chiral NHCs in asymmetric synthesis [14, 26–29].

The success encountered by NHCs is often attributed to their strong  $\sigma$ -donating ability that allows formation of very strong NHC-metal bonds and prevents catalyst decomposition [9, 30, 31]. Moreover, the impressive number of applications is possible because NHC ligands have rather flexible architectures whose stereoelectronics can be modified to a large extent, thus giving the possibility of an accurate tuning of the catalytic activity. In this review, which is not exhaustive, we will report on the fundamental insights that the theoretical community (often supported by experimental groups) has contributed to improve our understanding of NHCs in late transition metal catalysis [10]. Specifically, we describe here some applications of NHCs in gold, palladium and platinum catalysis.

## 2 Gold

Gold catalysis has emerged in the last few years as the most intriguing source of novel catalytic transformations of interest to the organic community [32, 33]. The first NHC–Au complex was isolated in 1973 [34], but it is only recently that these compounds, mainly as gold(I) species of formula [(NHC)AuCl], have gained in popularity, taking advantage of straightforward synthetic routes developed recently [35]. The importance acquired by NHC–Au catalysis has been reviewed recently by

Nolan and co-workers, who published a comprehensive review on the topic that included reference up to early 2008 [36]. The rapid advance in Au-assisted catalysis has certainly benefited from mechanistic insights provided by the theoretical community, and in this review we will describe some exemplary cases where computational chemistry unraveled unexpected reaction pathways or provided support to the mechanistic hypothesis originating from the analysis of the catalytic and synthetic experiments. In particular, we will focus on Au-promoted enyne cycloisomerizations, and alkene and propargylic ester activation.

## 2.1 Reactivity of Propargylic Esters and Related Reactions: The “Golden Carousel”

Propargylic esters, where the ester moiety usually performs a 1,2- or 1,3-shift upon electrophilic activation of the alkyne (see Fig. 1), have recently emerged as a special class of substrates [37, 38]. In fact, the intramolecular attack of the ester function, far from inhibiting their reactivity, triggers further carbene- and allene-based transformations.

Recently Correa et al. reported a DFT study on the activation of propargylic acetate by a gold(I) catalyst containing the IMe NHC ligand (IMe = 2,3-dimethylimidazol-2-ylidene), proposing that the three species can interconvert easily to form a “golden carousel”; see Fig. 2 [24]. Starting from **1**, the carboxylic O atom can promote the 5-*exo-dig* attack of to the C2 atom of the alkynyl group leading to the five-membered cyclic intermediate **1-2**, which presents a single Au–C  $\sigma$ -bond. Intermediate **1-2** can further evolve, via a ring-opening reaction, into the Au–vinyl carbenoid intermediate **2** which is only 0.4 kcal/mol less stable than the starting Au-coordinated ester **1**. The overall **1**  $\rightarrow$  **2** skeletal rearrangement corresponds to the 1,2-shift of the carboxylic group from the propargylic position to the internal C2

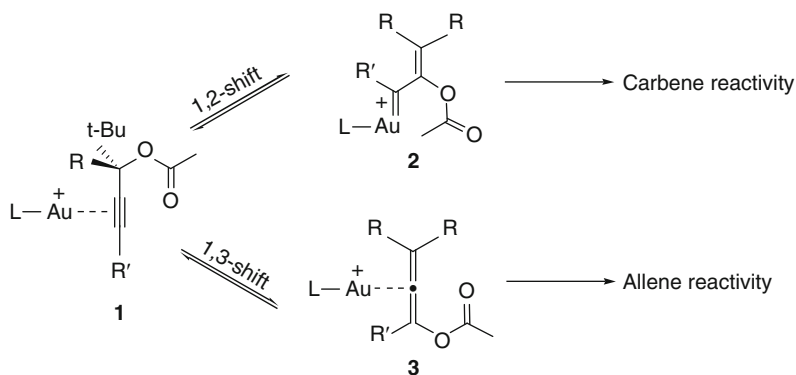


**Fig. 1** Schematic representation of the basic skeleton conversions of propargylic esters

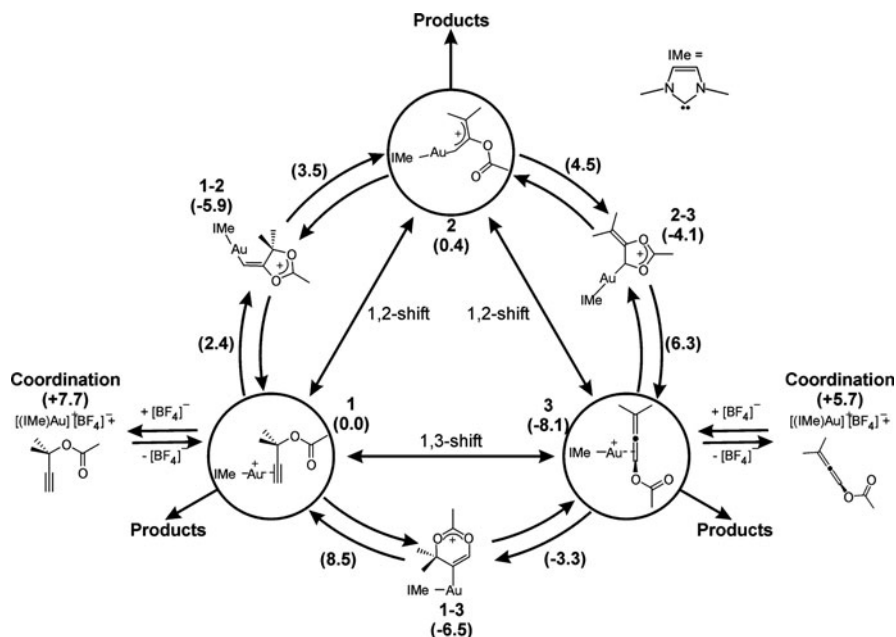


**Fig. 2** Schematic representation of the energetics associated with the  $1 \leftrightarrow 2 \leftrightarrow 3 \leftrightarrow 1$  equilibrium. Energies, in parenthesis and in kcal/mol, are calculated relative to **1**. Numbers close to the arrows represent the energy of the transition state connected with that reaction step

atom of the alkynyl group. Intermediate **2** is the gate to the carbene type reactivity of the starting propargylic ester structure.

The second 1,2-shift starts with the 5-*exo-trig* attack of the carboxylic O atom of **2** at the C1 atom of the alkynyl group, leading to the five-membered cyclic intermediate **2-3**. Then, the Au shift towards the nearby C2  $\text{sp}^2$  atom causes the ring opening of **2-3**, leading to the Au-allene species **3**. In this species, which is roughly 8 kcal/mol more stable than intermediate **1**, the Au center can coordinate equally well to both the C=C moieties of the allene functionality. Intermediate **3** is the gate to the allene type reactivity of the starting propargylic ester structure.

However, the DFT calculations also indicated that the Au-coordinated propargylic ester **1** can be transformed into the most stable Au-allene species **3** through a shorter reaction pathway corresponding to a direct 1,3-shift. In fact, the 6-*endo-dig* attack of the carboxylic O atom of **1** to the C1 atom of the alkynyl group leads to the six-membered cyclic intermediate **1-3**, which can further evolve, via a ring opening step, into the Au-allene species **3**.

Comparison between the reaction pathways corresponding to a double 1,2-shift and to the direct 1,3-shift suggested that the double 1,2-shift  $1 \rightarrow 2 \rightarrow 3$  route is somewhat preferred since the highest transition state along this pathway (transition state **2-3**  $\rightarrow$  **3**) is lower in energy than the highest transition state along the direct 1,3-shift pathway (transition state **1**  $\rightarrow$  **1-3**). Nevertheless, the small preference for

the double 1,2-shift route, roughly 2–3 kcal/mol, indicates that different Au ligands and/or substrates could modify this conclusion.

Overall, the DFT calculations were fundamental in illuminating that all reaction steps around the golden carousel of Fig. 2 present rather accessible energy barriers both in the forward and in the backward direction, and that there is not a remarkably more stable structure where the system collapses, and that would determine the overall reactivity. Indeed, the chemical picture that emerged from the calculations is that of a rapid equilibrium between all key intermediates. Of course, this picture is valid for the simple propargylic ester skeleton **1**, and it is clear that different Au ligands and/or substrates could modify this preference for the double 1,2-shift. This could explain the experimentally observed preference for 1,2- or 1,3-shift as a function of the substrate structure [39–43]. The exact way off the golden carousel depends on the energy barriers associated with reactions involving intermediates **1**, **2**, and **3** and leading to products irreversibly.

The catalytic cycle of Fig. 2 was also investigated by replacing the NHC ligand by a phosphine, namely  $\text{PMe}_3$ . This indicated that potentially relevant differences induced by NHC and  $\text{PR}_3$  are connected to the most stable intermediate around the cycle. In the presence of the IMe ligand the most stable intermediate along the cycle is **3**, while in the presence of  $\text{PMe}_3$  intermediate **1–2**, the energetic antipodes of **3**, is comparable in energy. This suggests that in the case of NHC ligands, intermediate **3** could be the preferential way off the cycle, with an allene-based reactivity. Differently, in the case of phosphines, the almost isoenergetic intermediates **1** and **2**, which are easily accessible from the relatively stable **1–2** intermediate, could represent the preferential ways off the cycle.

The golden carousel of Fig. 2 constitutes the first step towards the construction of more complex structures. This is well exemplified in the cyclization of the dyenine **4** into the mixture of products **5**, **6**, and **7** of Fig. 3.

Experimental results indicated that NHCs proved more selective than phosphines for the synthesis of the unexpected product **7** [23, 44], the formation of which was not easy to rationalize with the accepted mechanistic pathways. A combined experimental/mechanistic study by Nolan and Cavallo showed that **5** and **6** were likely formed via 1,2-migration of the acetate group of **4**, while **7** would be produced via an unprecedented 1,3-OAc shift to form the allene-ene intermediate **8** first, as suggested by the golden carousel, followed by a cyclization and 1,2-OAc shift of **8** leading to **7**. This hypothesis, which translates the apparent 1,2-OAc shift from **4** to **7** into a 1,3-OAc migration followed by a 1,2-OAc “retromigration”,

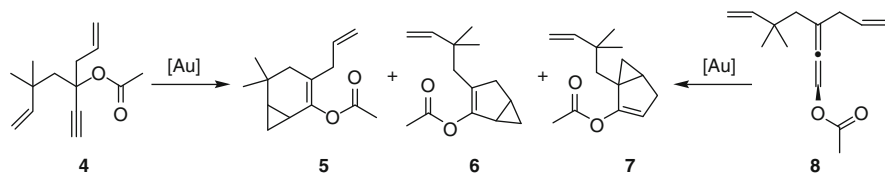


**Fig. 3** Schematic representation of the two possible routes to the cyclized product **5**, **6**, and **7**

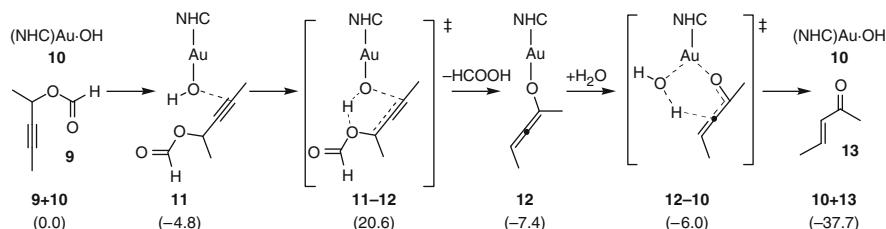


**Fig. 4** Schematic representation of the energetics associated with the 9–13 transformation. Energies, in *parenthesis* and in kcal/mol, are calculated relative to separated 9 + 10

is supported by the experimental evidence that cyclization of the allenyl acetate **8** afforded with a greater proportion **7** over **5** and **6** [25].

Still on the reactivity of propargylic esters, Maseras and Nolan reported an experimental and computational study on the formation of  $\alpha,\beta$ -unsaturated ketones and aldehydes from propargylic acetates in the presence of water, which was found to be crucial to achieve this transformation [45]. DFT calculations were fundamental to screen among a number of possible reaction mechanism, and to converge to that shown in Fig. 4. The first step of the mechanism supported by the DFT calculations corresponds to the unprecedented transfer of the OH fragment bound to gold center in **10** to the alkynyl functionality of **9** with formation of the Au-allenolate **12** and release of a HCOOH molecule. The second and final step of the catalytic cycle was found to be the attack of a water molecule to **12** with release of the  $\alpha,\beta$ -unsaturated ketone **13**. The rate limiting step of the catalytic cycle was found to be formation of the Au-allenolate **12** via transition state **11–12** and the relatively low barrier of 20.6 kcal/mol, while attack of a water molecule to **12** occurs with the negligible barrier of 1.4 kcal/mol only [45].

## 2.2 Alkenes and Allenes Reactivity

The first report involving NHC–Au complexes in alkene activation appeared in 2006 by Peris, Fernandez, and co-workers [46]. Immediately after, allylic esters also appeared as an interesting class of compounds in the context of gold catalysis [47, 48]. In fact, allylic rearrangement provides an efficient and atom-economical access to primary oxo derivatives.

Nolan and co-workers proposed that the rearrangement of allylic acetates involves a  $\pi$ -activation/oxo cyclization sequence [49]; see Fig. 5. From the comparison of the experimental results achieved with different NHC ligands they concluded that the key parameter to rationalize these transformations was the steric hindrance of the ligand, rather than its electronic properties. In particular, they proposed that a bulky ligand would shield the cationic gold center more efficiently than a smaller ligand, thus preventing catalyst decomposition.

Since other hypotheses could be envisaged for the mechanism of allylic esters isomerization [48], this transformation was recently the subject of a detailed DFT

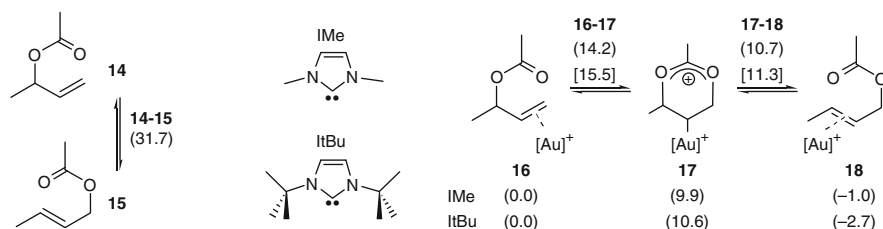


**Fig. 5** Schematic representation of the energetics associated with the **14–15** transformation. Energies, in *parenthesis* and in kcal/mol, are calculated relative to separated **9 + 10**

study by Maseras and co-workers [50]. They first investigated the uncatalyzed **14–15** reaction and calculated that, in this case, the transformation occurs in one step via a six-membered transition state and with the relatively high barrier of 31.7 kcal/mol; see Fig. 5. Analysis of the atomic charges, and of the length of the breaking and forming bonds at the transition state, suggested that the transition state can be viewed as an anionic acetate fragment interacting with a positive carbocation. Then they analyzed the reaction with the simple (NHC)–Au<sup>+</sup> catalyst, and they compared a system with the relatively unhindered IMe NHC ligand, with a system presenting the bulky ItBu NHC ligand; again see Fig. 5. After alkene coordination to the gold catalyst, **16** in Fig. 5, the reaction proceeds through an intramolecular nucleophilic attack of the carbonyl O atom on the C–C double bond that, through transition state **16–17** roughly 14–15 kcal/mol above **16**, leads to the six-membered 1,3-acetoxonium intermediate **17**, roughly 10 kcal/mol above **16**. This intermediate evolves, through transition state **17–18**, roughly 10–11 kcal/mol above **16**, into intermediate **18** that corresponds to the rearranged product coordinated to the gold catalyst. Comparison of the results obtained with the two NHC ligands indicated that the bulkiness of the NHC ligands has a negligible influence on the energetics of this transformation, further supporting the hypothesis that the lower experimental performances of systems presenting an unhindered NHC ligands could be due to the lower stability with respect to decomposition of the corresponding catalytically active [(NHC)Au<sup>+</sup>][BF<sub>4</sub><sup>–</sup>] cationic adduct [51].

In the same paper they also considered the effect of the BF<sub>4</sub><sup>–</sup> counterion showing that the anion interacts with the cationic systems by making hydrogen bonds with the organic substrate, but the effect on the energy profile was found to be negligible. The authors concluded that the anion is always able to find an appropriate position in the environment of the cationic system, resulting in similar electrostatic interactions along the whole reaction pathway.

The same group investigated the intermolecular hydroalkoxylation of allenes by methanol [52], see Fig. 6, reporting on the mechanistic aspects of this reaction, with a particular focus on regioselectivity. They showed that the most favored reaction pathway corresponds to a nucleophilic attack of MeOH to a gold(I)-coordinated allene, which occurs irreversibly [53]. The rate-limiting step was found to correspond to the initial attack of the alcohol on the allene, through transition states **22–23** and **25–26**; see Fig. 6. This initial step leads to the formation of the Au–σ-



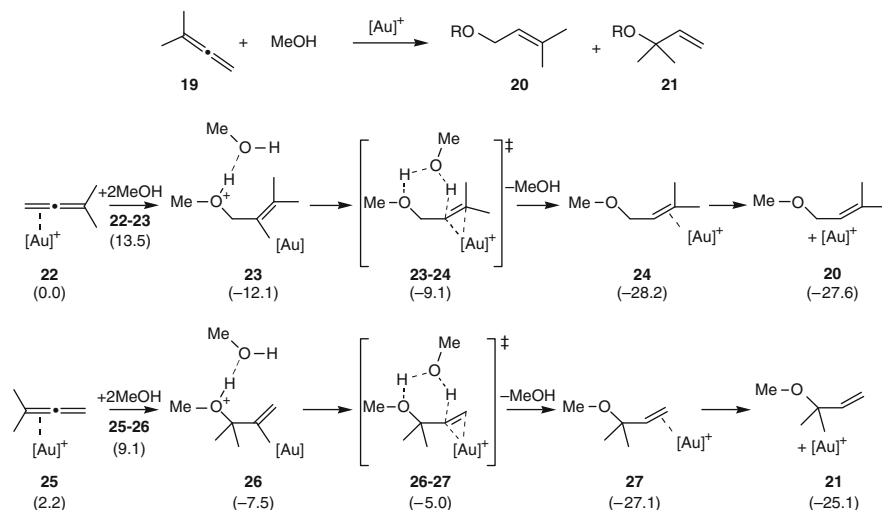


**Fig. 6** Schematic representation of the energetics of allene conversion into allylic ethers. Energies, in parenthesis and in kcal/mol, are calculated relative to **22**

alkenyl intermediates **23** and **26**, both of them more stable than the starting complex. Proton transfer assisted by an additional  $MeOH$  molecule, through transition states **23–24** and **26–27**, leads to the coordinated products **24** and **27**, followed by  $Au$  dissociation that leads to the observed products. The overall process is calculated to occur with retention of the alkene geometry.

Interestingly, calculations predicted that the rate-limiting initial attack of  $MeOH$  to the coordinated allene occurs preferentially at the methylated end of the allene, which is in contrast with the experimental data that resulted in the preferential formation of the allylic ether **21** rather than **20**. Since allene hydroalkoxylation was calculated to be irreversible (both **20** and **21** are roughly 25 kcal/mol more stable than the initial allene **19**), a viable explanation considered product isomerization; see Fig. 7. The proposed pathway for the NHC– $Au$  catalyzed allylic ether isomerization was calculated to start with coordination of the  $C=C$  double bond to gold, structures **24** and **27** in Fig. 7, which activates the alkene to nucleophilic attack from  $MeOH$ . This step is aided by hydrogen bonding to the allylic oxygen, and occurs through rather low energy cyclic transition states; see structures **27–28** and **28–24** in Fig. 7. Attack of either regioisomeric allylic ethers forms a central chair-shaped cyclic intermediate **28**, which allows the interconversion of the products, finally yielding the more stable regioisomer. In conclusion, based on DFT calculations the authors were able to demonstrate that the two regioisomeric products are in equilibrium, and as a result only the most stable one, corresponding to alkoxylation in the terminal position, is observed experimentally.

Computational studies have also focused on the reactivity of bisallenes. In particular, Chung and co-workers recently reported a mixed experimental and computational paper on N-tethered 1,5-bisallenes cyclization in presence of an  $Au(I)$  catalyst containing the IPr NHC ligand [54]. Interestingly, bisallenes such

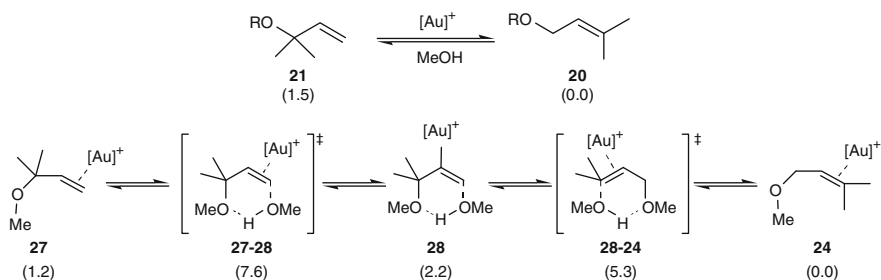


**Fig. 7** Schematic representation of the energetics associated with isomerization of allylic ethers. Energies, in *parenthesis* and in kcal/mol, are calculated relative to **24**

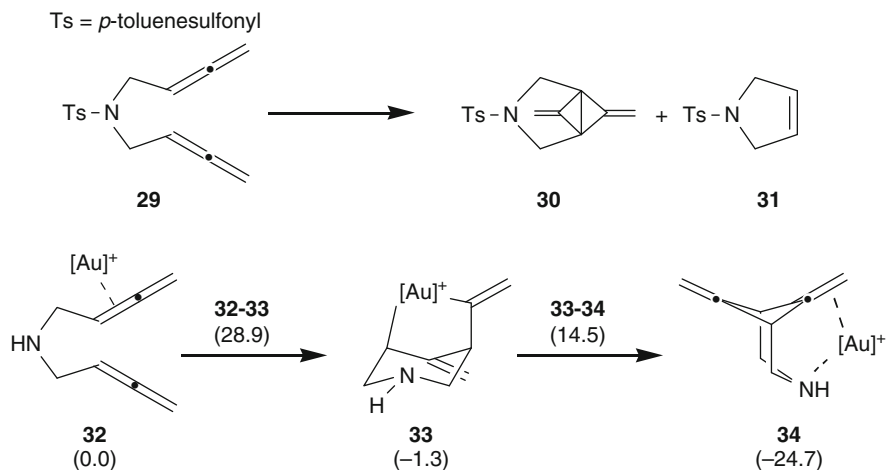


**Fig. 8** Schematic representation of the energetics associated with cyclization of bisallenenes. Energies, in *parenthesis* and in kcal/mol, are calculated relative to **32**

as **29** are converted principally into the 6,7-dimethylene-3-azabicyclo[3.1.1]heptane skeleton **30**, with the simple heterocycle **31** as a minor product. DFT calculations on a simplified model were fundamental to suggest a stepwise mechanism proceeding with the initial formation of a  $\eta^1$ -allenyl gold(I) complex, such as **32**, followed by sequential carbon–carbon bond formations through the unprecedented intermediate **33**, leading finally to the azabicyclo product **34**. The rate limiting step is the formation of the novel intermediate **33** (Fig. 8).

### 2.3 Ion Paring in Gold Complexes

Generally, gold catalysts are introduced in the reaction media in the form of a chloride salt that then reacts with silver tetrafluoroborate. The positive charge of the

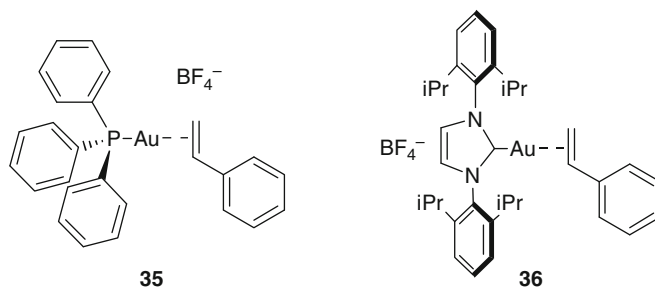


**Fig. 9** Schematic representation of the geometries of ion pairs based on phosphine and NHC gold cationic complexes in combination with  $\text{BF}_4^-$

catalyst, and the usually low polarity of the solvent, means that the reacting system is likely associated with a tetrafluoroborate anion after the precipitation of silver chloride. Ion pairing have been found to play a role in gold catalyzed reactions that involve the activation of unsaturated carbon–carbon bonds [33, 55, 56]. However, the anion–cation interaction in gold(I) complexes has rarely been investigated from a theoretical point of view [57, 58]. Probably the first report is that of Macchioni and co-authors, who reported a mixed NMR and computational study concerning the determination of the relative cation–anion orientations in the two complexes  $[(\text{PPh}_3)\text{Au}(4\text{-Me-styrene})][\text{BF}_4^-]$  which is an example of a phosphine-based gold(I) catalyst, and  $[(\text{IPr})\text{Au}(4\text{-Me-styrene})][\text{BF}_4^-]$ , which is an example of an NHC-based gold(I) catalyst. By combination of NMR measurements and accurate theoretical modeling, they concluded that the counterion in phosphine-based styrene–gold(I) catalyst is in the near proximity of the metal center, interacting actively with the substrate (see structure 35 in Fig. 9), whereas in the examined NHC-based styrene–gold(I) catalyst the counterion resides mainly far away from the gold site (see structure 36 in Fig. 9). The preferential position of the counterion seems to be tunable through the choice of the ancillary ligand, and DFT calculations were fundamental to rationalize the role of electrostatic properties in determining the preferential ion pair geometry. Of course, these conclusions could open the way to greater control of the properties and activity of these catalysts, and are in good agreement with the fact that counterion effects in gold(I) catalyzed activation of unsaturated substrates are much more frequent when phosphines [59–62] are used as ancillary ligand vs NHCs [52].

### 3 Palladium

NHC–palladium complexes are, undoubtedly, among the most commonly used transition metal catalysts for homogeneous catalysis. This class of complexes has notably allowed major breakthroughs in C–C and C–N forming cross-coupling reactions [63–68]. This success has overshadowed other interesting applications

of (NHC)Pd systems such as, for example, oxidations. Herein we will describe some of the applications where computational chemistry has provided experimentally relevant insights.

### 3.1 Pd-Catalyzed Aerobic Oxidations

Although challenging, Pd-catalyzed aerobic oxidation is a versatile method for the selective oxidation of organic molecules and makes use of molecular oxygen as the oxidant [69–73]. The reaction mechanism is considered to be a two-stage mechanism consisting of Pd(II)-mediated oxidation of the substrate followed by dioxygen oxidation of Pd(0), and computational chemistry has been extremely useful in providing a detailed understanding of the catalytic cycle.

Focusing on the use of NHC–Pd(OAc)<sub>2</sub> (Ac = acetate) complexes for aerobic oxidation of alcohols to carbonyl compounds as an exemplary case [74, 75], Fig. 10 displays the mechanism initially postulated. The first step is substrate coordination to the starting complex **37** with concomitant loss of water, followed by an intramolecular deprotonation to generate the alkoxide intermediate **40**. The next step is a  $\beta$ -hydride transfer that leads to the Pd-hydride intermediate **41**. Reductive elimination of acetic acid from **41** leads to the Pd(0) species **42**, that can either decompose or can be trapped and oxidized by molecular oxygen to give the peroxocomplex **43**. Protonation of **43** would give back the initial complex **38** closing the catalytic cycle. This mechanistic proposal has been studied by several research groups in order to validate and understand it fully [74–83].

In particular, Sigman and co-workers calculated that, under optimal conditions, the rate-limiting step is the generation of intermediate **41** [78]. In case of the oxidation of *sec*-phenylethyl alcohol, the geometry of transition state **40–41** correlates very well

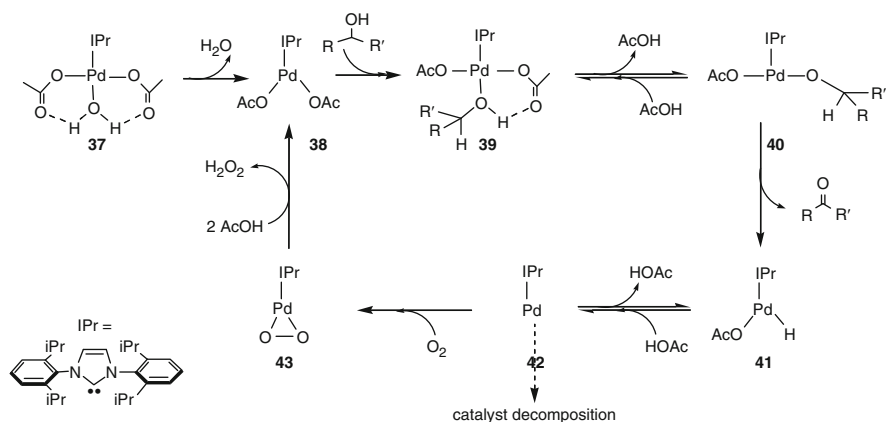


**Fig. 10** Mechanism for Pd-catalyzed aerobic oxidation of alcohols

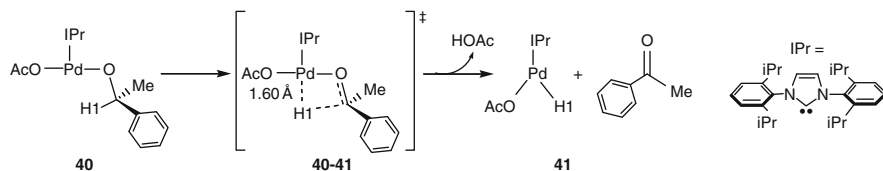


**Fig. 11** Key geometries of the  $\beta$ -H transfer step in the Pd-catalyzed oxidation of alcohols

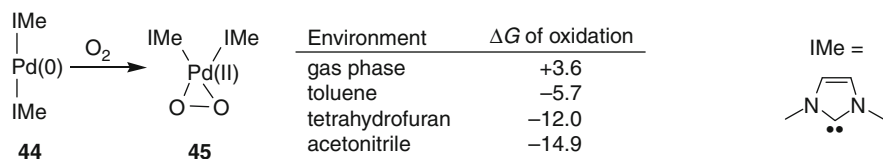


**Fig. 12** Schematic representation of the  $O_2$  addition to complex **44** and relative  $\Delta G$ , in kcal/mol

with that of a product-like transition state. Geometry analysis of **40–41** reveals that the distance between H1 and Pd is only 1.60 Å (see Fig. 11), indicating that the hydride is nearly completely transferred to the Pd center. Comparison of the calculated free energy barrier for  $\beta$ -H transfer with that calculated for the deuterated analog resulted in a rather large kinetic isotope effect, 3.8, in good agreement with the experimental value of 5.5, further supporting the overall mechanistic picture.

Further calculations indicated that in **40** the acetate counterion is in the coordination sphere of the Pd square planar complex, weakly chelated via the carbonyl oxygen. In transition state **40–41** the acetate counterion rotates out of the plane during the  $\beta$ -hydride elimination with a gain in rotational degrees of freedom. This result fits very well with the experimental activation parameters at 50 °C. The  $\Delta S^\ddagger$  contribution is close to unity for the oxidation of *sec*-phenylethyl alcohol and largely positive for the oxidation of 2-decanol and benzyl alcohol. The positive  $\Delta S^\ddagger$  values indicate that there is less “organization” in the transition state with respect to intermediate **40**.

The interaction of the Pd center with  $O_2$  was also modeled in detail. Stahl et al. investigated the fundamental reaction between dioxygen and Pd(0) complexes (i.e., systems that resemble intermediate **42**) [80]. They showed experimentally that the oxidation proceeds smoothly for a bis-NHC complex. Then they clarified the mechanism of the reaction between  $(\text{IMe})_2\text{Pd}(0)$  and  $O_2$  to yield  $(\text{IMe})_2\text{Pd}(\text{II})$  ( $\eta^2\text{-O}_2$ ) computationally (see Fig. 12). First they evaluated the thermodynamic driving force for the oxygenation of **44**. The  $\Delta G$  of the reaction was calculated in the gas phase and in several different solvents. The reaction was found to be endoergonic by 3.6 kcal/mol in the gas phase, but increasingly favorable in solvent with increasing polarity (see Fig. 12). This strong solvent effect was correlated to the significant dipole moment associated with the dioxygen complex **45** relative to the negligible dipole moment in **44**. The  $\Delta G$  of oxidation was evaluated, also

replacing the IMe ligands with phosphine ligands, namely  $\text{PMe}_3$ . In the case of  $(\text{PMe}_3)_2\text{Pd}$ , coordination of oxygen was calculated to be considerably less favorable, +10.3 and  $-2.8$  kcal/mol in the gas phase and in acetonitrile, respectively, relative to complex **44**. This sharp difference between NHC and phosphine was ascribed to the stronger  $\sigma$ -donor character of NHC ligands relative to phosphines, a conclusion supported by natural population analysis that revealed that the peroxy oxygen atoms of the NHC complex possess a greater negative natural charge than those of the  $\text{PMe}_3$  complex.

After investigating the thermodynamics of  $\text{Pd}(0)$  oxygenation, they turned their attention to the reaction mechanism. The proposed reaction pathway is displayed in Fig. 13. Molecular  $\text{O}_2$  approaches the Pd center end-on and forms the  $\text{Pd}(\eta^1\text{-O}_2)$  adduct **46** in which the NHC ligands are still *trans* to each other. The next step is isomerization into the  $\text{Pd}(\eta^1\text{-O}_2)$  *cis* complex **47**. This step proceeds with a barrier of about 8 kcal/mol. Complex **47**, 6.0 kcal/mol above **46**, exhibits an O–O bond length of 1.32 Å and was described as a Pd(I) superoxide adduct with an open-shell triplet configuration. Formation of the second Pd–O bond from **47** requires a spin-crossover from the triplet to the singlet electronic surface. Once this crossing has occurred, formation of the second Pd–O bond, leading to the  $\text{Pd}(\eta^2\text{-O}_2)$  complex **45** proceeds without an energy barrier.

The unrestricted DFT calculations provided relevant insights into the energetics and the mechanism of oxygenation of  $(\text{NHC})_2\text{-Pd}(0)$  complexes. The discovery that the thermodynamics of oxygen coordination depends strongly on solvent polarity not only resulted in the detection of reversible oxygenation of  $(\text{IMe})_2\text{Pd}(0)$ , but also has implications on the conditions under which the reaction is normally performed. In fact, the non-polar solvents commonly used in catalysis potentially enhance the chances of  $\text{O}_2$  dissociation that contributes to catalyst decomposition.

Stahl et al., instead, studied the insertion of molecular  $\text{O}_2$  into a  $\text{Pd}(\text{II})$ –hydride bond to produce a  $\text{P}(\text{II})$ –OOH hydroxide species [83]. Competition between the two reaction pathways shown in Fig. 14 was investigated.

The first pathway, labeled as the hydrogen atom abstraction pathway, starts with interaction of the  $\text{O}_2$  molecule in the triplet state to extract the H atom of the Pd–hydride species **48**, to arrive at intermediate **49** that lies 19.1 kcal/mol above **48**. At this point, with a concerted rearrangement of the hydroperoxide group, intermediate **49** collapses into the closed shell Pd–hydroperoxide complex **50**,

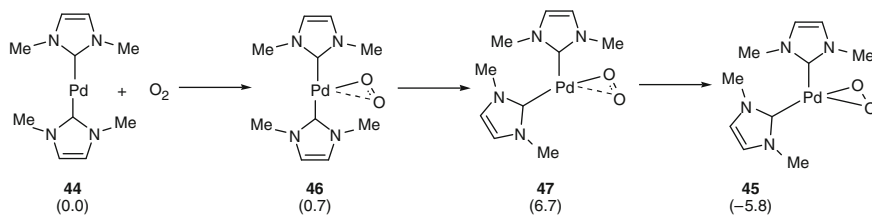


**Fig. 13** Schematic representation of the energetics associated with the oxygenation of the  $(\text{IMe})_2\text{-Pd}(0)$  complex. Energies, in *parenthesis* and in kcal/mol, are calculated relative to **44** +  $\text{O}_2$

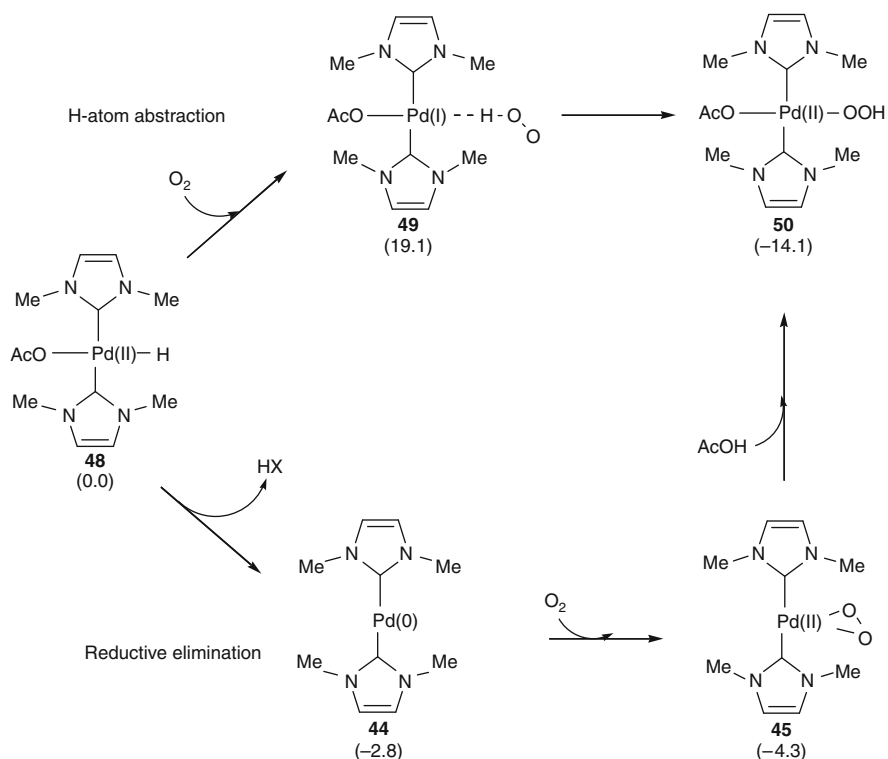


**Fig. 14** Schematic representation of the energetics associated with the oxygenation of the (IME) 2-Pd-H complex **48**. Energies, in parenthesis and in kcal/mol, are calculated relative to **48** +  $O_2$

with an energy gain of 14.1 kcal/mol. The alternative reaction pathway, labeled as the reductive elimination pathway, starts with reductive elimination of AcOH from **48** to yield **44**, 2.8 kcal/mol lower in energy, followed by  $O_2$  oxidative addition to **45**, with an energy gain of 4.3 kcal/mol, and completes with AcOH addition leading to the final hydroperoxide **50**. The two reaction pathways were found to be in competition, although the authors speculated that the elimination reaction pathways should be the working pathway under the typical conditions used for this reaction [83].

The peculiar ability of Pd(0) complexes to activate small but fundamental primary building blocks, such as  $O_2$ , was also evidenced by the ability of (IPr)Pd( $PCy_3$ ) to activate molecular  $H_2$  to form unprecedented *trans* Pd-dihydride complexes by Nolan and co-workers [84]. The thermodynamics of this transformation was investigated computationally. The initial coordination of molecular hydrogen to the starting (IPr)Pd( $PCy_3$ ) complex **51** leads to the Pd- $H_2$  molecular adduct **52**, which is 3.4 kcal/mol above **51**. This complex can both isomerize to the nearly isoenergetic *cis* Pd-( $H$ )<sub>2</sub> dihydride complex **53**, or to the more stable *trans* Pd-( $H$ )<sub>2</sub> complex **54** (Fig. 15)

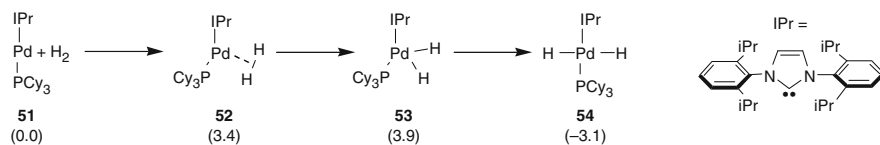


**Fig. 15** Schematic representation of the energetics associated with the hydrogenation of the (IPr) Pd(PCy<sub>3</sub>) complex **51**. Energies, in *parenthesis* and in kcal/mol, are calculated relative to **51** + H<sub>2</sub>

## 3.2 Pd-Catalyzed Cross Coupling Reactions

Palladium catalyzed cross-coupling reactions for the construction of carbon–carbon and carbon–heteroatom bonds provide convenient routes allowing the synthetic chemist to access a vast number of complex molecules and materials [63–68]. The traditional mechanism of Pd-catalyzed cross-coupling reactions involves three discrete steps. The catalyst is a Pd(0) complex, and the first step typically is the oxidative addition of a carbon–halide compound that transfers the first fragment to the Pd center to form a Pd(II) species. The second step is the transfer of the second fragment to the Pd(II)-alkyl complex, and offers a variety of solutions (alkene, alkyl–ZnBr, alkyl–NH<sub>2</sub>, as a few examples), which results in different types of cross-coupling. After the second fragment has also been loaded onto the Pd(II) center, the last step is the reductive elimination of the cross-coupling product with regeneration of Pd(0) catalyst. The relevance of Pd-mediated cross-coupling reactions has led to a number of computational studies that provided many insights into the mechanics of this class of reactions [85–91], although phosphine-based systems have been investigated in greater detail [80, 92–108]. Here we focus on those studies in which the complete catalytic cycle was investigated.

Focusing on the Heck reaction, Hu et al. modeled the cross-coupling of PhBr and CH<sub>2</sub>=CH<sub>2</sub> promoted by PdL<sub>2</sub> catalysts where L is a phosphine or a NHC ligand or an abnormal NHC ligand coordinated to the Pd center through the C5 carbon atom (see Fig. 16) [90]. They found that the rate-limiting step is the oxidative addition of PhBr to the starting species **55** to form the square planar intermediate **56**. For ethylene insertion into the Pd–Ph bond two pathways were examined. In the former, named the neutral pathway, dissociation of the L<sup>1</sup> ligand occurs prior to ethylene coordination, leading to intermediate **57**, while in the latter, named the cationic pathway, dissociation of Br<sup>−</sup> occurs prior to ethylene coordination, leading to intermediate **58**. Calculations indicated that the two pathways are not dramatically different in energy, although the phosphine-based system was calculated to have a higher tendency to react through the neutral pathway due to the easier dissociation of PMe<sub>3</sub> from the Pd center relative to dissociation of a NHC ligand. Minor differences were calculated for the system containing the abnormal NHC ligand relative to the system with two IMe NHC ligands. In all cases, ethylene insertion from both **57** and **58** presents a sizeable energy barrier, while the following β-H elimination from **59** to yield **60** and release the product was calculated as a rather easy step [90].





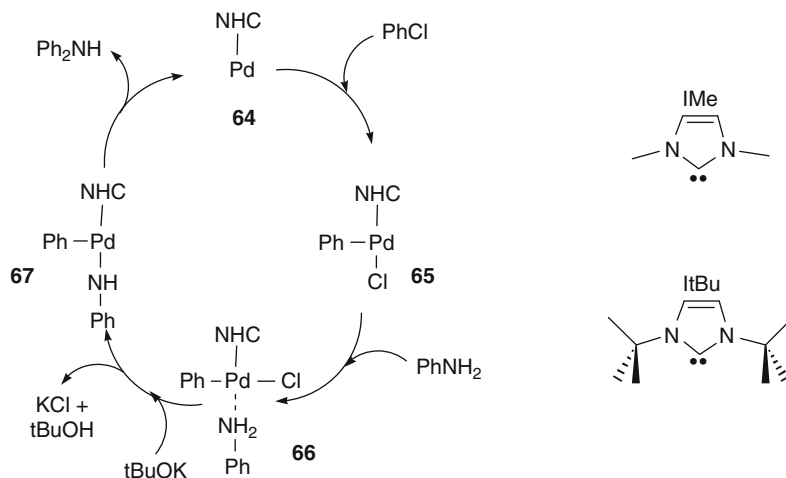


**Fig. 18** Schematic representation of the Pd-catalyzed amination of PhCl by PhNH<sub>2</sub>

experimental finding that the reaction is very selective towards alkyl–alkyl coupling with IPr, whereas alkene is the major product with IXy [89].

Arylamination is another class of NHC–Pd catalyzed cross-coupling reaction whose complete catalytic cycle was investigated. Specifically, Green et al. modeled the amination of PhCl by PhNH<sub>2</sub> (see Fig. 18) [91]. First, calculations indicated that the reactive species is the mono-carbene (NHC)Pd complex **64**, since the Pd center of the parent bis-carbene (NHC)<sub>2</sub>Pd complex is too electron rich to undergo oxidative addition. After addition of PhCl to **64** the system collapses into the T-shaped intermediate **65**, which can still coordinate a PhNH<sub>2</sub> molecule to yield intermediate **66**. Extraction of HCl from **66** with a base KOTBu in this case leads to intermediate **67** from which the arylaminated product is released via a reductive elimination step that closes the catalytic cycle. Also, oxidative addition, in the case of PhCl to **64**, is rate-determining compared to the subsequent reductive elimination of Ph<sub>2</sub>Nh from **67**. Interestingly, the steric bulkiness of the ItBu NHC ligand reduces the energy barrier of the oxidative addition of PhCl compared to the same barrier in the presence of the IMe ligand [91].

### 3.3 Reactivity Involving the Pd–NHC Bond

While the NHC ligand in Pd-catalysts is normally a spectator ligand, in some instances it can be directly involved in the reactive event. For example, the reductive elimination of 2-hydrocarbyl-imidazolium salts from hydrocarbyl-palladium complexes bearing NHC ligands represents an important deactivation route of NHC–Pd catalysts. McGuinness and co-workers were the first to associate the facile decomposition of hydrocarbyl palladium complexes and the elimination of a 2-substituted imidazolium salt (see Fig. 19) to a decrease in catalytic efficacy [109].



**Fig. 19** Elimination of 2-methylimidazolium from a methyl NHC–Pd complex

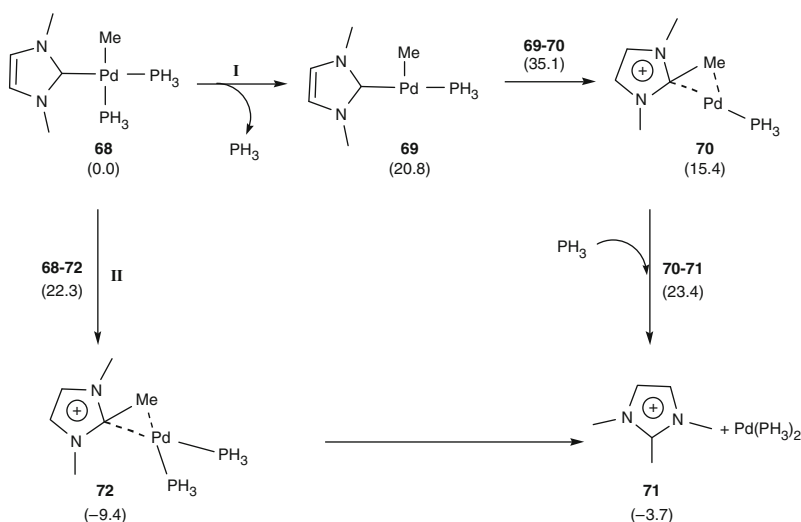
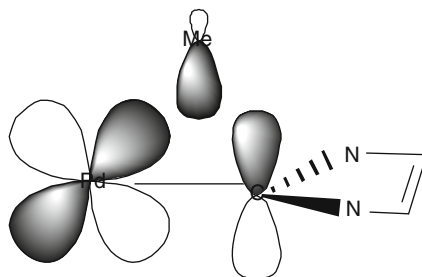


**Fig. 20** Schematic representation of the energetics associated with reductive elimination, prior phosphine dissociation, pathway I, and from four coordinated Pd, pathway II. Energies, in parenthesis, are calculated relative to **57**

An extensive study on the alkyl-carbene elimination from carbene/diphosphine and carbene/diphosphites hydrocarbyl–Pd(II) complexes has been reported by Cavell and co-workers [110]. They first considered a simplified model of the catalyst where the tertiary phosphine ligands were replaced by simple  $\text{PH}_3$  groups, **68** in Fig. 20. In principle, two reaction pathways are possible. In the former, pathway I in Fig. 20, reductive elimination occurs after dissociation of one phosphine. In the latter, pathway II in Fig. 20, reductive elimination occurs without phosphine dissociation. Focusing on pathway I, dissociation of one phosphine from **68** is of course an endothermic process and leads to the T-shaped complex **69**. Reductive elimination of 2-methylimidazolium through transition state **69–70** requires an energy barrier of only 14.3 kcal/mol, and the system collapses into complex **70**, with a strong interaction between the 2-methylimidazolium fragment and the Pd center. Complex **70** evolves into the final products through a relatively low barrier of some 11 kcal/mol, with simultaneous coordination of a free  $\text{PH}_3$  molecule. The overall activation barrier for this pathway has been calculated to be 35.1 kcal/mol.

**Fig. 21** Molecular orbital description of the transition state of the reductive elimination **68–72**



Focusing on the concerted pathway II, the first step is the formation of the three-centered intermediate **72** that occurs through transition state **68–72** and an energy barrier of 22.3 kcal/mol. This indicates that the concerted pathway is favored by 12.8 kcal/mol with respect to the dissociative one. Natural bond order analysis indicated an extensive involvement of the  $p(\pi)$  orbital on the carbene in the transition state (see Fig. 21). On closer examination, in the transition state **68–72**, there is a mixing between the  $p(\pi)$  orbital of  $C_{\text{carbene}}$ , the orbital of  $C_{\text{methyl}}$ , and the  $d$  orbitals of Pd ( $d_{xy}$ ). It is this mixing that allows the formation of the  $C_{\text{carbene}}-C_{\text{methyl}}$  bond.

The energetics of the reductive elimination were also calculated by replacing the model  $\text{PH}_3$  ligands with the bulkier and representative  $\text{P}(\text{OPh})_3$  phosphites. As a result of the different steric and electronic impact of  $\text{P}(\text{OPh})_3$  the activation barrier for the concerted reductive elimination decreases from 22.3 kcal/mol with  $\text{PH}_3$  to 14.1 kcal/mol with  $\text{P}(\text{OPh})_3$ . As is typical in organometallic catalysis, sterically demanding ligands result in an increased steric pressure in the first coordination sphere of a highly coordinated metal, which promotes reductive elimination [110].

Based on this study, Yates and co-workers calculated the effect of the N-substituents of the NHC fragment on the stability of (NHC)-Pd-hydrocarbonyl complexes to reductive elimination [111]. Their calculations clearly showed that complexes containing NHC ligands that bear branched-alkyl N-substituents should be the most resistant to reductive elimination, due to their electron donating capacity, and were found to be significantly more stable to reductive elimination than those complexes with electron withdrawing carbene N-substituents (i.e., chloride).

## 4 Platinum

Compared to Au and Pd, applications of NHC–Pt complexes in catalysis are less explored. Nonetheless, NHC–Pt complexes have shown outstanding catalytic activity in the field of olefins hydroxylation [112–115], and have shown promising results in the reductive cyclization of dienes [116], in the cycloisomerization of enynes [117], and in the hydroboration of alkenes [118]. For this reason, it is clear

that only a few computational efforts have been made in the field, and some of them have mostly focused on side reactions or structural characterization.

For example, the reactivity of NHC ligands bound to a Pt center was investigated by Nolan and Cavallo who reported on the insertion of an NHC fragment into the Pt–olefin bond [119]. The preparation of the  $(\text{NHC})_2\text{PtCl}_2$  potential catalyst from the (hexadiene) $\text{PtCl}_2$  precursor in THF leads to the surprising insertion of the NHC molecule into the Pt–olefin bond. Computational work clarified the exact mechanism of NHC insertion. Basically, three possible pathways for this transformation (see Fig. 22) were investigated. Pathway I assumes an intermolecular attack of a free NHC molecule on one of the C=C bond of the Pt complex **73**. Instead, pathways II and III both assume first the displacement of a C=C bound in **73** by an NHC molecule to give complex **75**, which can undergo intramolecular attack of the coordinated NHC ligand to the nearby C=C bound (pathway II), or intermolecular attack of a second NHC molecule to the C=C *trans* to the coordinated NHC ligand (pathway III).

Pathway I starts from complex **73** and proceeds through transition state **73–74** and an energy barrier of 4.3 kcal/mol to product **74** that is 39.5 kcal/mol more stable than the starting materials. Pathways II and III start both from **75**, in which an NHC ligand has displaced one of the C=C double bonds of the coordinated hexadiene from the Pt center. The intramolecular pathway II leads to the formation of **74** in a

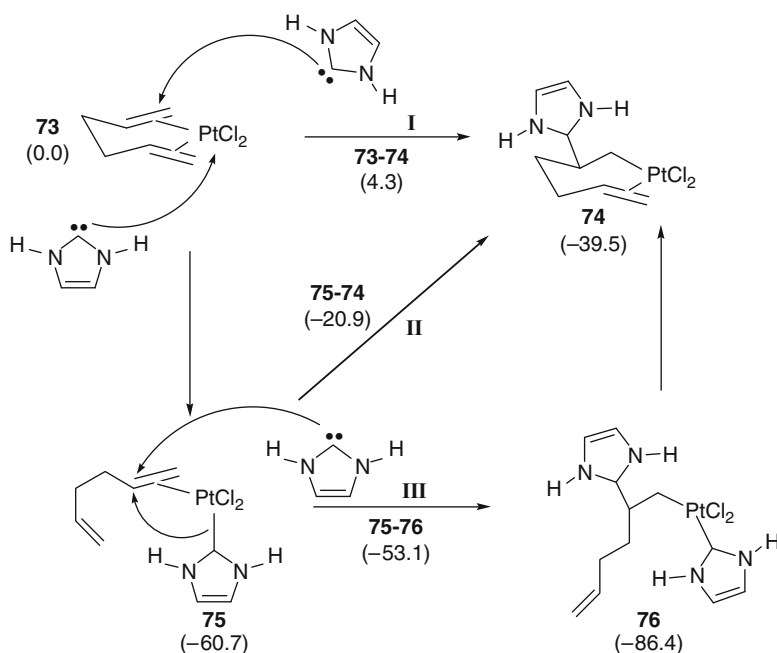


**Fig. 22** Schematic representation of the possible pathways for NHC insertion into the Pt–olefin bond of **73**. Energies in kcal/mol, relative to **73** + 2 free NHC molecules

single step, through transition state **75–74** and a barrier of 39.8 kcal/mol. Finally, the intermolecular pathway III, in which a free NHC molecule attacks the coordinated C=C double bond of **75**, leads to **76** through transition state **75–76** and a barrier of 7.6 kcal/mol. Dissociating an NHC ligand, with an energy cost of 47.3 kcal/mol leads from **76** to the final complex **74**. Based on these results the authors concluded that the preferred pathway is an intermolecular rather than intramolecular process. Further, calculations clearly showed that the intermediate leading to the final product is complex **75**.

Recently, Marinetti and co-workers reported mixed experimental and computational work on an NHC/diphosphine Pt(II) complex that was shown to be active in the cycloisomerization reaction of a N-tethered enyne such as **77**; see Fig. 23 [117].

The most relevant feature of this reaction is that the catalyst combines a chiral diphosphine ligand with an NHC ligand, which allows the isolation of axially chiral, configurationally stable, Pt complexes. These complexes were tested in the enantioselective cycloisomerization of **77** to yield **78** with reasonably good enantiomeric excesses (up to 73%) but also indicated that the axial configuration of the Pt complexes is likely to be lost during the cycloisomerization reaction. In order to

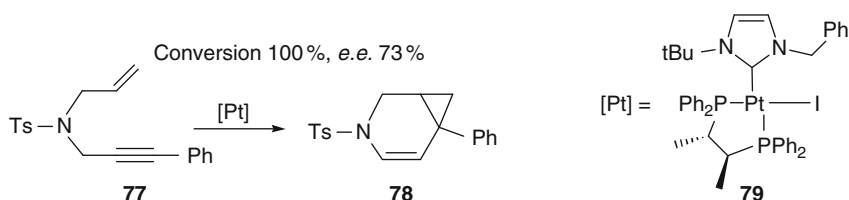


**Fig. 23** Schematic representation of enyne cycloisomerization promoted by NHC–Pt complexes

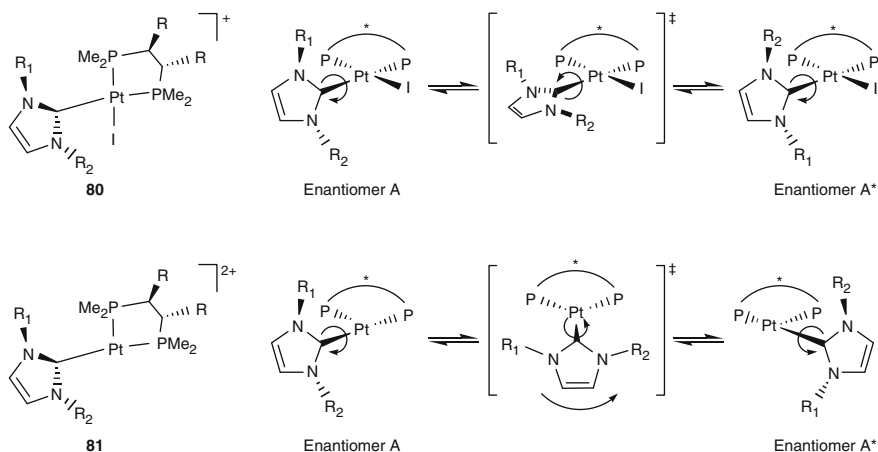


**Fig. 24** Schematic representation of Pt-complexes active in the cycloisomerization of N-tethered enyne **77**, and of the proposed mechanism of epimerization of the Pt complexes

investigate the configurational stability of these complexes, the possible epimerization pathways in the starting complex **80** and in the putative active species **81** that originates from dissociation of the iodine ligand were examined; see Fig. 24. Preliminary calculations on a model system bearing a symmetrical NHC ring ( $R^1=R^2=H$ ) indicated that the most viable pathway for epimerization in **80** is rotation of the NHC ligand around the Pt–C bond, while for **81** a pathway through a Y-shaped transition state with a migration (coined as a swing) of the NHC ligand to the empty coordination site is slightly preferred. In both cases the energy barrier amounts to only 3–4 kcal/mol. Increasing the bulkiness of one of the N-substituents of the NHC ligand ( $R^2=H$ ) resulted in an energy barrier of roughly 20 kcal/mol for rotation around the Pt–C bond in **80**, while the barrier for the migration (swing) pathway of **81** is substantially unchanged [117]. These results were in qualitative agreement with the observed easy epimerization of the tricoordinated Pt(II) complexes generated after removal of the iodine ligand.

## 5 Conclusions

In conclusion, we can state that the assistance and guidance of computational experiments has permitted us to understand fundamental processes and delineate possible reaction pathways explaining stoichiometric and catalytic reactions mediated by late transition metal–NHC systems. The examples provided are clear examples that a mix of computational and synthetic analyses are complimentary. For these reasons, we foresee continued synergy between computational and synthetic/catalytic chemists.

**Acknowledgments** Support of this work by the ERC (Advanced Research Grant to SPN) and the ENEA-GRID and CRESCO ([www.cresco.enea.it](http://www.cresco.enea.it)) in Portici, Italy (Grant to LC) is gratefully acknowledged.

## References

1. Arduengo AJ, Kline M, Calabrese JC, Davidson F (1991) *J Am Chem Soc* 113:9704
2. Díez-González S, Nolan SP (2007) *Coord Chem Rev* 251:874
3. Glorius F (2007) *Top Organomet Chem* 21:1
4. Alder RW, Blake ME, Chaker L, Harvey JN, Paolini F, Schutz J (2004) *Angew Chem Int Ed* 43:5896
5. Cavallo L, Correa A, Costabile C, Jacobsen H (2005) *J Organomet Chem* 690:5407
6. Bourissou D, Guerret O, Gabbaï FP, Bertrand G (2000) *Chem Rev* 100:39
7. Crudden CM, Allen DP (2004) *Coord Chem Rev* 248:2247
8. Nair V, Bindu S, Sreekumar V (2004) *Angew Chem Int Ed* 43:5130
9. Frenking G, Solà M, Vyboishchikov SF (2005) *J Organomet Chem* 690:6178
10. Díez-González S, Marion N, Nolan SP (2009) *Chem Rev* 109:3612
11. Weskamp T, Schattenmann WC, Spiegler M, Herrmann WA (1998) *Angew Chem Int Ed* 37:2490

12. Scholl M, Ding S, Lee CW, Grubbs RH (1999) *Org Lett* 1:953
13. Huang J, Stevens ED, Nolan SP, Peterson JL (1999) *J Am Chem Soc* 121:2674
14. Hoveyda AH, Schrock RR (2001) *Chem Eur J* 7:945
15. Fürstner A (2000) *Angew Chem Int Ed* 39:3012
16. Trnka TM, Grubbs RH (2001) *Acc Chem Res* 34:18
17. Jafarpour L, Nolan SP (2001) *J Organomet Chem* 617–618:17
18. Vázquez-Serrano LD, Owens BT, Buriak JM (2002) *Chem Commun* 2518
19. Hillier AC, Lee HM, Stevens ED, Nolan SP (2001) *Organometallics* 20:4246
20. Grasa GA, Viciu MS, Huang J, Nolan SP (2001) *J Org Chem* 66:7729
21. Grasa GA, Viciu MS, Huang J, Zhang C, Trudell ML, Nolan SP (2002) *Organometallics* 21:2866
22. Marion N, Navarro O, Mei J, Stevens ED, Scott NM, Nolan SP (2006) *J Am Chem Soc* 128:4101
23. Marion N, de Frémont P, Lemièrre G, Stevens ED, Fensterbank L, Malacria M, Nolan SP (2006) *Chem Commun* 2048
24. Correa A, Marion N, Fensterbank L, Malacria M, Nolan SP, Cavallo L (2008) *Angew Chem Int Ed* 47:718
25. Marion N, Lemièrre G, Correa A, Costabile C, Ramon RS, Moreau X, de Frémont P, Dahmane R, Hours A, Lesage D, Tabet JC, Goddard JP, Gandon V, Cavallo L, Fensterbank L, Malacria M, Nolan SP (2009) *Chem Eur J* 15:3243
26. Perry MC, Burgess K (2003) *Tetrahedron Asymmetry* 14:951
27. Funk TW, Berlin JM, Grubbs RH (2006) *J Am Chem Soc* 128:1840
28. Seiders TJ, Ward DW, Grubbs RH (2001) *Org Lett* 3:3225
29. Van Veldhuizen JJ, Garber SB, Kingsbury JS, Hoveyda AH (2002) *J Am Chem Soc* 124:4954
30. Jacobsen H, Correa A, Poater A, Costabile C, Cavallo L (2008) *Coord Chem Rev* 253:687
31. Radius U, Bickelhaupt FM (2009) *Coord Chem Rev* 253:678
32. Hashmi ASK, Hutchings GJ (2006) *Angew Chem Int Ed* 45:7896
33. Hashmi ASK (2007) *Chem Rev* 107:3180
34. Minghetti G, Bonati F (1973) *J Organomet Chem* 54:C62
35. Raubenheimer RH, Cronje S (2008) *Chem Soc Rev* 37:1998
36. Marion N, Nolan SP (2008) *Chem Soc Rev* 37:1776
37. Marion N, Nolan SP (2007) *Angew Chem Int Ed* 46:2750
38. Marco-Contelles J, Soriano E (2007) *Chem Eur J* 13:1350
39. Johansson MJ, Gorin DJ, Staben ST, Toste FD (2005) *J Am Chem Soc* 127:18002
40. Zhang L (2005) *J Am Chem Soc* 127:16804
41. Soriano E, Ballesteros P, Marco-Contelles J (2005) *Organometallics* 24:3182
42. Soriano E, Ballesteros P, Marco-Contelles J (2005) *J Org Chem* 70:9345
43. Bhanu Prasad BA, Yoshimoto FK, Sarpong R (2005) *J Am Chem Soc* 127:12468
44. Moreau X, Hours A, Fensterbank L, Goddard JP, Malacria M, Thorimbert S (2009) *J Organomet Chem* 694:561
45. Marion N, Carlqvist P, Gealageas R, de Frémont P, Maseras F, Nolan SP (2007) *Chem Eur J* 13:6437
46. Corberán R, Ramírez J, Poyatos M, Peris E, Fernández E (2006) *Tetrahedron Asymmetry* 17:1759
47. Buzas AK, Istrate FM, Gagosz F (2007) *Org Lett* 9:985
48. Porcel S, López-Carrillo V, García-Yebra C, Echavarren AM (2008) *Angew Chem Int Ed* 47:1883
49. Marion N, Gealageas R, Nolan SP (2007) *Org Lett* 9:2653
50. Gourlaouen C, Marion N, Nolan SP, Maseras F (2009) *Org Lett* 11:81
51. de Frémont P, Marion N, Nolan SP (2009) *Coord Chem Rev* 253:862
52. Zhang Z, Widenhoefer RA (2008) *Org Lett* 10:2079
53. Paton RS, Maseras F (2009) *Org Lett* 11:2237



54. Kim SM, Park JH, Kang YK, Chung YK (2009) *Angew Chem Int Ed* 48:4532
55. Li Z, Brouwer C, He C (2008) *Chem Rev* 108:3239
56. Jimenez-Nunez E, Echavarren AM (2008) *Chem Rev* 108:3326
57. Kovacs G, Ujaque G, Lledos A (2007) *J Am Chem Soc* 129:853
58. Pykkö P (2008) *Chem Soc Rev* 37:1967
59. Brouwer C, He C (2006) *Angew Chem Int Ed* 45:1744
60. Xia Y, Dudnik AS, Gevorgyan V, Li Y (2008) *J Am Chem Soc* 130:6940
61. Hamilton GL, Kang EJ, Mba M, Toste FD (2007) *Science* 317:496
62. LaLonde RL, Sherry BD, Kang EJ, Toste FD (2007) *J Am Chem Soc* 129:2452
63. Marion N, Nolan SP (2008) *Acc Chem Res* 41:1440
64. Wurtz S, Glorius F (2008) *Acc Chem Res* 41:1523
65. Kantchev EAB, O'Brien CJ, Organ MJ (2007) *Angew Chem Int Ed* 46:2768
66. Herrmann WA, Oefele K, Dv P, Schneider SK (2003) *J Organomet Chem* 687:229
67. Hillier AC, Grasa GA, Viciu MS, Lee HM, Yang C, Nolan SP (2002) *J Organomet Chem* 653:69
68. Nicolaou KC, Bulger PG, Sarlah D (2005) *Angew Chem Int Ed* 44:4442
69. Stahl SS (2005) *Science* 16:1824
70. Stahl SS (2004) *Angew Chem Int Ed* 43:3400
71. Sigman MS, Schult MJ (2004) *Org Biomol Chem* 2:2551
72. Stoltz BM (2004) *Chem Lett* 33:362
73. Sheldon RA, Arends IWCE, Ten Brink GJ, Dijkman A (2002) *Acc Chem Res* 35:774
74. Jensen DR, Schultz MJ, Mueller JA, Sigman MS (2003) *Angew Chem Int Ed* 42:3810
75. Schultz MJ, Hamilton SS, Jensen DR, Sigman MS (2005) *J Org Chem* 70:3343
76. Nielsen RJ, Goddard WA (2006) *J Am Chem Soc* 128:9651
77. Chowdhury S, Rivalta I, Russo N, Sicilia E (2008) *Chem Phys Lett* 456:41
78. Mueller JA, Goller CP, Sigman MS (2004) *J Am Chem Soc* 126:9724
79. Konnick MM, Guzei IA, Stahl SS (2004) *J Am Chem Soc* 126:10212
80. Popp BV, Wendlandt JE, Landis CR, Stahl SS (2007) *Angew Chem Int Ed* 46:601
81. Konnick MM, Gandhi BA, Guzei IA, Stahl SS (2006) *Angew Chem Int Ed* 45:2904
82. Konnick MM, Stahl SS (2008) *J Am Chem Soc* 130:5753
83. Popp BV, Stahl SS (2007) *J Am Chem Soc* 129:4410
84. Fantasia S, Egbert JD, Jurcik V, Cazin CSJ, Jacobsen H, Cavallo L, Heinekey DM, Nolan SP (2009) *Angew Chem Int Ed* 48:5182–5186
85. Lillo V, Mas-Marzá E, Segarra AM, Carbó JJ, Bo C, Peris E, Fernandez E (2007) *Chem Commun* 3380
86. O'Brien CJ, Kantchev EAB, Chass GA, Hadei N, Hopkinson AC, Organ MG, Setiadi DH, Tang TH, Fang DC (2005) *Tetrahedron* 61:9723
87. Albert K, Gisdakis P, Rosch N (1998) *Organometallics* 17:1608
88. Yandulov DV, Tran NT (2007) *J Am Chem Soc* 129:1342
89. Chass GA, O'Brien CJ, Niloufar H, Kantchev EAB, Wei-Hua M, De-Cai F, Hopkinson AC, Csizmadia IG, Organ MG (2009) *Chem Eur J* 15:4281
90. Lee MT, Lee HM, Hu CH (2007) *Organometallics* 26:1317
91. Green JC, Herbert BJ, Lonsdale R (2005) *J Organomet Chem* 690:6054
92. Penka EF, Schlaepfer CW, Atanasov M, Albrecht M, Daul C (2007) *J Organomet Chem* 692:5709
93. Goossen LJ, Koley D, Hermann HL, Thiel W (2005) *Organometallics* 25:54
94. Stambuli JP, Incarvito CD, Bühl M, Hartwig JF (2004) *J Am Chem Soc* 126:1184
95. Pérez-Temprano MH, Nova A, Casares JA, Espinet P (2008) *J Am Chem Soc* 130:10518
96. Fazaeli R, Ariafard A, Jamshidi S, Tabatabaie ES, Pishro KA (2007) *J Organomet Chem* 692:3984
97. Ahlquist M, Norrby P-O (2007) *Organometallics* 26:550
98. Barder TE, Biscoe MR, Buchwald SL (2007) *Organometallics* 26:2183
99. Senn HM, Ziegler T (2004) *Organometallics* 23:2980

100. Alvarez E, Conejero S, Paneque M, Petronilho A, Poveda ML, Serrano O, Carmona E (2006) *J Am Chem Soc* 126:13060
101. Braga AAC, Morgon NH, Ujaque G, Lledós A, Maseras F (2006) *J Organomet Chem* 691:4459
102. Braga AAC, Morgon NH, Ujaque G, Maseras F (2005) *J Am Chem Soc* 127:9298
103. Napolitano E, Farina V, Persico M (2003) *Organometallics* 22:4030
104. Nova A, Ujaque G, Maseras F, Lledós A, Espinet P (2006) *J Am Chem Soc* 128:14571
105. Ananikov VP, Musaev DG, Morokuma K (2005) *Organometallics* 24:715
106. Zuidema E, van Leeuwen PWNM, Bo C (2005) *Organometallics* 24:3703
107. Surawatanawong P, Fan Y-B, Hall MB (2008) *J Organomet Chem* 693:1552
108. Barder TE, Buchwald SL (2007) *J Am Chem Soc* 129:12003
109. McGuinness DS, Cavell KJ, Skelton BW, White AH (1998) *Organometallics* 17:565
110. McGuinness DS, Saendig N, Yates BF, Cavell KJ (2001) *J Am Chem Soc* 123:4029
111. Graham DC, Cavell KJ, Yates BF (2006) *Dalton Trans* 14:1768
112. Markò IE, Sterin S, Buisine O, Mignani R, Branlard P, Tinant B, Declercq JP (2002) *Science* 298:204
113. Markò IE, Sterin S, Buisine O, Berthon G, Michaud G, Tinant B, Declercq JP (2004) *Adv Synth Catal* 346:1429
114. Zhang Y, Zhao L, Patra PK, Ying JY (2008) *Adv Synth Catal* 350:662
115. Sprengers JW, Mars MJ, Duin MA, Cavell KJ, Elsevier CJ (2003) *J Organomet Chem* 679:149
116. Jung IG, Seo J, Lee SI, Choi SY, Chung YK (2006) *Organometallics* 25:4240
117. Brissy D, Skander M, Retailleau P, Frison G, Marinetti A (2009) *Organometallics* 28:140
118. Lillo V, Mata JA, Segarra AM, Peris E, Fernandez E (2007) *Chem Commun* 2184
119. Fantasia S, Jacobsen H, Cavallo L, Nolan SP (2007) *Organometallics* 26:3286



# Activation of Allenes by Gold Complexes: A Theoretical Standpoint

Max Malacria, Louis Fensterbank, and Vincent Gandon

**Abstract** This review provides an insight into the activation of allenes by gold complexes toward nucleophilic attack. The various possible geometries of allene–gold species, from  $\eta^2$ -allenes to  $\eta^1$  allylic cations, are described. From the data collected in the literature, it is clear that all of these intermediates have been met during computational analysis of reaction mechanisms. While some retain the stereochemical information of the starting optically active allenes, others may lose it by planarization. To shed light on that matter, the factors governing axial-to-center chirality transfer are described. Some concepts are illustrated by selected examples of catalytic transformations, the mechanisms of which have been studied computationally.

**Keywords** Allene · Cation · Chirality transfer · Cycloisomerization · Gold

## Contents

1	Introduction .....	158
2	Structure and Bonding of Au-Allene Complexes .....	160
2.1	$\eta^2$ -Allene Complexes Versus Allylic Cations .....	160
2.2	Consequences on Chirality Transfers .....	164
3	Reaction Mechanisms .....	170
3.1	Cycloisomerization of Ene-Vinyl Allenes .....	170
3.2	Cycloisomerization of 1-Aryl-1-allene-6-enes .....	173
3.3	Hydrative Carbocyclizations of Allenynes .....	173
3.4	Transformation N-Tethered of 1,5-Bisallenes into 6,7-Dimethyl-3-azabicyclo[3.1.1]heptanes .....	178
4	Conclusions .....	180
	References .....	180

---

M. Malacria and L. Fensterbank  
UPMC Univ Paris 06, Institut Parisien de Chimie Moléculaire (UMR CNRS 7201), C. 229, 4 Place  
Jussieu, 75005 Paris, France

V. Gandon (✉)  
ICMMO, UMR CNRS 8182, Université Paris-Sud 11, 91405 Orsay Cedex, France  
e-mail: vincent.gandon@u-psud.fr

## List of Abbreviations

Ac	Acetyl
Alk	Alkyl
biPh	Biphenyl
Bu	Butyl
ee	Enantiomeric excess
IPr	Bis(2,6-diisopropylphenyl)-imidazol-2-ylidene
Me	Methyl
mol	Mole(s)
NHC	<i>N</i> -Heterocyclic carbene
Ph	Phenyl
PNB	<i>p</i> -Nitrobenzoate
<i>t</i> -Bu	<i>tert</i> -Butyl
Tf	Triflate
Ts	Tosyl

## 1 Introduction

Allenes are versatile substrates that are widely used in transition and main group metal-catalyzed reactions. In that respect, numerous examples of gold-catalyzed transformations involving allenes have been reported (for selected reviews on gold-catalyzed transformations, see [1–11]). Their unique bonding situation comprising two perpendicular  $\pi$  systems allows the formation of up to four regioisomeric  $\eta^2$  complexes of type **I**, depending on the substitution pattern (Fig. 1) (for reviews on transition metal-allene complexes, see [12, 13]). The peculiar *sp*-hybridized central carbon can also give rise to  $\eta^1$   $\sigma$ -complexes, extreme cases being gold-stabilized allylic cations of type **II** or carbenes of type **III** (for experimental evidence of the coordination of Cu, Ag, and Au to allene central carbon, see [14]).

The complexation of gold onto allenes activates them towards the addition of oxygen-, nitrogen-, or carbon nucleophiles [1–11]. For instance, alcohols, amines, and electron-rich arenes can add to the external or central carbons to furnish hydroalkoxylation, hydroamination, or hydroarylation products (Fig. 2).

With  $\pi$ -systems as nucleophiles (alkenes, dienes, alkynes, allenes, ketones, ...), the formation of a bond at the external allene carbon may be followed, in a stepwise or asynchronous concerted fashion, by the creation of a second C–C bond at the

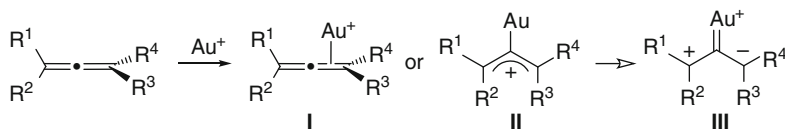


**Fig. 1** Various coordination modes of allenes

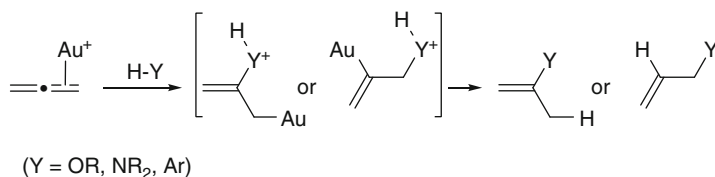


**Fig. 2** Prototypical addition of H-Y on a complexed allene bond

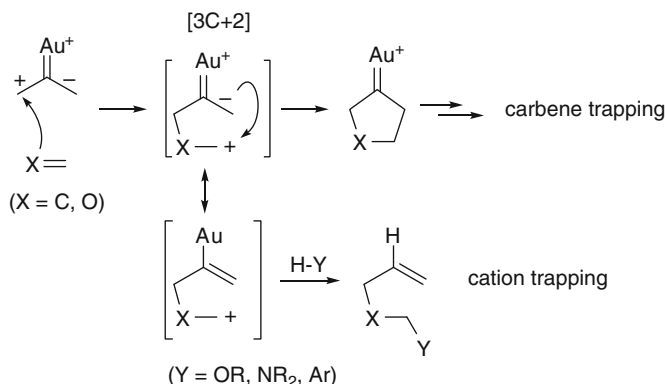


**Fig. 3** Prototypical addition of a  $\pi$ -system on a complexed allene generating a gold-stabilized carbene or a vinyl-gold species

other end (Fig. 3). Thus, allenes can also be activated as formal 3-carbon dipoles in  $[3C+n]$  cycloaddition reactions.<sup>1</sup> The isolated product will then depend on the evolution or trapping of the resulting cyclic carbene. On the other hand, the cationic intermediate resulting from the first nucleophilic attack can be trapped by nucleophiles such as alcohols, amines, or arenes.

In this contribution, we will cover the gold-catalyzed transformations involving allene substrates that have been investigated by means of computational studies. Because some of these transformations will be the subject of other chapters of this book, only selected features related to the present discussion will be mentioned. Among the transformations that will not be covered in detail herein, there are the  $[4C+nC]$  ( $n = 2$  or  $3$ ) cycloaddition of allenedienes (for combined experimental and theoretical studies, see [16, 17]), all reactions involving  $[3,3]$ -sigmatropic rearrangement through allenic esters (for a selected theoretical study, see [18]; for a combined experimental and theoretical study, see [19]), and the heterocyclization of allenes (for a selected combined experimental and theoretical study, see [20]; for a selected theoretical study, see [21]). Also, the reactions in which the allenes only serve as nucleophiles, such as in cycloisomerization of allenynes (for combined

<sup>1</sup>The  $[3+2]$  cycloaddition could be considered as a metallat-TMM, in analogy with [15].

experimental and theoretical studies, see inter alia [22, 23]; for the competition between allene and alkyne activation, see [24]) have been deliberately put aside. Thus, this chapter will focus on the cycloisomerization of vinyl-, homoallyl-, and allenylallenes, as well as the hydrative cyclization of allenynes (to the best of our knowledge, the gold-catalyzed transformations of allylallenes were not studied computationally; see [25, 26]).

## 2 Structure and Bonding of Au-Allene Complexes

The first part of this section describes the various species that have been computed using model allenes and  $\text{LAu}^+$  fragments, that is  $\eta^2$ -allene gold complexes and gold-stabilized allylic cations. Because the formation of the latter type of intermediates may cause the loss of the stereochemical information of the starting allene, a discussion about chirality transfers will follow as the second part.

### 2.1 $\eta^2$ -Allene Complexes Versus Allylic Cations

Throughout this section we will use the following descriptors to account for the geometry of the complexes (Fig. 4): the length of the complexed allene bond ( $d$ ), the angle between the two allene bonds ( $\alpha$ ), the angle defined by the gold center and the two carbon atoms of the complexed allene bond ( $\beta$ ), and the absolute value of the dihedral angle defined by the bonds between the allene substituents pointing *anti* to gold and the terminal allene carbons ( $\gamma$ ). In case of doubt,  $d$  and  $\beta$  always concern the right hand side of the molecule drawn.

To the best of our knowledge, no X-ray diffraction study regarding  $\eta^2$ -allene gold complexes has been reported (for X-ray structures of platinum-allene complexes, see inter alia [27, 28]). However, the reaction of tetramethyltetraaminoallene with  $\text{Au}(\text{PPh}_3)^+$  led to isolation and X-ray characterization of the allylic cation **1**, in which gold is coordinated to the central allene carbon (Fig. 5) [29]. The peculiar structure of this species was considered as a prototype of carbodicarbene-gold complex, a new kind of ligand that is receiving much attention on both experimental and theoretical levels [30–35].

In spite of the lack of X-ray derived geometries, the literature is rich in calculated structures, many of them being slipped  $\eta^2$ -allene complexes of type **I** (for the concept of slippage, see [36, 37]). In the typical one **2** depicted below (Fig. 6) [23],

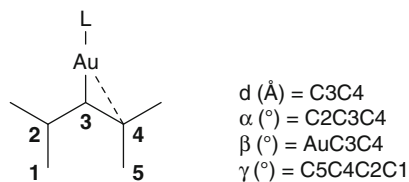


**Fig. 4** Geometrical parameters used in this chapter

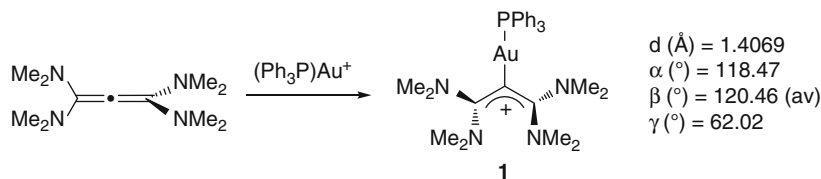


**Fig. 5** Key geometrical parameters obtained from the X-ray diffraction study of complex **1**

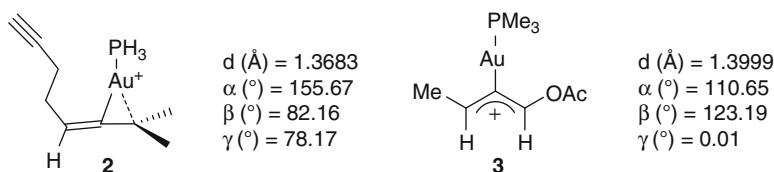


**Fig. 6** Computational levels: *left*: B3LYP/LANL2DZ(Au)/6-31+G\*(C, H, P); *right*: B3LYP/LANL2DZ(Au)/6-31G\*\*(C, H, O, P)

the complexed allene bond is shorter than in the carbodicarbene complex **1**, the allene is less bent, and the dihedral angle is larger.

On the other hand, an extreme case would be a planar allylic cation such as **3**, with geometrical features similar to **1** yet with a  $\gamma$  angle close to 0. Such species have been computed as well [38]. They show the most severely bent allene frameworks (shortest  $\alpha$  angle).

Based on the geometrical data gleaned in the literature (see all specific examples shown above and below, and [39, 40]), especially the  $\gamma$  angle, it would be tempting to divide allene–gold complexes into those three categories (Fig. 7):  $\eta^2$ -allene complexes **I** such as **2**, twisted allylic cations **II** such as **1** (also referred to as bent-allene complexes), and planar allylic cations **II'** such as **3**. However, inspection of the other geometrical parameters suggests that there is rather a continuum, at least between twisted and planar allylic cations.

The twist angle  $\gamma$  can be related to the allylic strain. While with two face-to-face hydrogen atoms, planar allylic cations such as **6** converge as minimum (Fig. 8), two face-to-face methyl groups move away from each other during optimization, giving rise to a twisted allylic cation such as **5** [38].

As far as allenyl esters are concerned, the moderate allylic strain generated by the  $sp^3$ -hybridized oxygen atom of the carboxyl group and the hydrogen atom leads to slightly twisted allylic cations such as **7** (Fig. 9), exhibiting  $\gamma$  angles around 25–30° [41]. As expected, the replacement of this hydrogen by a methyl group as in **8** induces a much larger twist angle (55–60°), yet smaller than in the case of two methyl groups (65°, see **5** in Fig. 8).

Transition states have been located for the transformation of species of type **I** into **II** or **II'**. For instance, the  $\eta^2$ -allene complex **9** (Fig. 10) rearranges into the planar allylic cation **3** at a low enthalpic cost of 2.4 kcal mol<sup>−1</sup> [38]. In addition, the transformation of **10** into the twisted allylic cation **11** requires only 0.1 kcal mol<sup>−1</sup> of enthalpy of activation.



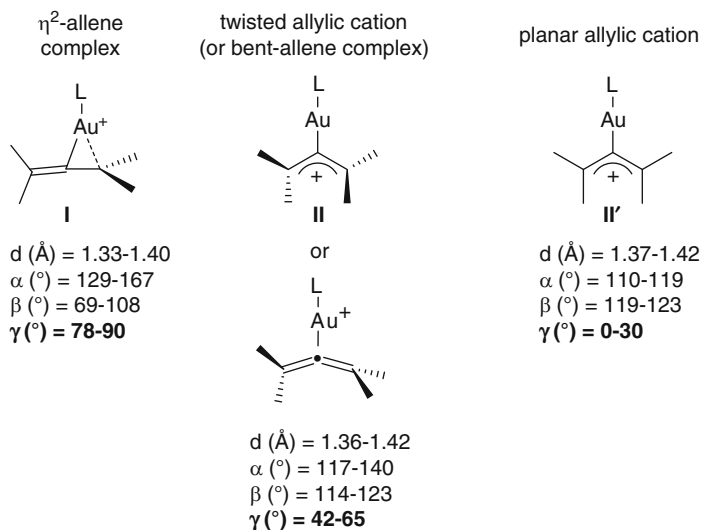


**Fig. 7** Ranges of values for key geometrical features extracted from the literature

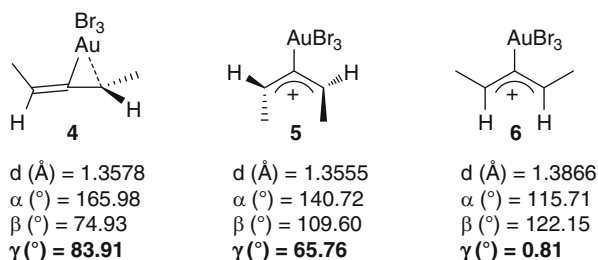


**Fig. 8** Gold complexes of 1,3-dimethylallene (computational level: B3LYP/LANL2DZ(Au)/6-31G\*\*(C, H, Br))

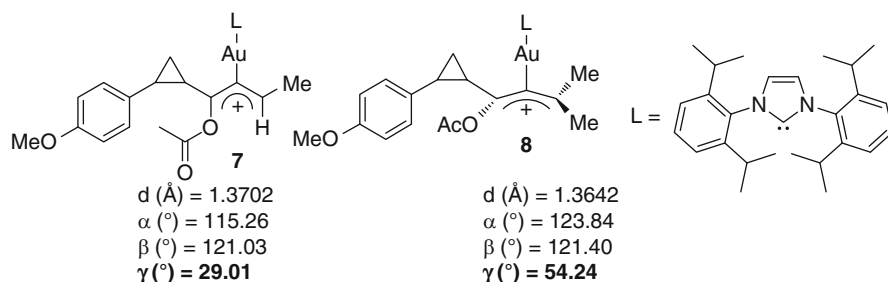


**Fig. 9** Computational level: B3LYP/LANL2DZ(Au)/6-31G\*(C, H, O, N)

Interestingly, the easily formed allylic cation **3** is the ground state of the system. The consequence of this rearrangement on the racemization of allenes under gold catalysis will be discussed in [Sect. 2.2](#).

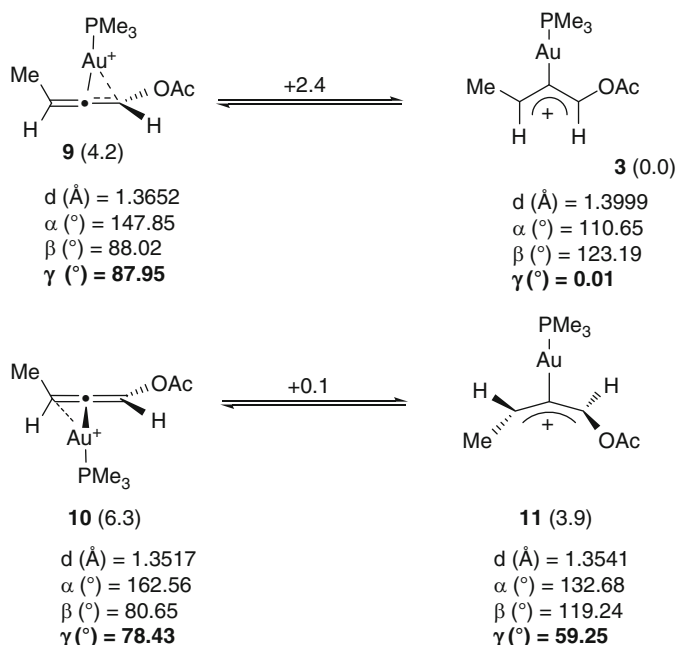


**Fig. 10** Interconversion between gold complexes of an allenyl ester (computational level: B3LYP/LANL2DZ(Au)/6-31G\*\*(C, H, O, P); relative enthalpies in kcal mol<sup>-1</sup>; the barrier heights from left to right are indicated over the *equilibrium arrows*)

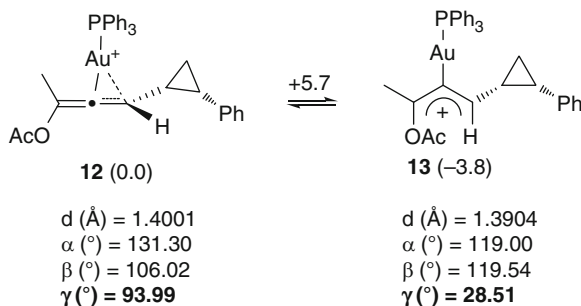


**Fig. 11** Interconversion between gold complexes of a cyclopropyl allene (computational level: B3LYP/LACVP(Au)/6-31G\*\*(C, H, O, P)//PB (CH<sub>2</sub>Cl<sub>2</sub>); relative Gibbs energy in kcal mol<sup>-1</sup>; the barrier height from left to right is indicated over the *equilibrium arrow*)

In the cyclopropylallenyl ester series, it was also found that the formation of allylic cations was exergonic and proceeded via low-lying transition states (Fig. 11) [42]. For instance, the  $\eta^2$ -allene complex **12** rearranges with a barrier of 5.7 kcal mol<sup>-1</sup> into the almost planar allylic cation **13**, slightly more stable by 3.8 kcal mol<sup>-1</sup> (Fig. 11).

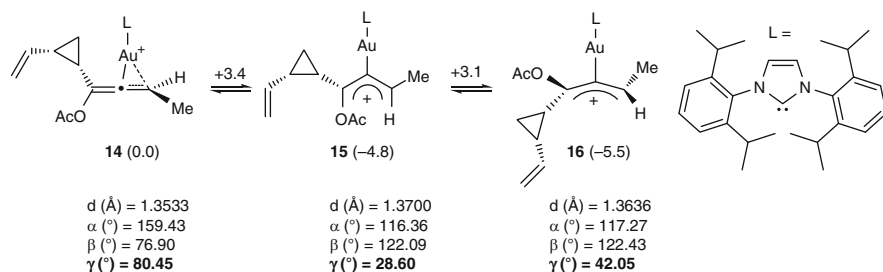


**Fig. 12** Interconversion between gold complexes of a cyclopropyl allene (computational level: B3LYP/LANL2DZ(Au)/6-31G\*\* (C, H, O, N)/IEF-PCM(CH<sub>2</sub>Cl<sub>2</sub>); relative enthalpies in kcal mol<sup>-1</sup>; the barrier heights from left to right are indicated over the equilibrium arrows)

Similarly, complex **14** transforms exothermically into the virtually planar allylic cation **15** via a transition state lying 3.4 kcal mol<sup>-1</sup> above the ground state (Fig. 12) [41]. The latter rearranges in a slightly exothermic fashion into the most severely twisted allylic cation **16** at an enthalpic cost of 3.1 kcal mol<sup>-1</sup>.

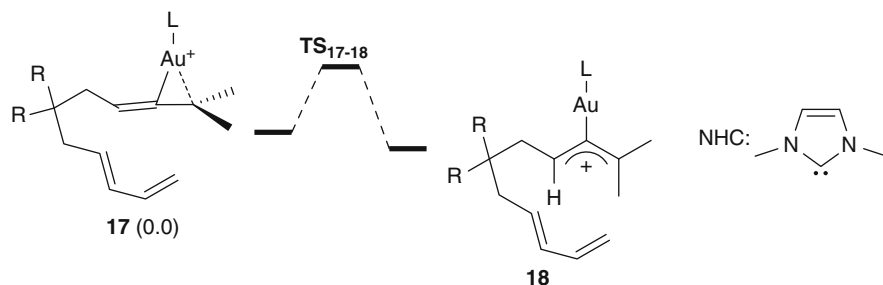
Two independent studies on allenediene systems allow one to gain some insight into ligand effects (Table 1) [16, 17]. In this particular series, the transformation of  $\eta^2$ -allene complexes of type **17** into gold-stabilized allylic cations **18** is moderately exergonic to quite endergonic. In terms of kinetics, it is somewhat faster with phosphines and phosphites than with an *N*-heterocyclic carbene.

Although quite difficult to rationalize, one can infer that the steric bulk of the ligand plays a role in determining the  $\gamma$  twist angle. Probably in order to minimize the steric hindrance between the substituents at L and those of the allylic cation pointing toward gold, the P(*t*-Bu)<sub>2</sub>(*o*-biphenyl) containing complex **18** displays the largest  $\gamma$  angle of the series (Fig. 13).

The apparent ease by which  $\eta^2$ -allene gold complexes rearrange into planar or virtually planar allylic cations implies that the stereochemistry of the starting allene is not expected to persist. However, gold-catalyzed reactions in which enantioenriched allenes transform into enantioenriched products have been reported, suggesting that a given reaction of a  $\eta^2$ -allene complex can be even faster than the formation of planar allylic cations. It could also be that twisted (chiral) allylic cations are involved. A discussion about this phenomenon is provided below.

## 2.2 Consequences on Chirality Transfers

Electrophilic activation of optically active allenes by transition metal complexes is a well-established strategy to generate enantioenriched products (for recent reviews on stereoselective gold catalysis involving allenes, see [43, 44]). In that respect, chiral  $\alpha$ - and  $\beta$ -hydroxyallenes or -aminoallenes can be cyclized in the presence of gold(I) or gold(III) salts into the corresponding five- and six-membered heterocycles with axis-to-center transfer of chirality, (for selected examples, see [45–55])

**Table 1** Ligand effect in the rearrangement of  $\eta^2$ -allene complexes into allylic cations

L	PH <sub>3</sub>	PMe <sub>3</sub>	PPh <sub>3</sub>	P( <i>t</i> -Bu) <sub>2</sub> ( <i>o</i> -biPh)	P(OMe) <sub>3</sub>	P(OPh) <sub>3</sub>	NHC
<b><i>R = H</i></b>							
$\Delta E_{\text{TS17-18}}$	5.2	—	—	—	5.1	—	8.4
$\Delta E_{17-18}$	−0.6	—	—	—	−0.3	—	5.6
<b>17</b>							
d (Å)	1.3696	—	—	—	1.3628	—	1.3609
$\alpha$ (°)	155.03	—	—	—	157.07	—	158.14
$\beta$ (°)	82.52	—	—	—	80.94	—	78.71
$\gamma$ (°)	77.01	—	—	—	77.82	—	76.72
<b>18</b>							
d (Å)	1.4079	—	—	—	1.4093	—	1.4104
$\alpha$ (°)	118.56	—	—	—	118.29	—	116.45
$\beta$ (°)	121.39	—	—	—	120.89	—	122.82
$\gamma$ (°)	8.56	—	—	—	9.91	—	3.38
<b><i>R = CO<sub>2</sub>Me</i></b>							
$\Delta G_{\text{TS17-18}}$	—	5.5	—	—	—	—	—
$\Delta G_{17-18}$	—	6.3	11.8	5.2	—	−2.39	—
<b>17</b>							
d (Å)	—	1.3582	1.3536	1.3553	—	1.3641	—
$\alpha$ (°)	—	159.20	165.07	159.01	—	154.14	—
$\beta$ (°)	—	80.11	77.78	76.72	—	80.28	—
$\gamma$ (°)	—	78.50	78.26	74.92	—	77.30	—
<b>18</b>							
d (Å)	—	1.4110	—	1.4014	—	1.4051	—
$\alpha$ (°)	—	116.52	—	116.62	—	118.35	—
$\beta$ (°)	—	122.48	—	120.71	—	121.73	—
$\gamma$ (°)	—	0.04	—	13.91	—	5.59	—

Relative energies in kcal mol<sup>−1</sup>. Computational level: ***R = H***: B3LYP/LANL2DZ(f)(Au)/6-31G\* (C, H, P, O, N)//CPCM(CH<sub>2</sub>Cl<sub>2</sub>)/LANL2DZ(f)/6-311++G\*\*; ***R = CO<sub>2</sub>Me***: M06/LACVP\*\*(Au)/6-31G\*(C, H, P, O)//LACV3P++\*(2f)/6-311++G\*\*/PB(CH<sub>2</sub>Cl<sub>2</sub>).

even in intermolecular versions [56, 57]. Whether the nucleophile attacks a species of type **I**, **II**, or **II'** is of prime importance to account for the transfer of chirality (Fig. 14). Indeed, although the stereochemical information is maintained in allene complexes of type **I**, it is lost when planar allylic cations **II'** are formed. Even if these species are not strictly planar, their rotation barrier is so low that racemization of the starting allene is expected to be much faster than any other reaction process

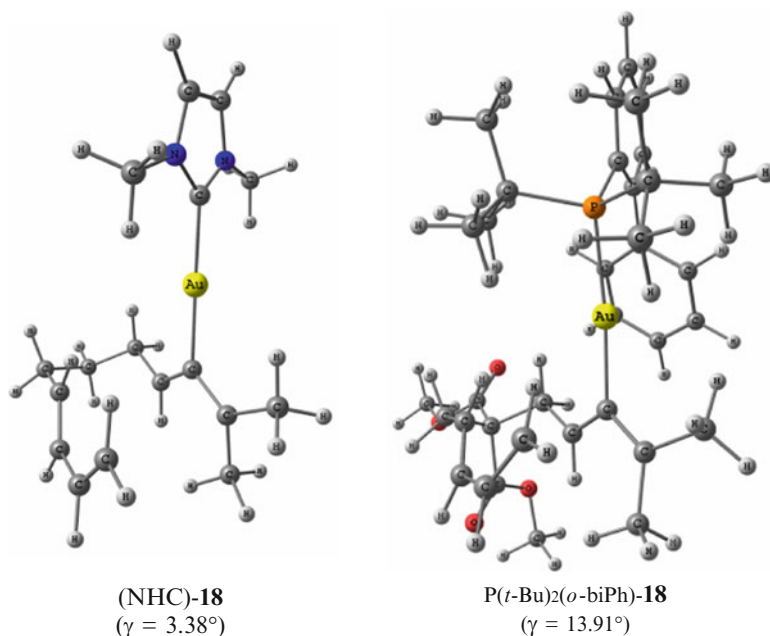


**Fig. 13** Influence of the gold ligand on the geometries of  $\eta^1$ -allenediene complexes

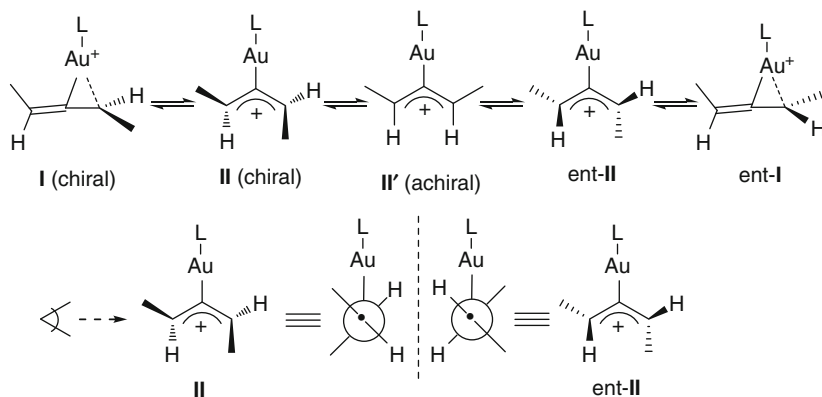


**Fig. 14** Gold complexes of 1,3-dimethylallene

(see below) (for examples of gold-catalyzed epimerization of allenes, see *inter alia* [58, 59]). On the other hand, twisted allylic cations **II** are chiral species which keep the memory of the chirality of the starting material. Concerted racemization of such complexes is expected to be easier than that of  $\eta^2$ -allene complexes, but more difficult than that of virtually planar allylic cations, leaving a good chance for another elementary step to take place.

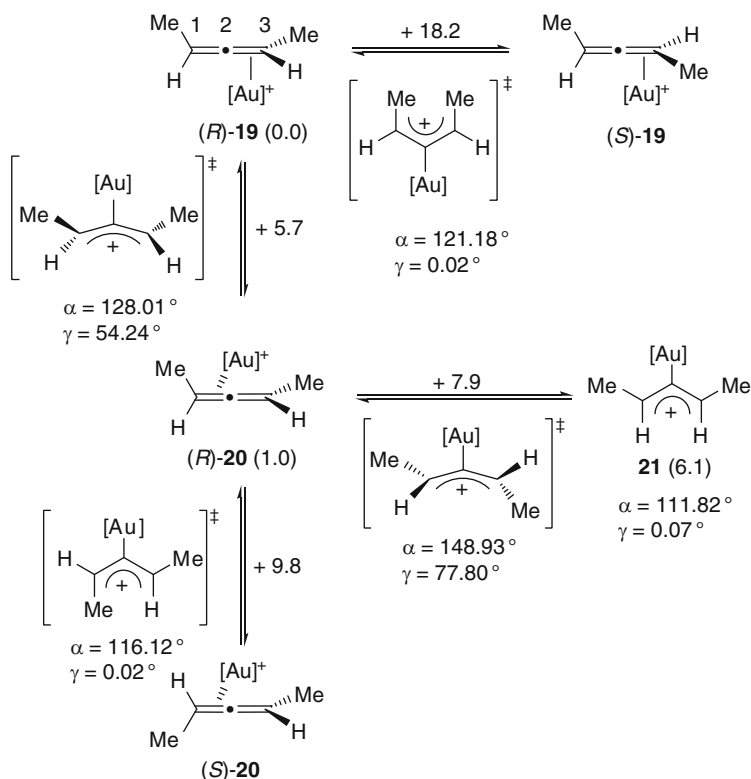


**Fig. 15** Interconversion between gold complexes of 1,3-dimethyl allene ([Au] = Au(PMe<sub>3</sub>); computational level: B3LYP/LANL2DZ(Au)/6-31G\*\*(C, H, P); relative enthalpies in kcal mol<sup>-1</sup>; the barrier heights from left to right and up to down are indicated in *parentheses*)

In the specific case of 1,3-dimethylallene and Au(PMe<sub>3</sub>)<sup>+</sup>, the complexes **19** and **20** were found to be more stable than the allylic cation **21** (Fig. 15) [38]. The latter was the only C2-coordinated compound which converged as a minimum. The other possible geometries of this kind were obtained as transition states. The 90° shift of the gold atom when going from (*R*)-**19** to (*R*)-**20** is achieved through a type **II** transition state and requires 5.7 kcal mol<sup>-1</sup> of enthalpy of activation.

On the other hand, the planar transition state TS<sub>(*R*)-19-(*S*)-19</sub>, which allows the stereomutation of the starting allene, lies 18.2 kcal mol<sup>-1</sup> above the minimum. Also the inversion of (*R*)-**20** can be achieved through the less hindered planar transition state TS<sub>(*R*)-20-(*S*)-20</sub> lying 9.8 kcal mol<sup>-1</sup> above the minimum. Apart from these two concerted racemization processes, the stereochemistry of the allene can also be lost when forming the planar cation **21**, through a twisted transition state lying 7.9 kcal mol<sup>-1</sup> above **20**.

Thus, with this simple unfunctionalized disubstituted allene, coordination to the central carbon atom is enthalpically disfavored, and the concerted racemizations require quite high enthalpies of activation. This may account for the good chirality

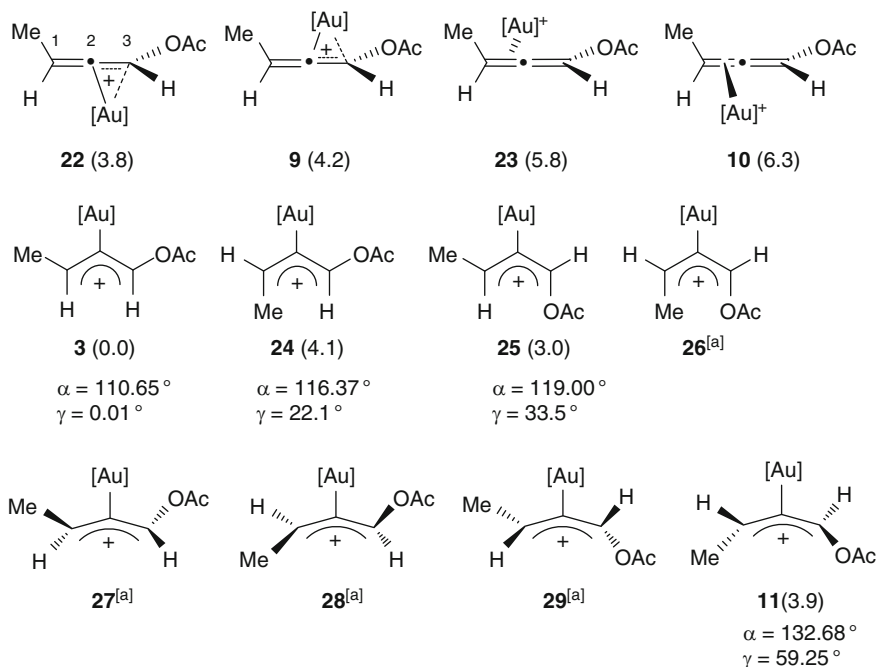


**Fig. 16** Various coordination modes of (*R*)-buta-1,2-dienyl acetate to gold (I) ([Au] = Au (PMe<sub>3</sub>); relative enthalpies in kcal mol<sup>-1</sup>; <sup>[a]</sup> these species did not converge and collapsed to the corresponding planar or twisted C2-coordinated compound)

transfers observed with 1,3-dialkyl or 1-phenyl-3-alkyl allenes [56, 57], the nucleophilic addition being faster than these competitive processes.

However, the presence of an electron-donating group at the allene can modify this trend. For instance, Fig. 16 shows all possible complexes of a given allenyl acetate. Within this family, 8 of the 12 possible candidates converged as minima. The allylic cation **3** is now the ground state of the system, all other isomers being at least 3.0 kcal mol<sup>-1</sup> less stable. The participation of the oxygen atom to the conjugation is clearly revealed by the short C3O distance of 1.31 Å. It is worthy of note that two other C2-coordinated allenes are more stable (**25**) or of similar energy (**11**) compared to the most stable  $\eta^2$ -allene complex **22**.

All species are connected via low-lying transition states, two examples being shown on Fig. 10. The racemization of complexes **24** and **25**, which are not strictly planar but very close to planarity, requires only 0.1 and 0.01 kcal mol<sup>-1</sup> respectively of enthalpy of activation. For this reason, all allylic cations exhibiting modest  $\gamma$  twist angles have been depicted as planar species throughout this chapter. Interestingly, the 45° shift of the metal from the  $\eta^2$  allene complex **10** to the twisted allylic cation **11** is also straightforward (Fig. 10,  $\Delta H_{298}^\ddagger = 0.1$  kcal mol<sup>-1</sup>). On the other hand, the 90° rotation of the CHOAc group converting **9** into **3** requires 2.4 kcal mol<sup>-1</sup> of enthalpy of activation (Fig. 10). It is also worth mentioning that the stereochemistry of the twisted allylic cation **11** may also invert via a planar transition state (Fig. 17).

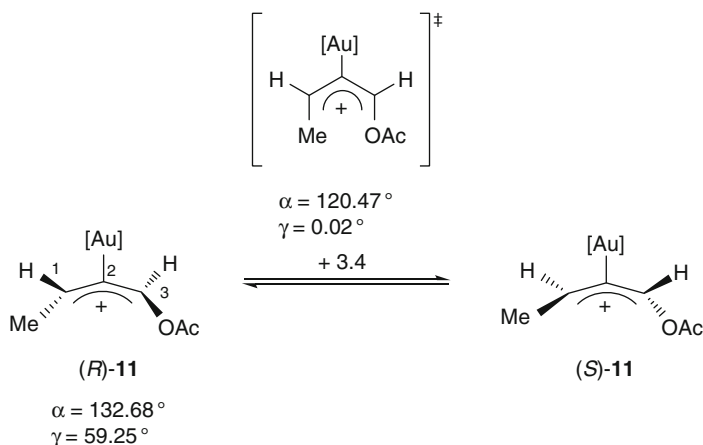


**Fig. 17** Racemization of a twisted allylic cations ([Au] = Au(PMe<sub>3</sub>); relative enthalpies in kcal mol<sup>-1</sup>; the barrier height is indicated over the *equilibrium arrow*)

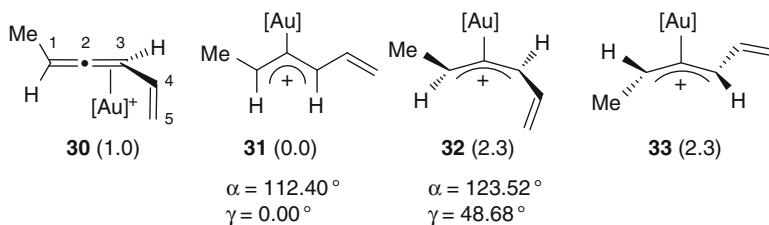


**Fig. 18** Selected examples of gold complexes of disubstituted hexa-1,3,4-triene ([Au] = Au(PMe<sub>3</sub>); relative enthalpies in kcal mol<sup>-1</sup>)

The case of vinyl allenes was also investigated (Fig. 18). The allylic cation **31** was obtained as the ground state. Again, the conjugation was obvious from the C3C4 bond length of 1.43 Å. Thus, these species can also be considered as pentadienyl cations exhibiting helical chirality [60]. In contrast with the 1,3-dimethyl allene system described above, although slightly less stable than the  $\eta^2$ -coordinated allene, the bent structures **32** and **33** could be modeled.

Importantly, no more planar structure could be modeled in the case of trisubstituted allenes (Fig. 19). Besides, the ground states are now twisted complexes such as **35** or **38**.

Therefore, it seems quite clear that the 1,3-allylic strain is a critical feature to ensure chirality transfer because it prevents the formation of planar cations and also slows down the racemization of allenes. Because twisted structures retain the stereochemical information of the substrate, a reaction that requires the formation of C2-coordinated allenes may give rise to a transfer of chirality. This transfer should be even more efficient as the substitution of the allene increases (see next paragraph).



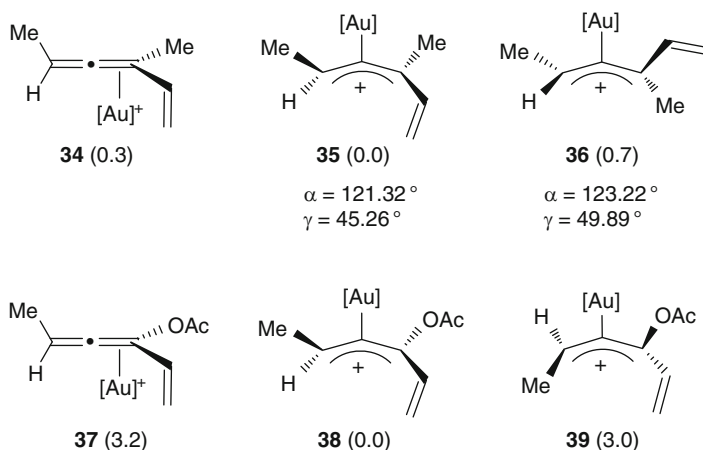


**Fig. 19** Selected examples of gold complexes of trisubstituted hexa-1,3,4-triene ([Au] = Au(PMe<sub>3</sub>); relative enthalpies in kcal mol<sup>-1</sup>)

### 3 Reaction Mechanisms

Having described the various species that have been computed between allenes and LAu<sup>+</sup> fragments, we will now focus on their involvement in chemical transformations.

#### 3.1 Cycloisomerization of Ene-Vinyl Allenes

The gold(I)-catalyzed cycloisomerization of ene-vinyl allenes allows the formation of polycyclic compounds in a highly diastereoselective fashion [61, 62]. For instance, in the presence of AuCl(PPh<sub>3</sub>)/AgSbF<sub>6</sub> (2 mol%), ene-vinyl allenes **40–42** and **46–48** cyclized in 10–30 min at room temperature (**40–42**) or 0 °C (**46–48**) to give the desired tricyclic compounds (Fig. 20).

Propargyl acetates such as **52–56**, **62**, and **63** undergo the same kind of transformation (Fig. 21).

In this case, allenyl esters are formed in situ via a well-known rearrangement, notably being catalyzed by gold (see [18] and references therein). This transformation provides in situ the vinyl allene moiety exhibiting the required substitution pattern for the next step (Fig. 22).

The mechanism has been studied by DFT computations [61]. The first transition state connects the gold-stabilized cyclopentenylidene **B** with the twisted species **A** similar to those described in the previous section (Fig. 23). Because of the analogy between these complexes and pentadienyl cations, this process can also be viewed as a metalla-Nazarov cyclization (for reviews on the Nazarov cyclization, see [63–67]; for selected representative examples of catalyzed Nazarov reactions, see [67–73]). Next, the gold carbene **B** is trapped by the pendant C=C bond to furnish

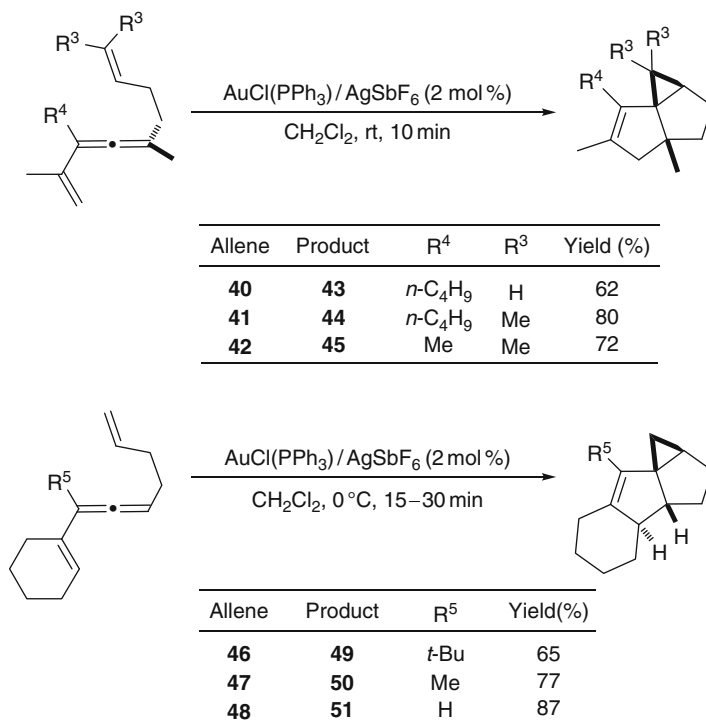


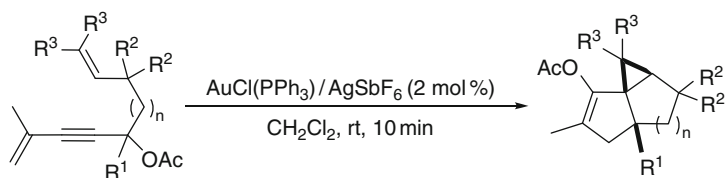
**Fig. 20** Au(I)-catalyzed cycloisomerization of ene-vinyl allenes

the cyclopropyl ring of **C** (electrophilic cyclopropanation). As expected, when starting from trisubstituted allenes (see Sect. 2), the intermediate allylic cation **A** is not planar and thus keeps the stereochemical information.

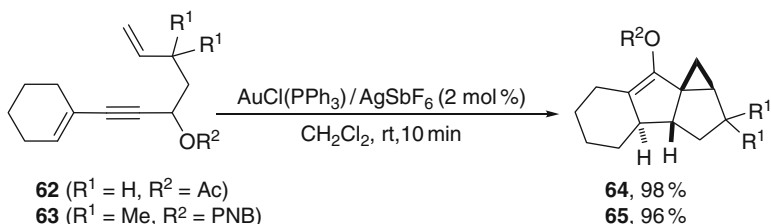
Of the four possible twisted geometries, only those with the vinyl group *anti* to the metal fragment are reactive relatively to the cyclization process (Fig. 24).

Figure 25 shows the cyclization of the allylic cation **68**, ground state of the system, and that of **66**, 3.0 kcal mol<sup>-1</sup> less stable. From the former, the formation of the gold-stabilized carbene **67** requires only 7.6 kcal mol<sup>-1</sup> of enthalpy of activation. Interestingly, any of these two diastereomers should lead to the same enantiomer after cyclization; therefore an efficient transfer of chirality is expected, at least if the cyclization is faster than the racemization of the twisted intermediates.

To verify this hypothesis experimentally, gold(I)-catalyzed cycloisomerizations of optically active ene-vinyl allenes were attempted (Fig. 26) [38, 61]. In (*S*)-**69**, because the allene moiety is only disubstituted, the formation of achiral planar allylic cations is expected to be straightforward, leading to a racemic product. Indeed, its transformation furnished the tetracyclic compound **70** in 87% yield and 0% enantiomeric excess. Based on a chiral GC-analysis of an aliquot of the reaction mixture taken after 10 min, it was clear that the starting compound was already completely racemized. A similar loss of stereochemical information was



Acetate	Product	n	R <sup>1</sup>	R <sup>2</sup>	R <sup>3</sup>	Yield(%)
<b>52</b>	<b>57</b>	1	H	Me	H	92
<b>53</b>	<b>58</b>	1	H	H	H	92
<b>54</b>	<b>59</b>	1	Me	H	H	97
<b>55</b>	<b>60</b>	1	Me	H	Me	95
<b>56</b>	<b>61</b>	2	Me	H	H	88



**Fig. 21** Au(I)-catalyzed cycloisomerization of enyl acetates

**Fig. 22** 3,3-Rearrangement of propargyl acetates into allenyl acetates

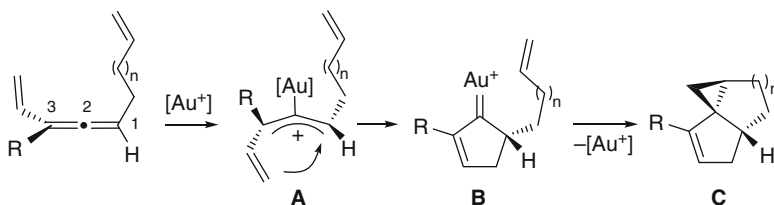
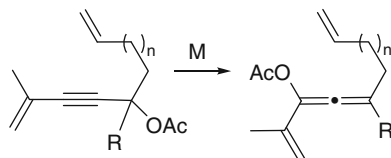


**Fig. 23** Cycloisomerization of ene-vinyl allenes (R = H, Me, OAc)

observed during the gold(I)-catalyzed cycloisomerization of disubstituted vinyl allenes into cyclopentadienes [74].

On the other hand, the cyclizations of the trisubstituted allene (*R*)-**71** gave rise to a perfect transfer of chirality (Fig. 26). Under the same experimental conditions, efficient chirality transfers were also observed during the cycloisomerization of the

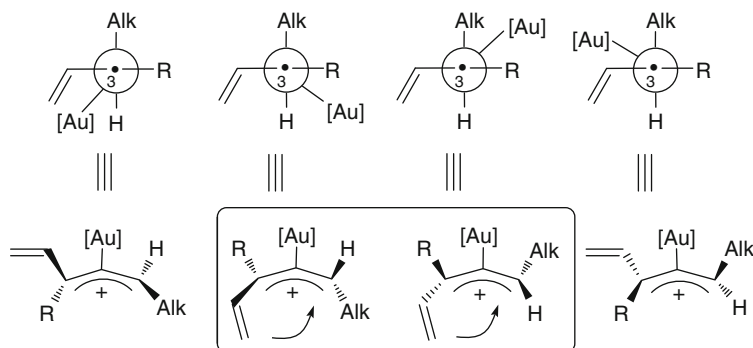


**Fig. 24** Diastereomeric allene gold complexes

propargylic esters (*R*)-**75** and (*R*)-**77**. This result is not surprising since these substrates rearrange into trisubstituted allenyl esters before cyclization.

Thus, in a reaction which transits through allylic cations, the stereochemical information can persist and be transferred nonetheless. With allenes as starting material, the best chance to achieve such a transfer is to use at least trisubstituted substrates.

### 3.2 Cycloisomerization of 1-Aryl-1-allene-6-enes

As a second example of activation of allenes toward the nucleophilic attack of a double bond, we have chosen the formal intramolecular [3+2] cycloaddition of 1-aryl-1-allene-6-enes [75]. The treatment of these substrates with  $[\text{PPh}_3\text{AuCl}]/\text{AgSbF}_6$  leads to *cis*-fused dihydrobenzo[*a*]fluorenes (Fig. 27).

*trans*-Cyclohexenyl compounds could also be isolated sometimes and proved to be plausible intermediates en route to the *cis*-fused products (Fig. 28).

This finding suggests that the first cyclization occurs at the allene by a 6-*endo* attack of the remote double bond to give cation **B** (Fig. 29). This step could be modeled, yielding transition states of similar energy for the *cis* and the *trans* cyclizations. The *trans* cation was found to be slightly more stable than the *cis*; however, the following Friedel–Crafts type cyclization is kinetically favored in the case of the *cis* cation. The high *cis*-selectivity for the final products was attributed to the intervention of adventitious acid.

Because the coordinates of the computed intermediates were not provided, we cannot comment on the geometries. The nature of the ligand used on the gold atom during the calculations was not specified either.

### 3.3 Hydrative Carbocyclizations of Allenynes

It was reported that, in the presence of water, gold may trigger the nucleophilic attack of alkynes onto allenes [76]. This case is interesting since, in the absence of

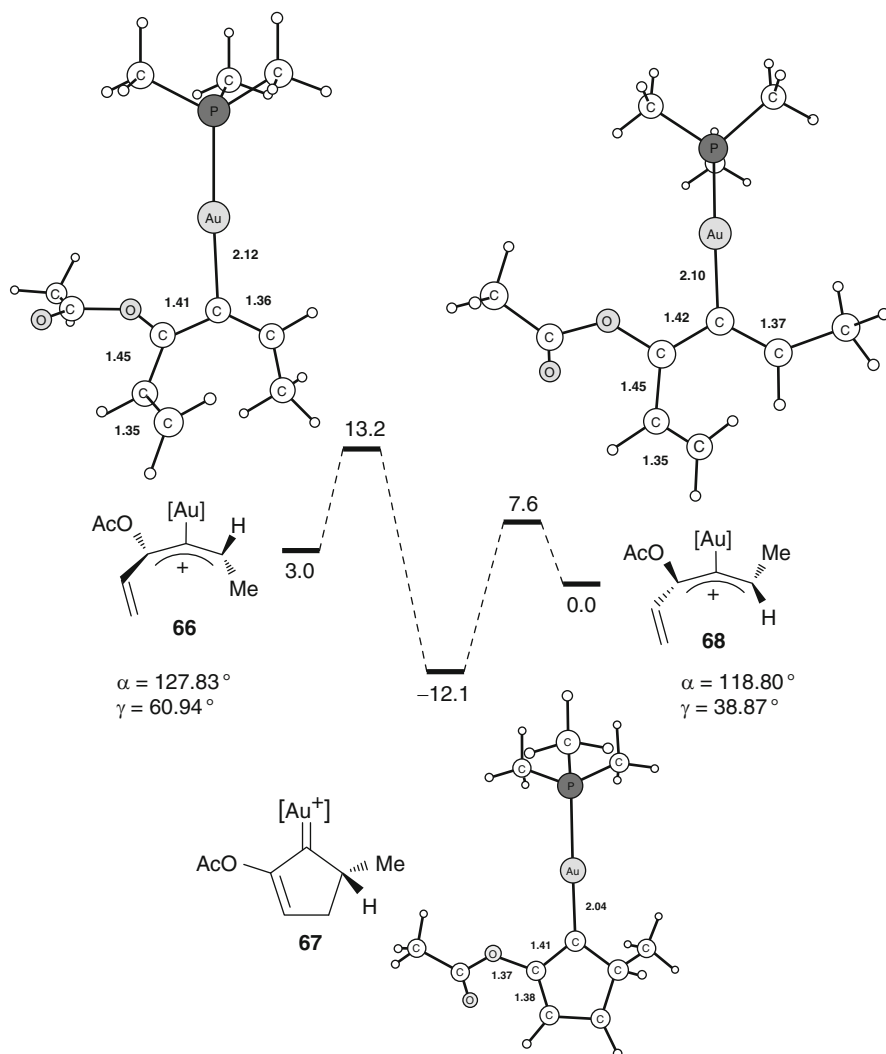


**Fig. 25** Cycloisomerizations of the diastereomeric allene gold complexes **66** and **68** leading to the same enantiomer **67** (distances in Å; relative enthalpies in kcal mol<sup>-1</sup>; [Au] = AuPMe<sub>3</sub><sup>+</sup>; computational level: B3LYP/LANL2DZ(Au)/6-31G\*\*(C, H, P))

water, the reverse process is typically observed, i.e., the activation of alkynes toward the nucleophilic attack of an allene [22–24]; for the role of water in Pt-catalyzed cycloisomerization of enynes, see [77]. This unexpected type of reactivity was unearthed within the 1,4- and 1,6-allenyne series (Fig. 30). In such cyclizations, water attacks regioselectively at the terminal alkyne carbon, while the internal

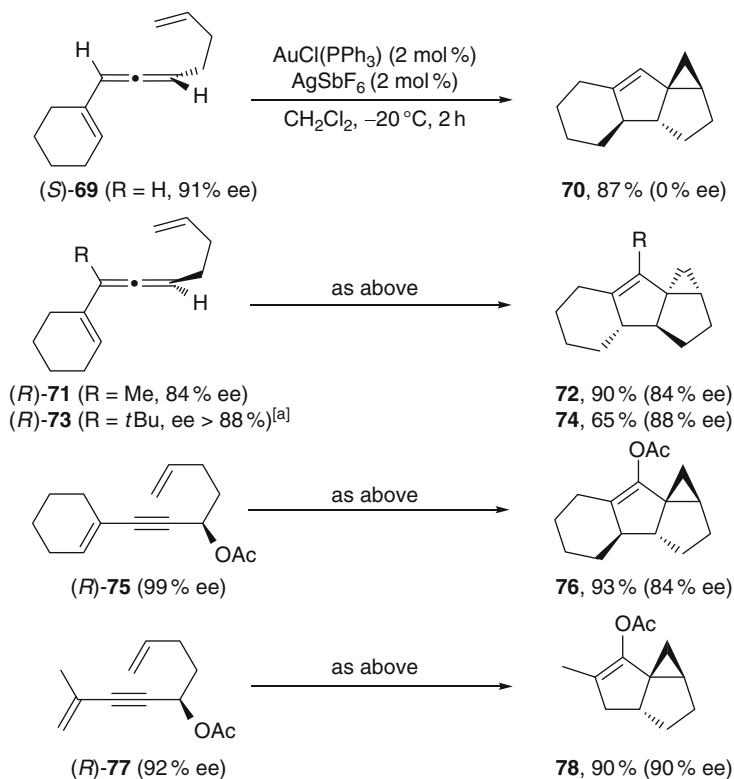


**Fig. 26** Gold(I)-catalyzed cycloisomerization of enantioenriched ene-vinyl allenenes (<sup>[a]</sup> the enantiomeric excess could not be determined)

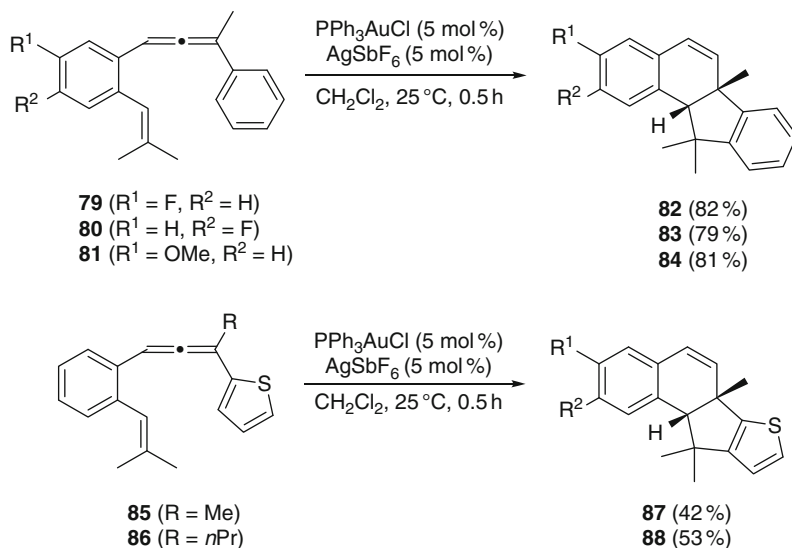


**Fig. 27** Au(I)-catalyzed intramolecular [3+2] cycloadditions of 1-aryl-1-allene-6-enes

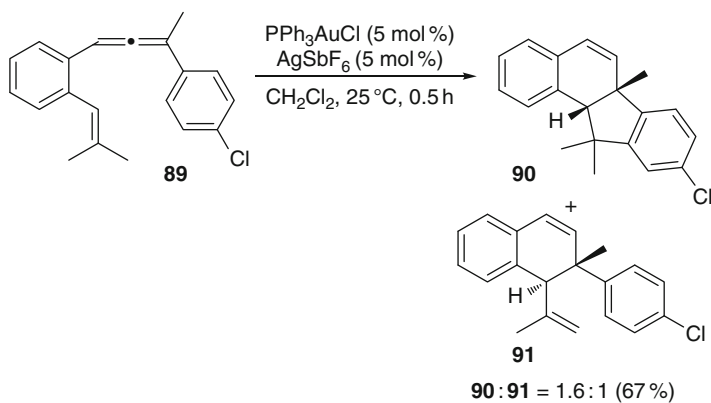
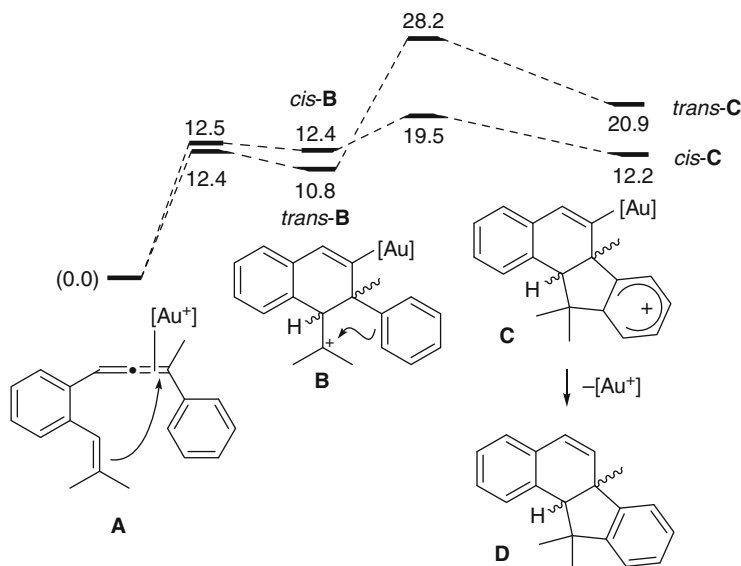


Fig. 28



**Fig. 29** Proposed mechanism, energy profile ( $\text{kcal.mol}^{-1}$ ) (computational level B3LYP/LANL2DZ)

alkyne carbon attacks the allene. Cyclic ketones are formed with moderate to good levels of diastereoselectivity.

Interestingly, chirality transfers were achieved when starting from enantioenriched allenes (Fig. 31). In agreement with the conclusions reached in Sect. 2.2, the disubstituted allene (*S*)-**106** suffers racemization subsequently with the reaction

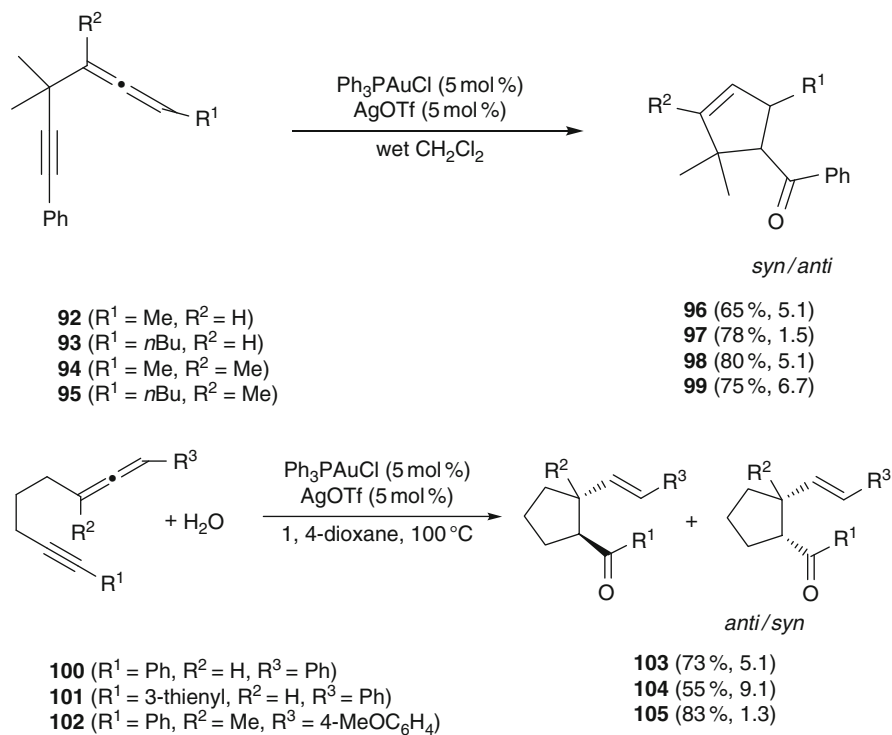


**Fig. 30** Au(I)-catalyzed hydrative cyclizations of 1,4- and 1,6-allenynes

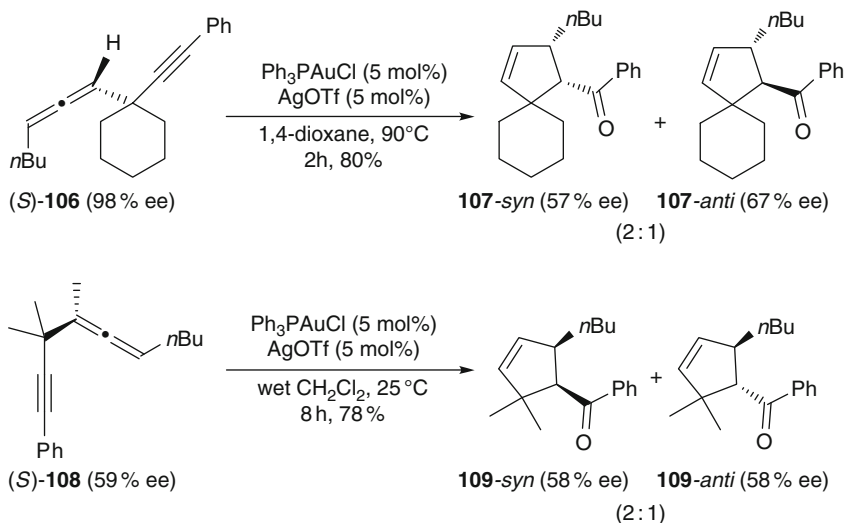


**Fig. 31** Hydrative cyclization of enantioenriched allenynes



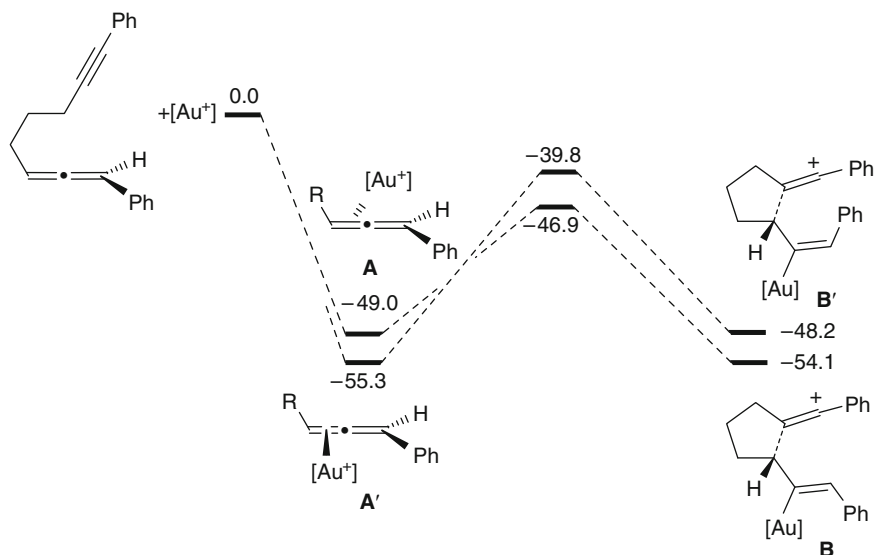


**Fig. 32** Proposed mechanism, energy profile ( $\text{kcal.mol}^{-1}$ ) ( $[\text{Au}] = \text{AuPH}_3$ ; computational level B3LYP/LANL2DZ)

process, and therefore the chirality transfer is moderate in this case. In contrast, the disubstituted allene framework of (*S*)-**108** allows perfect transfer of the stereochemical information to the reaction product.

The proposed mechanism for this transformation involves the formation of an allene gold complex, a 5-*exo* attack of the triple bond to form an aryl-stabilized vinyl cation, and the trapping of the latter by water. It was partially validated by a theoretical study on a model 1,6-allenylne (Fig. 32) [76]. Again, no coordinates were reported, so we cannot comment on the geometries. Nevertheless this mechanism leads to *trans* double bond as kinetically and thermodynamically preferred over the *cis* pathway.

### 3.4 Transformation *N*-Tethered of 1,5-Bisallenes into 6,7-Dimethyl-3-azabicyclo[3.1.1]heptanes

Azadimethylbicyclo[3.1.1]heptanes have been prepared by means of gold-catalyzed cycloisomerization of bisallenenes with an *N*-R tether. This unprecedented framework exhibits two exocyclic double bonds (Fig. 33) [78].

The mechanism was thoroughly studied by DFT computations. The preferred pathway is a stepwise process depicted below (Fig. 34). The first transition state is

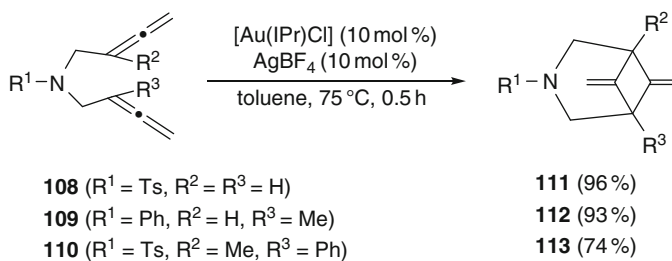


**Fig. 33** Au(I)-catalyzed cycloisomerization of 1,5-bisallenenes

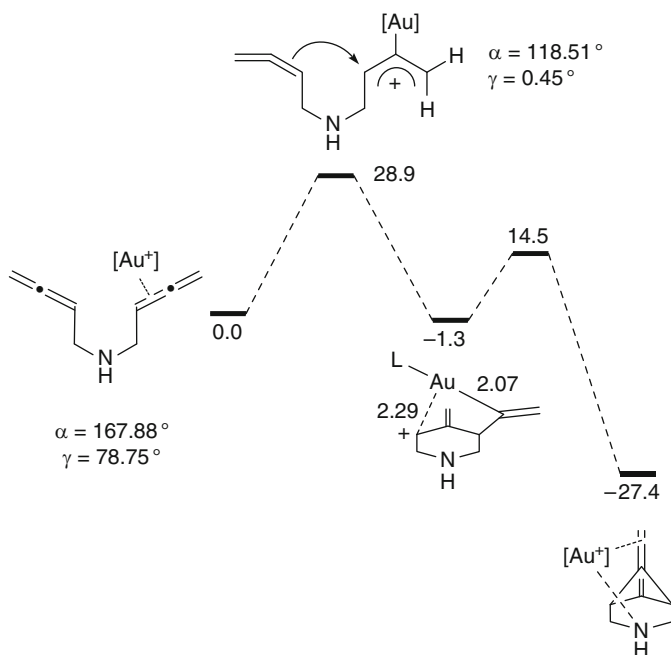


**Fig. 34** Proposed mechanism, energy profile ( $\text{kcal mol}^{-1}$ ) ([Au] = Au(imidazol-2-ylidene); computational level B3LYP/LANL2DZ(Au)/6-31G(d)(N, H, C))

a planar allylic cation which lies  $28.9 \text{ kcal mol}^{-1}$  above the starting complex where gold is coordinated to the central allene carbon in an almost perfect  $\eta^2$ -fashion, both Au–C bonds being  $2.34 \text{ \AA}$ . The intermediate resulting from this 6-*endo* attack of the uncomplexed allene internal double bond is a new type of long-range gold-stabilized carbocation. This T-shaped intermediate brings closer together the vinyl-gold moiety with the carbocation, allowing, through a second transition state lying at  $14.5 \text{ kcal mol}^{-1}$ , the formation of the cyclobutyl ring.

## 4 Conclusions

This compilation of computational studies related to gold-catalyzed transformation of allenes clearly shows the involvement of  $\eta^2$ -allene gold complexes as starting points of reaction mechanisms. As such, the activated allene is prone to nucleophilic attack. However, one has to keep in mind that  $\eta^2$ -allene gold complexes easily rearrange into allylic cations, which can also undergo nucleophilic attack or cycloaddition reactions. The interconversion between these two kinds of species is often kinetically and thermodynamically favorable. Intuitively, it is tempting to discard allylic cations from reaction mechanisms which allow axial-to-center chirality transfer, because allylic cations are reputed to be planar achiral species. However, the 1,3-allylic strain may prevent planarity, giving rise to chiral  $\eta^1$  intermediates. The racemization process of such twisted species may be slow enough to allow a bond formation to take place at one or two allene carbons. If not formed as minima, allylic cations may also be encountered as transition states in which, depending on the substitution pattern of the starting allene, the stereochemical information may be saved or lost.

**Acknowledgements** This work was supported by UPS, UPMC, and CNRS.

**Note added in proof:** The two following articles, dealing with the theoretical analysis of the activation of allenes by gold complexes, were published during the production of this chapter. Fernández I, Cossio FP, de Cózar A, Lledós A, Mascareñas JL (2010) *Chem Eur J* 16:12174–12157; Wang ZJ, Benitez D, Tkatchouk E, Goddard III WA, Toste FD (2010) *J Am Chem Soc* 132:13064–13071.

## References

1. Fürstner A, Davies PW (2007) *Angew Chem Int Ed* 46:3410–3449
2. Gorin DJ, Toste FD (2007) *Nature* 446:395–403
3. Hashmi ASK (2007) *Chem Rev* 107:3180–3211
4. Marion N, Nolan SP (2008) *Chem Soc Rev* 37:1776–1782
5. Li Z, Brouwer C, He C (2008) *Chem Rev* 108:3239–3265
6. Arcadi A (2008) *Chem Rev* 108:3266–3325
7. Gorin DJ, Sherry BD, Toste FD (2008) *Chem Rev* 108:3351–3378
8. Michelet V, Toullec PY, Genêt J-P (2008) *Angew Chem Int Ed* 47:4268–4315
9. Jiménez-Núñez E, Echavarren AM (2008) *Chem Rev* 108:3326–3350
10. Belmont P, Parker E (2009) *Eur J Org Chem* 6075–6089
11. Garcia P, Malacria M, Aubert C, Gandon V, Fensterbank L (2010) *ChemCatChem* 2:493–497
12. Jacobs TL (1982) In: Landor SR (ed) *The chemistry of the allenes*, vol 2. Academic Press, London, p 277
13. Shaw BL, Stringer AJ (1973) *Inorg Chim Acta Rev* 7:1
14. Chenier JHB, Howard JA, Mile B (1985) *J Am Chem Soc* 107:4190–4191
15. Trost BM, Chan DMT (1983) *J Am Chem Soc* 105:2315–2325
16. Alonso I, Trillo B, López F, Montserrat S, Ujaque G, Castedo L, Lledós A, Mascareñas JL (2009) *J Am Chem Soc* 131:13020–13030
17. Benitez D, Tkatchouk E, Gonzalez AZ, Goddard WA III, Toste FD (2009) *Org Lett* 11:4798–4801

18. Correa A, Marion N, Fensterbank L, Malacria M, Nolan SP, Cavallo L (2008) *Angew Chem Int Ed* 47:718–721
19. Marion N, Lemi re G, Correa A, Costabile C, Ram n RS, Moreau X, de Fr mont P, Dahmane R, Hours A, Lesage D, Tabet J-C, Goddard J-P, Gandon V, Cavallo L, Fensterbank L, Malacria M, Nolan SP (2009) *Chem Eur J* 15:3243–3260
20. Alcaide B, Almendros P, Mart nez del Campo T, Soriano E, Marco-Contelles JL (2009) *Chem Eur J* 15:9127–9138
21. Zhu R-X, Zhang D-J, Guo J-X, Mu J-L, Duan C-G, Liu C-B (2010) *J Phys Chem A* 114:4689–4696
22. Lemi re G, Gandon V, Agenet N, Goddard J-P, de Kozak A, Aubert C, Fensterbank L, Malacria M (2006) *Angew Chem Int Ed* 45:7596–7599
23. Cheong PH-Y, Morganelli P, Luzung MR, Houk KN, Toste FD (2008) *J Am Chem Soc* 130:4517–4526
24. Zriba R, Gandon V, Aubert C, Fensterbank L, Malacria M (2008) *Chem Eur J* 14:1482–1491
25. Buzas A, Gagosz F (2006) *J Am Chem Soc* 128:12614–12615
26. Horino Y, Yamamoto T, Ueda K, Kuroda S, Toste FD (2009) *J Am Chem Soc* 131:2809–2811
27. Briggs JR, Crocker C, McDonald WS, Shaw BL (1981) *J Chem Soc Dalton Trans* 121–125
28. Hewitt G, De Boer JJ (1971) *J Chem Soc A (Inorg Phys Theor)* 817–822
29. F rstner A, Alcarazo M, Goddard R, Lehmann CW (2008) *Angew Chem Int Ed* 47:3210–3214
30. Tonner R, Frenking G (2007) *Angew Chem Int Ed* 46:8695–8698
31. Tonner R, Frenking G (2008) *Chem Eur J* 14:3273–3289
32. Dyker CA, Lavallo V, Donnadi u B, Bertrand G (2008) *Angew Chem Int Ed* 47:3206–3209
33. Kaufhold O, Hahn FE (2008) *Angew Chem Int Ed* 47:4057–4061
34. Melaimi M, Parameswaran P, Donnadi u B, Frenking G, Bertrand G (2009) *Angew Chem Int Ed* 48:4792–4795
35. Alcarazo M, Lehmann CW, Anoop A, Theil W, F rstner A (2009) *Nat Chem* 1:295–301
36. Eisenstein O, Hoffmann R (1981) *J Am Chem Soc* 103:4308–4320
37. Senn HM, Bl chl PE, Togni A (2000) *J Am Chem Soc* 122:4098–4107
38. Gandon V, Lemi re G, Hours A, Fensterbank L, Malacria M (2008) *Angew Chem Int Ed* 47:7534–7538
39. Paton RS, Maseras F (2009) *Org Lett* 11:2237–2240
40. Xia Y, Dudnik AS, Gevorgyan V, Li Y (2008) *J Am Chem Soc* 130:6940–6941
41. Garayalde D, G mez-Bengoa E, Huang X, Goeke A, Nevado C (2010) *J Am Chem Soc* 132:4720–4730
42. Maule n P, Krinsky JL, Toste FD (2009) *J Am Chem Soc* 131:4513–4520
43. Bongers N, Krause N (2008) *Angew Chem Int Ed* 47:2178–2181
44. Widenhoefer RA (2008) *Chem Eur J* 14:5382–5391
45. Hoffmann-R der A, Krause N (2001) *Org Lett* 3:2537–2538
46. Morita N, Krause N (2004) *Org Lett* 6:4121–4123
47. Gockel B, Krause N (2006) *Org Lett* 8:4485–4488
48. Buzas A, Istrate F, Gagosz F (2006) *Org Lett* 8:1957–1978
49. Hyland CTJ, Heged s LS (2006) *J Org Chem* 71:8658–8660
50. Morita N, Krause N (2006) *Eur J Org Chem* 4634–4641
51. Patil NT, Lutete LM, Nishina N, Yamamoto Y (2006) *Tetrahedron Lett* 47:4749–4751
52. Zhang Z, Liu C, Kinder RE, Han X, Qian H, Widenhoefer RA (2006) *J Am Chem Soc* 128:9066–9073
53. Morita N, Krause N (2006) *Angew Chem Int Ed* 45:1897–1899
54. Liu Z, Wasmuth AS, Nelson SG (2006) *J Am Chem Soc* 128:10352–10353
55. Deutsch C, Gockel B, Hoffmann-R der A, Krause N (2007) *Synlett* 1790–1794
56. Nishina N, Yamamoto Y (2006) *Angew Chem Int Ed* 45:3314–3317
57. Zhang Z, Widenhoefer RA (2008) *Org Lett* 10:2079–2081
58. Zhang Z, Bender CF, Widenhoefer RA (2007) *J Am Chem Soc* 129:14148–14149
59. Sherry BD, Dean Toste F (2004) *J Am Chem Soc* 127:15978–15979

60. Faza ON, López CS, Álvarez R, de Lera AR (2006) *J Am Chem Soc* 128:2434–2437
61. Lemièrè G, Gandon V, Cariou K, Hours A, Fukuyama T, Dhimane A-L, Fensterbank L, Malacria M (2007) *Org Lett* 9:2207–2209
62. Lemièrè G, Gandon V, Cariou K, Hours A, Fukuyama T, Dhimane A-L, Fensterbank L, Malacria M (2009) *J Am Chem Soc* 131:2993–3006
63. Frontier AJ, Collison C (2005) *Tetrahedron* 61:7577–7606
64. Pellissier H (2005) *Tetrahedron* 61:6479–6517
65. Tius MA (2005) *Eur J Org Chem* 2193–2206
66. Tius MA (2003) *Acc Chem Res* 36:284
67. Habermas KL, Denmark SE, Jones TK (1994) *Org React* 45:1–158
68. Walz I, Togni A (2008) *Chem Commun* 4315–4317
69. Rueping M, Ieawsuwan W, Antonchick AP, Nachtsheim BJ (2007) *Angew Chem Int Ed* 46:2097–2100
70. Liang G, Trauner D (2004) *J Am Chem Soc* 126:9544–9545
71. Janka M, He W, Frontier AJ, Eisenberg R (2004) *J Am Chem Soc* 126:6864–6865
72. Aggarwal VK, Belfield AJ (2003) *Org Lett* 5:5075–5078
73. Cordier P, Aubert C, Malacria M, Lacôte E, Gandon V (2009) *Angew Chem Int Ed* 48:8757–8760
74. Lee JH, Toste FD (2007) *Angew Chem Int Ed* 46:912–914
75. Chaudhuri R, Liao H-Y, Liu RS (2009) *Chem Eur J* 15:8895–8901
76. Yang C-Y, Lin G-Y, Liao H-Y, Datta S, Liu R-S (2008) *J Org Chem* 73:4907–4914
77. Baumgarten S, Lesage D, Gandon V, Goddard J-P, Malacria M, Tabet J-C, Gimbert Y, Fensterbank L (2009) *ChemCatChem* 1:138–143
78. Kim SM, Park JH, Kang YK, Chung YK (2009) *Angew Chem Int Ed* 48:4532–4535

# Heterocyclization of Allenes Catalyzed by Late Transition Metals: Mechanisms and Regioselectivity

Benito Alcaide, Pedro Almendros, Teresa Martínez del Campo, Elena Soriano, and José Marco-Contelles

**Abstract** Regiocontrolled metal-catalyzed preparations of enantiopure tetrahydrofurans, dihydropyrans, and tetrahydrooxepines have been developed starting from  $\gamma$ -allenols derived from 4-oxoazetidine-2-carbaldehydes and D-glyceraldehyde. Regioselectivity control in the O–C functionalization of  $\gamma$ -allenols can be achieved through the choice of catalyst, protecting group, or tether. Because of the increasing power and availability of computers, and the simultaneous development of well-tested and reliable theoretical methods, the use of computational chemistry as an adjunct to experimental research has increased rapidly. Computational studies can be carried out to assist in understanding experimental data, such as the exploration of reaction mechanisms that are not readily studied by experimental means. As a consequence, density functional calculations were performed to predict the regioselectivity of the  $\gamma$ -allenol cycloetherification to the five-, six-, and seven-membered oxacycles on the basis of the tether nature, the presence of a protecting group, and characteristics of the metals, and to gain insight into the mechanism of the oxycyclizations. The interactions between computational and experimental chemistry are often brief. However, it should be desirable to keep this close association for long periods. This chapter must be considered as an interesting symbiotic relationship on the field of organic synthesis using metal (Au, Pd, and Pt) catalysis.

**Keywords** Allenes · Gold · Heterocyclization · Palladium · Reaction mechanisms

---

B. Alcaide (✉), and T.M. del Campo

Grupo de Lactamas y Heterociclos Bioactivos, Departamento de Química Orgánica I, Unidad Asociada al CSIC, Facultad de Química, Universidad Complutense de Madrid, 28040 Madrid, Spain

e-mail: alcaideb@quim.ucm.es

P. Almendros (✉), E. Soriano, and J. Marco-Contelles

Instituto de Química Orgánica General, CSIC, Juan de la Cierva 3, 28006 Madrid, Spain

e-mail: Palmendros@iqog.csic.es, esoriano@iqog.csic.es

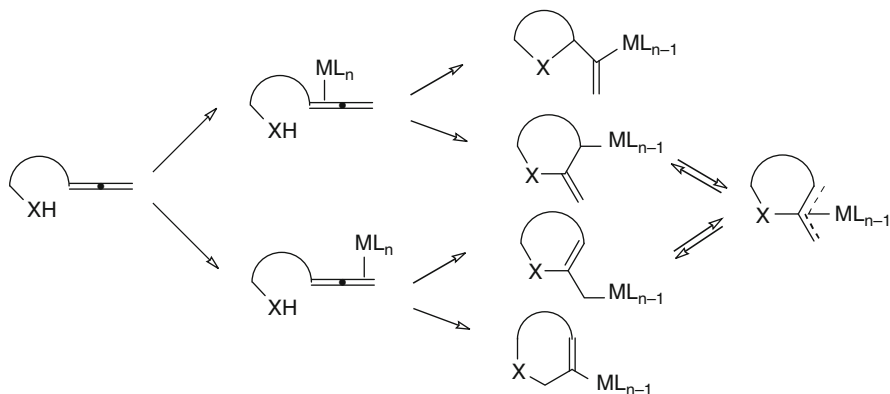
## Contents

1	Introduction .....	184
2	Metal-Catalyzed Heterocyclization Reactions of 2-Azetidinone-Tethered $\gamma$ -Allenols ....	185
2.1	Experimental Study .....	185
2.2	Computational Study .....	189
3	Metal-Catalyzed Heterocyclization Reactions of $\gamma$ -Allenols Derived from D-Glyceraldehyde .....	208
3.1	Experimental Study .....	208
3.2	Computational Study .....	209
4	Conclusion .....	221
	References .....	222

## 1 Introduction

In the nineteenth century, organic chemistry was primarily an experimental, empirical science. Throughout the twentieth century, the emphasis has been continually shifting to a more theoretical approach. The term theoretical chemistry may be defined as the mathematical description of chemistry. The term computational chemistry is usually used when a mathematical method is sufficiently well developed that it can be automated for implementation on a computer. As a technique, computational chemistry has the advantage of producing answers cheaply and quickly (compared to, e.g., thermodynamic measurements), and for hypothetical structures, like transition states. This is a point of concern at the same time because it is both easy to make errors that remain undetected and often difficult to judge the significance of a result. As a consequence, a key question that an experimental chemist in collaboration with a theoretical chemist must face up to is: must we assume that any computed number is exact?

On the other hand, tetrahydrofuran, dihydropyran, and oxepane ether rings are ubiquitous structural units that are extensively encountered in a number of biologically active natural products and functional molecules, and therefore their stereocontrolled synthesis remains an intensive research area (for selected reviews, see [1–6]). Allene heterocyclization chemistry has attracted considerable attention in recent years (for general and comprehensive reviews, see [7–9]). However, regioselectivity problems are significant (*endo-trig* vs *exo-dig* vs *endo-dig* vs *exo-trig* cyclization) (Scheme 1). Intramolecularization of the reactions, usually by placing the group at such a distance that five- or six-membered rings are formed, should automatically solve the positional selectivity problems because larger rings are disfavored. In particular, transition metal-catalyzed reactions of  $\alpha$ -allenols leading to heterocyclization products have attracted a great deal of interest (for a review, see [10]; for selected examples of Ag-mediated heterocyclizations of  $\alpha$ -allenols, see [11, 12]; for selected gold-catalyzed cyclizations of  $\alpha$ -allenols, see [13, 14–17]; for selected Pd-catalyzed cyclizative coupling reactions of  $\alpha$ -allenols, see [18, 19]; for Ag- and Pd-promoted heterocyclizations of  $\alpha$ -allenols, see [20]; [21]). However, relatively little work has been performed on intramolecular cyclizations of  $\gamma$ -allenols



**Scheme 1** Possible regioisomers observed in the heterocyclization of allenols using metal catalysis

(for Au-catalyzed cyclizations of  $\gamma$ -allenols, see [22]; for Au- and Pt-mediated oxycyclization of  $\gamma$ -allenols, see [23]; for Ag- and Sn-catalyzed cyclizations of  $\gamma$ -allenols, see [24]).

The regioselectivity of the metal-catalyzed cyclizations of  $\gamma$ -allenols derived from 4-oxoazetidine-2-carbaldehydes and D-glyceraldehyde will be discussed in this chapter. The regioselectivities observed in these reactions were substantially different, and suggested that the regioselectivity was strongly modulated by the nature of the metal (gold vs palladium vs lanthanum), by the status of the hydroxyl group in the  $\gamma$ -allenol (i.e., free or protected), or by the  $\gamma$ -allenol tether nature. On the other hand, very few aspects of organic chemistry can be computed exactly, but almost every aspect of organic chemistry may be described in a qualitative or approximate quantitative computational scheme. Often a qualitative or approximate computation can give useful insight into organic chemistry if we understand what it tells us and what it doesn't. The fact that the agreement of theoretically predicted and experimentally observed selectivities for the gold-, palladium-, and platinum-catalyzed oxycyclization reactions of  $\gamma$ -allenols was very good in all cases clearly points to a beneficial collaboration between experimental and computational chemists.

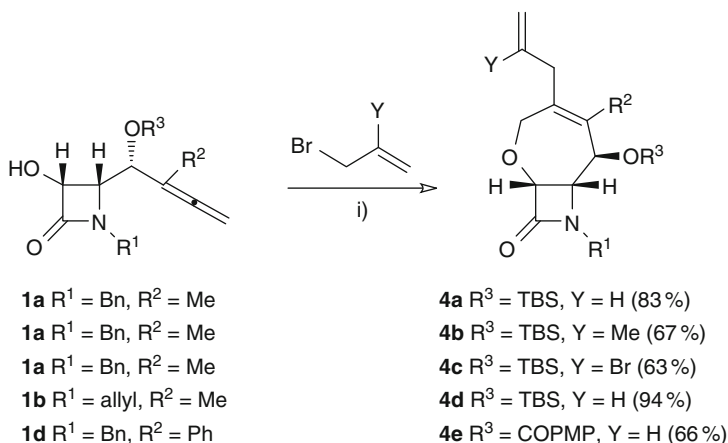
## 2 Metal-Catalyzed Heterocyclization Reactions of 2-Azetidinone-Tethered $\gamma$ -Allenols

### 2.1 Experimental Study

First, the general reactivity of 2-azetidinone-tethered  $\gamma$ -allenols toward the regio-selective hydroalkoxylation reaction was tested with substrate **1a** by the use of  $[\text{PtCl}_2(\text{CH}_2=\text{CH}_2)]_2$ ,  $\text{AgNO}_3$ ,  $\text{AuCl}$ , and  $\text{AuCl}_3$  as catalysts.  $[\text{PtCl}_2(\text{CH}_2=\text{CH}_2)]_2$







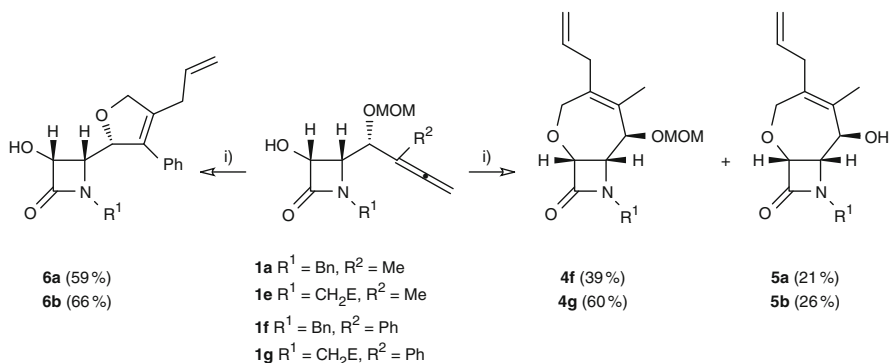
**Scheme 4** Palladium-promoted preparation of seven-membered oxacycles **4a–e**. Reagents and conditions: (i) 5 mol%  $\text{PdCl}_2$ , DMF, RT. PMP = 4-MeOC<sub>6</sub>H<sub>4</sub>. TBS = *tert*-butyldimethylsilyl

6-*endo* cyclization (for the sole report on lanthanide-catalyzed hydroalkoxylations of allenols; see [32]). In addition, partial epimerization was observed through the isolation of *epim*-**3a**. Worthy of note, the  $\text{Pd}^{\text{II}}$ -catalyzed cyclizative coupling reaction of  $\gamma$ -allenols **1a**, **1b**, and **1d** with allyl halides gave impressive yields (up to 94%) of the desired seven-membered adducts **4a–e** (Scheme 4) as the sole products, resulting from a 7-*endo* oxycyclization.<sup>1</sup> Notably, the judicious choice of catalyst (Au, La, or Pd) allows modulation the ring size (five, six, or seven) of the fused oxacycle.

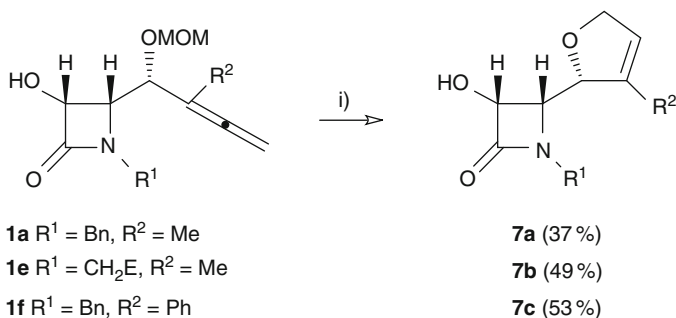
Having demonstrated the stability of the benzoate and TBS-protective groups to the  $\text{Au}^{\text{III}}$ - or  $\text{Pd}^{\text{II}}$ -catalyzed conditions, it was decided to see whether (methoxymethyl)oxy substitution has a beneficial impact on the cyclization reactions. In the event, MOM cleavage was observed to an appreciable extent during the reaction of methyl- $\gamma$ -allenols **1a** and **1e** with allyl bromide in the presence of  $\text{PdCl}_2$  (Scheme 5). Surprisingly, the  $\text{PdCl}_2$ -catalyzed reaction between allyl bromide and phenyl- $\gamma$ -allenols **1f** and **1g** afforded the dihydrofurans **6a** and **6b**, corresponding to the heterocyclizative coupling of the MOM-deprotected  $\alpha$ -allenols (Scheme 5). Interestingly, when both methyl- and phenyl- $\gamma$ -allenols **1a**, **1e**, and **1f** were treated with  $\text{AuCl}_3$  the 2,5-dihydrofurans **7a–c** were the sole products (Scheme 6). These transformations may involve a chemoselective (5-*endo-trig* vs 7-*endo-trig*) allenol oxycyclization with concomitant MOM ether deprotection.

Taking into account the above results, it was decided to test whether the metal-catalyzed preparation of bicycles **2** and **4** can be directly accomplished from MOM protected  $\gamma$ -allenol derivatives **8**. In the event, MOM ethers **8a**, **8b**, **8c**, and **8d** remained unaltered in the presence of  $\text{PdCl}_2$  and allyl bromide. In contrast, when

<sup>1</sup>The Pd-catalyzed cyclizative coupling reaction of  $\gamma$ -allenols with allyl halides has not yet been reported. For its pioneered used in  $\alpha$ -allenols, see [18].



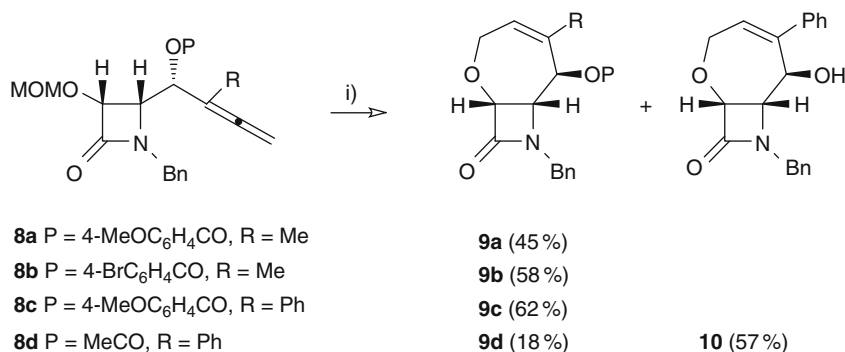
**Scheme 5** Palladium-catalyzed heterocyclization reaction of  $\gamma$ -allenol derivatives **1a**, and **1e–g**. Reagents and conditions: (i) 5 mol%  $\text{PdCl}_2$ , allyl bromide, DMF, RT. MOM =  $\text{MeOCH}_2$ . E =  $\text{CO}_2\text{Me}$



**Scheme 6** Gold-catalyzed heterocyclization reaction of  $\gamma$ -allenol derivatives **1a**, **1e**, and **1f**. Reagents and conditions: (i) 5 mol%  $\text{AuCl}_3$ ,  $\text{CH}_2\text{Cl}_2$ , RT. MOM =  $\text{MeOCH}_2$ . E =  $\text{CO}_2\text{Me}$

allenic MOM ethers **8a**, **8b**, **8c**, and **8d** were treated with  $\text{AuCl}_3$ , the 5-*exo* mode completely reverted to a 7-*endo* cyclization to afford bicycles **9a–d** and **10** in fair yields (Scheme 7). It seems that the reactivity in this type of  $\text{Au}^{\text{III}}$ -catalyzed reactions is determined by the presence or absence of a methoxymethyl protecting group at the  $\gamma$ -allenol oxygen atom, as the free  $\gamma$ -allenols **1a–c** gave 5-*exo* hydroalkoxylation, while MOM protected  $\gamma$ -allenol derivatives **8a**, **8b**, **8c**, and **8d** exclusively underwent a 7-*endo* oxycyclization. Thus, it has been demonstrated that regioselectivity control in the metal-catalyzed O–C functionalization of  $\gamma$ -allenols can be achieved both through the choice of catalyst (Au vs La vs Pd) as well as through the nature of the  $\gamma$ -allenol (free vs protected). It appears to be the first time that such an effect has been reported.

According to the Au- and Pd-catalyzed results, the heterocyclization reaction is very sensitive to the presence of the MOM ether functionality. To expand further the utility of the metal-catalyzed cycloetherification, allenes incorporating a (methoxymethyl)oxy group were studied under the lanthanide amide methodology.



**Scheme 7** Au<sup>III</sup>-catalyzed heterocyclization reaction of MOM protected  $\gamma$ -allenol derivatives **8a**, **8b**, **8c**, and **8d**. Reagents and conditions: (i) 5 mol% AuCl<sub>3</sub>, CH<sub>2</sub>Cl<sub>2</sub>, RT. MOM = MeOCH<sub>2</sub>

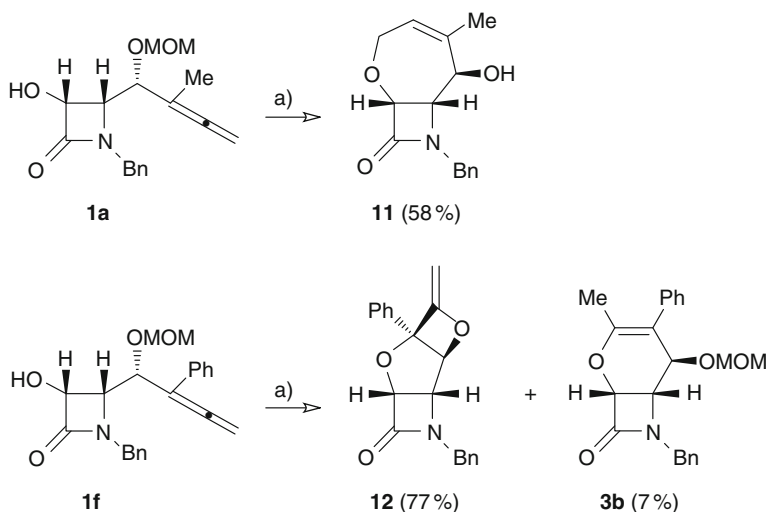
Along the line of this research, the La-catalyzed reaction of MOM-protected  $\gamma$ -allenols **8a**, **1a**, and **1f** was investigated. When compound **8a** was submitted to the lanthanide amide conditions, the starting material remained unaltered even after 2 days of reaction. When the reaction of methyl-allene **1a** was conducted in the presence of a catalytic amount of La[N(SiMe<sub>3</sub>)<sub>2</sub>]<sub>3</sub>, the MOM-free seven-membered adduct **11** was exclusively obtained (Scheme 6).<sup>2</sup> Intrigued by this unusual outcome, we set out to perform the lanthanum-catalyzed reaction of phenyl-allene **1f**. With this consideration in mind, the C-methyl group on allene was replaced by a sterically more demanding C-phenyl group which, based on the above Au- and Pd-results, was anticipated not to change the electronic property of the propa-1,2-dienyl moiety significantly. However, to our delight, the reaction proceeded smoothly to afford the strained tricycle **12** in a remarkably high isolated yield of 77%; additionally, a small amount (7% yield) of the dihydropyran **3b** was observed (Scheme 8). Thus, by a subtle variation in the substitution pattern of the allene component (Ph vs Me), the La-preferential formation of the seven-membered regioisomer can be reversed.

To understand the highly regio- and diastereoselective nature of these metal-catalyzed transformations, a theoretical study on the ring-closure steps of free and protected azetidin-2-one tethered  $\gamma$ -allenols **1** and **8** was undertaken.

## 2.2 Computational Study

With regard to computational methods, density functional theory (DFT) calculations were performed using the Gaussian 03 package [33]. The hybrid functional

<sup>2</sup>The preferential regioselective 7-*endo* cyclization here differs markedly from that of the only reported La-mediated oxycyclization of a  $\gamma$ -allenol, namely the 6-*endo*/6-*exo* cyclization of hexa-4,5-dien-1-ol leading to 6-methyl-3,4-dihydro-2*H*-pyran and 2-methylenetetrahydro-2*H*-pyran as a 4:1 mixture. See [32].



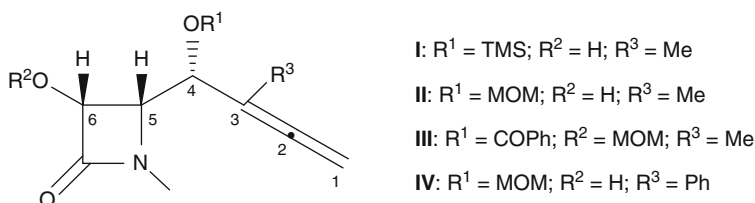
**Scheme 8**  $\text{La}^{\text{III}}$ -catalyzed heterocyclization reaction of  $\gamma$ -allenol derivatives **1a** and **1f**. Reagents and conditions: (a) 5 mol%  $\text{La}[\text{N}(\text{SiMe}_3)_2]_3$ , toluene, reflux. MOM =  $\text{MeOCH}_2$

B3LYP of Becke Lee, Yang, and Parr was used [34, 35]. The 6-34G(d) basis set was used for main-group atoms, while the metal centers Au, Pd, and La have been described by LANL2DZ basis set [36], where the innermost electrons are replaced by a relativistic ECP and the valence electrons are explicitly treated by a double- $\zeta$  basis set. The optimized geometries were characterized by harmonic analysis, and the nature of the stationary points was determined according to the number of negative eigenvalues of the Hessian matrix. The intrinsic reaction coordinate (IRC) pathways from the transition structures have been followed using a second-order integration method to verify the connections with the correct local minima [37, 38]. The reported energies, enthalpies, and free-energies include the vibrational gas-phase zero-point energy term and thermal corrections, respectively. Solvent effects have been obtained through single-point calculations on the gas-phase optimized geometries. The Conductor Polarizable Continuum Model (CPCM) [39] as implemented in the Gaussian 03 package has been used, with the parameters chosen by default.  $\text{CH}_2\text{Cl}_2$ , DMF, and toluene were selected as model solvents, with a dielectric constant  $\epsilon = 8.93$ , 39.0, and 2.38, respectively. Natural bond orbital (NBO) analyses (*NBO Version 3.1*, Glendening ED, Reed AE, Carpenter JE, Weinhold F. For original literature, see [40, 41]) have been performed by the module NBO v.3.1 implemented in Gaussian 03 to evaluate the NPA charges at the optimization level.

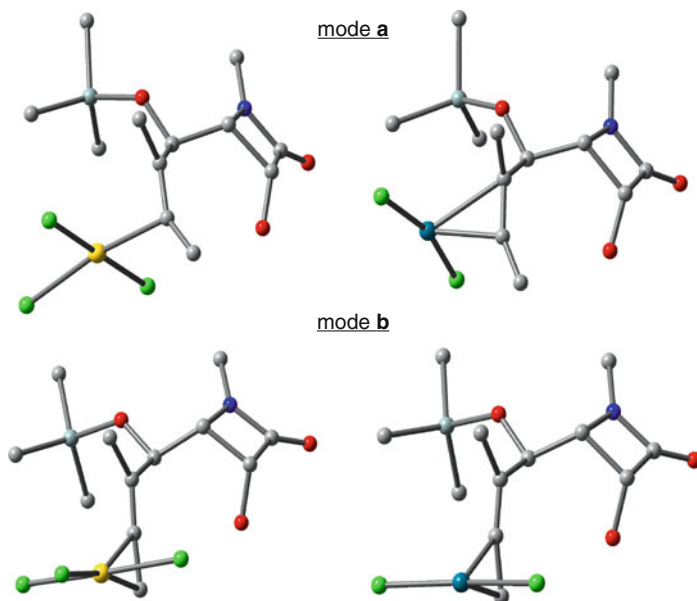
To get insights into the factors that control the regioselectivity of the transition metal catalyzed cyclization and the role of substituents, a theoretical study has been carried out on different precursors. Taking into account the experimental observations and the computational resources, precursors **I–III** (see below) were selected as theoretical models for the gold- and palladium-catalyzed reactions. In order to

elucidate general mechanistic aspects of the intramolecular lanthanide-catalyzed hydroalkoxylation/cyclization of  $\gamma$ -allenols **4**, to determine factors that govern the observed high regio- and stereoselectivity as well as to highlight the role of substituents, we have performed a computational study on the hydroalkoxylation of precursors **I**, **II**, and **IV** (Fig. 1) as theoretical models. Additionally, we have selected  $\text{La}[\text{N}(\text{SiH}_3)_2]_3$  complex to simulate the precatalyst species.

The above experimental results suggest a different activation of the allene moiety by complexation with the catalyst. Unfortunately, the computed NPA charges on the reactant complex **I**- $\text{AuCl}_3$  and **I**- $\text{PdCl}_2$  reveal a similar trend. Thus, complexation on proximal allenic double bond (mode **a**, Fig. 2) induces a higher electrophilic character over C3 (Table 1, see also Fig. 3 for orbital topology), hence preferentially promoting a 5-*exo-trig* cyclization. Because of the hindrance



**Fig. 1** Structures for the selected theoretical model precursors

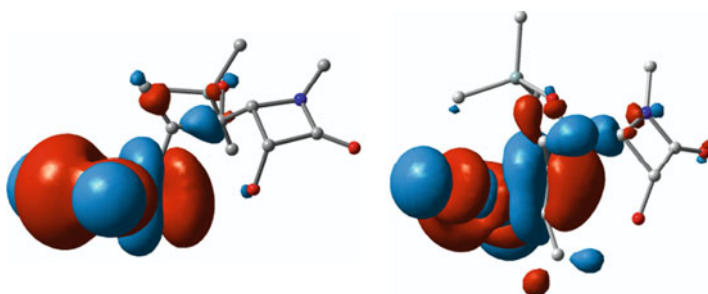


**Fig. 2** Optimized structures of the reactant complexes. Mode **a** refers to coordination of the proximal allene C=C, and **b** to coordination of the distal C=C. Hs have been omitted for clarity

**Table 1** NPA atomic charges on the reactant complexes. The charge for the uncomplexed precursor is also shown to appreciate the effect of the catalyst

Mode		C1	C2	C3	C4	C5	C6	O	M	MCl <sub>n</sub>
–		–0.495	+0.072	–0.122	+0.091	–0.073	+0.026	–0.738	–	–
<b>a</b>	AuCl <sub>3</sub>	–0.386	–0.188	+0.158	+0.065	–0.075	+0.027	–0.740	+0.996	–0.319
<b>a</b>	PdCl <sub>2</sub>	–0.418	–0.012	+0.050	+0.083	–0.076	+0.028	–0.738	+0.716	–0.339
<b>b</b>	AuCl <sub>3</sub>	–0.473	+0.133	–0.065	+0.108	–0.066	+0.029	–0.764	+1.011	–0.297
<b>b</b>	PdCl <sub>2</sub>	–0.428	+0.057	–0.065	+0.104	–0.064	+0.029	–0.763	+0.719	–0.289

Mode **a**: coordination of the proximal allene C=C; **b**: coordination of the distal C=C

**Fig. 3** Topology of the acceptor molecular orbital LUMO on the complexed structures precursor of **I** according to the mode of coordination **a** (left) and **b** (right)

between the catalyst and TMS group, the allene moiety coordinates the metal center only through C2 (Au–C2 = 2.211 Å), forming a slipped  $\eta^1$ -reactant complex, **I**-AuCl<sub>3</sub>, whereas the less sterically demanding PdCl<sub>2</sub> forms a  $\eta^2$ -complex by coordination of C2 and C3 (2.057 and 2.279 Å, respectively). The engagement of the distal allenic double bond (mode **b**, Fig. 2) enhances the electrophilic character at the central allene carbon C2 (Table 1). The lower steric hindrance induced by the methyl substituent allows the formation of a more symmetric complex with the gold-catalyst (Au–C1 = 2.283, Au–C2 = 2.489 Å). In the case of the complex formed by  $\pi$ -coordination of the proximal allenic double bond, the net charge transfer from the  $\pi$ -system to the catalyst is slightly larger than that computed from the distal bond (MCl<sub>n</sub>, Table 1), which makes a more electrophilic allene moiety (mainly at C3).

On the basis of these electronic data, these binding modes would promote preferably the 5-*exo-trig* or 6-*exo-dig* cyclization by intramolecular nucleophilic addition over alternative paths, to form tetrahydrofuran or dihydropyran-skeletons, respectively. However, the fact that divergent results are observed suggests that other factors must come into play. First, studies have been focused on the AuCl<sub>3</sub>-catalyzed cycloisomerization of **I**. The computed energy values clearly reveal a kinetic preference for the formation of the fused-tetrahydrofuran scaffold (Table 2). Thus, the free energy barrier to reach the transition structure **TS**<sub>I-5</sub> is 5.1 and 8.2 kcal mol<sup>–1</sup> lower than the corresponding transition structure for the addition

**Table 2** Enthalpy and free energy in the gas phase, and free energy in solution (kcal mol<sup>-1</sup>) for the cyclization of **1** by alternative regioisomeric 5-*exo-trig*, 6-*exo-dig*, and 7-*endo-trig* paths

	AuCl <sub>3</sub>			PdCl <sub>2</sub>		
	$\Delta H_{\text{gas}}$	$\Delta G_{\text{gas}}$	$\Delta G_{\text{sol}}$	$\Delta H_{\text{gas}}$	$\Delta G_{\text{gas}}$	$\Delta G_{\text{sol}}$
<b>I-MCl<sub>n</sub></b>	0.0	0.0	<b>0.0</b>	0.0	0.0	<b>0.0</b>
<b>TS<sub>1-5</sub></b>	3.7	6.1	<b>1.9</b>	6.2	7.5	<b>4.8</b>
<b>IN<sub>1-5</sub></b>	-4.0	-2.7	<b>-5.5</b>	-2.8	-1.2	<b>-2.3</b>
<b>TS<sub>1-6</sub></b>	8.3	9.6	<b>7.0</b>	15.2	15.9	<b>9.5</b>
<b>IN<sub>1-6</sub></b>	-3.5	-2.6	<b>-5.8</b>	-2.1	-0.8	<b>-1.9</b>
<b>TS<sub>1-7</sub></b>	14.2	15.0	<b>10.1</b>	15.9	17.9	<b>11.2</b>
<b>IN<sub>1-7</sub></b>	-3.2	-2.5	<b>-10.0</b>	-1.5	0.1	<b>-2.2</b>

to the central (**TS<sub>1-6</sub>**) and terminal allene carbon (**TS<sub>1-7</sub>**), respectively (Fig. 4). These results agree with experimental evidence.

From a thermodynamic viewpoint, the formation of the tetrahydrooxepine intermediate (**IN<sub>1-7</sub>**) is slightly more exothermic than the formation of the tetrahydrofuran (**IN<sub>1-5</sub>**) and dihydropyran (**IN<sub>1-6</sub>**) intermediates. In this regard, the most stable structure in the gas phase is the tetrahydrofuran complex, but solvent effects exert greater influence on the stabilization of the seven-membered ring. The transition structures and subsequent intermediates show the formation of a weak hydrogen bond between one of the chloride ligands and the acidic hydroxyl-hydrogen (for **TS<sub>1-5</sub>**, **TS<sub>1-6</sub>**, **TS<sub>1-7</sub>**: 2.240, 3.793, 2.242 Å; for **IN<sub>1-5</sub>**, **IN<sub>1-6</sub>**, **IN<sub>1-7</sub>**: 1.790, 1.691, 1.875 Å). This interaction slightly stabilizes the structures as compared with non-hydrogen-bonded structures (when this alternative is possible). The fact that the cyclization generates a quaternary center in an asymmetric manner when a 5-*exo*-cyclization route is followed is due to steric effects in the transition state. Thus, while **TS<sub>1-5</sub>** lacks unfavorable steric interactions, the formation of the epimer proceeds through a transition structure, **TS<sub>1-5'</sub>** (Fig. 5), exhibiting a distortion of the allenic group in order to alleviate the steric interaction with the protons at the lactam ring (distance terminal allenic proton-lactam proton = 2.034 Å in **TS<sub>1-5'</sub>**, shorter than sum of van der Waals radii, vs distance methyl proton-lactam proton = 2.307 Å in **TS<sub>1-5</sub>**). This effect results in a transition structure 5.3 kcal mol<sup>-1</sup> higher in energy than **TS<sub>1-5</sub>**, which accounts for the observed stereoselectivity.

The higher stability of the transition structure **TS<sub>1-5</sub>**, and hence the kinetic preference for the formation of the five-membered oxacycle, is mostly due to the electronic effects described above. In addition, steric hindrance imposed by the TMS protecting group plays a significant role. As can be seen in Fig. 4, the bulky TMS group on the tether center causes compression of the internal angle (C3–C4–C5 = 108.2°) to relieve the steric pressure with the allenic moiety and lactam ring, so the reactive centers at the ends of the system are moved closer together, thus favoring the cyclization and improving the reaction rate (Thorpe–Ingold effect). In contrast, the formation of the larger seven-membered ring proceeds through a transition structure **TS<sub>1-7</sub>** where the methyl substituent can rest in the same plane as the TMS group. This conformation is reached without angle compression; in fact,



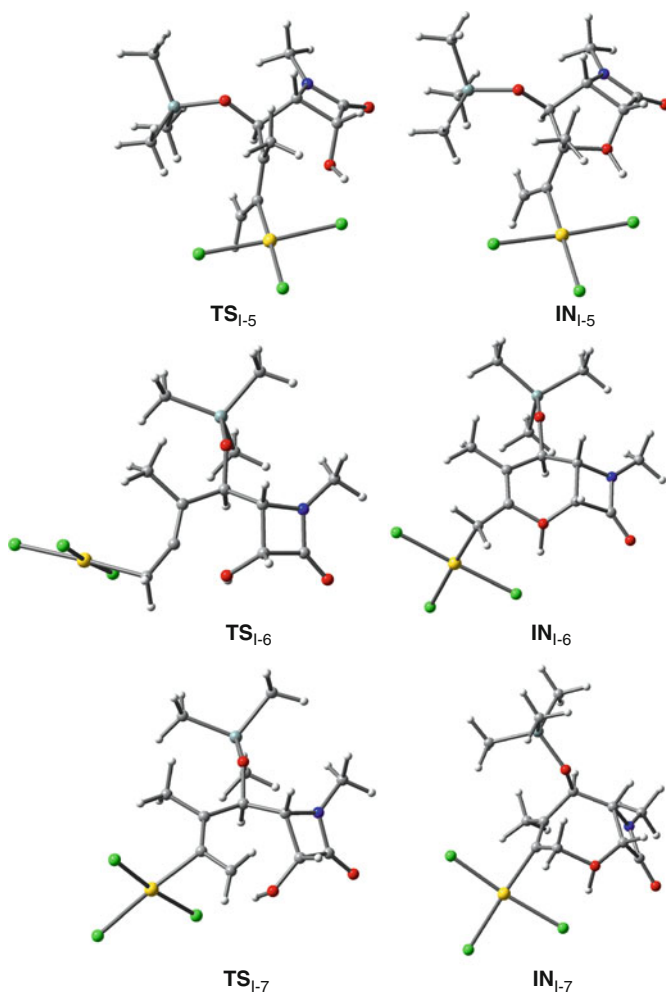


**Fig. 4** Optimized structures of the transition structures and intermediates for the oxycyclization step following alternative paths

it proceeds with an angle opening ( $C3-C4-C5 = 119.7^\circ$ ) since the ring strain imposed by the lactam and endocyclic alkene group restrains the tether flexibility and the interaction between reactive centers. It should be noted, however, that a ring-puckering change upon optimization to the intermediate, **IN<sub>I-7</sub>**, is observed to relieve steric congestion in the cyclized adduct (Fig. 4).

Protonolysis of the  $\sigma$ -carbon–gold bond would yield the bicycle type **5** with simultaneous regeneration of the  $Au^{III}$ -species. This process may proceed through two conceivable paths from the vinyl-Au complex **IN<sub>I-5</sub>**: via direct 1,3-H shift (*path a*), or through a stepwise migration assisted by the catalyst (*path b*) (Scheme 9).

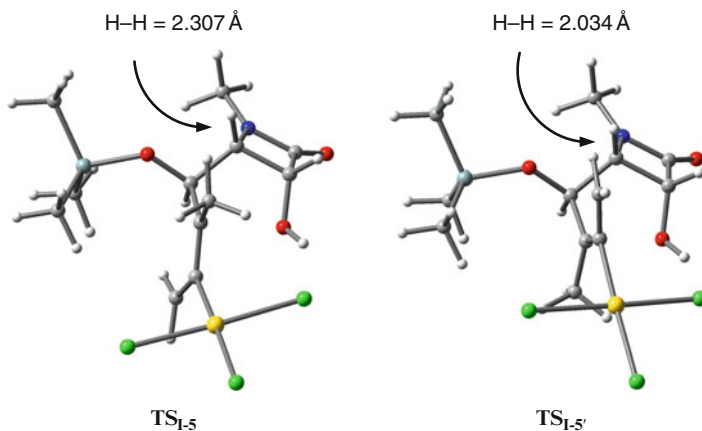
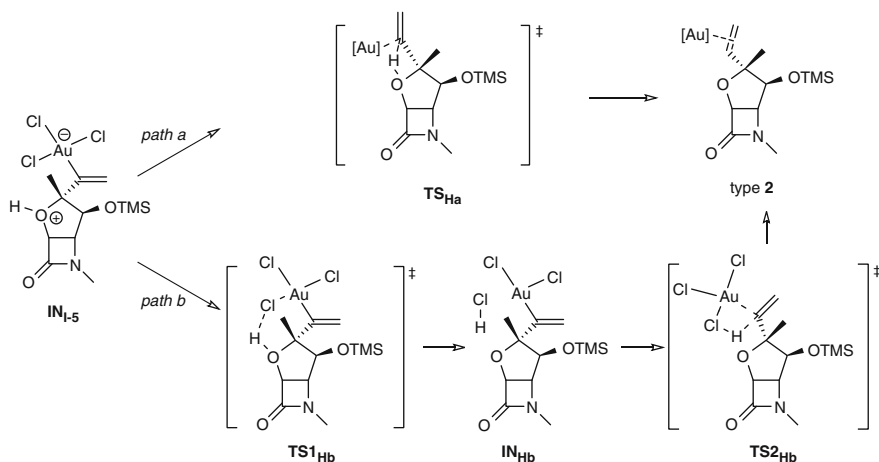


**Fig. 5** Transition structures for the 5-*exo-trig* cyclization, showing critical steric interactions which account for the observed stereochemistry



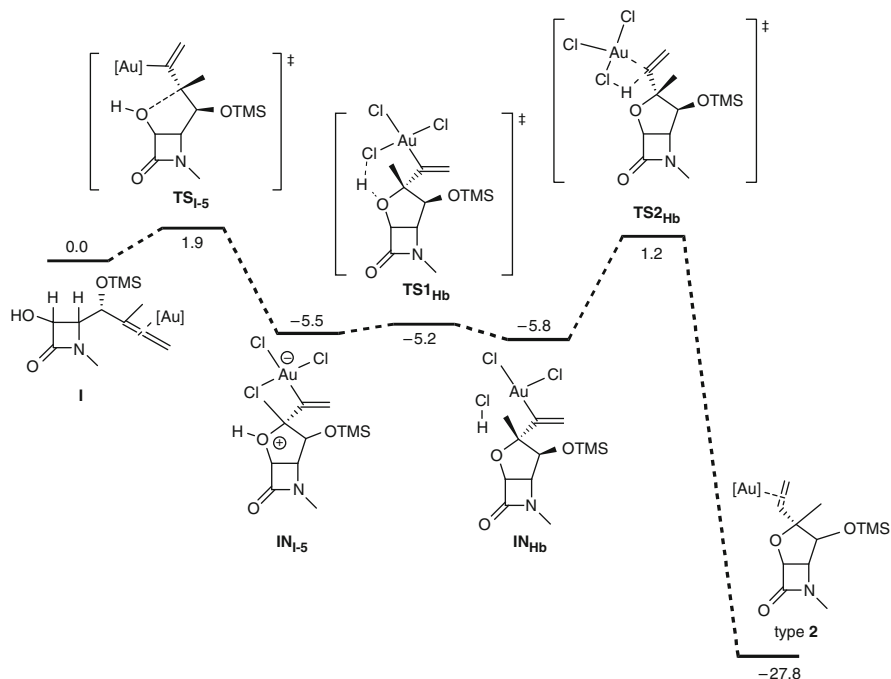
**Scheme 9** Possible pathways for obtaining the bicycle of type **2** through protonolysis

The results, summarized in Table 3, clearly point to the stepwise mechanism as the most likely route. It should be noted that the first step is nearly thermoneutral and takes place with a negligible activation barrier ( $\Delta G_{\text{sol}} = 0.3 \text{ kcal mol}^{-1}$ ) affording an intermediate, **IN<sub>Hb</sub>**, which still exhibits a strong Au–Cl interaction (2.559 Å). This suggests that the ligand remains partially attached to the metal along the assisted H-shift. The last step could then be the cleavage of the Au–C bond by HCl, to liberate the bicycloadduct. Thus, the formation of the C–H bond and regeneration of the catalyst proceeds in a highly exothermic step through the transition structure **TS<sub>2Hb</sub>**, which involves a free energy barrier of  $7.0 \text{ kcal mol}^{-1}$ .

**Table 3** Free energy differences in solution (in kcal mol<sup>-1</sup>) for the 1,3-H shift from the 5-*exo* and 7-*endo* cyclized adducts

	AuCl <sub>3</sub>		PdCl <sub>2</sub>	
	<i>n</i> = 5	<i>n</i> = 7	<i>n</i> = 5	<i>n</i> = 7
<b>IN<sub>I-n</sub></b>	0.0 (−5.5)	0.0 (−10.0)	0.0 (−2.3)	0.0 (−2.2)
<b>TS<sub>Ha</sub></b>	19.8 (14.3)	19.2 (9.2)	20.8 (18.5)	21.3 (19.1)
<b>TS<sub>1Hb</sub></b>	0.3 (−5.2)	0.4 (−9.6)	−0.1 (−2.4)	−0.4 (−2.6)
<b>IN<sub>Hb</sub></b>	−0.3 (−5.8)	−0.9 (−10.6)	−0.2 (−2.5)	−0.5 (−2.7)
<b>TS<sub>2Hb</sub></b>	6.7 (1.2)	8.6 (−2.4)	7.0 (4.7)	8.8 (6.6)
<b>Product</b>	−22.3 (−27.8)	−19.6 (−29.6)	−19.7 (−22.0)	−16.0 (−18.2)

Free energy differences relative to the reactant complex are shown in *parenthesis*

**Fig. 6** Free energy profile [kcal mol<sup>-1</sup>] for the transformation of  $\gamma$ -allenol **I** into the tetrahydrofuran **type 2**

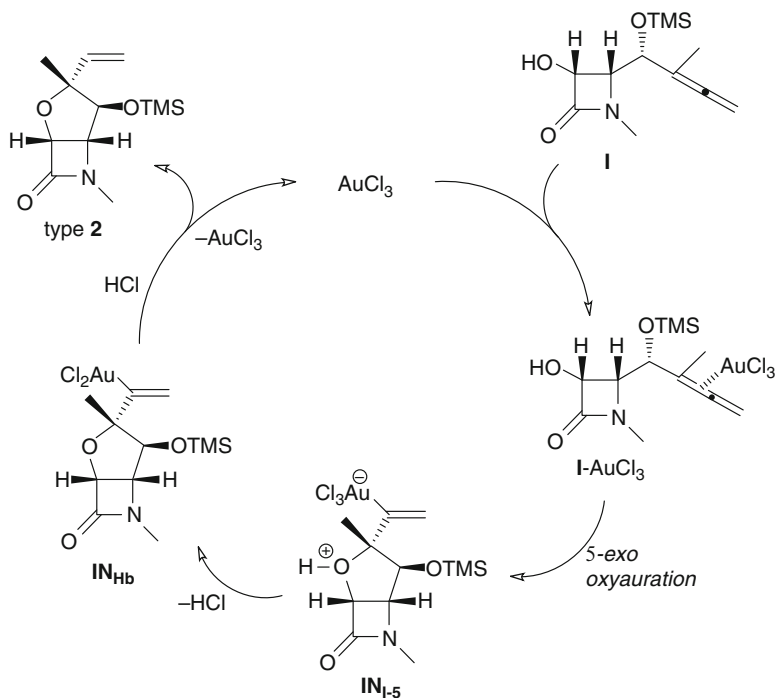
The direct transformation (path a), via **TS<sub>Ha</sub>**, requires a free energy of activation considerably higher ( $\Delta G_{\text{sol}}^{\ddagger} = 19.8 \text{ kcal mol}^{-1}$ ). Therefore, the stepwise path is predicted to be considerably favored (by  $13.1 \text{ kcal mol}^{-1}$ ) over the concerted path, which hence can be ruled out as operative. Overall, the 1,3-H shift is a strongly exothermic process ( $-22.3 \text{ kcal mol}^{-1}$ ), pointing to a somewhat irreversible character.

To sum up, the Au<sup>III</sup>-catalyzed cyclization of  $\gamma$ -allenol **I** (Fig. 6) takes place regio- and stereoselectively through a 5-*exo* hydroalkoxylation because of a kinetic preference governed by electronic and steric factors.

Thus, a possible pathway for the achievement of bicyclic tetrahydrofuran type **2** from  $\gamma$ -allenol **I** may initially involve the formation of a complex **I**-AuCl<sub>3</sub> through coordination of the gold trichloride to the proximal allenic double bond. Next, regioselective 5-*exo* oxyauration forms zwitterionic species **IN<sub>I-5</sub>**. Loss of HCl followed by protonolysis of the carbon–gold bond of **IN<sub>Hb</sub>** affords product type **2** and regenerates the gold catalyst (Scheme 10).

The Pd<sup>II</sup>-catalyzed cyclizative coupling reaction of  $\gamma$ -allenols **1** with allyl halides gave the tetrahydrooxepine- $\beta$ -lactams **4** (Scheme 4), resulting from a 7-*endo* oxycyclization. However, the computed results for the plausible cyclization modes on the allenol model **I** show the same trend as that seen before for the Au<sup>III</sup>-catalyzed process, namely, a kinetic preference for the 5-*exo-trig* cyclization, although the 7-*endo-trig* cyclization proceeds with a barrier only 6.4 kcal mol<sup>-1</sup> higher (vs  $\Delta G_{\text{sol}}^{\ddagger} = 8.2$  kcal mol<sup>-1</sup> for Au<sup>III</sup>-catalysis). This poorer kinetic preference may be due to a lower polarization of the allene upon  $\pi$ -coordination to the metal (Table 1). In this context, every alternative process has been explored to determine the factors that promote the 7-*endo* over the 5-*exo* cyclization and the allyl coupling over the H-shift.

While the transition structure for the 5-*exo-trig* cyclization appears slightly later for the Pd<sup>II</sup>- than for the Au<sup>III</sup>-catalyzed process (2.429 vs 2.457 Å, respectively),



**Scheme 10** Possible pathways for obtaining the bicycle of type **2** through protonolysis

the alternative 7-*endo-trig* is earlier (2.055 vs 1.942 Å, respectively). Likewise, the transition structures (very weak for **TS<sub>I-6</sub>**) and subsequent intermediates show the formation of a hydrogen bond between the closest halide ligand and the hydroxyl-proton (for **TS<sub>I-5</sub>**, **TS<sub>I-6</sub>**, **TS<sub>I-7</sub>**: 2.177, 2.607, 2.145 Å; for **IN<sub>I-5</sub>**, **IN<sub>I-6</sub>**, **IN<sub>I-7</sub>**: 1.708, 1.707, 1.741 Å), which is stronger (shorter) than for the related Au<sup>III</sup>-complexed structures. This effect makes the first event of the 1,3-H shift (formation of **IN<sub>Hb</sub>** intermediate, *path b*, Scheme 1) a barrierless step (Table 3). Although pallada-tetrahydrooxepine and pallada-furan intermediates show equivalent structural and energetic properties, initial efforts have been focused on the former; discussion on the latter is presented below. The HCl formed shows a higher enlargement of the Pd–Cl (hence, weaker interaction) as compared with the same state **IN<sub>I-7</sub>** for the Au counterpart ( $\Delta d_{\text{M-Cl}}$  = 0.10 vs 0.06 Å, respectively; for optimized structures and selected geometric parameters for Au<sup>III</sup> and Pd<sup>II</sup>-mediated protonolysis of **IN<sub>I-7</sub>**), which suggests an easier HCl release. The final formation of the C–H bond and regeneration of the catalyst requires overcoming a low energy barrier, 8.3 kcal mol<sup>−1</sup>. Figure 7 depicts the optimized geometries for the protonolysis process of **IN<sub>I-7</sub>** catalyzed by AuCl<sub>3</sub>, according to the two proposed reaction paths in Scheme 9. For a comparison, Table 4 summarizes the evolution of the most relevant structural parameters along the reaction coordinate for both paths for the protonolysis of **IN<sub>I-7</sub>** mediated by AuCl<sub>3</sub> and PdCl<sub>2</sub>.

Alternatively, the presence of an allyl halide promotes a coupling reaction by trapping with the intermediate **IN<sub>Hb</sub>**. This process should be favored by the easy HCl release/metal decoordination. Furthermore, a close inspection of the vinyl-intermediates **IN<sub>I-n</sub>** suggests that this reaction would take place more favorably for the pallada-tetrahydrooxepine than for the pallada-furan intermediate because of a lower steric hindrance around the reactive centers. The allyl coupling with the alkenyl Pd<sup>II</sup> intermediate occurs by insertion of the C=C bond of allylic halide to give a  $\sigma$ -C–Pd intermediate, which then undergoes a *trans*  $\beta$ -elimination affording the oxepane product (Fig. 8) ([42]; for studies on Pd<sup>II</sup>-catalyzed coupling-cyclization of  $\alpha$ - or  $\beta$ -amino allenes with allylic halides, see [43–45]). The weakly Pd-coordinated HCl in **IN<sub>Hb</sub>** can be easily displaced by the incoming allyl bromide in a fast ligand-interchange displacement mechanism, which yields the  $\eta^2$ -complex **IN<sub>I-AL</sub>** upon  $\pi$ -coordination to the metal. The alkene in this  $\eta^2$ -complex may adopt four perpendicular conformations [46, 47], relative to the Pd–C(alkenyl) vector, involving different orientations of the methyl bromide moiety.<sup>3</sup> Herein, only the conformation giving rise to the lowest energy profile for the insertion, where the –CH<sub>2</sub>Br rests on the opposite side of the ring and endocyclic oxygen is shown. The  $\pi$ -coordination gives rise to symmetrical Pd–alkene bonds [Pd–C(H<sub>2</sub>) = 2.246 and Pd–C(H) = 2.264 Å], and a lengthened C=C bond ( $\Delta d$  = 0.044 Å

<sup>3</sup>In addition to these perpendicular conformations, four parallel structures with the C=C parallel to the  $\sigma$ -Pd–C bond could also be envisioned. However, in these cases the local minima either do not exist at all or are so shallow that the geometry optimizations eventually lead to the perpendicular complexes.

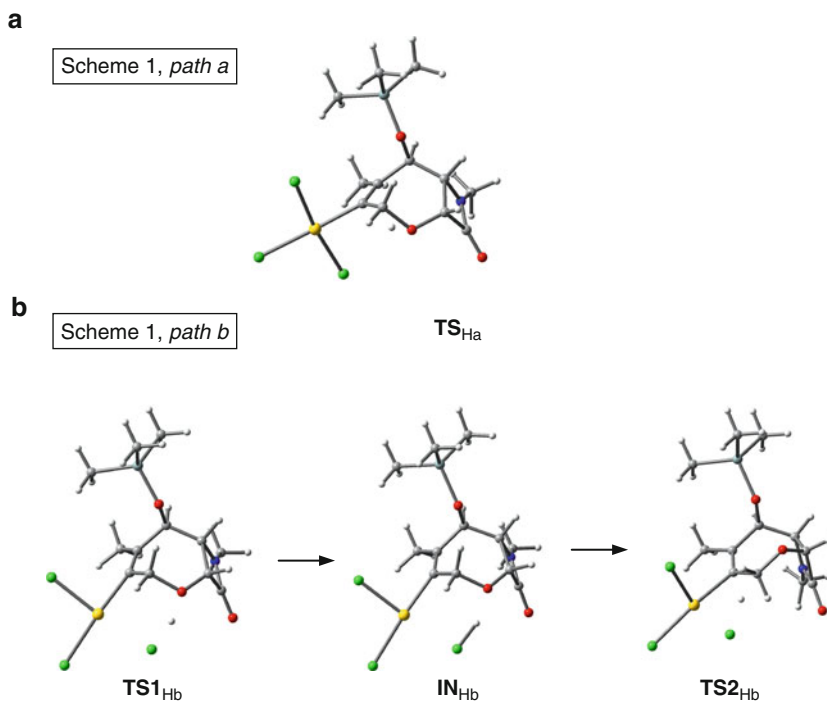


**Fig. 7** Optimized geometries for Au<sup>III</sup>-mediated protonolysis process following a concerted (*path a*) or stepwise route (*path b*)

**Table 4** Selected optimized structural parameters (in Å) for the Au<sup>III</sup>- and Pd<sup>II</sup>-mediated protonolysis of IN<sub>1-7</sub> according to the paths *a* and *b* proposed in Scheme 9

	Au <sup>III</sup>				Pd <sup>II</sup>			
	O–H	C2–H	H–Cl	Au–Cl	O–H	C2–H	H–Cl	Pd–Cl
<b>IN<sub>1-7</sub></b>	1.044	3.000	1.875	2.495	1.103	2.493	1.741	2.457
<b>TS<sub>Ha</sub></b>	1.345	1.465	2.762	2.391	1.320	1.493	2.842	2.396
<b>TS<sub>1Hb</sub></b>	1.367	2.558	1.466	2.521	1.136	2.518	1.678	2.469
<b>IN<sub>Hb</sub></b>	1.617	2.667	1.365	2.556	1.685	2.730	1.349	2.558
<b>TS<sub>2Hb</sub></b>	3.425	1.524	1.536	2.524	3.429	1.453	1.577	2.489
<b>Type 7</b>	3.423	1.090	2.655	2.387	3.413	1.090	2.761	2.330

from the uncomplexed precursor to **IN<sub>1AL</sub>**). The formation of this  $\eta^2$ -complex is exothermic by  $-7.5 \text{ kcal mol}^{-1}$ . The coordinated alkene undergoes a 2,1-insertion into the Pd–alkyl bond in a stepwise process (the regioselectivity found here is quite similar to those found in the insertion reactions of alkenes with many neutral Pd<sup>II</sup> complexes [48]; It can readily be explained by a polarization of the  $\pi$ -orbital in alkene toward the CH<sub>2</sub> group [49]), that proceeds through the formation of a Pd-complex **IN<sub>2AL</sub>**. This intermediate is formed via **TS<sub>1AL</sub>**, where the four atoms

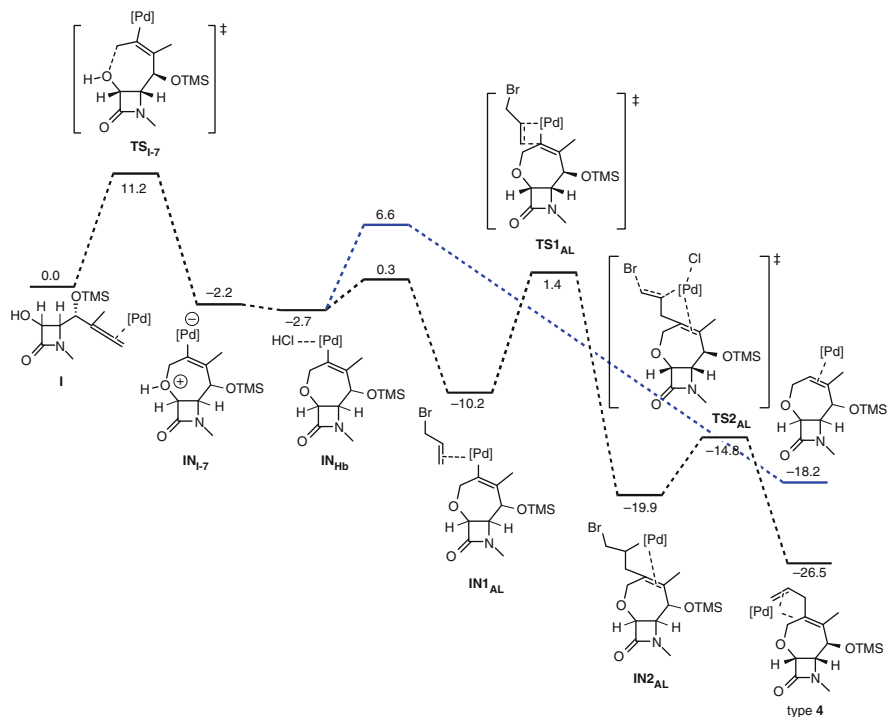


**Fig. 8** Free energy profile [kcal mol<sup>-1</sup>] for the transformation of  $\gamma$ -allenol **I** into the tetrahydrodrooxepine type **4**. Formation of the corresponding bicycle from protonolysis of the intermediate **IN<sub>Hb</sub>** is shown in blue for comparison

forming new bonds (Pd–C = 2.079 and C–C = 2.097 Å) are roughly planar (deviation of 8.2°). Intriguingly, a *cis-trans* isomerization of the chloride ligand takes place to reach the transition state, probably in order to reduce the back-bonding interaction and favor the Pd–C bond formation. A moderate activation barrier is found for this elementary step (11.6 kcal mol<sup>-1</sup>), being the formation of the palladacyclobutane complex favored from a thermodynamical viewpoint (–9.7 kcal mol<sup>-1</sup>).

The cycloalkene fragment in the Pd-complex **IN2<sub>AL</sub>** still appears strongly, though asymmetrically, bound to the metal (Pd–C2 = 2.169, Pd–C3 = 2.232 Å), so the intermediate shows a distorted square-planar geometry around the metal with a vacant position *trans* to the new  $\sigma$ -Pd–C bond. Then, the intermediate **IN2<sub>AL</sub>** may suffer a  $\beta$ -heteroatom elimination ([50–57]; for the stereoselectivity of  $\beta$ -heteroatom elimination, see [58–61]) to give the coupling product type **4** regenerating the active catalyst PdCl<sub>2</sub>. Here, the liberated HCl play a very important role in promoting the dehalopalladation and inhibiting the  $\beta$ -H elimination [56, 62]. It has been postulated that halide ions would assist the  $\beta$ -heteroatom elimination through an E2-like mechanism promoted by halide ion coordination to Pd [63]. This *trans*  $\beta$ -elimination step takes place via **TS2<sub>AL</sub>**, where the lengths of the

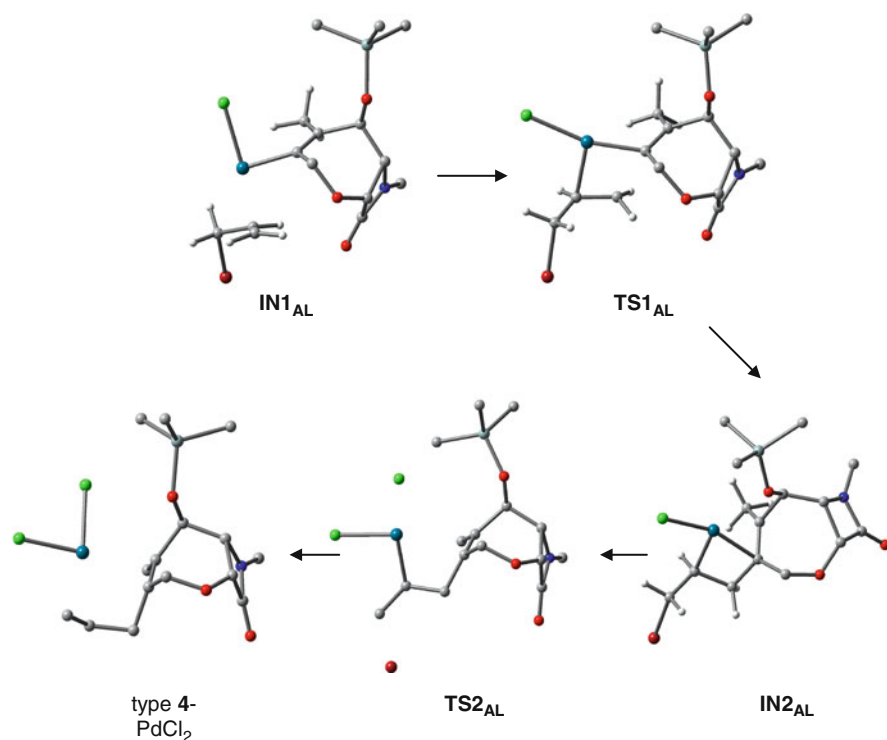
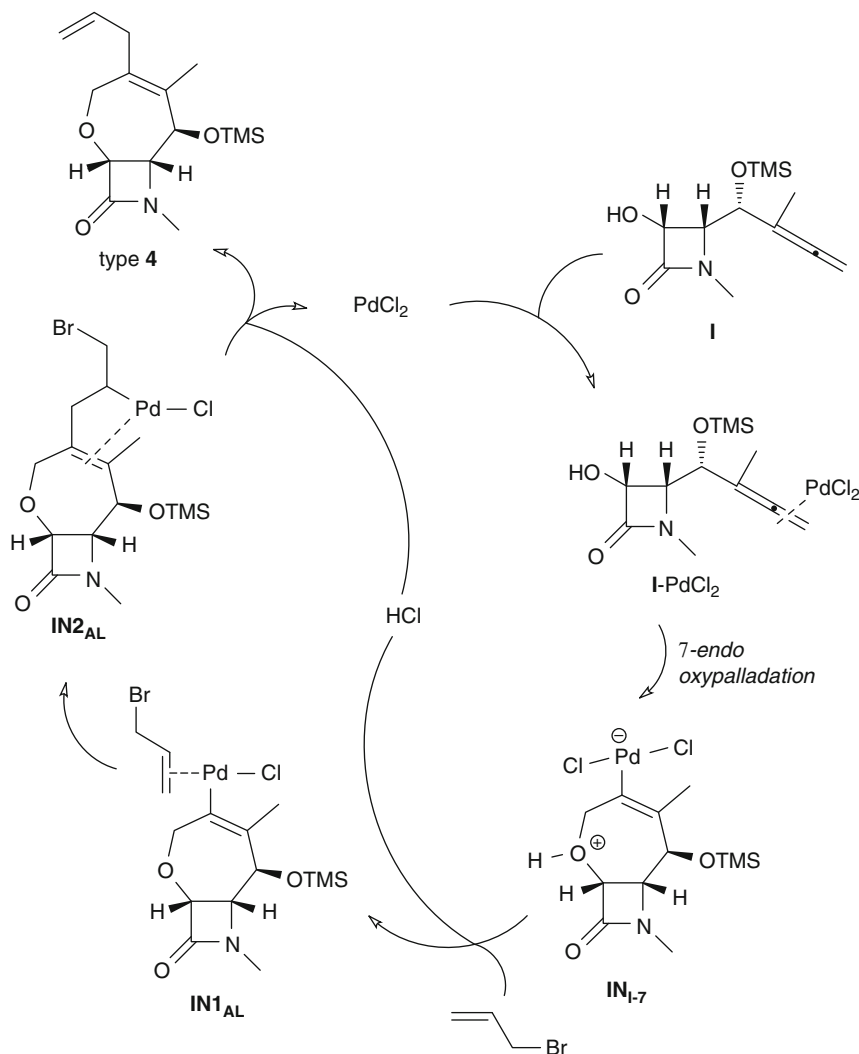


**Fig. 9** Optimized structures for the Pd<sup>II</sup>-allyl coupling. Some Hs have been omitted for clarity

forming and breaking bonds (2.481 Å for the Pd–Cl bond, 2.088 Å for the Br–C) on one hand, and enlargement of the Pd–alkene distance (2.703 and 3.205 Å) and advanced opening of the tetracycle (C–C–C = 113.2°) on the other indicate a large asynchronicity. The formation of the diene product thus proceeds in a final exothermic step by surmounting a low activation barrier (5.1 kcal mol<sup>−1</sup>). Figure 9 shows the optimized structures for the olefin insertion and β-dehalopalladation processes. Alternatively, a *syn* β-dehalopalladation might be envisaged, in analogy with the β-H-elimination in related Pd<sup>II</sup>-promoted processes (for a computational study, see [64]). Nevertheless, the computed results indicate that this pathway is less favored from a kinetic viewpoint since the transition structure to the metallacyclobutane intermediate is 5.2 kcal mol<sup>−1</sup> higher in energy than the equivalent for the alternative β-dehalopalladation.

Scheme 11 outlines a mechanistic proposal for the achievement of compounds type 4. Initial Pd<sup>II</sup>-coordination to the 1,2-diene moiety gave an allenepalladium complex **I**-PdCl<sub>2</sub>. Species **I**-PdCl<sub>2</sub> suffers an intramolecular cycloetherification reaction to give the intermediate palladatetrahydrooxepine **IN<sub>L7</sub>**, which reacted with allyl bromide via **IN<sub>1AL</sub>** to form intermediate **IN<sub>2AL</sub>**. A *trans* β-heteroatom elimination generates tetrahydrooxepine-β-lactams type 4 with concomitant regeneration of the Pd<sup>II</sup> species (Scheme 11).

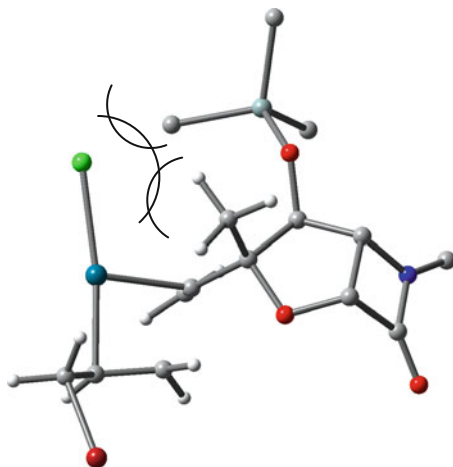




**Scheme 11** Mechanistic explanation for the  $\text{Pd}^{\text{II}}$ -catalyzed heterocyclization reaction of  $\gamma$ -allenol **I**

It is worth noting that the cyclization/coupling process affords cycloadducts **4** from a *7-endo-trig* cyclization instead of that from the kinetically preferred *5-exo-trig*-cyclization intermediate. This latter plausible mechanism, however, has been found to involve a highly congested transition structure for the olefin insertion (Fig. 10), which accounts for the rather high activation barrier for this step ( $25.4 \text{ kcal mol}^{-1}$ ),  $14.8 \text{ kcal mol}^{-1}$  higher than that from the seven-membered

**Fig. 10** Transition structure for the alternative allyl-coupling with the 5-*exo* cyclized intermediate



ring intermediate. Therefore, given that the cyclization and HCl formation are likely reversible processes under the reaction conditions, it could be argued that the kinetic preference for the coupling event from the seven-membered ring relative to other cyclic adducts and also to the protonolysis of the metal–carbon bond, along with the greater stability of the coupling product vs H-shift adduct, should funnel the reaction toward the observed product.

Protection of the  $\alpha$ -hydroxyl functionality with an MOM moiety has been shown to induce a different process when  $\text{AuCl}_3$  is used as catalyst (Scheme 6):  $\gamma$ -allenols **1** are transformed into dihydrofurans **7** by a chemoselective 5-*endo-trig* cyclization over the ether protecting group. On the basis of these experimental findings, a calculation has been carried out on the  $\gamma$ -allenol model **II**. The optimized structures are depicted in Fig. 11. In this case, the results suggest that the formation of the gold–dihydrofuran intermediate complex **IN<sub>II-5endo</sub>** is kinetic and thermodynamically favored over the competing 5-*exo-trig* and 7-*endo-trig* cyclization (Table 5).

The active participation of the protecting group as nucleophilic entity is due to stereoelectronic and thermodynamic effects. The reaction takes place through a planarized five-membered cyclic transition structure, **TS<sub>II-5endo</sub>**, as dihedral angle values highlight ( $\text{C1-C2-C3-C4} = 1.4^\circ$ ,  $\text{C2-C3-C4-O} = -12.2^\circ$ ,  $\text{C3-C4-O-C1} = 13.2^\circ$ ,  $\text{C4-O-C1-C2} = 11.5^\circ$ ,  $\text{O-C1-C2-C3} = 6.1^\circ$ , see Fig. 12). The metal lies in the  $\text{C1-C2-C3}$  allene plane ( $0.8^\circ$  in **TS<sub>II-5endo</sub>** vs  $6.1^\circ$  and  $17.8^\circ$  in **TS<sub>II-5</sub>** and **TS<sub>II-7</sub>**, respectively) which enhances the electrophilic activation of C1. The conformation in **TS<sub>II-5endo</sub>**, easily reached with small structural distortion from the reactant complex, allows an effective orbital overlap between the lone-pair orbital  $n$  and  $\pi^*$  orbital and charge transference to the electrophilic fragment, which results in a stabilization of the transition state as compared with alternative

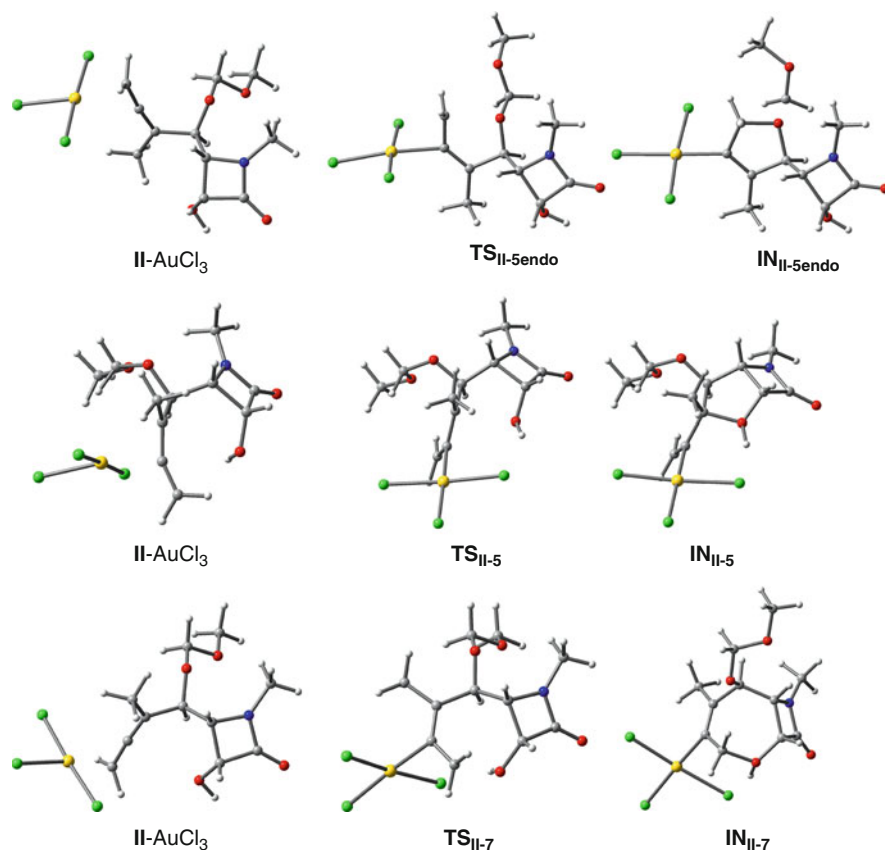


**Fig. 11** Optimized structures of the Au<sup>III</sup>-catalyzed cyclization step of  $\gamma$ -allenol **II** following the competing 5-*endo-trig*, 5-*exo-trig*, and 7-*endo-trig* modes

**Table 5** Enthalpy and free energy differences in gas and in solution for the competing Au<sup>III</sup>-catalyzed cyclization modes of  $\gamma$ -allenol **II**

	$\Delta H$	$\Delta G$	$\Delta G_{\text{sol}}$
<b>II-AuCl<sub>3</sub></b>	0.0	0.0	0.0
<b>TS<sub>II-5</sub></b>	3.5	6.9	7.9
<b>IN<sub>II-5</sub></b>	-3.4	-0.4	0.3
<b>TS<sub>II-7</sub></b>	12.5	15.8	14.1
<b>IN<sub>II-7</sub></b>	-1.8	1.0	-0.2
<b>TS<sub>II-5endo</sub></b>	5.1	4.2	6.9
<b>IN<sub>II-5endo</sub></b>	-2.9	-3.5	-12.7

routes. It should be noted that the bulky  $\alpha$ -substituent in  $\gamma$ -allenol **I** would preclude the effective interaction between the activated allene carbon and the oxygen atom. Additionally, as can be deduced from Table 5, the formation of the

fused bicycle is associated with a less favored entropy contribution than the non-fused dihydrofuran ( $\Delta S^\ddagger_{\text{II-5}} = -7.9$ ,  $\Delta S^\ddagger_{\text{II-7}} = -11.2$ , and  $\Delta S^\ddagger_{\text{II-5endo}} = +2.9$  cal mol<sup>-1</sup>K<sup>-1</sup>, respectively). It leads to a lower free energy of activation to achieve **TS**<sub>II-5endo</sub> than other transition structures. Also, it implies that the formation of **IN**<sub>I-5endo</sub> has a thermodynamic driving force greater than that corresponding to the transformation into the alkenyl palladium intermediates **IN**<sub>II-5</sub> or **IN**<sub>II-7</sub> (Fig. 12).

According to the results detailed above, the regioselectivity of the Au<sup>III</sup>-catalyzed cyclization of  $\gamma$ -allenols **4** mainly depends on two factors: the electronic properties of the acceptor carbon atom of the allene induced by the catalyst, and the structural properties of the  $\alpha$ -substituent.

In sharp contrast, protection of the  $\gamma$ -hydroxyl group inhibits the 5-*exo* cyclization, being the 7-*endo* mode, the operative pathway, to yield fused tetrahydrooxepines **9** (Scheme 7). To shed light on this result, both cyclization modes have been explored for precursor **III**. In this case, the calculations provide a clear picture and indicate that the 5-*exo-trig* cyclization transition structure **TS**<sub>III-5</sub> is 5.1 kcal mol<sup>-1</sup> less stable than the 7-*endo* cyclization **TS**<sub>III-7</sub> due to strong steric effects. The intramolecular attack on the internal allenic carbon is inhibited by steric hindrance

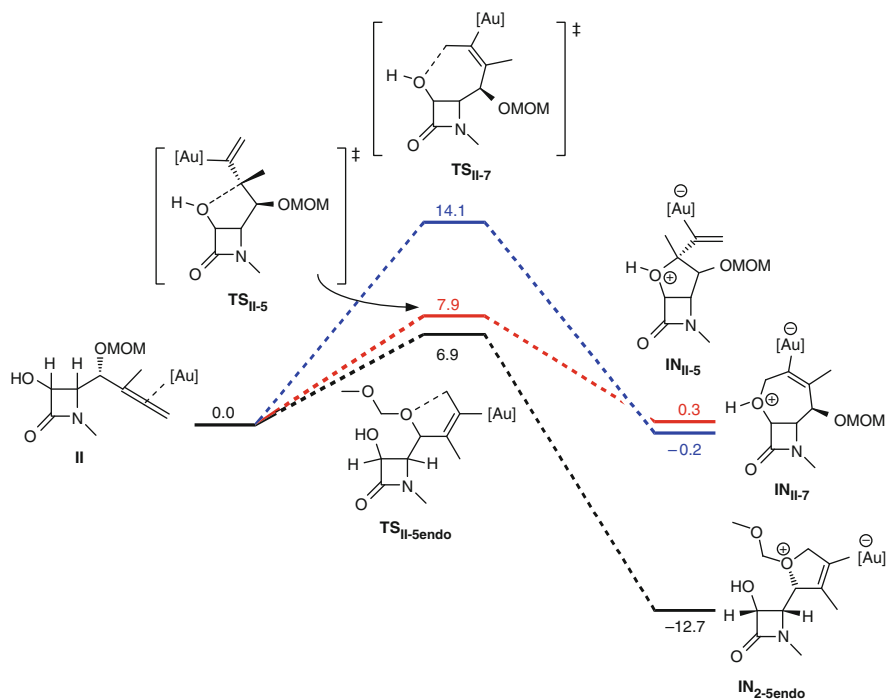


**Fig. 12** Free energy profile [kcal mol<sup>-1</sup>] for the Au-catalyzed oxycyclization of  $\gamma$ -allenol **II** through alternative pathways

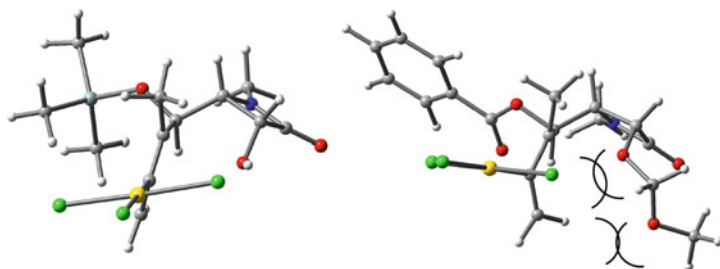
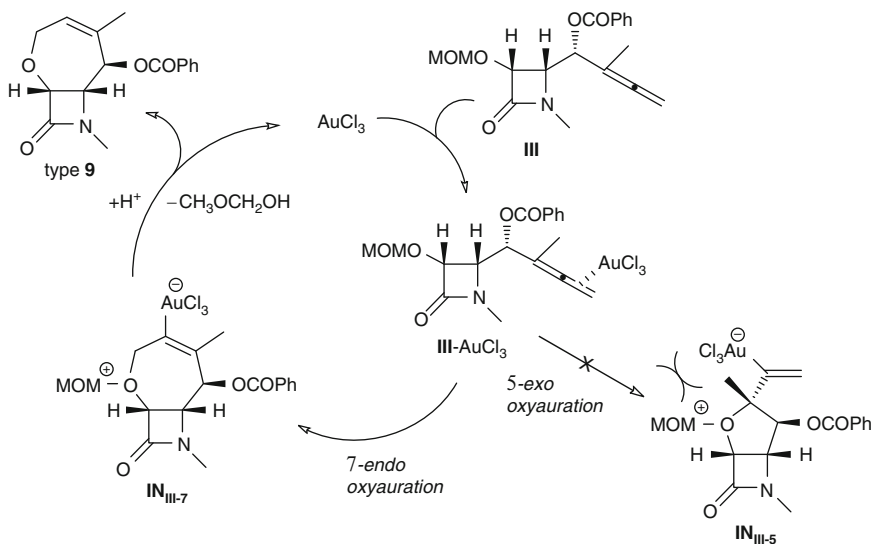


**Fig. 13** Comparison between the transition structures  $\text{TS}_{\text{I-5}}$  and  $\text{TS}_{\text{III-5}}$

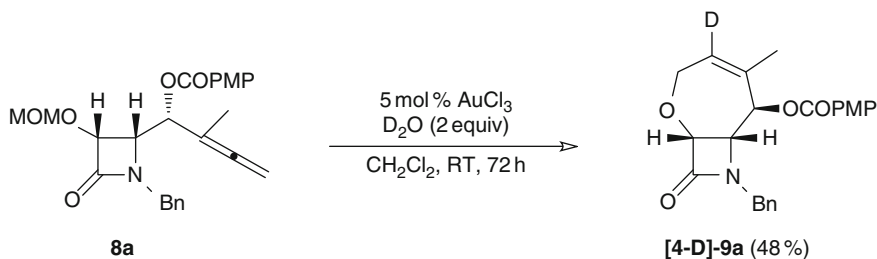
between the (methoxymethyl)oxy group and the catalyst (Fig. 13). A comparison with the preferential 5-*exo* transition structure of **I** ( $\text{TS}_{\text{I-5}}$ ) reveals that  $\text{TS}_{\text{III-5}}$  not only lacks the stabilizing H-bond interaction between the hydroxyl and the ligand catalyst found in  $\text{TS}_{\text{I-5}}$ , but also shows a destabilizing steric interaction owing to the protecting group. The O–C3 distance in  $\text{TS}_{\text{III-5}}$  is shorter (2.384 Å) than in  $\text{TS}_{\text{I-5}}$  (2.457 Å), which further enhances the steric repulsion, as indicated by the deviation of the metal from the  $\pi$ -plane ( $9.7^\circ$  vs  $0.1^\circ$  in  $\text{TS}_{\text{I-5}}$ ) and the torsion of the C1–C2–C3–C4 angle ( $41.4^\circ$  vs  $-7.1^\circ$  in  $\text{TS}_{\text{I-5}}$ ). Thus the transition structure is achieved with a higher structural distortion from ideal values. The subsequent alkenyl gold intermediate  $\text{IN}_{\text{III-5}}$  should be formed by opening of the C1–C2–C3–C4 dihedral angle as the O–C3 distance decreases, but this torsion would increase the strong steric congestion between the catalyst or the alkene fragment. In fact, the calculations reveal that  $\text{TS}_{\text{III-5}}$  evolves to a highly unstable uncyclized intermediate (O–C3 = 2.367), only  $0.01 \text{ kcal mol}^{-1}$  more stable than  $\text{TS}_{\text{III-5}}$ , so it must revert to the reactant Au-complex, which funnels the reaction toward the formation of the tetrahydrooxepine

The pathway proposed in Scheme 12 looks valid for the formation of products type **9** from MOM protected  $\gamma$ -allenol derivative **III**. It could be presumed that the initially formed allenegold complex **III**–AuCl<sub>3</sub> undergoes an intramolecular attack (7-*endo* vs 5-*exo* oxyauration) by the (methoxymethyl)oxy group, giving rise not to species  $\text{IN}_{\text{III-5}}$  but to the tetrahydrooxepine intermediate  $\text{IN}_{\text{III-7}}$ . Protonolysis of the carbon–gold bond linked to an elimination of methoxymethanol would then liberate the bicycle type **9** with concomitant regeneration of the Au<sup>III</sup> species. Probably the proton in the last step of the catalytic cycle comes from the trace amount of water present in the solvent or the catalyst. In the presence of MOM group, 5-*exo* cyclization falters. As calculations reveals, 5-*exo* oxyauration via  $\text{IN}_{\text{III-5}}$  is restricted by the steric hindrance between the (methoxymethyl)oxy group and the substituents at the quaternary stereocenter.

With the aim of trapping the organogold intermediate to confirm the mechanism of this reaction, deuterium labeling studies with deuterium oxide were performed. Under the same conditions but with the addition of 2 equiv. of D<sub>2</sub>O, heterocyclization reaction of MOM protected  $\gamma$ -allenol **8a** catalyzed by AuCl<sub>3</sub> in dichloromethane afforded [4-D]-**9a** in 48% yield, indicating that a



**Scheme 12** Mechanistic explanation for the  $\text{Au}^{\text{III}}$ -catalyzed heterocyclization reaction of MOM protected  $\gamma$ -allenol derivatives **III**



**Scheme 13**  $\text{Au}^{\text{III}}$ -catalyzed heterocyclization reaction of MOM protected  $\gamma$ -allenol derivative **8a**. Reagents and conditions: 5 mol%  $\text{AuCl}_3$ ,  $\text{D}_2\text{O}$  (2 equiv.),  $\text{CH}_2\text{Cl}_2$ , RT, 72 h. MOM =  $\text{MeOCH}_2$ . PMP = 4- $\text{MeOC}_6\text{H}_4$

deuterium atom was incorporated at the alkenyl carbon (Scheme 13). The fact that the  $\text{AuCl}_3$ -catalyzed conversion of allenol **8a** into bicycle **9a** in the presence of 2 equiv. of  $\text{D}_2\text{O}$  afforded **[4-D]-9a**, as judged by the disappearance of the peak at 6.35 ppm in the  $^1\text{H}$  NMR spectrum, which is the signal of the proton H4 on the 2-oxa-8-azabicyclo[5.2.0]non-4-en-9-one (**9a**), suggests that deuterolysis of the carbon–gold in species type **IN<sub>III</sub>-7** has occurred. Along with the clarification of the reaction mechanism, it should point out at the same time that, although metal-catalyzed oxycyclization reactions of allenenes are well-known in hydroxyallenes, heterocyclization of alkoxyallenes is not an easy task and still remains a real challenge.

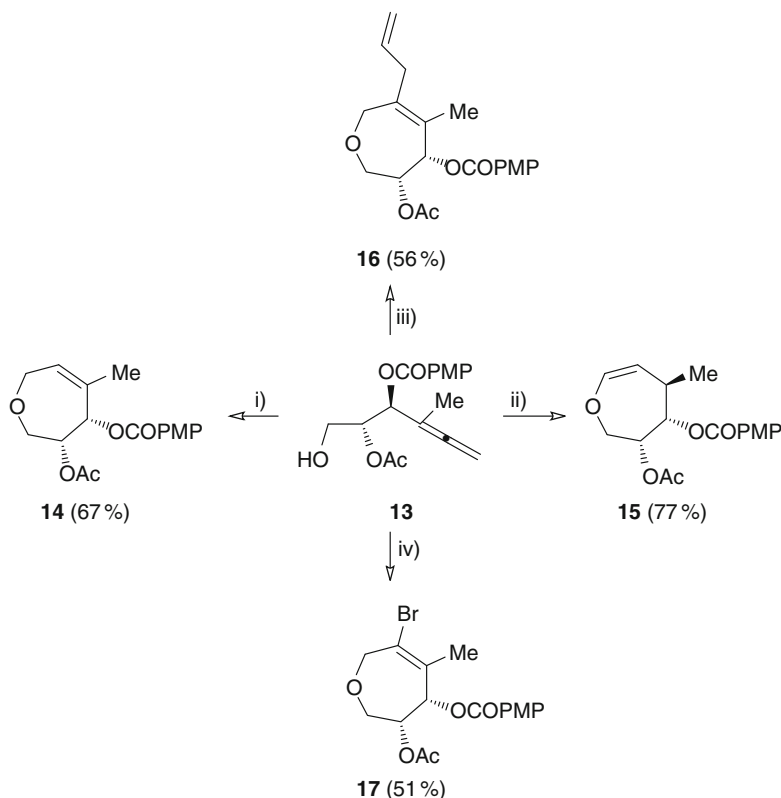
### 3 Metal-Catalyzed Heterocyclization Reactions of $\gamma$ -Allenols Derived from D-Glyceraldehyde

#### 3.1 Experimental Study

From the above results for 2-azetidinone-tethered  $\gamma$ -allenol precursors, it is revealed as an initially kinetically favored 5-*exo-trig* cyclization whereas the 7-*endo-trig* cyclization mode appeared as a less favorable route (activation barrier 6–8 kcal mol<sup>-1</sup> higher), in part because the ring strain imposed by the  $\beta$ -lactam ring and endocyclic alkene group restrains the tether flexibility and the successful interaction between reactive centers. Therefore attention should also be directed to the influence of the nature of the tether between the allene moiety and the functionality.

In order to address the role of the tether, the reactivity of  $\gamma$ -allenols lacking a  $\beta$ -lactam ring toward the regioselective metal-mediated heterocyclization reaction was tested with substrate **13**. Treatment of  $\gamma$ -allenol **13** with AgNO<sub>3</sub> in THF–H<sub>2</sub>O (1:1) at reflux temperature furnished the desired tetrahydrooxepine **14** although only in modest yield (38%), the best cycloisomerization result being obtained on using AuCl<sub>3</sub> (5 mol%) (Scheme 14). The preferential regioselective 7-*endo* cyclization here differs markedly from that of the reported Au-mediated oxycyclization of  $\gamma$ -allenols [22, 65], namely a 5-*exo* cyclization leading to 2-vinyltetrahydrofurans. Interestingly, a similar regioselectivity is observed with [PtCl<sub>2</sub>(CH<sub>2</sub>=CH<sub>2</sub>)]<sub>2</sub> as the catalyst (the only available Pt-mediated oxycyclization of a  $\gamma$ -allenol is the 6-*exo* cyclization of 2,2-diphenyl-hexa-4,5-dien-1-ol leading to 6-methyl-3,3-diphenyl-3,4-dihydro-2*H*-pyran; see [23]). However, product **14** is not detected, its isomer **15** being the sole reaction product. Conjugation of the double bond with the lone pair of the oxygen atom under Pt-catalyzed conditions is believed to promote the formation of **15**. The PdCl<sub>2</sub>-catalyzed reaction between allyl bromide and  $\gamma$ -allenol **13** afforded the tetrasubstituted tetrahydrooxepine **16** in a totally regioselective fashion (Scheme 15), as was observed for the related  $\beta$ -lactam precursor [65].<sup>4</sup> Next, it was decided to test whether a related transformation could be accessible through the palladium(II)-catalyzed oxybromination of  $\gamma$ -allenol **13**. Indeed, bromotetrahydrooxepine **17** was achieved as single isomer in reasonable yield (Scheme 14). Of special interest is the reversal on the regioselectivity in the nucleophilic insertion of  $\gamma$ -allenol **13**, by comparison with the recently reported cyclization of simple  $\gamma$ -allenic alcohols under similar Pd–Cu bimetallic reaction conditions (these authors obtained bromoalkenyl tetrahydrofurans, while in the current report a bromotetrahydrooxepine was obtained [66]).

<sup>4</sup>These are the first examples of Pd-catalyzed cyclizative coupling reaction of acyclic-tethered  $\gamma$ -allenols with allyl halides. For its pioneered used in  $\alpha$ - and  $\beta$ -allenols, see [18].



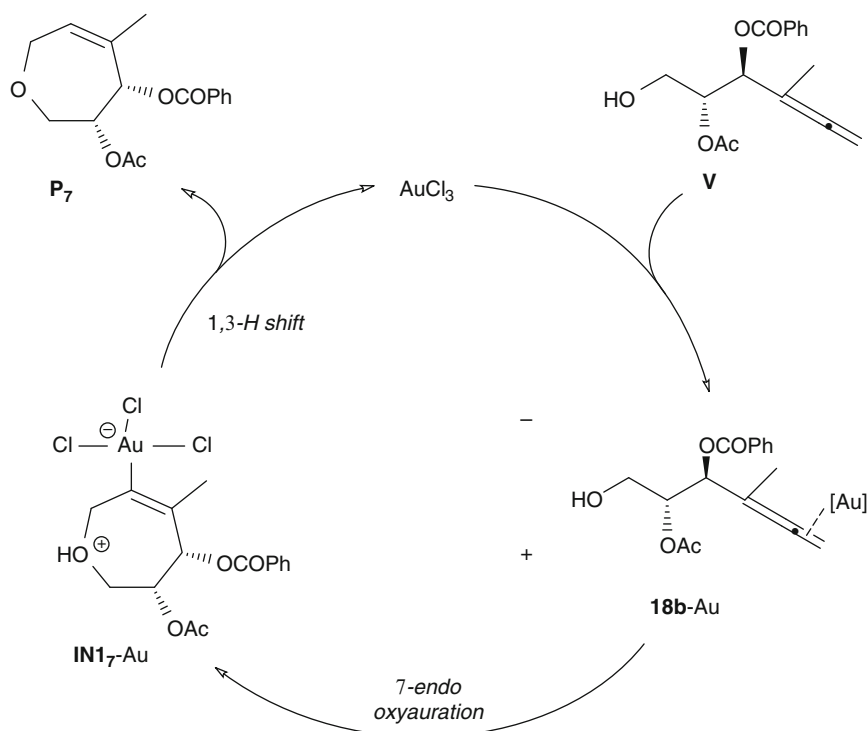
**Scheme 14** Metal-promoted preparation of tetrahydrooxepines **14–17**. Reagents and conditions: (i) 5 mol%  $\text{AuCl}_3$ ,  $\text{CH}_2\text{Cl}_2$ , RT, 3 h; (ii) 1 mol%  $[\text{PtCl}_2(\text{CH}_2=\text{CH}_2)]_2$ , 2 mol% TDMPP,  $\text{CH}_2\text{Cl}_2$ , RT, 2 h; (iii) allyl bromide, 5 mol%  $\text{PdCl}_2$ , DMF, RT, 2 h; (iv) 7 mol%  $\text{Pd}(\text{OAc})_2$ , LiBr,  $\text{Cu}(\text{OAc})_2$ ,  $\text{K}_2\text{CO}_3$ , MeCN,  $\text{O}_2$ , RT, 9 h. PMP = 4-MeOC<sub>6</sub>H<sub>4</sub>. TDMPP = tris(2,6-dimethoxyphenyl)phosphine

All of these metal-catalyzed transformations may involve a chemoselective (7-*endo-trig* vs 6-*endo-dig* vs 5-*exo-trig*)  $\gamma$ -allenol cycloetherification.

### 3.2 Computational Study

With regard to computational methods, all stationary points were located and characterized at the DFT level by means of the B3LYP hybrid functional using the Gaussian 03 program package [67]. The gold, platinum, and palladium atoms were described by a double- $\zeta$  basis set with the effective core potential of Hay and Wadt (LANL2DZ) [68], and the 6-31G(d) basis set [69–73] was used for the other elements. The optimized geometries were characterized by harmonic analysis, and





**Scheme 15** Mechanistic explanation for the  $\text{Au}^{\text{III}}$ -catalyzed hydroalkoxylation reaction of  $\gamma$ -allenol **V**

the nature of the stationary points was determined according to the number of negative eigenvalues of the Hessian matrix. In several cases, the IRC pathways from the transition structures have been followed by using a second-order integration method to verify the proper connections with reactants and products [37, 38]. The reported enthalpies and free-energies include the thermal corrections. Relative enthalpies and free-energies (298 K,  $\text{kcal mol}^{-1}$ ) are provided in the manuscript. Solvent effects were allowed for through single-point calculations on the gas-phase optimized geometries. The CPCM [39] as implemented in the Gaussian 03 package was used, with the parameters chosen by default.  $\text{CH}_2\text{Cl}_2$  and DMF were selected as model solvents, with dielectric constants  $\epsilon = 8.93$  and 39.0, respectively. NBO analyses [40, 41] were performed with the module NBO v.3.1 implemented in Gaussian 03 to evaluate the NPA charges and Wiberg bond indexes (WBIs) at the optimization level.

Aiming to shed some light onto the dependence of the regioselectivity with the tether, a computational study of the possible competing cycloetherification routes has been carried out.  $\gamma$ -Allenol **V** (Fig. 14) has been selected as theoretical model, a

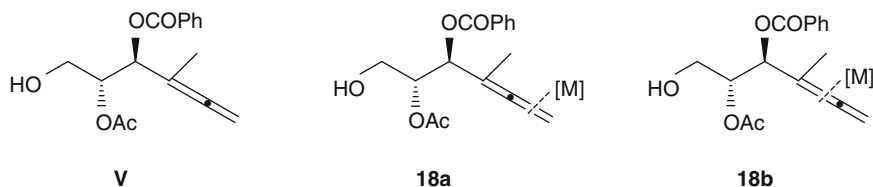


**Fig. 14** Structure of  $\gamma$ -allenol **V** as selected theoretical model for computational studies

**Table 6** NPA charge, bond lengths, Wiberg bond index of the M–C interactions, and free energy differences between complexes of type **a** and **b**

	ML <sub>x</sub>	NPA charge ML <sub>x</sub>	C <sub>n</sub> –C <sub>n+1</sub> (Å)	M–C <sub>n</sub> (Å)	M–C <sub>n+1</sub> (Å)	Wiberg bond index	Wiberg bond index	$\Delta G^a$ (kcal mol <sup>–1</sup> )
<b>18a</b>	AuCl <sub>3</sub>	–0.335	1.389	2.205	2.800	0.309	0.078	
	PtCl <sub>2</sub> (CH <sub>2</sub> CH <sub>2</sub> )	–0.196	1.378	2.165	2.603	0.355	0.194	
	PdCl <sub>2</sub>	–0.326	1.403	2.035	2.366	0.492	0.351	
<b>18b</b>	AuCl <sub>3</sub>	–0.268	1.356	2.291	2.464	0.258	0.168	–3.1
	PtCl <sub>2</sub> (CH <sub>2</sub> CH <sub>2</sub> )	–0.167	1.363	2.211	2.284	0.353	0.307	–9.5
	PdCl <sub>2</sub>	–0.304	1.385	2.124	2.121	0.480	0.428	–10.8

Free energy differences relative to **18a**

closely related structure to the parent precursor **13**, in order to include main effects and optimize computational resources.

The coordination of an allene to a metal may lead to several types of structures. For the model system **V**, two  $\eta^2$  complexes involving one of the C=C bonds have been found, **18a** and **18b** (Fig. 14), whose properties depend on the substitution pattern of the allene [74]. Thus, the  $\pi$ -coordination of the proximal C=C leads to a partially  $\eta^1$  slipped reactant complex to reduce steric repulsion with the methyl substituent, as the M–C distances and computed WBI suggest (Table 6). On the contrary, the coordination of the distal double bond drives to an almost symmetric  $\eta^2$  structure for the three catalysts, showing also higher WBI, i.e., more significant bonding, and globally shorter M–C lengths. These results point to stronger coordination and more stable complexes, supported by the calculated free energy difference between both types of coordination modes. The data summarized in Table 6 also suggest that the PdCl<sub>2</sub> generates a more electron-deficient allene fragment, probably due to the lack of a *trans* ligand and, hence, back-bonding donation from the metal.

Alternative conformations of the starting complexes, such as  $\sigma$ -allylic cation structures [74], could not be optimized as minima but were obtained as transition states. Therefore, it can be stated that the ground state for the complexes is the form **18b**. These similar trends for the catalytic systems suggest the same activation mode of the allene moiety upon complexation with the metal. The free energy differences computed for the intramolecular nucleophilic addition to the allene following the plausible heterocyclization paths are depicted in Table 7 and Fig. 15 (for AuCl<sub>3</sub>).

**Table 7** Enthalpies and free energy in the gas phase, and free energy in solution (kcal mol<sup>-1</sup>) for the cyclization of **V** by alternative regioisomeric 5-*exo-trig*, 6-*exo-dig*, and 7-*endo-trig* hetero-cyclization pathways

	AuCl <sub>3</sub>			PtCl <sub>2</sub> (CH <sub>2</sub> CH <sub>2</sub> )			PdCl <sub>2</sub>		
	$\Delta H_{\text{gas}}$	$\Delta G_{\text{gas}}$	$\Delta G_{\text{sol}}$	$\Delta H_{\text{gas}}$	$\Delta G_{\text{gas}}$	$\Delta G_{\text{sol}}$	$\Delta H_{\text{gas}}$	$\Delta G_{\text{gas}}$	$\Delta G_{\text{sol}}$
<b>18b</b>	0.0	0.0	<b>0.0</b>	0.0	0.0	<b>0.0</b>	0.0	0.0	<b>0.0</b>
<b>TS1<sub>5</sub></b>	6.6	8.6	<b>4.9</b>	15.5	17.6	<b>15.2</b>	14.6	16.0	<b>15.3</b>
<b>IN1<sub>5</sub></b>	-7.3	-3.7	<b>-12.5</b>	2.9	6.4	<b>4.2</b>	-2.8	0.0	<b>1.4</b>
<b>TS1<sub>6</sub></b>	3.9	6.5	<b>2.5</b>	11.0	13.7	<b>13.6</b>	11.3	13.1	<b>16.2</b>
<b>IN1<sub>6</sub></b>	-21.9	-18.5	<b>-26.5</b>	-8.3	-5.5	<b>-6.9</b>	-17.7	-16.0	<b>-10.4</b>
<b>TS1<sub>7</sub></b>	5.1	6.6	<b>2.2</b>	11.3	14.2	<b>13.5</b>	12.2	12.3	<b>13.9</b>
<b>IN1<sub>7</sub></b>	-4.9	-0.9	<b>-11.2</b>	5.8	7.8	<b>2.7</b>	-0.4	2.3	<b>2.6</b>

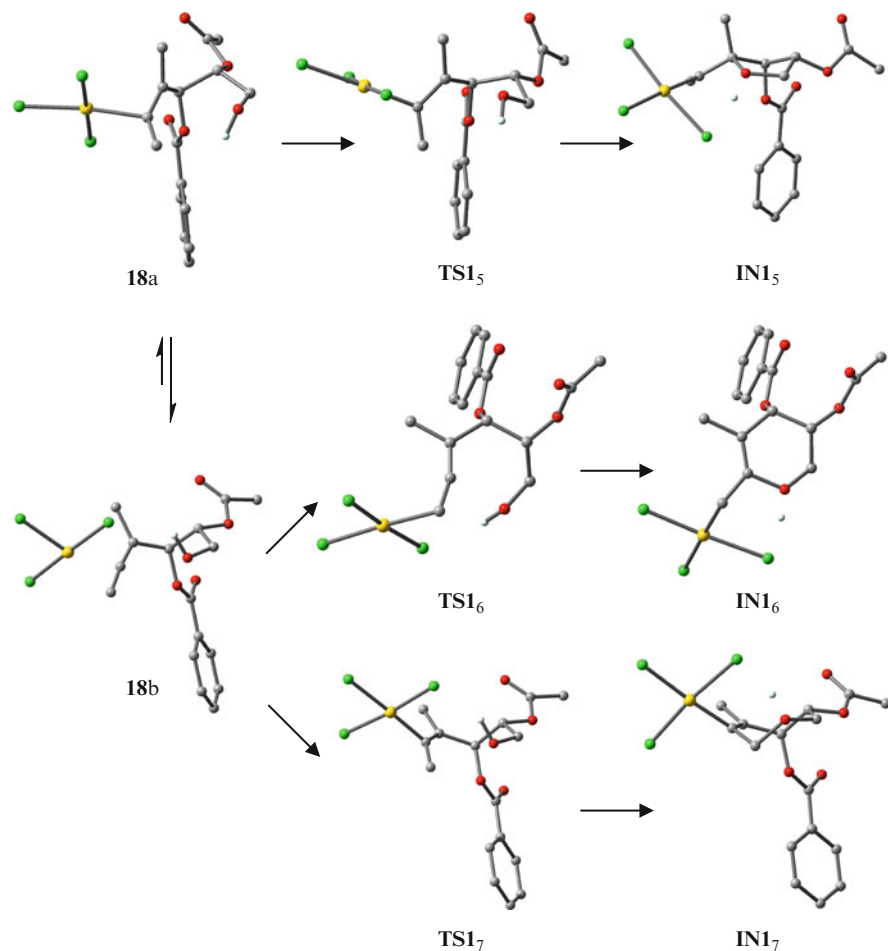


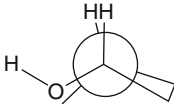
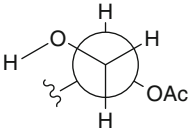
**Fig. 15** Optimized structures of the transition structures and intermediates for the AuCl<sub>3</sub> hetero-cyclization step following alternative paths

The computed energy values reveal that the 5-*exo-trig* cyclization (transition structure **TS1<sub>5</sub>**) takes place with a higher activation barrier than the 6-*exo-dig* mode (**TS1<sub>6</sub>**), which in turn proceeds with a higher barrier than the 7-*endo-trig* cyclization (**TS1<sub>7</sub>**). Furthermore, this tendency is systematically shown by the three catalyst systems. This kinetic preference contrasts sharply with that estimated for the precursors bearing a  $\beta$ -lactam ring as tether part, since the energy of activation increased progressively with the ring-size and the formation of the fused-tetrahydrofuran scaffold was clearly favored.

From a thermodynamic viewpoint, the formation of the dihydropyran intermediate (**IN1<sub>6</sub>**) is more exothermic than the formation of the tetrahydrofuran (**IN1<sub>5</sub>**) and tetrahydrooxepine (**IN1<sub>7</sub>**) intermediates. These divergences between both kinds of precursors can be easily understood by a close inspection of the transition structures. Focusing on the dihedral angle O(H)–C–C–C for the three alternative cyclizations for the three catalysts and comparing them with the  $\beta$ -lactam precursor, critical differences can be observed (Table 8). The restraint imposed by the  $\beta$ -lactam forces an *eclipsed* conformation for both the transition and intermediate fused structures, whereas for the acyclic precursor the transition state can be reached through a lower energy *staggered* conformation because of the improved tether flexibility. This effect not only reduces drastically the energy barrier for the cycloetherifications but also the 6-*exo-dig* and 7-*endo-trig* cyclization become the kinetically preferred pathways. In addition, **TS1<sub>6</sub>** and **TS1<sub>7</sub>** evolve to the metalla-alkenyl intermediates **IN1<sub>6</sub>** and **IN1<sub>7</sub>**, respectively, where the dihydropyran and tetrahydrooxepine rings formed adopt the lowest energy conformation, i.e., half-chair [75, 76] and chair [77, 78], respectively.

In summary, the calculated energy values indicate that the 7-*endo*-cycloetherification is kinetically favored over alternative cyclization modes, although **TS1<sub>6</sub>** for the 6-*exo* mode is only slightly less stable than **TS1<sub>7</sub>**. Even if these data agree with experimental evidence, the low energy difference between **TS1<sub>6</sub>** and **TS1<sub>7</sub>** does not justify the manifest regioselectivity. Therefore, the full reaction profiles for all the catalytic systems have been examined.

**Table 8** Dihedral angle O(H)–C–C–C for the first step (in degrees). The values for the AuCl<sub>3</sub>-mediated reaction of the  $\beta$ -lactamic structure are also shown for comparative purposes

				
	AuCl <sub>3</sub>	AuCl <sub>3</sub>	PtCl <sub>2</sub> (CH <sub>2</sub> CH <sub>2</sub> )	PdCl <sub>2</sub>
<b>TS1<sub>5</sub></b>	0.3	58.8	64.2	61.3
<b>IN1<sub>5</sub></b>	3.7	31.3	32.2	31.4
<b>TS1<sub>6</sub></b>	7.3	71.0	70.2	71.3
<b>IN1<sub>6</sub></b>	1.0	63.7	64.0	63.4
<b>TS1<sub>7</sub></b>	21.2	64.9	61.2	56.0
<b>IN1<sub>7</sub></b>	2.5	57.8	56.9	57.6

The alkenyl-metal intermediates **IN1<sub>n</sub>** show the formation of a hydrogen bond between one of the chloride ligands and the acidic hydroxylic hydrogen [1.75–1.85, 1.75–1.86, and 1.76–1.77 for AuCl<sub>3</sub>, PtCl<sub>2</sub>(CH<sub>2</sub>CH<sub>2</sub>), and PdCl<sub>2</sub>, respectively], which promotes the proton shift and protonolysis of the  $\sigma$ -carbon–metal bond to afford the cyclized product (a plausible direct 1,3-hydrogen shift was previously ruled out on the basis of the high energy barrier [79]). The formal 1,3-H migration is therefore assisted by the catalyst and takes place through two steps: formation of HCl and cleavage of the M–C bond through protonolysis by HCl to liberate the cycloadduct and regenerate the active catalyst. The first is a barrierless step when thermal corrections to the energy are taken into account. This step yields a transient intermediate structure (**IN2<sub>n</sub>**; for instance, for AuCl<sub>3</sub>-catalyzed processes, see Fig. 16) where the HCl formed remains weakly coordinated to the metal, thus promoting the last step.

The final step proceeds through the early four-membered ring transition structure **TS2<sub>n</sub>** that still exhibits short M–C and Cl–H breaking bonds and a large C–H forming bond (Table 9). This step is slightly exothermic whatever the catalyst. The free energy barrier required to reach the transition state for the seven-membered

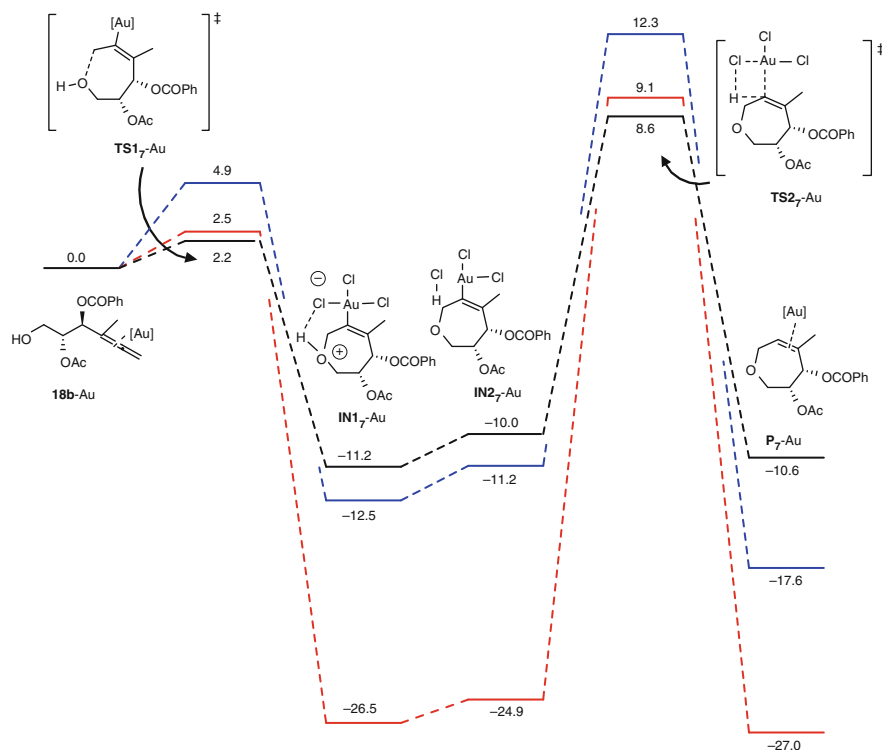


**Fig. 16** Free energy profile (kcal mol<sup>-1</sup>) for the transformation of  $\gamma$ -allenol **V** into the tetrahydroxepine **P<sub>7</sub>** (black line). Formation of the alternative five- (blue) and six-membered ring (red) cyclic ethers are shown for comparison

**Table 9** Key structural parameters (measured in Å) for the protonolysis step

	AuCl <sub>3</sub>			PtCl <sub>2</sub> (CH <sub>2</sub> CH <sub>2</sub> )			PdCl <sub>2</sub>		
	Cl–H	M–Cl	C–H	Cl–H	M–Cl	C–H	Cl–H	M–Cl	C–H
<b>TS2<sub>5</sub></b>	1.592	2.516	1.435	1.594	2.501	1.458	1.607	2.493	1.401
<b>P<sub>5</sub></b>	2.652	2.394	1.088	2.907	2.376	1.087	3.021	2.335	1.085
<b>TS2<sub>6</sub></b>	1.567	2.534	1.508	1.529	2.502	1.626	1.654	2.431	1.470
<b>P<sub>6</sub></b>	3.372	2.370	1.096	3.339	2.364	1.096	3.215	2.318	1.095
<b>TS2<sub>7</sub></b>	1.506	2.550	1.535	1.498	1.514	1.602	1.547	2.502	1.469
<b>P<sub>7</sub></b>	2.686	2.390	1.090	2.814	2.386	1.091	2.812	2.330	1.089

**Table 10** Free energy differences (in kcal mol<sup>−1</sup>), relative to the starting complex **18b**, for the protonolysis step

	AuCl <sub>3</sub>			PtCl <sub>2</sub> (CH <sub>2</sub> CH <sub>2</sub> )			PdCl <sub>2</sub>		
	<i>n</i> = 5	<i>n</i> = 6	<i>n</i> = 7	<i>n</i> = 5	<i>n</i> = 6	<i>n</i> = 7	<i>n</i> = 5	<i>n</i> = 6	<i>n</i> = 7
<b>TS2<sub>n</sub></b>	12.3	9.1	8.6	22.3	18.5	17.9	19.2	15.5	14.7
<b>Product</b>	−17.6	−27.0	−10.6	−9.4	−26.9	−6.9	−2.5	−12.1	−3.5

ring intermediate, **TS2<sub>7</sub>**, is lower than for the six-membered ring counterpart, **TS2<sub>6</sub>** (Table 10). That is, **TS2<sub>7</sub>** is more stable than **TS2<sub>6</sub>**, probably because a stronger  $\sigma$ -Csp<sup>2</sup>–H bond is being formed. In this context, the high barrier computed for the protonolysis of the vinyl-metal intermediates **IN1<sub>5</sub>** (**TS2<sub>5</sub>**, Table 10) is remarkable, in contrast to the  $\beta$ -lactam counterpart. To check whether it is due to steric repulsions with the bulky ester, we estimated the activation barrier for its epimer **IN1<sub>5</sub>'** lacking this effect. The pertinent transition structure **TS2<sub>5</sub>'** is even less stable (0.9 kcal mol<sup>−1</sup>) than **TS2<sub>5</sub>** because of steric interactions with endocyclic protons in a puckered, highly functionalized, tetrahydrofuran ring. The full free energy profiles for the formation of tetrahydrofuran, dihydropyran, and tetrahydrooxepine frameworks are depicted together in Fig. 16 for comparative purposes. The data are in good agreement with experimental observations as they indicate a kinetically favored formation of the tetrahydrooxepine skeleton.

All these data point out that a possible pathway for the AuCl<sub>3</sub>-catalyzed formation of the tetrahydrooxepine derivative from  $\gamma$ -allenol **V** might thus initially involve the formation of a complex **18b** through coordination of the gold trichloride to the distal allenic double bond. Next, a regioselective 7-*endo* oxyauration through nucleophilic addition to the terminal allenic carbon forms the alkenyl–Au intermediate **IN1<sub>7</sub>**. A subsequent loss of HCl and rate-limiting protonolysis of the carbon–gold bond provides the tetrahydrooxepine and regenerates the gold catalyst (Scheme 15).

The computed results for the plausible Pt<sup>II</sup>-catalyzed heterocyclizations for allenol **V** show the same trend to that seen before for the Au<sup>III</sup>-catalyzed process, namely, a kinetic preference for the nucleophilic addition to the terminal Csp<sup>2</sup>-allene carbon (7-*endo-trig* heterocyclization mode, Table 7). Likewise, the transition structure for the rate-limiting protonolysis step for the seven-membered, **TS2<sub>7</sub>**, is more stable than those for the dihydropyran (**TS2<sub>6</sub>**) and tetrahydrofuran (**TS2<sub>5</sub>**) cycloadducts (Table 10). One might expect, therefore, the favored formation of the same oxacycle **P<sub>7</sub>**. However, experimental results showed that product **14** is not

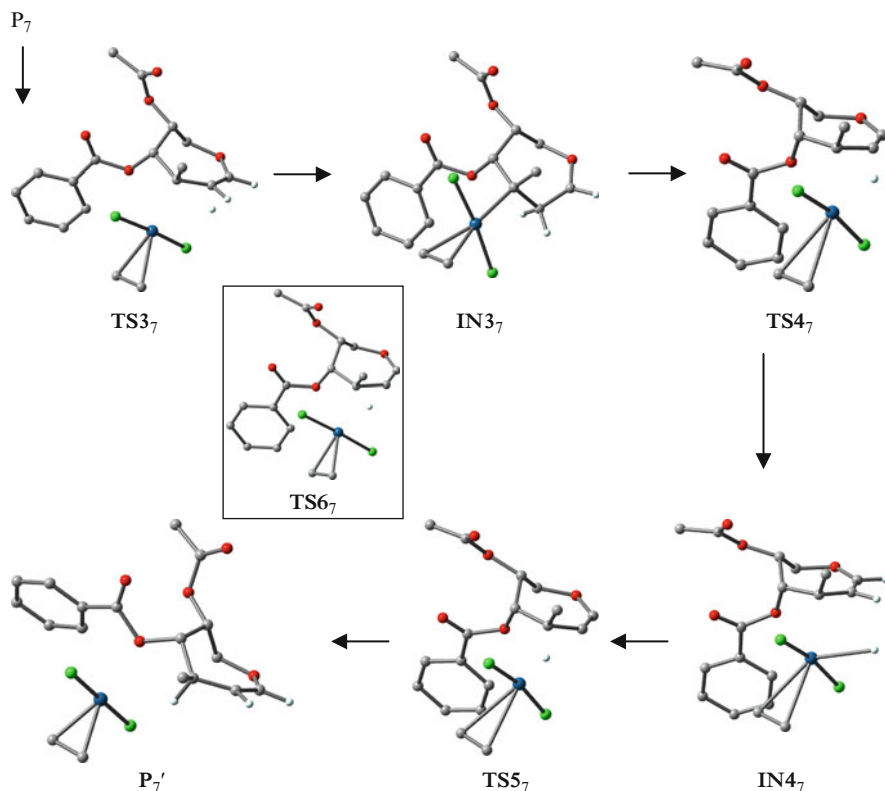


**Fig. 17** Optimized structures of the stepwise hydrogen shift involved in the isomerization of  $P_7$  into  $P_7'$ . A three-step Pt-mediated mechanism is favored over the alternative uncatalyzed two-step mechanism through  $TS_{67}$ . Most of the Hs have been omitted for the sake of clarity

detected in the Pt-catalyzed reaction of  $\gamma$ -allenol **13** (Scheme 14), its isomer **15** being the sole reaction product. Conjugation of the double bond with the lone pair of oxygen atoms under Pt-catalyzed conditions might be evoked to account for the formation of this structure. So the role of the catalyst in this divergence was questioned.

Coming back to the theoretical model, the transformation of  $P_7$  into  $P_7'$  involves a formal 1,3-hydrogen migration. This process can be viewed as two consecutive 1,2-H shift steps rather than a direct 1,3-H shift (Fig. 17). In this context it has been found to be a rather synchronous transition structure (C–H breaking bond = 1.406, C–H forming bond = 1.470 Å),  $TS_{37}$ , where the moving atom establishes an H-bond with the catalyst (1.849 Å). This effect stabilizes the transition structure, giving rise to a moderate activation barrier (17.3 kcal mol<sup>-1</sup>) to be overcome.<sup>5</sup>

<sup>5</sup>An alternative transition structure has been located lacking this H-bond between the ligand and the moving hydrogen, that lies 16.2 kcal mol<sup>-1</sup> above  $TS_{37}$ .

The pertinent IRC calculations have verified that **TS3<sub>7</sub>** connects **P<sub>7</sub>** with **IN3<sub>7</sub>** in an endothermic, reversible step (8.8 kcal mol<sup>-1</sup>). Finally, it has been proposed that the last 1,2-H migration may be a stepwise process taking place assisted by the metal center via  $\beta$ -H elimination. Mechanistic studies on transition-metal-catalyzed  $\beta$ -H elimination processes [80–82] have revealed that they can proceed through four-membered ring intermediate structures [83, 84] in which H coordinates to a metal center before  $\beta$ C–H bond dissociation takes place. Nevertheless, the long Pt...H distance (2.945 Å) suggests that **IN3<sub>7</sub>** should not be a marked  $\beta$ -agostic structure [85]. The transition structure involved in this step, **TS4<sub>7</sub>**, exhibits the lengthening of the Pt–C (2.304 Å) and C–H (1.201 Å) breaking bonds and shortening of the Pt–H (2.179 Å) and C–C (1.449 Å) bonds. Detailed examination of the imaginary frequency mode confirms that the most important geometric change takes place on the H atom between the C atom and the metal center. Then **TS4<sub>7</sub>** evolves to the platinahydride intermediate **IN4<sub>7</sub>**, where the complete migration of H from the methylene moiety (C–H 3.113 Å) to Pt (Pt–H 1.535 Å) has taken place.

The last step could therefore drive to the isomer **P<sub>7</sub>'** from the **IN4<sub>7</sub>** intermediate through the transition state **TS5<sub>7</sub>**, as confirmed by IRC analysis. This transition structure shows the H approaching to C by closure of the C–Pt–H bond angle (from 83.7° in **IN4<sub>7</sub>** to 25.9°). It should be noted that a weak Pt–O interaction between the catalyst and the benzylic oxygen atom is detected along the stepwise 1,2-H shift (2.994, 2.723, and 2.367, for **IN4<sub>7</sub>**, **TS5<sub>7</sub>**, and **P<sub>7</sub>'**, respectively), due to the oxophilic nature of the Pt, which likely stabilizes **TS5<sub>7</sub>** and accounts for the stability of the complexed **P<sub>7</sub>'** and, amazingly, the chirality at the new stereocenter. This step is exothermic and the barrier to attain **TS5<sub>7</sub>** is low (4.4 kcal mol<sup>-1</sup> from **IN4<sub>7</sub>**). Otherwise, the uncatalyzed 1,2-shift from **IN3<sub>7</sub>** has been estimated to proceed through a high energy transition structure (**TS6<sub>7</sub>**) lying 22.2 and 28.3 kcal mol<sup>-1</sup> above **TS4<sub>7</sub>** and **TS5<sub>7</sub>**, respectively. These data support the stepwise 1,2-H migration assisted by the metal complex. Figure 18 outlines the free energy profile for the

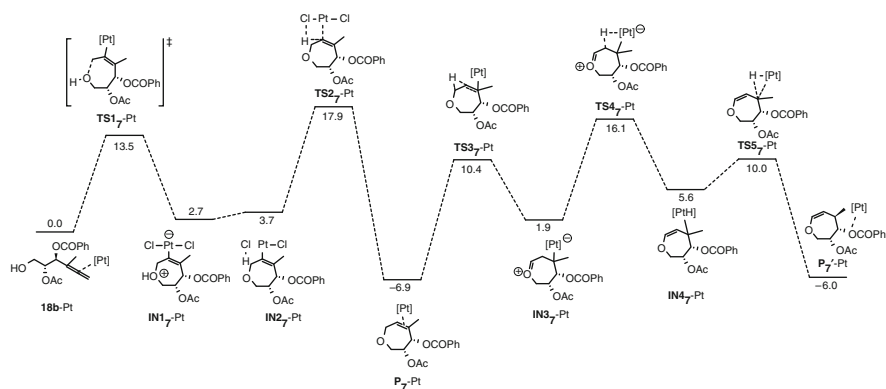
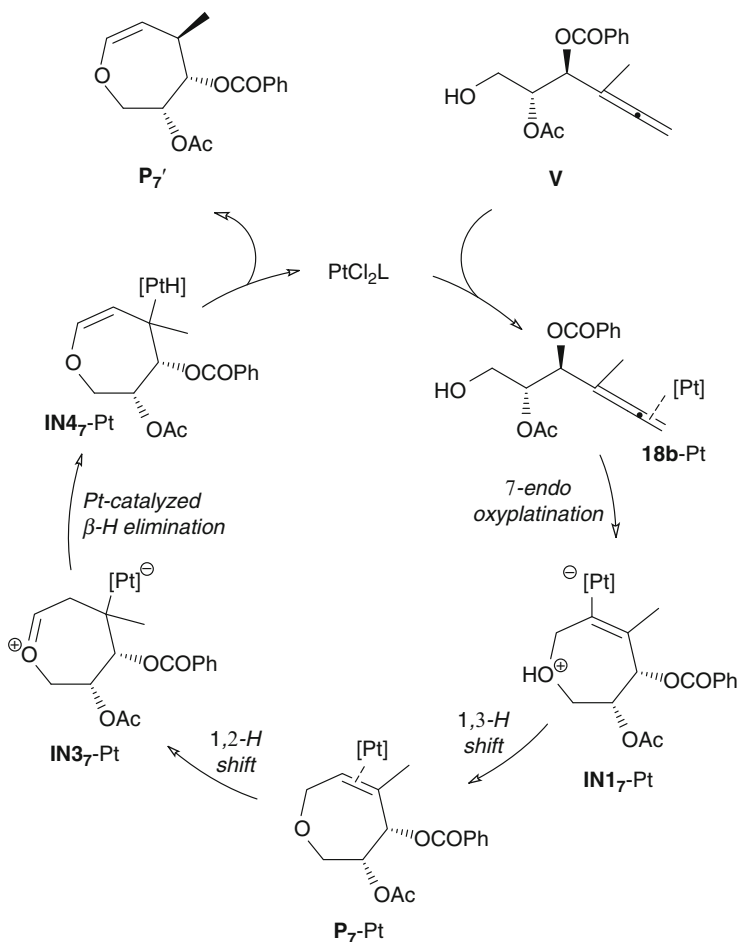


**Fig. 18** Free energy profile [kcal mol<sup>-1</sup>] for the Pt-catalyzed transformation of  $\gamma$ -allenol **V** into the tetrahydrooxepine **P<sub>7</sub>'**





**Scheme 16** Mechanistic explanation for the  $\text{Pt}^{\text{II}}$ -catalyzed hydroalkoxylation reaction of  $\gamma$ -allenol **V**

transformation of  $\gamma$ -allenol **V** into the tetrahydrooxepine **P7'** (cyclic ether of type **15**, Scheme 14).

According to these results, a likely pathway for the achievement of tetrahydrooxepine of type **15** (Scheme 14) initially involves the formation of a  $\pi$ -complex **18b** through coordination of the metal to the distal diene moiety of  $\gamma$ -allenol. Next, a kinetically preferred 7-endo heterocyclization to form species **IN17** is followed by 1,3 hydrogen shift affording the  $\pi$ -complexed oxacycle **P7**. This tetrahydrooxepine scaffold isomerizes to **P7'** through a 1,2-hydrogen migration, assisted by a halide ligand, a Pt-catalyzed  $\beta$ -hydrogen elimination to generate the platinahydride intermediate **IN47**, and a final protonolysis step (Scheme 16). The **P7**  $\rightarrow$  **P7'** isomerization is not observed under  $\text{AuCl}_3$  catalysis, probably due to the fact that gold shows

no tendency to undergo  $\beta$ -hydride elimination reactions; indeed, gold-hydrides are a rare species and difficult to access [86, 87]. Thus, even if the formation of **IN3<sub>7</sub>** is possible, as long as it is reversible and the subsequent  $\beta$ -H elimination is blocked, the reaction stops once **P<sub>7</sub>** has been generated.

The Pd-catalyzed heterocyclization also shows the same regioselectivity as that observed under Au- and Pt-catalysis, i.e., the initial 7-*endo-trig* cyclization takes place preferentially by nucleophilic addition of the hydroxylic oxygen to the activated terminal allene carbon (Table 7). In the same way, the transition structure for the protonolysis step for the seven-membered cycloadduct, **TS2<sub>7</sub>**, appears about 1 and 4.5 kcal mol<sup>-1</sup> below the related for the dihydropyran (**TS2<sub>6</sub>**) and tetrahydrofuran (**TS2<sub>5</sub>**) scaffolds, respectively. However, the presence of an allyl halide alternatively promotes a coupling reaction by trapping of the kinetically preferred alkenyl-Pd intermediate **IN<sub>7</sub>-Pd**. This process is favored by the easy HCl release from the coordination to the metal center [Pd–Cl(H) = 2.592 Å in **IN2<sub>7</sub>-Pd** vs 2.487 Å in **IN1<sub>7</sub>-Pd**]. As noted above, the cyclization intermediates **IN1<sub>n</sub>** show the shortest H–Cl distances for Pd as catalyst. The allyl coupling with the alkenyl Pd<sup>II</sup> intermediate occurs through a three-step mechanism: (1) ligand displacement from the metal coordination sphere, (2) insertion into the allylic halide C=C bond to give a  $\sigma$ -C–Pd intermediate, and (3) *trans*  $\beta$ -elimination to afford the oxepane product (Fig. 19). The Pd-coordinated HCl is easily displaced by the incoming allyl bromide in a fast ligand-interchange displacement mechanism to yield the  $\eta^2$ -complex **IN1<sub>Al</sub>** upon  $\pi$ -coordination of the C=C double bond to the metal. This coordination gives rise to almost symmetrical Pd–alkene bonds [Pd–C(H<sub>2</sub>) 2.221 and Pd–C(H)

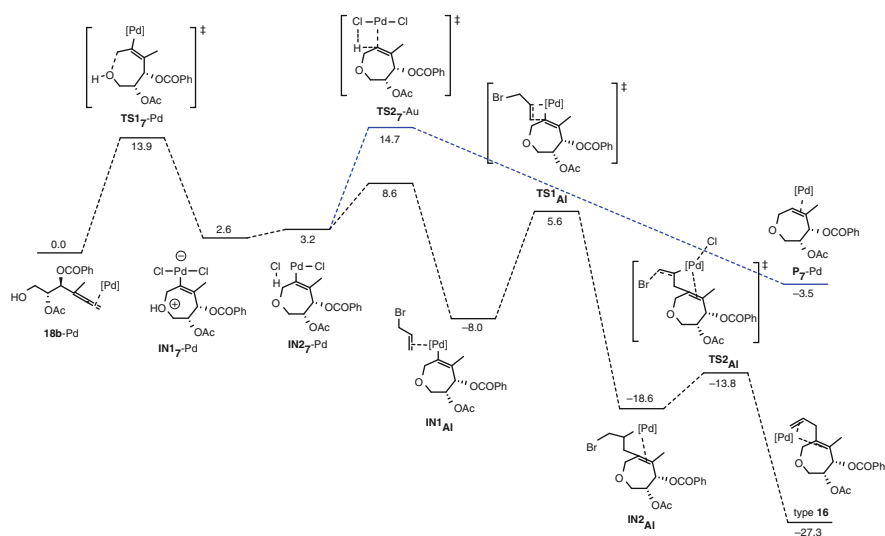


**Fig. 19** Free energy profile [kcal mol<sup>-1</sup>] for the transformation of  $\gamma$ -allenol **V** into the tetrahydrooxepine of type **16**. Formation of the corresponding bicycle **P<sub>7</sub>** from protonolysis of the intermediate **IN2<sub>7</sub>** is shown in blue for comparison

2.252 Å], and a lengthened C=C bond ( $\Delta d$  0.049 Å on going from the uncoordinated precursor to the  $\pi$ -complex **IN1<sub>Al</sub>**). This step is exothermic (by 11.2 kcal mol<sup>-1</sup>), and requires a low activation barrier to succeed (5.3 kcal mol<sup>-1</sup>).

The coordinated alkene undergoes a 2,1-insertion into the Pd-alkyl bond in a stepwise process<sup>6</sup> that proceeds through the formation of a  $\eta^2$ -Pd-complex (Pd-C 2.203 and 2.282 Å), **IN2<sub>Al</sub>**. This intermediate is formed via the four-membered ring **TS1<sub>Al</sub>**, in which the four atoms forming new bonds (Pd-C 2.077 and C-C 2.133 Å) are roughly planar (deviation of 7.4°). A *cis/trans* isomerization of the chloride ligand takes place to reach the transition state, probably in order to reduce the back-bonding interaction and to favor the Pd-C bond formation. Likewise, a moderate activation barrier is found for the insertion of the allylic bromide into the Pd-C bond (13.6 kcal mol<sup>-1</sup>), the formation of **IN2<sub>Al</sub>** being favored from a thermodynamic viewpoint (-10.6 kcal mol<sup>-1</sup>). The  $\eta^2$ -Pd-complex then suffers a  $\beta$ -heteroatom elimination<sup>7,8</sup> to give the coupling product and the active catalyst PdCl<sub>2</sub>. As has been noted, the liberated HCl plays a key role in promoting the dehalopalladation and inhibiting the usual  $\beta$ -H elimination (see footnote 7).<sup>9</sup> Lu et al. have postulated that halide ions would assist the  $\beta$ -heteroatom elimination, through an E2-like mechanism promoted by halide ion coordination to Pd.<sup>10</sup> Accordingly, the *trans*  $\beta$ -elimination step takes place via **TS2<sub>Al</sub>**, that exhibits an advanced tetracycle opening (forming bond Pd-Cl = 2.466 and breaking bond C-Br = 2.097 Å, opening of the bond angle C-C-C = 115.6°). This transition structure finally drives to the dienic product. The  $\beta$ -dehalopalladation proceeds in an exothermic step by surmounting a low activation barrier (4.8 kcal mol<sup>-1</sup>).

The free energy profile is shown in Fig. 19 and reveals similar features to that computed for 2-azetidinone-tethered methyl- $\gamma$ -allenols. Thus, the Pd-catalyzed cyclizative coupling reaction between  $\gamma$ -allenols and allyl halides is a kinetic and thermodynamically favored process over the cyclization, and proceeds through a common 7-*endo*-oxypalladation followed by a stepwise energy-downhill coupling with the alkene.

The proposed mechanism is summarized in Scheme 17. Initial coordination of the distal allene bond of the precursor to the catalyst provides the allenepalladium complex **18b**-Pd. This starting complex undergoes an intramolecular cycloetherification reaction to give the palladatetrahydrooxepine **IN1<sub>7</sub>**, that easily releases HCl providing **IN2<sub>7</sub>**. A subsequent displacement from the metal coordination sphere of the HCl by allyl bromide gives intermediate **IN1<sub>Al</sub>**, which after insertion of the allylic chain and *trans*  $\beta$ -heteroatom elimination generates tetrahydrooxepine of type **16** (Scheme 17) with concomitant regeneration of the Pd-catalyst.

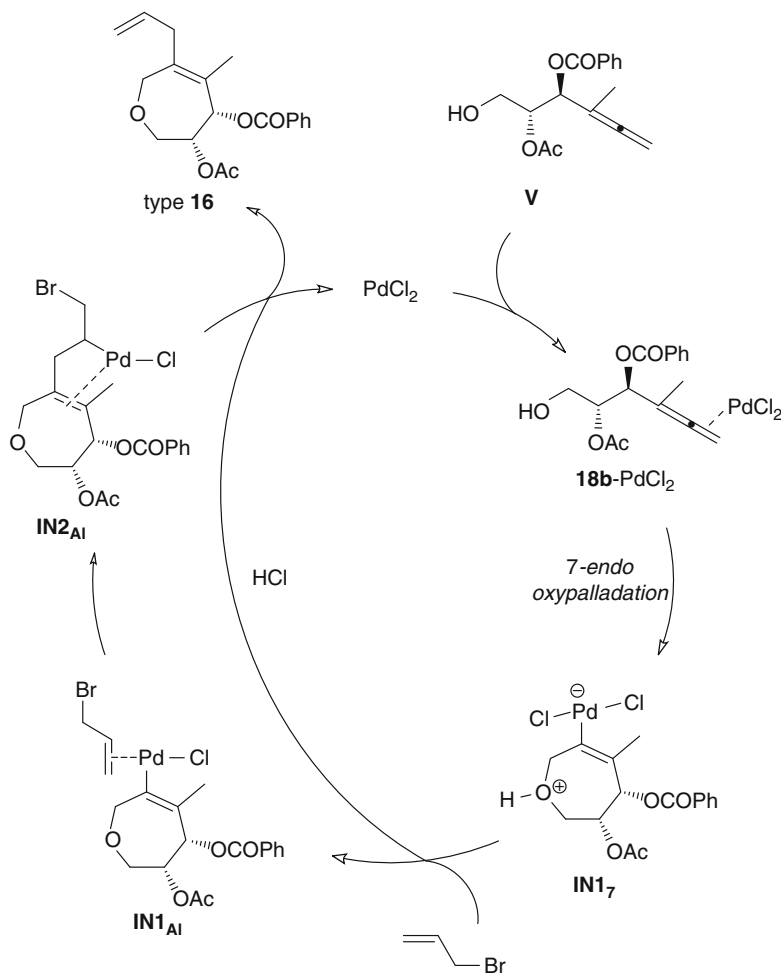
<sup>6</sup>The regioselectivity found here is quite similar to those found in the insertion reactions of alkenes with many neutral Pd<sup>II</sup> complexes. See [48, 49].

<sup>7</sup>See [50–57].

<sup>8</sup>For the stereoselectivity of  $\beta$ -heteroatom elimination, see [58–61].

<sup>9</sup>See [62].

<sup>10</sup>See [63].



**Scheme 17** Mechanistic explanation for the  $\text{Pd}^{\text{II}}$ -catalyzed heterocyclization reaction of  $\gamma$ -allenol **V**

## 4 Conclusion

In summary, regiocontrolled gold-, platinum-, lanthanum-, and palladium-catalyzed heterocyclization reactions of  $\gamma$ -allenols derived from 4-oxoazetidine-2-carbaldehydes and D-glyceraldehyde leading to a variety of enantiopure tetrahydrofurans, dihydropyrans, and tetrahydrooxepines have been developed. Besides, DFT calculations were performed to obtain insight on various aspects of this reactivity of  $\gamma$ -allenols. Calculations methods predicted a tether-, a protecting group-, and a metal-dependent heterocyclization for  $\gamma$ -allenols. These theoretical predictions are fully confirmed by the experimental results. Recently, synthetic

chemists have shown an increased interest in the use of computational chemistry as a tool, next to spectroscopic and other physical techniques. Mostly what we are after is an explanation for both experimental product ratios and mechanistic rationalization. The results presented herein may encourage the dialog between synthetic chemists and our more theoretical colleagues, throwing some light on the search for transition states and the comparison between the activation energies obtained for alternative reactions.

## References

1. Larrosa I, Romea P, Urpí F (2008) *Tetrahedron* 64:2683
2. Wolfe JP, Hay MB (2007) *Tetrahedron* 63:261
3. Clarke PA, Santos S (2006) *Eur J Org Chem* 2405
4. Snyder NL, Haines HM, Peczu MW (2006) *Tetrahedron* 62:9301
5. Hou XL, Yang Z, Yeung KS, Wong HNC (2005) In: Gribble GW, Joule JA (eds) *Progress in heterocyclic chemistry*, vol 17. Elsevier, Oxford, p 142
6. Eicher T, Hauptmann JS (eds) (2003) *The chemistry of heterocycles: structure, reactions, syntheses, and applications*. Wiley-VCH, Weinheim
7. Ma S (2005) *Chem Rev* 105:2829
8. Krause N, Hashmi ASK (eds) (2004) *Modern allene chemistry*. Wiley-VCH, Weinheim
9. Zimmer R, Dinesh CU, Nandan E, Khan FA (2000) *Chem Rev* 100:3067
10. Brasholz M, Reissig HU, Zimmer R (2009) *Acc Chem Res* 42:45
11. Marshall JA, Yu RH, Perkins JF (1995) *J Org Chem* 60:5550
12. Flögel O, Reissig HU (2004) *Eur J Org Chem* 2797
13. Hoffmann-Röder A, Krause N (2001) *Org Lett* 3:2537
14. Morita N, Krause N (2006) *Eur J Org Chem* 4634
15. Hashmi ASK, Blanco MC, Fischer D, Bats JW (2006) *Eur J Org Chem* 1387
16. Volz F, Krause N (2007) *Org Biomol Chem* 5:1519
17. Aksn Ö, Krause N (2008) *Adv Synth Catal* 350:1106
18. Ma S, Gao W (2002) *J Org Chem* 67:6104
19. Yu F, Lian X, Ma S (2007) *Org Lett* 9:1703
20. Xu D, Li Z, Ma S (2002) *Chem Eur J* 8:5012
21. Alcaide B, Almendros P, Rodríguez-Acebes R (2006) *J Org Chem* 71:2346
22. Zhang Z, Widenhoefer RA (2007) *Angew Chem Int Ed* 46:283
23. Zhang Z, Liu C, Kinder RE, Han X, Qian H, Widenhoefer RA (2006) *J Am Chem Soc* 128:9066
24. Arbour JL, Rzepa HS, White AJP, Hii KK (2009) *Chem Commun* 7125
25. Belmont P, Parker E (2009) *Eur J Org Chem* 6075
26. Lipshutz B, Yamamoto Y (2008) *Chem Rev* 108(8):2793–3442
27. Hutchings GJ, Brust M, Schmidbaur H (eds) (2008) *Chem Soc Rev* 37(9):1759–2134
28. Bongers N, Krause N (2008) *Angew Chem Int Ed* 47:2178
29. Hutchings GJ (2008) *Chem Commun* 1148
30. Muzart J (2008) *Tetrahedron* 64:5815
31. Hashmi ASK (2007) *Chem Rev* 107:3180
32. Yu X, Seo S, Marks TJ (2007) *J Am Chem Soc* 129:7244
33. Frisch MJ, Trucks GW, Schlegel HB, Scuseria GE, Robb MA, Cheeseman JR, Montgomery JA Jr, Vreven T, Kudin KN, Burant JC, Millam JM, Iyengar SS, Tomasi J, Barone V, Mennucci B, Cossi M, Scalmani G, Rega N, Petersson GA, Nakatsuji H, Hada M, Ehara M, Toyota K, Fukuda R, Hasegawa J, Ishida M, Nakajima T, Honda Y, Kitao O, Nakai H, Klene M,

- Li X, Knox JE, Hratchian HP, Cross JB, Bakken V, Adamo C, Jaramillo J, Gomperts R, Stratmann RE, Yazyev O, Austin AJ, Cammi R, Pomelli C, Ochterski JW, Ayala PY, Morokuma K, Voth GA, Salvador P, Dannenberg JJ, Zakrzewski VG, Dapprich S, Daniels AD, Strain MC, Farkas O, Malick DK, Rabuck AD, Raghavachari K, Foresman JB, Ortiz JV, Cui Q, Baboul AG, Clifford S, Cioslowski J, Stefanov BB, Liu G, Liashenko A, Piskorz P, Komaromi I, Martin RL, Fox DJ, Keith T, Al-Laham MA, Peng CY, Nanayakkara A, Challacombe M, Gill PMW, Johnson B, Chen W, Wong MW, González C, Pople JA (2003) Gaussian 03, Revision B.03. Gaussian, Inc., Wallingford CT
34. Lee C, Yang W, Parr R (1988) *Phys Rev B* 37:785
35. Becke A (1993) *J Chem Phys* 98:5648
36. Hay PJ, Wadt WR (1985) *J Chem Phys* 82:270
37. Fukui K (1981) *Acc Chem Res* 14:363
38. González C, Schlegel HB (1990) *J Chem Phys* 94:5523
39. Barone V, Cossi M (1998) *J Phys Chem A* 102:1995
40. Reed AE, Weinhold F (1983) *J Chem Phys* 78:4066
41. Reed AE, Curtiss LA, Weinhold F (1988) *Chem Rev* 88:899
42. Prasad JS, Liebeskind LS (1988) *Tetrahedron Lett* 29:4257
43. Ma S, Gao W (2000) *Tetrahedron Lett* 41:8933
44. Ma S, Yu F, Gao W (2003) *J Org Chem* 68:5943
45. Ma S, Yu F, Li J, Gao W (2007) *Chem Eur J* 13:247
46. Michalak A, Ziegler T (1999) *Organometallics* 18:3998
47. Deeth RJ, Smith A, Brown J (2004) *J Am Chem Soc* 126:7144
48. Michalak A, Ziegler T (2000) *Organometallics* 19:1850
49. Cabri W, Candiani I (1995) *Acc Chem Res* 28:2
50. Harrington PJ, Hegedus LS, McDaniel KF (1987) *J Am Chem Soc* 109:4335
51. Francis JW, Henry PM (1991) *Organometallics* 10:3498
52. Kimura M, Horino Y, Mukai R, Tanaka S, Tamaru Y (2001) *J Am Chem Soc* 123:10401
53. Ozawa F, Okamoto H, Kawagishi S, Yamamoto S, Minami T, Yoshifuji M (2002) *J Am Chem Soc* 124:10968
54. Manabe K, Kobayashi S (2003) *Org Lett* 5:3241
55. Kabalka GW, Dong G, Venkataiah B (2003) *Org Lett* 5:893
56. Yoshida M, Gotou T, Ihara M (2004) *Chem Commun* 1124
57. Liu G, Lu X (2001) *Org Lett* 3:3879
58. Frost CG, Howarth J, Williams MJ (1992) *Tetrahedron Asymmetry* 3:1089
59. Daves GD Jr (1990) *Acc Chem Res* 23:201
60. Zhu G, Lu X (1995) *Organometallics* 14:4899
61. Alcaide B, Almendros P, Martínez del Campo T (2006) *Angew Chem Int Ed* 45:4501
62. Lu X, Zhu G, Wang Z (1998) *Synlett*: 115, and references therein
63. Zhang Z, Lu X, Xu Z, Zhang Q, Han X (2001) *Organometallics* 20:3724
64. Balcells D, Maseras F, Keay BA, Ziegler T (2004) *Organometallics* 23:2784
65. Alcaide B, Almendros P, Martínez del Campo T, Soriano E, Marco-Contelles JL (2009) *Chem Eur J* 15:1901
66. Jonasson C, Horváth A, Bäckvall JE (2000) *J Am Chem Soc* 122:9600
67. Gaussian Inc. (2004) Gaussian 03, Wallingford CT
68. Hay PJ, Wadt WR (1985) *J Chem Phys* 82:299
69. Ditchfield R, Hehre WJ, Pople JA (1971) *J Chem Phys* 54:724
70. Hehre WJ, Ditchfield R, Pople JA (1972) *J Chem Phys* 56:2257
71. Hariharan PC, Pople JA (1973) *Theo Chim Acta* 28:213
72. Hariharan PC, Pople JA (1974) *Mol Phys* 27:209
73. Gordon MS (1980) *Chem Phys Lett* 76:163
74. Gandon V, Lemièrre G, Hours A, Fensterbank L, Malacria M (2008) *Angew Chem Int Ed* 47:7534

75. Kalsi PS (2005) Stereochemistry conformation and mechanism, 6th edn. New Age International, New Delhi, Chap. 4
76. Mastryukov VS, Chen KH, Allinger NL (2001) *J Phys Chem A* 105:8562
77. Ermolaeva LI, Mastryukov VS, Allinger NL, Almennigen A (1989) *J Mol Struct* 196:151
78. Leong MK, Mastryukov VS, Boggs JE (1998) *J Mol Struct* 445:149
79. Alcaide B, Almendros P, Martínez del Campo T, Soriano E, Marco-Contelles JL (2009) *Chem Eur J* 15:1909
80. Samec JSM, Bäckvall JE, Andersson PG, Brandt P (2006) *Chem Soc Rev* 35:237
81. Crabtree RH (2001) The organometallic chemistry of the transition metals. Wiley, New York
82. Niu S, Hall MB (2000) *Chem Rev* 100:353
83. Ackerman LJ, Green MLH, Green JC, Bercaw JE (2003) *Organometallics* 23:188
84. Shultz LH, Brookhart M (2001) *Organometallics* 20:3975
85. Brookhart M, Green MLH, Parkin GP (2007) *Natl Acad Sci USA* 104:6908
86. Hoffmann-Röder A, Krause N (2005) *Org Biomol Chem* 3:387
87. Hashmi ASK, Hutchings GJ (2006) *Angew Chem Int Ed* 45:7896

# Gold-Catalyzed Cycloadditions Involving Allenes: Mechanistic Insights from Theoretical Studies

Sergi Montserrat, Gregori Ujaque, Fernando López, José L. Mascareñas, and Agustí Lledós

**Abstract** Allenes, owing to their special structural characteristics related to the presence of two  $\pi$  bonds in a formally strained manner, are particularly prone to undergo gold-activated reactions, particularly cycloaddition processes. Theoretical studies based on DFT calculations have been very useful to explain observed reactivities and advance mechanistic proposals.

**Keywords** Allene · Cycloaddition · DFT studies · Gold catalysis · Reaction mechanisms

## Contents

1	Introduction .....	225
2	Interaction Between Gold and Allenes .....	227
3	Gold-Catalyzed Cycloadditions Between Allenes and Dienes .....	230
3.1	[4C + 3C] Cycloadditions .....	230
3.2	[4C + 2C] Cycloadditions .....	236
4	Other Cycloadditions Involving Allenes .....	242
5	Concluding Remarks .....	245
	References .....	246

---

S. Montserrat, G. Ujaque, and A. Lledós (✉)

Departament de Química, Universitat Autònoma de Barcelona, Bellaterra, Barcelona 08193, Spain  
e-mail: agusti@klingon.uab.cat

F. López

Instituto de Química Orgánica General (CSIC), Juan de la Cierva 3, Madrid 28006, Spain

J.L. Mascareñas

Departamento de Química Orgánica, Universidade de Santiago de Compostela, Santiago de Compostela 15782, Spain



## 1 Introduction

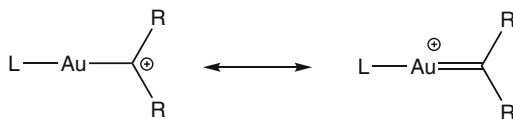
Cycloaddition reactions have been used as key steps in innumerable syntheses for more than a century and therefore can be considered as one of the most useful organic reactions [1]. Most classical cycloadditions are pericyclic reactions as they involve cyclic transition states and a concerted rearrangement of the electrons that causes  $\sigma$ - and  $\pi$ -bonds to break and form simultaneously. In the case of carbon unsaturated systems, most cycloadditions have involved the use of alkenes and/or dienes as reactants. However, in the last two decades cycloadditions of allenes have grown considerably [2, 3].

Some reviews and monographs on the chemistry of allenes have been published in the last 10 years [4–6]. Allenes have a unique reactivity as  $\pi$ -conjugated systems since they are cumulated dienes. In addition they can be chiral species if the four substituents are different, and this property provides additional bonus from the synthetic point of view. Particularly relevant is the chemistry of allenes involving transition metal catalyzed processes, most of them consisting of metalation and cyclization reactions [7].

Several transition metals can activate C–C multiple bonds. Special mention must be made of Pt- and especially Au-complexes that show higher and better activity compared to complexes of other previously used metals [8, 9]. The increasing relevance of gold catalysis over the last 10 years is reflected by the number of reviews that have appeared in the literature in a short period (2006–2008) [8–15]. This special reactivity of gold complexes can be related to their coordination characteristics and reluctance to undergo redox processes, as well as to the relativistic effects present in gold [16, 17]. In this sense, Pt and Au complexes activate C–C multiple bonds towards nucleophilic attacks because there is a good  $\sigma$ -interaction from the  $\pi$  system to the metal, but a small  $\pi$  back-donation of the metal to the unsaturated unit. Hence, the multiple bond becomes more electrophilic [8].

This kind of activation drives a variety of interesting and otherwise unfeasible transformations. However, nowadays experimental studies of the reaction mechanism are scarce [18, 19], and seriously hampered by the impossibility of isolating reaction intermediates. Regarding theoretical studies, although they are not very numerous yet, they are increasing quite rapidly [20–25]. One of the controversial points about Au-catalyzed reaction mechanisms has to do with the nature of the crucial species that has been proposed as intermediate in several transformations: a gold-carbene or gold-stabilized carbocation (Fig. 1) [8, 26–29].

**Fig. 1** Scheme of the two discussed structures to describe the Au–C bond usually proposed as intermediate in several Au-catalyzed reactions



Here we present a brief review of theoretical studies carried out to elucidate the mechanisms of Au-catalyzed cycloadditions involving allene subunits. For theoretical studies on other types of Au-catalyzed reactions concerning allenes see [30–37] and other chapters within this special issue.

## 2 Interaction Between Gold and Allenes

The coordination of alkynes and alkenes to a cationic Au metal center involves a  $\eta^2$  mode. The principal interaction occurs between the  $\pi$ -orbital of the multiple bond and vacant  $6s/6p$  orbitals of the metal center. In contrast, the interaction of an allene moiety to a metal center may occur in different ways but can be classified as two types [38]:  $\eta^2$  complexes involving one of the two C=C bonds (as alkynes and alkenes) and species in which only the central allene carbon is directly coordinated to the metal center (Fig. 2). Depending on the substituents on the allene, different structures of each category can be formed. For instance, structure **I** represents a similar contribution of the two carbon atoms of the double bond in the coordination with the metal center, but distorted structures with a major contribution of central or external carbon can be favored by the presence of electron-donating or electron-withdrawing groups, respectively. The second category can also be represented by different structures such as  $\sigma$ -allylic cations **II**, zwitterionic carbenes **III**, or  $\eta^1$ -coordinated bent allenes **IV**. Remarkably, if the allene is chiral, the stereochemical information is conserved if the interaction gives structures of type **I** or  $\eta^1$ -coordinated bent allenes **IV**. However, the chirality of the allene is lost in structures of types **II** and **III** with the three carbons and their substituents in the same plane.

To understand better the driving forces of this interaction, Malacria and coworkers carried out a computational study in 2008 on the interaction of allenes with gold complexes [38]. Their results suggest that the adopted structures resulting from the interaction between the allene subunit and gold are very dependent on the nature of the allene substituents as well as on the properties of the particular gold complex employed.

For instance, relative energy of the species formed by the interaction among 1,3-dimethyl allene and AuPMe<sub>3</sub> or AuBr<sub>3</sub> were analyzed (Fig. 3a,b). The interaction of the allene with both complexes gives  $\eta^2$ -structures (type **I**) **1a** and **1b**, and two different isomers very close in energy, **2a** and **2b**. Moreover,  $\sigma$ -allylic cations (type **II**) **3a** and **3b** were also observed. Interestingly, this type of structure is more stabilized

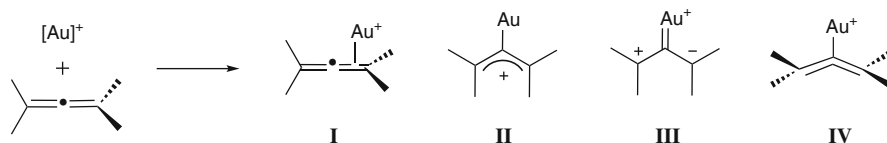


**Fig. 2** Scheme of the possible structure representation for the interaction of an allene moiety and a gold metal center

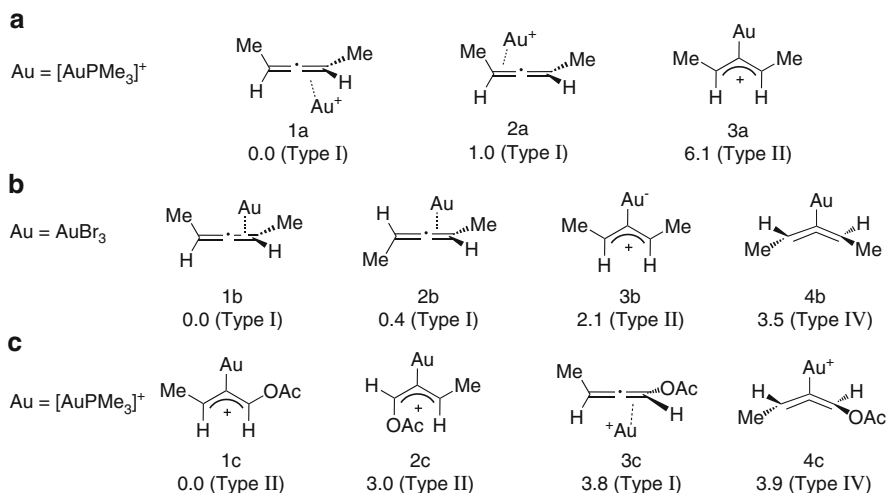


**Fig. 3** Structures of the localized minima for the different gold-allene systems (energies in kcal/mol)

for the  $\text{AuBr}_3$  system **3b** than for  $\text{AuPMe}_3$  **3a**, with relative energies of 2.1 and 6.1 kcal/mol, above the most stable isomer (**1b** and **1a**), respectively. A  $\eta^1$ -coordinated bent allene (type IV) **4b** was observed in the  $\text{AuBr}_3$  system but not with cationic  $\text{AuPMe}_3$ .

The effect of the allene substituents in the interaction with  $\text{AuPMe}_3$  was also analyzed by replacing a methyl group in the allene moiety by acetate. Interestingly, the ground state for this system was a  $\sigma$ -allylic cation structure (type II) **1c**. Most stable of the other minima obtained are indicated in Fig. 3c. The relative stability of the allylic cation structure **1c** with regard to the  $\eta^2$ -coordinated structure **3c** (3.8 kcal/mol) can be explained in terms of electron-donor characteristics of the acetate group, confirmed by the short C–O distance of 1.31 Å in species **1c**.

It is noteworthy that some recent theoretical studies have shown that allenic species, not observed experimentally, could be key intermediates for some Au-catalyzed isomerization and cycloaddition reactions of unsaturated systems [39–43].

One example is the reactivity of a propargylic ester with two cationic AuL catalysts ( $\text{L} = \text{PMe}_3$  and 2,3dimethylimidazol-2-ylidene *Ime*, Fig. 4) [42]. Three key intermediates were identified (**i-1**, **i-2**, **i-3**), along with the reaction pathways interconnecting each other. Gold propargylic ester species **i-1** can evolve to gold vinyl carbenoid species **i-2** through a 1,2-acyl migration, whereas a 1,3-acyl migration gives rise to the gold allene species **i-3**. The theoretical calculations also showed that a second 1,2-acyl migration can interconnect **i-2** with **i-3**. Analysis of the energy barriers and the energy values of all the intermediates allow one to conclude that the three key species **i-1**, **i-2**, and **i-3** are in rapid equilibrium. The authors introduced the term “golden carousel” in order to describe such behavior. Interestingly, the allene **i-3** intermediate is more stable than **i-1** and **i-2**, by approximately 8 kcal/mol. This could suggest that intermediate **i-3** acts as a reservoir of active species.

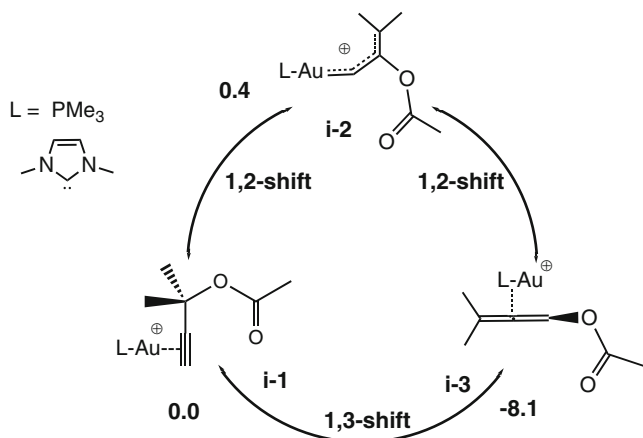


**Fig. 4** Scheme of the three localized intermediates of the interaction of a propargylic ester with Au complexes. Zero point corrected energies in solution for Au *Ime* system, in kcal/mol

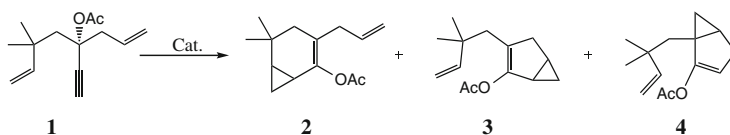


**Fig. 5** Scheme of the Au-catalyzed reaction of the dienyne **1**

These similar relative energies are in concordance with the variety of products that have been observed within this kind of catalysis.

In 2009, a similar theoretical analysis was presented by the same authors for the Au-catalyzed reaction of dienyne **1** (Fig. 5) [43]. Products **2–4** were observed in different ratio depending on the catalyst. Their calculations indicate that this catalytic reaction involves several competitive reactions pathways. A mechanism via a gold vinyl carbenoid (such as **i-2**) can explain the formation of products **2** and **3**, whereas a pathway with a gold allene intermediate (such as **i-3**) was proposed for the formation of product **4**. Therefore, metal-allene intermediates seem to be involved in this kind of isomerizations catalyzed by gold complexes.

A gold(I)-catalyzed rearrangement of acyloxypropargyl oxiranes was described by Faza, Soriano, de Lera, and coworkers [39]. The theoretical mechanistic study of reactant **5** (Fig. 6) indicated that several gold catalyzed isomerizations are energetically accessible; all these mechanisms go through different allenic intermediates. The calculations indicate that three different mechanisms can explain the formation of **6** through some rearrangement steps. Figure 6 shows the initial key intermediates for the different mechanisms: the initial coordination of the triple bond to the metal center gives rise an allenic intermediate **i-4**, by a 1,3-ester migration, or through a carbenic intermediate **i-5**, by a 1,2-ester migration. Additionally, the oxirane activation by the Au-complex can evolve to the allenic intermediate **i-6** that might also afford **6** after

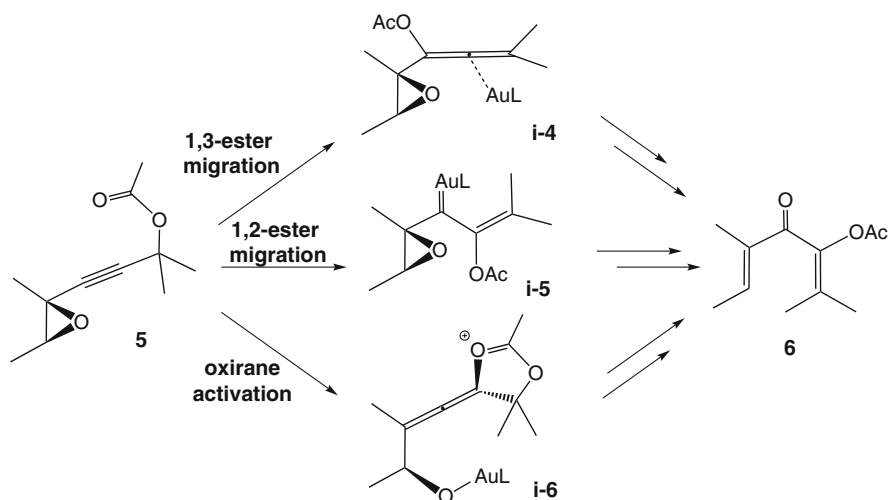


**Fig. 6** Simplified scheme of the three possible mechanisms for the Au-catalyzed rearrangement of reactant **5**

several steps. The preferred mechanism (1,3 ester migration) for this facile synthetic transformation involves a sequence of more than eight steps with all the functional groups in the substrate playing a crucial and synergistic role.

### 3 Gold-Catalyzed Cycloadditions Between Allenes and Dienes

#### 3.1 [4C + 3C] Cycloadditions

In 2008, Mascareñas and co-workers developed a new [4C + 3C] intramolecular cycloaddition of allenedienes (**7**) to synthesize seven-membered ring subunits (**8**) based on a Pt(II)-catalyzed process [44]. One year later they also demonstrated that the same reactions can also be performed using Au(I) catalysts, under milder conditions (Fig. 7) [45].

One of the key features of these methods is the ability of Pt and Au complexes to form allylic cationic species **i-7** from non functionalized allenes (Fig. 8) [46, 47]. This allylic cation moiety participates as three carbon-2 $\pi$ -electron component in the subsequent [4C + 3C] cycloaddition with the diene. Hence, the number of electrons involved in this cycloaddition are six [4 $\pi e^-$  + 2 $\pi e^-$ ], similar to the well-known Diels–Alder reaction. As for a common Diels–Alder reaction, this [4C + 3C] cycloaddition involves the formation of two  $\sigma$ -carbon bonds by rearrangement of three  $\pi$ -bonds. However, a seven-membered ring is formed, **i-8**. Intermediate **i-8** can be stabilized by retrodonation of the metal center to the former central-carbon of the allene, a situation that can be understood as a metal-carbene or a metal-stabilized carbocation.

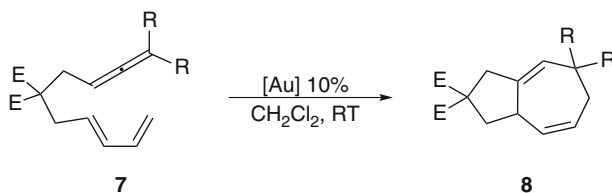


**Fig. 7** General scheme of the experimental Au-catalyzed [4C+3C] cycloaddition

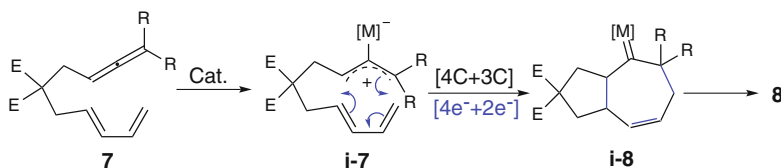
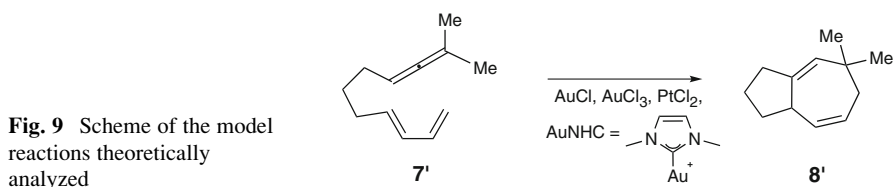


**Fig. 8** Scheme of the electronic rearrangement of the Au- and Pt-catalyzed [4C+3C] cycloaddition



A mechanistic analysis of the Au-catalyzed [4C + 3C] intramolecular cycloaddition of allenediene **7'** was carried out using DFT methods. Figure 9 shows the model system used in the calculations, which were carried out with AuCl, AuCl<sub>3</sub>, Au(NHC), and PtCl<sub>2</sub> complexes as catalysts [45].

The results suggest analogous mechanisms for all of these catalysts. The catalytic cycle is shown in Fig. 10. The mechanism starts with the  $\eta^2$ -coordination (type **I**) of one of the two double bonds of the allene **7'** to the metal center. Both species **A** and **A'** evolve to a  $\sigma$ -allylic cation **B** (type **II**) that allows the subsequent concerted [4C + 3C] intramolecular cycloaddition step forming the heptacyclic structure **C**. The last step is a 1,2-H shift leading to a new double C–C bond coordinated to the metal center (**D**). The catalytic cycle is closed by product (**8'**) decooordination and catalyst regeneration.

Intermediates **A** and **A'** were localized for all the catalysts, and the energy difference between them is relatively small, within a range of 2.5 kcal/mol. Hence, there is an equilibrium between both coordination modes. For most of the catalysts, **A'** is the most stable intermediate. However, the formation of the allylic cation intermediate **B** is more accessible from the species **A**. The transition state of this process adopts a slipped  $\eta^1$ -coordination to the central carbon atom of the allene (type **II'**). Intermediate **B** evidences a  $\sigma$ -allylic cation structure (type **II**) with an

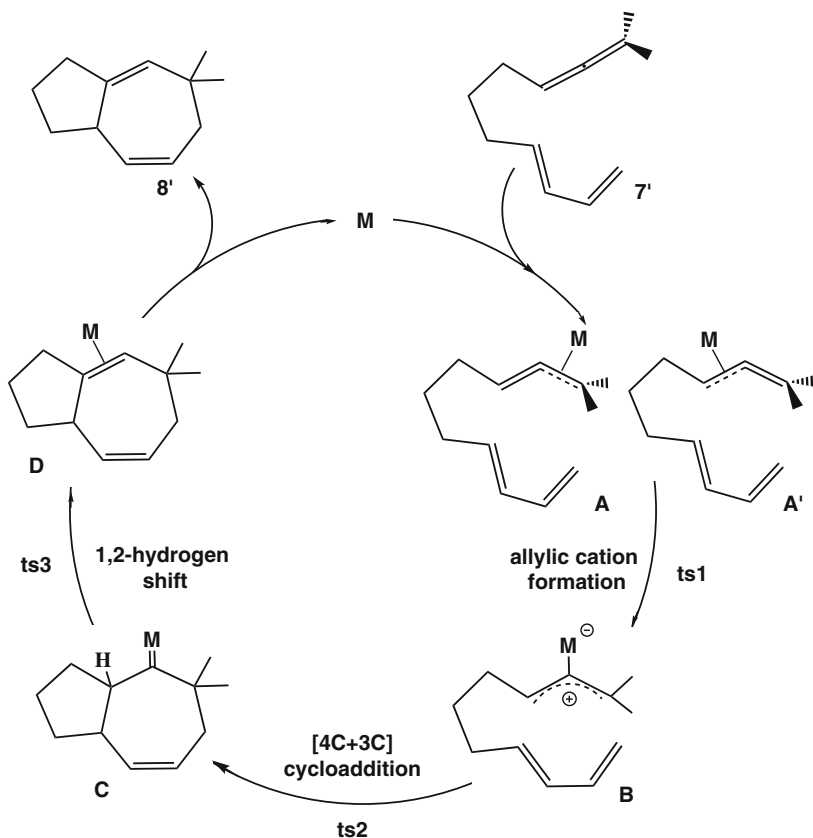


**Fig. 10** Catalytic cycle proposed from the theoretical analysis for the [4C+3C] cycloaddition

angle close to  $120^\circ$  between the three allene carbons. Moreover, the planarity around the allene moiety, including the three methyls and hydrogen substituents, is also observed (Fig. 11).

The [4C + 3C] intramolecular cycloaddition is a concerted and diastereoselective process. All the attempts to localize a stepwise mechanism or a minimum with only one C–C bond formed were unsuccessful. The cycloaddition can take place in two different arrangements of the diene over the metal-allyl moiety giving rise to diastereoisomeric cycloadducts, *Cexo* and *Cendo*. The transition states leading to these two diastereoisomers can be depicted as *exo*- or *endo*-like structures (Fig. 12). These two pathways were explored in the case of the  $\text{PtCl}_2$ -catalyzed process. The energy barrier of the **ts2** *endo*-like cycloaddition is 5.7 kcal/mol higher than that of the **ts2** *exo*-like. According to the experimentally observed diastereoselectivity, the *exo*-like pathway is clearly favored, as the *endo* product was not observed. Interestingly, the *endo*-like transition state shows that in this conformation the cycloaddition would take place in an asynchronous manner, with the external C–C bond

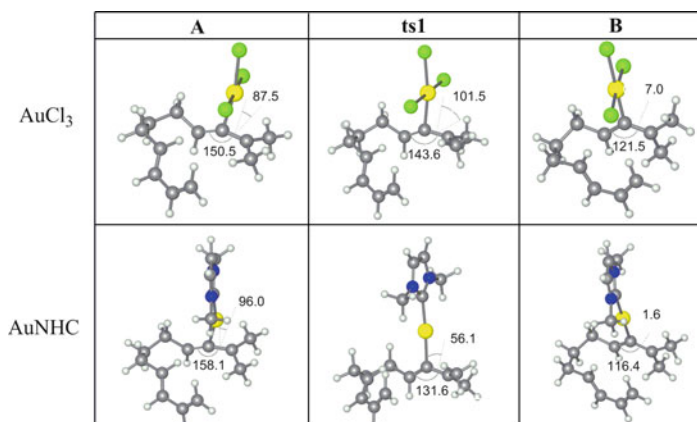


**Fig. 11** Geometries of **A**, **ts1** and **B** for AuCl<sub>3</sub> and Au(NHC). Angle formed by the three allene carbons and dihedral Au–C–C–CH<sub>3</sub> are shown (angles in degrees)

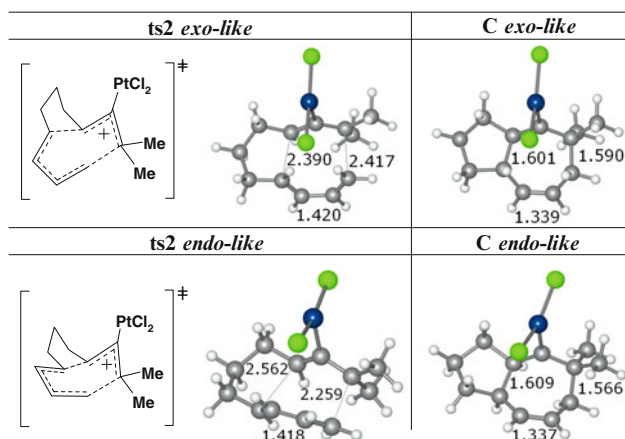


**Fig. 12** Geometries of *exo* and *endo-like* **ts2** and **C** intermediate for PtCl<sub>2</sub> system, (distance in Å)

being more formed (2.259 Å) than the internal one (2.562 Å) (Fig. 12). The major stability of the *exo-like* process probably stems from steric effects. Moreover the **C<sub>endo</sub>** and **D<sub>endo</sub>** intermediates are ~2 kcal/mol and ~6 kcal/mol less stable than their *exo-like* counterparts, respectively. With regard to Au catalysts, a similar situation is expected. Thus, the most favored transition states corresponded to an *exo-like* concerted cycloaddition and all of them were found to be highly synchronous, except for Au(NHC) (Table 1).

The [4C + 3C] cycloaddition forms the bicyclic intermediate **C** with the aforementioned C–M bond type that can be defined as gold stabilized cation or gold carbene. In this sense, and being aware of the actual controversy on the nature of



**Table 1** Distances of the two forming C–C bonds of the [4C+3C] cycloaddition transition state **ts2** and the C–M bonds for intermediates **B** and **C** (distances in Å)

	C–C <sub>dist</sub> on <b>ts2</b> <i>exo-like</i>			C–M <sub>dist</sub>		
	Internal	External	Difference	<b>B</b>	<b>C</b>	Difference
AuCl	2.378	2.353	0.025	2.048	1.972	0.076
AuCl <sub>3</sub>	2.436	2.464	−0.028	2.069	2.028	0.041
Au(NHC)	2.448	2.292	0.156	2.081	2.047	0.034
PtCl <sub>2</sub>	2.390	2.417	−0.027	1.959	1.848	0.111

the bond of these species [26–29], it is worth noting that **C** intermediates showed a shorter C–M bond than the precursor intermediate **B**, therefore supporting some double bond nature of **C** (Table 1). The biggest difference in C–M value (0.111 Å) was observed in the case of PtCl<sub>2</sub>. This is also in agreement with the well accepted higher ability of Pt compared to Au of stabilizing and forming carbenic C=M bonds [48].

The 1,2-H shift is a one-step process for all the catalysts studied by these authors except for Au(NHC) system. In this latter case the carbene intermediate **C** evolves to a different conformer **C'** (through transition state **ts3'**), prior to undergoing the 1,2-H migration, which eventually occurs through transition state **ts3** (Fig. 13). The principal difference between both conformers, **C** and **C'**, can be described by the H–C–C–M dihedral angle: 161.1° for intermediate **C** and 91.2° for **C'** (Fig. 13). In any case, the barrier for the formation of **D** from **C'** is rather low (3.3 kcal/mol). Thus, in practice, the process from **C** to **D** could be also considered as a single step process with Au(NHC).

The conformational change observed for the Au(NHC) system is also required for the 1,2-H shift (**ts3**) with the others catalysts, as can be deduced from their respective transition states **ts3** (Table 2). Hence, this conformational change seems to be required for the 1,2-H shift, in order to optimize the interaction between the 1s hydrogen orbital and the free 2p<sub>z</sub> orbital of the carbene. The H–C–C–M dihedral values of **C** and **ts3** for all the catalyst are shown in Table 2. As can be deduced from this data, the dihedral angle in **ts3**, corresponding to the 1,2-H migrations is almost identical for all catalysts, close to 90°, and just slightly bigger for PtCl<sub>2</sub>.

The energy profiles for AuCl, AuCl<sub>3</sub>, Au(NHC), and PtCl<sub>2</sub> are shown in Fig. 14 (formation of **C'** is omitted since it doesn't change the general mechanistic analysis nor the overall energy barriers of the process). The energy barriers of the allylic cation formation (**ts1**), [4C + 3C] cycloaddition (**ts2**) and 1,2-H shift or (**ts3**) are shown in Table 3.

The energy barriers for the allylic cation formation and the relative stability of intermediate **B** showed that this process is very dependent on the nature of the catalyst. This step involves an increase of the electron density on the metal center. Accordingly, the more the complex is electron-accepting, the easier the process. Hence, the lowest barrier for AuCl<sub>3</sub> compared with AuCl is reasonable. The low barriers and the relative stability of intermediate **C** ensure a fast and irreversible [4C + 3C] cycloaddition step for all the catalysts.

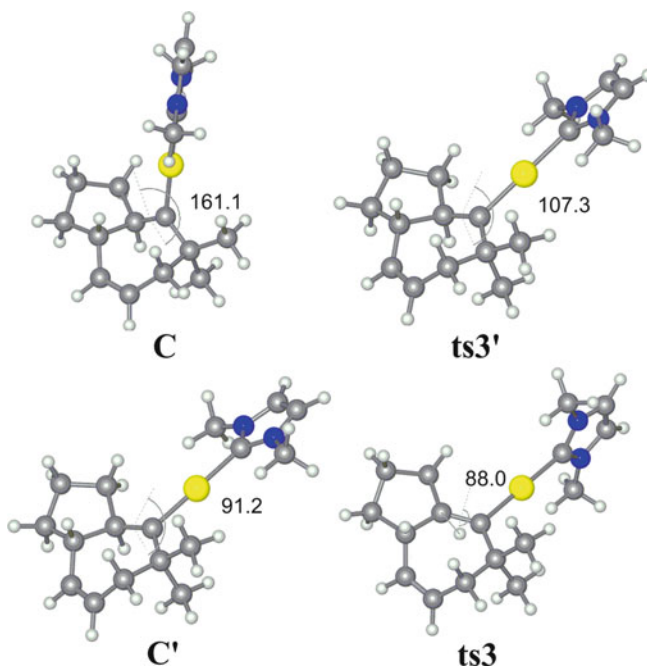


**Fig. 13** Geometries of the species involved on the 1,2-hydrogen shift for Au(NHC) catalyst. The H–C–C–M dihedral values are shown (angles in degrees)

**Table 2** Values of the H–C–C–M dihedral parameter for C conformers and 1,2-H-shift transition state **ts3** (angles in degrees)

	<b>C</b>	<b>ts3'</b>	<b>C'</b>	<b>ts3</b>
AuCl	157.4	–	–	88.3
AuCl <sub>3</sub>	150.7	–	–	88.1
Au(NHC)	161.1	107.3	91.2	88.0
PtCl <sub>2</sub>	114.1	–	–	92.5

According to these authors, the 1,2-H-shift has the highest energy barrier for all the analyzed catalysts (AuCl, AuCl<sub>3</sub>, Au(NHC), PtCl<sub>2</sub>). However, in the case of a family of [AuPR<sub>3</sub>]<sup>+</sup> catalysts, and considering  $\Delta G$ , Benitez et al. have found that the [4C + 3C] cycloaddition can be rate-determining [49]. The relative energy barriers of the different catalysts are in agreement with the experimental observation: the reaction catalyzed by PtCl<sub>2</sub>, which exhibits the highest energy barrier, usually requires high temperatures, whereas a good conversion was obtained for AuCl and AuCl<sub>3</sub> catalysts at room temperature. For Au(NHC), that exhibits the smallest barrier of 8.6 kcal/mol, the reaction can be carried out at 0 °C in less than 1 h.

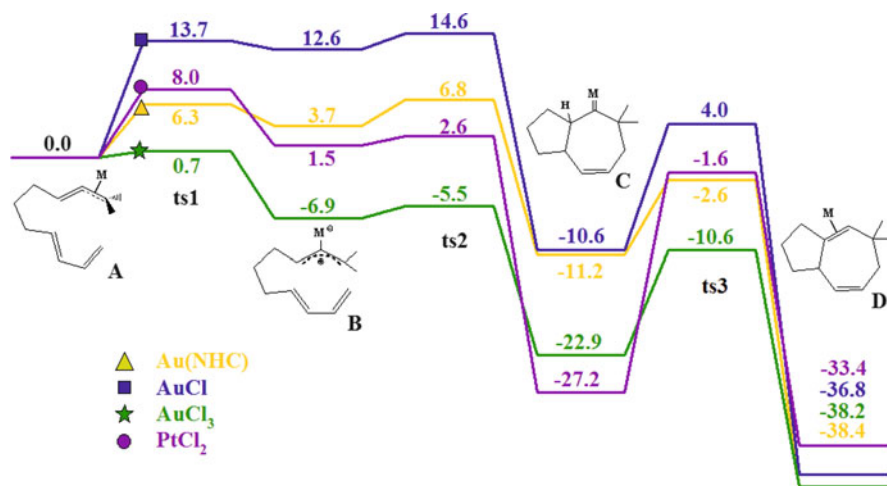


**Fig. 14** Energy profile for all the analyzed catalyst (relative gas phase electronic energies in kcal/mol)

**Table 3** Relative energy barriers for each one of the three reaction steps (relative gas phase electronic energies in kcal/mol)

	ts1	ts2	ts3
AuCl	13.7	2.0	14.6
AuCl <sub>3</sub>	0.7	1.4	12.3
Au(NHC)	6.3	3.1	8.6
PtCl <sub>2</sub>	8.0	1.1	25.6

Therefore, Au-catalysts are more active than PtCl<sub>2</sub>, and the cationic species Au(NHC) is the most effective from those computationally studied. The different behavior between Au and Pt halides catalysts could be traced to the formation of a stronger carbene-Pt bond which implies a major relative stability of intermediate C and hence a lower reactivity because of the higher energy barrier for the subsequent 1,2-H shift.

### 3.2 [4C + 2C] Cycloadditions

It has been experimentally shown that, for the reaction of specific allenedienes with Au-complexes equipped with more electron-accepting ligands such as phosphites and phosphoramidites, the major reaction product becomes the [4C + 2C] cycloadduct **9** instead of the [4C + 3C] adduct **8** (Fig. 15). The formation of these adducts as well as their relative proportions depends on the substrate (the 4 + 2

Entry	Substrate, 7	Product	8 : 9 <sup>b</sup>	9, Yield <sup>c</sup>
1	7a, X = C(CO <sub>2</sub> Et) <sub>2</sub>		1 : 10	9a, 72%
2	7b, X = C(CO <sub>2</sub> Me) <sub>2</sub>		1 : 13	9b, 79%
3	7b, X = C(CO <sub>2</sub> Me) <sub>2</sub>		1 : 19	9b, 85% <sup>d</sup>
4	7c, X = NTs		0 : 1	9c, 80% <sup>d</sup>
5	7d, X = C(CO <sub>2</sub> Me) <sub>2</sub>		0 : 1	9d, 91%
6 <sup>e</sup>	7e, X = NTs		0 : 1	9e, 97%
7 <sup>e</sup>	7f, X = C(CO <sub>2</sub> Et) <sub>2</sub>		0 : 1	9f, 72%
8 <sup>e</sup>	7g, X = NTs		0 : 1	9g, 84%

**Fig. 15** General scheme of the observed experimental [4+3] and [4+2] cycloadditions catalyzed by Au-complexes with strong electron-acceptor ligands. Selected experimental<sup>a</sup> examples. <sup>a</sup>Conditions: (ArO)<sub>3</sub>PAuCl (10 mol%) and AgSbF<sub>6</sub> (10 mol%) in CH<sub>2</sub>Cl<sub>2</sub> (0.15 M) at 0 °C for 1 h. <sup>b</sup>Ratio determined by <sup>1</sup>H-NMR in the crude reaction mixtures. <sup>c</sup>Isolated yields. <sup>d</sup>5 min at –15 °C. <sup>e</sup>40 min at 0 °C

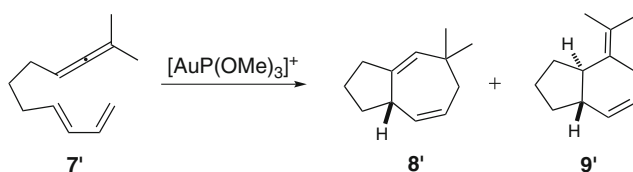


**Fig. 16** Scheme of the model reaction theoretically studied to explore the different mechanisms that lead to 8' and 9'

requires disubstitution of the allene), reaction conditions and specific catalyst employed [50].

Several reaction pathways for the formation of the [4C + 2C] adduct were analyzed by Montserrat et al. by means of DFT calculations, using [(MeO)<sub>3</sub>PAu]<sup>+</sup> as model catalyst and allenediene 7', with two methyl substituents at the distal position of the allene, as model substrate (Fig. 16) [50].

A stepwise process involving a carbocationic intermediate **E** that in principle could evolve to any of both products (8' or 9') was evaluated (Fig. 17). An analogous

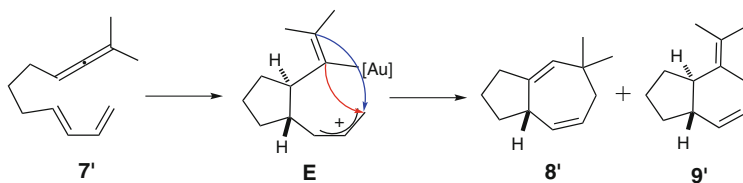


**Fig. 17** Scheme of a hypothetical intermediate for the [4C+2C] cycloaddition mechanism

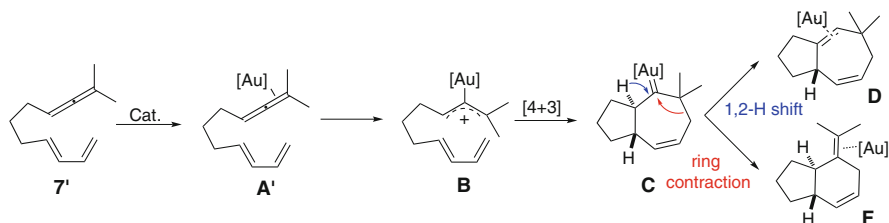


**Fig. 18** Scheme of the theoretical proposal mechanism for the formation of the [4C+3C] and [4C+2C] products

intermediate including a benzylic cation, rather than the allylic one of **E**, was proposed to be an intermediate in Au-catalyzed [2 + 2] cycloaddition of allenes [51]. However, in spite of an intensive theoretical exploration of the potential surface, such intermediate **E** or related species could not be located, presumably due to the instability of the nonsubstituted allylic cation structure **E**. In all the attempts, the activation of **7'** leads to **B** which undergoes a concerted [4C + 3C] cycloaddition, with a very low energy barrier.

Interestingly, the experimental [4C + 2C] cycloadduct product **9** showed the same stereochemistry (hydrogens in *trans*) as the [4C + 3C] cycloaddition products **8** [44, 45, 50]. Moreover, preliminary attempts to develop asymmetric Au(I)-catalyzed cycloaddition using chiral phosphoramidites as gold ligands showed that both [4C + 3C] and [4C + 2C] products were obtained with equal enantiomeric excess [50]. Hence, the formation of both products must have a common diastereo and enantio determining mechanistic step. These facts together with the low barriers found for the formation of the [4C+3C] cycloaddition suggested that the [4C+2C] product **9'**, as well as the [4C+3C] cycloadduct **8'**, could be formed after the initial [4C+3C] cycloaddition step from **B**. Indeed the calculations showed that 1,2-alkyl migration on the cycloheptenyl carbene intermediate **C** can be a pathway competitive with the 1,2-H shift, thus leading to **9'**. This step implies a ring contraction in the carbene intermediate **C** and would provide the [4C+2C] species **F** (Fig. 18). Similar conclusions were also assumed by Benitez et al.[49].

The energy profile for the [AuP(OMe)<sub>3</sub>]<sup>+</sup>-catalyzed reaction is shown in Fig. 19. The formation of the allylic cation and subsequent [4C+3C] cycloaddition convey low energy barriers. The structure of the transition state **ts2** showed that the cycloaddition

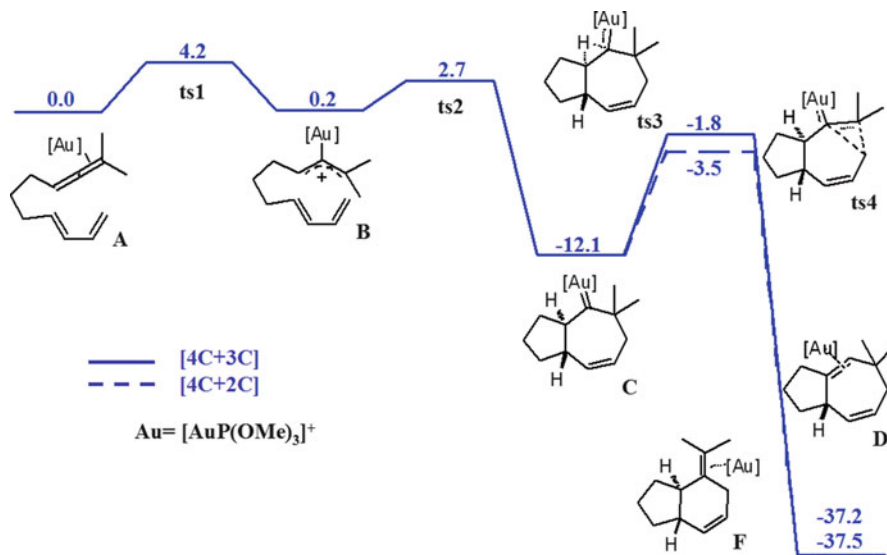


**Fig. 19** Energy profile of the reaction of **7'** with  $[\text{AuP}(\text{OMe})_3]^+$  catalyst (relative gas phase electronic energies in kcal/mol)

process is quite asynchronous. The C–C bond distances are  $d_{\text{C-C}_{\text{internal}}} = 2.055 \text{ \AA}$  and  $d_{\text{C-C}_{\text{external}}} = 2.730 \text{ \AA}$ .

Intermediate **C** is a key divergent point. On one hand it can provide the seven-membered ring adduct by means of a 1,2-H-shift. As in the case of the  $\text{Au}(\text{NHC})$  catalyst, this process takes place in two steps: a preliminary conformational change (**C'** for the  $\text{Au}(\text{NHC})$  system) and the hydrogen shift. Analogously, the barrier for the latter is also very low, 2.2 kcal/mol, and can be considered as a single step. The transition state for 1,2-H shift (**ts3**) showed a value of  $87.2^\circ$  for the dihedral H–C–C–M (Fig. 20). On the other hand it can lead to [4+2] adducts by means of a ring contraction process. The transition state for the required 1,2-alkyl-migration (**ts4**) has a conformation similar to that present in intermediate **C** (the dihedral angle for structures **C** and **ts4** are  $160.9^\circ$  and  $166.3^\circ$ , respectively). In **ts4** the cycloheptyl subunit is being broken ( $d_{\text{C-C}_{\text{broken}}} = 2.033 \text{ \AA}$ ) and the distance of the forming C–C bond to obtain the cyclohexyl is relatively short ( $d_{\text{C-C}_{\text{forming}}} = 1.908 \text{ \AA}$ ) (Fig. 20).

Table 4 shows the energy barriers for the two competitive steps (1,2-H shift and 1,2-alkyl migration) for different Au-complexes. In concordance with the experimental observations, an electron-acceptor ligand at gold ( $[\text{AuP}(\text{OMe})_3]^+$ ) favors the 1,2-alkyl migration compared to the 1,2-H shift. Conversely, with the electron-donor N-heterocyclic carbene ligand ( $\text{Au}(\text{NHC})$ ) the 1,2-H-shift is energetically favored.

Benitez et al. also performed a theoretical analysis of these reaction mechanisms [49], and reported an analog mechanism for the [4C+3C] cycloaddition of allenedienes. Importantly, their results with a more hindered phosphine ligand

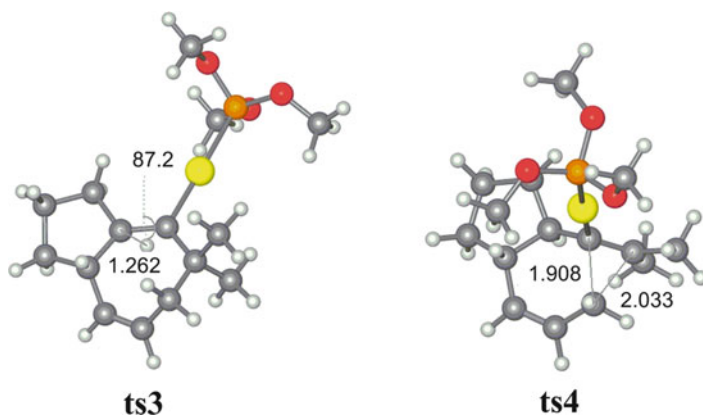


**Fig. 20** Geometries of transition states of the 1,2-hydrogen shift (**ts3**) and 1,2-alkyl migration (**ts4**) for  $[\text{AuP}(\text{OMe})_3]^+$  analyzed system (angles in degrees, distances in Å)

**Table 4** Energy barriers of the competitive pathways, 1,2-H-shift and 1,2-C-migration for the analyzed Au-catalyst (relative gas phase electronic energies in kcal/mol)

	<b>ts3</b>	<b>ts4</b>	Difference
$\text{AuP}(\text{OMe})_3$	10.3	8.6	−1.7
$\text{AuPH}_3$	8.1	8.5	0.4
$\text{AuCl}$	14.6	17.7	3.1
$\text{Au}(\text{NHC})$	8.7	10.8	2.1

( $\text{P}(\text{t}(\text{Bu})_2\text{Ph})$ ) suggested that steric effects can affect the Au–C bonding properties and therefore the reactivity of the process and the ratio of [4+2] and [4+3] adducts. Regarding the nature of the Au–C bond on carbene intermediate **C**, a natural bond orbital (NBO) analysis showed that the Au–carbene bond is formed by weak  $\sigma$  and  $\pi$  components. The  $\sigma$ -interaction takes place between the C  $sp^2$  lone pair overlapping with the 6s gold orbital, which is partially populated by donation of the ligand. The  $\pi$ -component is a donation from a  $d\pi$  Au-orbital to the empty  $p\pi$ -orbital on a carbon atom. As a conclusion from the combination of theoretical and experimental results, these authors suggest that the 1,2-alkyl migration is relatively insensitive to the electronic ligand effect, whereas 1,2-H-shift is affected by the increased population of the C  $p\pi$ -orbital, partially full by donation from the Au  $d\pi$ -electrons. The steric properties of the ligand seem to be a key factor determining this donation from the  $d\pi$  Au-orbital to the C- $p\pi$ -orbital, thus affecting the products ratio.

The theoretical calculations carried out by Monserrat et al. are consistent with the experimental observations that the NHC type of ligands with high donor character the reaction prefers to evolve by conformational change and 1,2-H migration to give cycloheptenyl systems. On the other hand, acceptor ligands like triarylphosphites

give rise to a lower energy barrier for the ring contraction step. This donor-acceptor explanation for the [4+3]/[4+2] dichotomy is also fully consistent with recent experiments published by Furstner et al. on the behavior of NHC-carbene ligands with similar  $\sigma$ -donating properties but different  $\pi$ -acceptor character [52].

The effect of allene substituents on these two competitive pathways was also analyzed [50]. Experimental data suggest that decreasing the substitution leads to a lower reactivity, so that unsubstituted allenes remain unaltered when submitted to the reaction conditions. The theoretical analysis of a reactant analog to **7'** lacking the methyl groups in the terminal allene position, **10'**, revealed that the [4C+3C] cycloaddition could take place in a single step that couples the allene activation and the [4+3] cycloaddition (Fig. 21). Nevertheless, this direct [4C+3C] cycloaddition for this non-substituted substrate **10'** is higher in energy (energy barrier of 6.8 kcal/mol) than that required for reactant precursor **7'**. This different behavior can be explained in terms of a higher difficulty for the formation of the allylic cation due to the lower capacity of less substituted carbons to stabilize positive charges. The 1,2-H shift and the competitive 1,2-alkyl migration steps could be computationally located. The energy barrier of the 1,2-H shift pathway was 11.1 kcal/mol, similar to those for **7'** (10.3 kcal/mol). However, the energy barrier of 1,2-alkyl migration pathway was 23.8 kcal/mol, and hence the process is clearly less favorable than for **7'** (8.6 kcal/mol). According to these values, the formation of the [4+2] cycloadducts seems to be strongly dependent on the ability of allene distal substituents to stabilize the positive charge that is being generated at this carbon center during the 1,2-alkyl migration (**ts4**). This stabilization is obviously higher when this carbon has two alkyl groups, and decreases with the number of alkyl substituents.

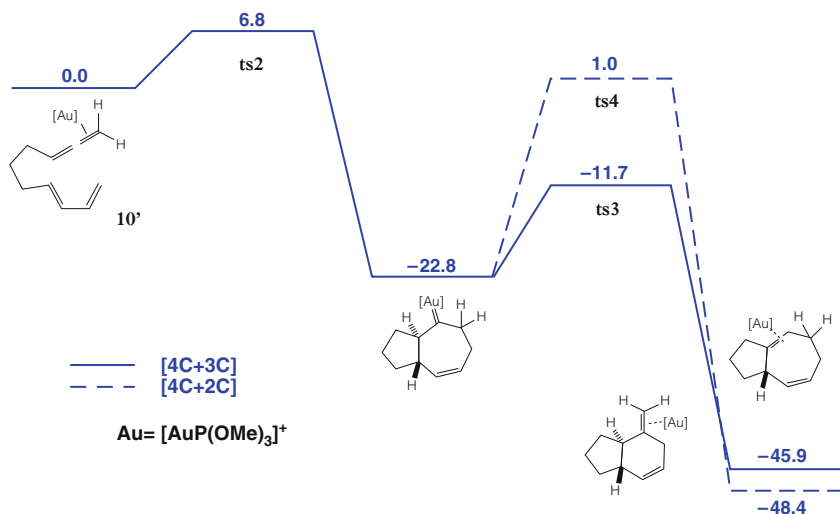


**Fig. 21** Energetic profile founded for the reaction with the non-substituted allene (relative gas phase electronic energies in kcal/mol)



## 4 Other Cycloadditions Involving Allenes

This section is devoted to Au-catalyzed cycloadditions between allenes and alkenes whose mechanisms have been theoretically analyzed.

A gold-catalyzed intramolecular [3+2] cycloaddition of 1-aryl-1-allene-6-enes to give *cis*-fused products was recently reported by Liu and coworkers (Fig. 22a) [53]. In the case of substrate **11**, products **12**, **13**, and **14** were experimentally observed (Fig. 22b). The authors carried out a mechanistic DFT study to evaluate the observed [3+2] *cis*-stereoselectivity of product **12**.

The proposed mechanism starts with coordination of the disubstituted double bond of the allene to the metal center to give complex **i-9** (Fig. 23). This intermediate evolves through an intramolecular 6-*endo-dig* cyclization by nucleophilic attack of the internal carbon of the alkene.

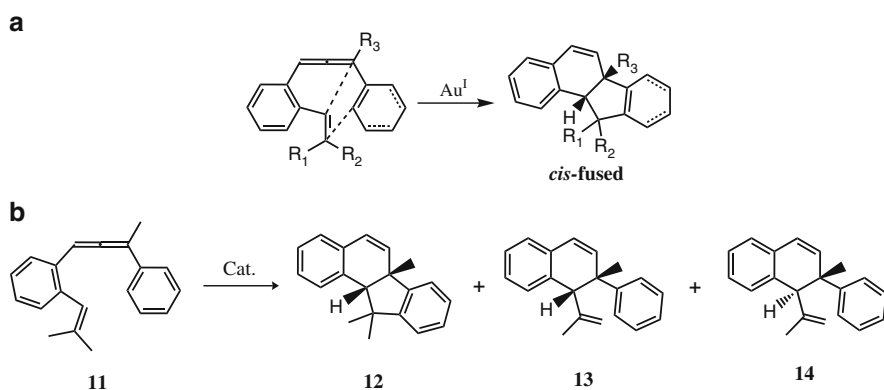


**Fig. 22** General reaction for Au-catalyzed [3+2] cycloaddition of 1-aryl-1-allene-6-enes

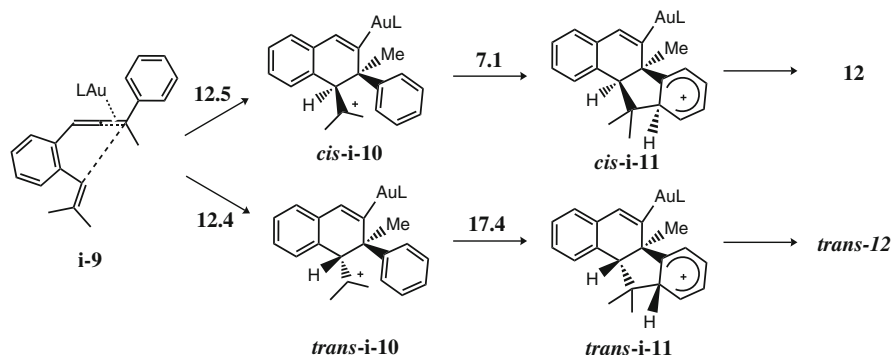


**Fig. 23** Calculated intermediates for the stepwise [3+2] cycloaddition. Zero point energy barriers in kcal/mol [53]

intermediates **cis-i-10** and **trans-i-10**. The calculations indicate that indeed a mixture of **cis-i-10** and **trans-i-10** isomers can be formed, as the energy barriers are similar (12.4 kcal/mol and 12.5 kcal/mol, respectively), as well as their relative stability (**trans-i-10** is 1.6 kcal/mol more stable than **cis-i-10**). Both intermediates can form the **cis-i-11** or **trans-i-11** adducts through an intramolecular arylation process (formally the whole process is a [3+2] cycloaddition). However, the *cis*-pathway is clearly favored over the *trans*-, the energy barriers being 7.1 and 17.4 kcal/mol, respectively. These results follow the experimental trend since the *trans*-isomer was never observed.

Surfing through the literature one can find other cycloaddition reactions that involve the participation of allene and alkene moieties, though the allene is not formally present in the starting material. Propargyl acetates **15** evolve through an Au-catalyzed [3,3] rearrangement into allenyl acetate intermediate **i-12** (Fig. 24). The reaction mechanism of this rearrangement was theoretically analyzed by Malacria and coworkers [54]. This is a clear example of the relatively easy interconversion between propargylic acetates and allenyl species, as previously commented on (Fig. 4). The allene intermediate **i-12** exhibits different reactivity depending on the number of substituents  $R_1$ ,  $R_2$ , and  $R_3$  (methyls or hydrogens) and the length of the ( $n = 1, 2$ ). Three products **16**, **17**, and **18** were isolated. The first one implies a [4+2] cycloaddition, whereas additional rearrangements are necessary to obtain the other two products.

The gold catalyzed reaction of allenyl acetate species **i-12** was theoretically analyzed, and calculations led to propose the mechanism shown in Fig. 25. The coordination of gold to the allenic intermediate **i-12** may give rise to two different

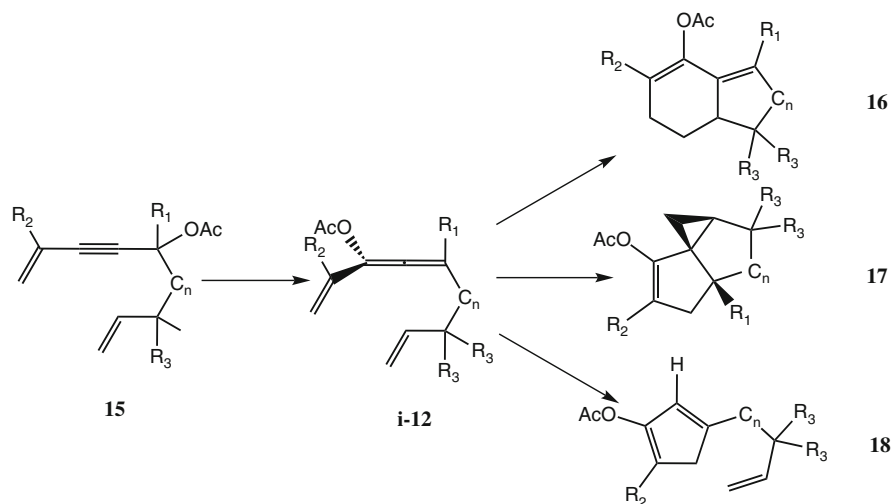


**Fig. 24** Scheme of the Au-catalyzed reaction of propargyl acetate **15** and structure of the proposed allenic intermediate **i-12** [54]

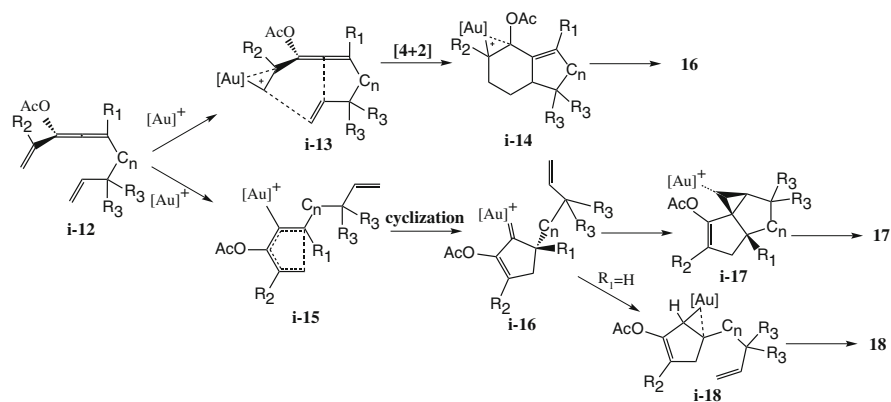


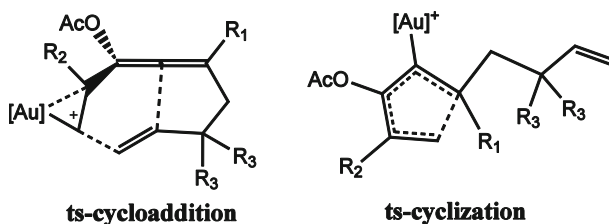
**Fig. 25** Scheme of the proposed mechanism via the allenic intermediate **i-12** for the Au-catalyzed reaction of propargyl acetate **15** [54]

intermediates: complexes of type **i-13** with the alkene coordinated, or **i-15** with allene coordination. In turn, **i-13** can evolve through a [4+2] cycloaddition that forms a bicyclic intermediate **i-14**. On the other hand, **i-15** is structurally similar to a bent-allene (type **II'**, Fig. 2) that retains the chirality of the starting allene. A Nazarov-like cyclization of **i-15** forms the cyclopentenylidene **i-16**. The presence of the alkene group allows the electrophilic cyclopropanation forming the species **i-17** as a competitive pathway of the 1,2-hydride migration that forms species **i-18** when  $R_1=H$ .

Regarding the [4+2] cycloaddition process, a reaction mechanism was computationally found with or without the assistance of the catalyst. The energy barriers (enthalpies at 298 K) of the uncatalyzed pathway were relatively high, over 23 kcal/mol independent of the substituents. The Au-catalyzed pathway reduced the energy barrier of this process by ~4 kcal/mol, except for  $R_2=Me$ . Both cycloaddition pathways take place in a concerted asynchronous manner forming first the bond between the external carbons of the alkenes, followed by the other with the central allene carbon.

The relative stability of **i-13** and **i-15** is similar, so the chemoselectivity of this reaction is determined by the relative energy barriers of the [4+2] cycloaddition and the Nazarov-like cyclization steps. Table 5 shows the difference values calculated for the energy barriers of both competitive [4+2] cycloaddition and cyclization pathways, depending on  $R_1$ ,  $R_2$ ,  $R_3$  for  $n = 1$  (no dependence on the length chain was observed). The calculations found that the cyclization step is favored over the cycloaddition. Then, although the products of both competitive pathways were observed experimentally, the theoretical study predicts only formation of products **17** and **18**. However, the experimental observed trend with the substituents is consistent with the calculations. The cycloaddition pathway is favored when the allene is tetrasubstituted  $R_1=Me$ , and the vinyl moiety is monosubstituted  $R_2=H$ ; otherwise the formation of cyclopentadiene **i-16** is clearly favored (Table 5).

**Table 5** Differences between the energy barriers of the two competitive pathways [4+2] cycloaddition and cyclization for a sort of reactants depending on the substituted  $R_1$ ,  $R_2$  and  $R_3$ . Catalyzed by Au(PMe<sub>2</sub>Ph) calculated enthalpy differences at 298 K in kcal/mol



$R_1$	$R_2$	$R_3$	$\Delta\Delta H_{298}(\text{ts-cyclization favored})^\#$
H	H	H	11.5
Me	H	H	5.2
H	Me	H	18.2
H	H	Me	10.4
Me	H	Me	2.5
H	Me	Me	17.3

## 5 Concluding Remarks

The analysis of the reaction mechanisms for gold-catalyzed cycloaddition reactions by means of theoretical methods involving allenes has been assessed in the present chapter. The complexation of the allene moiety to the metal center is always described as the first step towards its reactivity. Regarding this interaction between gold(I)-complexes and allenes, several isomers with relatively similar energies can be formed. The stability of these species is highly dependent on both the allenic substituents and the nature of the ligands at gold. Therefore, the participation of different allenic intermediates is crucial to understanding the extensive reactivity observed in these gold-catalyzed processes.

One of the most important gold-catalyzed cycloadditions is that involving allenes and dienes. This reactivity is shown to give different products, six- and seven-membered rings depending on the nature of the catalyst. According to the theoretical studies, the mechanism proposed for the [4C+3C] intramolecular cycloaddition has three main steps: (1) allene coordination of the catalyst and formation of an allylic cation, (2) cycloaddition leading to a seven-membered ring intermediate, and (3) 1,2 H-shift and formation of the [4C+3C] cycloaddition product.

The reaction mechanism for the formation of the [4C+2C] product is shown to be rather similar, sharing the two initial steps (1) and (2) that provide the seven-membered ring intermediate. The difference is introduced in the third step. This reaction step (3) involves a ring contraction (1,2 alkyl migration, instead of a 1,2 H-shift) giving rise to the six-membered ring cycloaddition product. The preferred formation of 4+3 or 4+2 adducts can be certainly controlled by modifying the

characteristics of the gold ligand. Therefore more electron-donor ligands like NHC favor the 4+3 pathway whereas electronacceptor triphosphite type of ligands favor the ring contraction process leading to the formal [4+2] adducts.

Theoretical analysis of other gold-catalyzed reactions involving allenes and alkenes has provided an explanation of the chemo- and stereoselectivity observed. Theoretical studies have also shown the implication of allenes as intermediates in gold-catalyzed reactions of other precursors such as propargylic derivatives.

To conclude, theoretical analyses of gold-catalyzed processes are still scarce, although they have witnessed an important impulse in recent years. In general the theoretical calculations have been quite consistent with the experimental results and helped to propose mechanistic alternatives and explain reactivity behavior. No doubt the use of increasingly sophisticated theoretical tools will be of great help to advance further new gold-catalyzed processes and refine those already developed. In particular, the rich and diverse reactivity of allenes in gold-catalyzed reactions promises to take advantage of the theoretical progress.

**Acknowledgements** We are grateful to the Spanish MICINN (Projects CTQ2008-06866-CO2-01, SAF2007-61015, Consolider Ingenio 2010 CSD2007-00006, and FPU fellowship to S. M.), to Generalitat de Catalunya (2009/SGR/68), and to Xunta de Galicia (INCITE09 209 122 PR).

## References

1. Kobayashi S, Jørgensen KA (2002) Cycloaddition reactions in organic synthesis. Wiley-VCH, Weinheim
2. Alcaide B, Almendros P, Aragoncillo C (2010) Exploiting [2+2] cycloaddition chemistry: achievements with allenes. *Chem Soc Rev* 39:783–816
3. Huang X, Zhang L (2007) Two step formal [3+2] cycloaddition of enones/enals and allenyl MOM ether: gold highly diastereoselective synthesis of cyclopentanone enol ether containing an all-carbon quaternary center. *J Am Chem Soc* 129:6398–6399
4. Ma S (2005) Typical advances in the synthetic applications of allenes. *Chem Rev* 105: 2829–2871
5. Krause N, Hashmi ASK (2004) Modern allene chemistry, vol 1 and 2. Wiley-VCH, Weinheim
6. Ma S (2009) Electrophilic addition and cyclization reactions of allenes. *Acc Chem Res* 42: 1679–1688
7. Ma S (2007) Recent advances in the chemistry of allenes. *Aldrichim Acta* 40:91–102
8. Fürstner A, Davies PW (2007) Catalytic carbophilic activation: catalysis by platinum and gold  $\pi$  acids. *Angew Chem Int Ed* 46:3410–3449
9. Zhang L, Sun J, Kozmin SA (2006) Gold and platinum catalysis of enyne cycloisomerization. *Adv Synth Catal* 348:2271–2296
10. Hashmi ASK, Hutchings GJ (2006) Gold catalysis. *Angew Chem Int Ed* 45:7896–7936
11. Hashmi ASK (2007) Gold-catalyzed organic reactions. *Chem Rev* 107:3180–3211
12. Jiménez-Nuñez E, Echavarren AM (2007) Molecular diversity through gold catalysis with alkynes. *Chem Commun* 333–346
13. Li Z, Brouwer C, He C (2008) Gold-catalyzed organic transformations. *Chem Rev* 108: 3239–3265

14. Shen HC (2008) Recent advances in syntheses of heterocycles and carbocycles via homogeneous gold catalysis. Part 1: heteroatom addition and hydroarylation reactions of alkynes, allenes and alkenes. *Tetrahedron* 64:3885–3903
15. Shapiro ND, Toste FD (2010) A reactivity-driven approach to the discovery and development of gold-catalyzed organic reactions. *Synlett* 675–691
16. Gorin DJ, Toste D (2007) Relativistic effects in homogeneous gold catalysis. *Nature* 446: 395–403
17. Pyykkö P (2004) Theoretical chemistry of gold. *Angew Chem Int Ed* 43:4412–4456
18. Jiménez-Núñez E, Echavarren AM (2008) Gold-catalyzed cycloisomerizations of enynes: a mechanistic perspective. *Chem Rev* 108:3326–3350
19. Liu L-P, Hammond GB (2009) Reaction of cationic gold(I) with allenates: synthesis of stable organogold(I) complexes and mechanistic investigations on gold-catalyzed cyclizations. *Chem Asian J* 4:1230–1236
20. Straub BF (2004) Gold(I) or gold(III) as active species in  $\text{AuCl}_3$ -catalyzed cyclization/cycloaddition reactions? A DFT study. *Chem Commun* 1726–1728
21. Soriano E, Marco-Contelles J (2009) Mechanistic insights on the cycloisomerization of polyunsaturated precursors catalyzed by platinum and gold complexes. *Acc Chem Res* 42: 1026–1036
22. Comas-Vives A, González-Arellano C, Corma A et al (2006) Single-site homogeneous and heterogeneous gold(III) hydrogenation catalysis: mechanistic implications. *J Am Chem Soc* 128:4756–4765
23. Nieto-Oberhuber C, López S, Muñoz MP et al (2005) Divergent mechanisms for the skeletal rearrangement and [2+2] cycloaddition of enynes catalyzed by gold. *Angew Chem Int Ed* 44: 6146–6148
24. Nieto-Oberhuber C, Pérez-Galán P, Herrero-Gómez E et al (2008) Gold(I)-catalyzed intramolecular [4+2] cycloadditions of arylalkynes or 1,3-enynes with alkenes: scope and mechanism. *J Am Chem Soc* 130:269–279
25. Cuenca AB, Montserrat S, Hossain KM et al (2009) Gold(I)-catalyzed intermolecular oxyarylation of alkynes: unexpected regiochemistry in the alkylation of arenes. *Org Lett* 11: 4906–4909
26. Fürstner A, Morency L (2008) On the nature of the reactive intermediates in gold-catalyzed cycloisomerization reactions. *Angew Chem Int Ed* 47:5030–5033
27. Hashmi ASK (2008) “High noon” in gold catalysis: carbene versus carbocation intermediates. *Angew Chem Int Ed* 47:6754–6756
28. Benitez D, Shapiro ND et al (2009) A bonding model for gold(I) carbene complex. *Nat Chem* 1:482–486
29. Echavarren AM (2009) Carbene or cation? *Nat Chem* 1:431–433
30. Lemièrre G, Gandon V, Agenet N et al (2006) Gold(I)- and gold(III)-catalyzed cycloisomerization of allenynes: a remarkable halide effect. *Angew Chem Int Ed* 45:7596–7599
31. Cheong PH-Y, Morganelli P et al (2008) Gold-catalyzed cycloisomerization of 1,5-allenynes via dual activation of an ene reaction. *J Am Chem Soc* 130:4517–4526
32. Yang C-Y, Lin G-Y et al (2008) Gold-catalyzed hydrative carbocyclization of 1,5- and 1,7-allenynes mediated by  $\pi$ -allene complex: mechanistic evidence supported by the chirality transfer of allenyne substrates. *J Org Chem* 73:4907–4914
33. Xia Y, Dudnik AS, Gevorgyan V, Li Y (2008) Mechanistic insights into the gold-catalyzed cycloisomerization of bromoallenyl ketones: ligand-controlled regioselectivity. *J Am Chem Soc* 130:6940–6941
34. Paton RS, Maseras F (2009) Gold(I)-catalyzed intermolecular hydroalkoxylation of allenes: a DFT study. *Org Lett* 11:2237–2240
35. Alcaide B, Almendros P et al (2009) Metal-catalyzed cyclization of  $\beta$ - and  $\gamma$ -allenols derived from D-glyceraldehyde synthesis of enantiopure dihydropyrans and tetrahydrooxepines: an experimental and theoretical study. *Chem Eur J* 15:9127–9138

36. Zhu R-X, Zhang D-J et al (2010) Mechanism study of the gold-catalyzed cycloisomerization of  $\alpha$ -aminoallenes: oxidation state of active species and influence of counterion. *J Phys Chem A* 114:4689–4696
37. Dudnik AS, Xia Y, Li Y, Gevorgyan V (2010) Computation-guided development of Au-catalyzed cycloisomerizations proceeding via 1,2-Si or 1,2-H migrations: regiodivergent synthesis of silylfurans. *J Am Chem Soc* 132:7645–7655
38. Gandon V, Lemièrre G, Hours A, Fensterbank L, Malacria M (2008) The role of bent acyclic allene gold complexes in axis-to-center chirality transfers. *Angew Chem Int Ed* 39:7534–7538
39. González Pérez A, Silva López C, Marco-Contelles J et al (2009) Mechanism of the gold-catalyzed rearrangement of (3-acyloxyprop-1-ynyl)oxiranes: a dual role of the catalyst. *J Org Chem* 74:2982–2991
40. Mauleón P, Krinsky JL, Toste D (2009) Mechanistic studies on Au(I)-catalyzed [3,3]-sigmatropic rearrangements using cyclopropane probes. *J Am Chem Soc* 131:4513–4520
41. Garayalde D, Gómez-Bengoa E, Huang X et al (2010) Mechanistic insights in gold-stabilized nonclassical carbocations: gold-catalyzed rearrangement of 3-cyclopropyl propargylic acetates. *J Am Chem Soc* 132:4720–4730
42. Correa A, Marion N, Fensterbank L, Malacria M, Nolan SP, Cavallo L (2008) Golden carousel in catalysis: the cationic gold/propargylic ester cycle. *Angew Chem Int Ed* 47:718–721
43. Marion N, Lemièrre G, Correa A et al (2009) Gold- and platinum-catalyzed cycloisomerization of enynyl esters versus allenyl esters: an experimental and theoretical study. *Chem Eur J* 15: 3243
44. Trillo B, López F, Gulías M, Castedo L, Mascareñas JL (2008) Platinum-catalyzed intramolecular [4C+3C] cycloaddition between dienes and allenes. *Angew Chem Int Ed* 47:951–954
45. Trillo B, López F, Montserrat S, Ujaque G, Castedo L, Lledós A, Mascareñas JL (2009) Gold-catalyzed [4C+3C] intramolecular cycloaddition of allenedienes: synthetic potential and mechanistic implications. *Chem Eur J* 15:3336–3339
46. Funami H, Kusama H, Iwasawa N (2007) Preparation of substituted cyclopentadienes through platinum (II)-catalyzed of 1,2,4-trienes. *Angew Chem Int Ed* 46:909–911
47. Lee JH, Toste FD (2007) Gold(I) catalyzed synthesis of functionalized cyclopentadienes. *Angew Chem Int Ed* 46:912–914
48. Heinemann C, Hertwig HR, Wesendrup R et al (1995) Effects on bonding in cationic transition-metal-carbene complexes: a density-functional study. *J Am Chem Soc* 117: 495–500
49. Benitez D, Tkatchouk E et al (2009) On the impact of steric and electronic properties of ligands on gold(I)-catalyzed cycloaddition reactions. *Org Lett* 11:4798–4801
50. Alonso I, Trillo B, López F, Montserrat S et al (2009) Gold-catalyzed [4C+3C] cycloadditions of allenedienes including an enantioselective version with new phosphoramidite-based catalysts. Mechanistic aspects of the divergence between [4C+3C] and [4C+2C] pathways. *J Am Chem Soc* 131:13020–13030
51. Luzung MR, Mauleón P, Toste D (2007) Gold(I)-catalyzed [2+2]-cycloaddition of allenes. *J Am Chem Soc* 129:12402–12403
52. Alcarazo M, Stork T, Anoop A et al (2010) Steering the surprisingly modular  $\pi$ -acceptor properties of N-heterocyclic carbenes: implications for gold catalysis. *Angew Chem Int Ed* 49: 2542–2546
53. Chaudhuri R, Liao H-Y, Liu R-S (2009) Gold-catalyzed intramolecular [3+2] cycloadditions of 1-aryl-1-allene-6-enes. *Chem Eur J* 15:8895–8901
54. Lemièrre G, Gandon V, Cariou K et al (2009) Generation and trapping of cyclopentenylidene gold species: four pathways to polycyclic compounds. *J Am Chem Soc* 131:2993–3006

# Index

## A

Acetalcyclopropenes, 22, 35  
 3-Acetoxy 1,2,4-trienes, 118  
 Acetoxallene, 93  
 Acridines, 39  
 8-(3-Acyloxyprop-1-ynyl)oxiranes  
 Acyloxypropargyl oxiranes, 229  
 Alcohols, Pd-catalyzed aerobic  
   oxidation, 141  
 Alkenes, electrophilic activation, 9  
   hydrogenation, 92  
   nucleophiles, 68  
   reactivity, 136  
 Alkenyl alkynylamides,  
   cycloisomerization, 40  
 Alkoxycyclization, 64  
 Alkyl-carbene elimination, 148  
 Alkynes, 2, 83  
   attack of alkene, 89  
   metal-catalyzed addition of alkene, 32  
 Alkynophilic character, 1  
 Alkynophilicity, 12, 85  
 Alkynyl aldehydes,  $\alpha$ -substituted, 49  
 Alkynyl- $\beta$ -ketoesters, cycloisomerization, 48  
 Allenedienes, cycloaddition, 230  
 Allenes, 2, 157, 183, 225  
   coordination modes, 158  
   cycloadditions with dienes, 230  
   hydroalkoxylation, 92  
   hydroamination, 9  
   interaction with gold, 227  
   reactivity, 136  
   stability, 100

$\gamma$ -Allenols, 2-azetidinone-tethered, 185  
   cycloetherification, 183  
   metal-catalyzed heterocyclization, 208  
 Allenynes, hydrative  
   carbocyclizations, 173  
 Allylpropargylethers, 60  
 Allylsilanes, cycloisomerization, 45  
 Allylstannanes, cycloisomerization, 45  
 Aminoallenes, 8  
 1-Aryl-1-allene-6-enes, Au-catalyzed  
   [3+2]cycloaddition, 242  
   cycloisomerization, 173  
 Arylamination, 147  
 Au-allene, 160  
 Au-phosphines, 9  
 Au(III) 7  
 [AuXL] 4  
 Aura-Nazarov cyclization, 119  
 Aurophilicity, 3, 4  
 Azadimethylbicyclo[3.1.1]heptanes, 178

## B

B3LYP/6-311G(d,p) 8  
 Bicyclic derivatives, 50  
 Bicyclo[3.1.0]hexenes, 51  
 Bicyclo[4.1.0]hexanes, 53  
 Bicyclobutene, 56  
 Bicyclopropane, 50  
   derivatives, cycloisomerization, 51  
 Binepine, 63  
 1,5-Bisallenenes, 178  
 Bromoallenyl ketone, 8



**C**

Carbene–carbocation continuum, 88  
Carbenes, 18  
Carbocation model, 18  
Carbon nucleophiles, 68  
Carbon–carbon bonds, 2  
Carbon–heteroatom bonds, 2  
Carbophilic activation, 1, 31  
Catalysis, transition metals, 131  
Cations, 157  
Chirality, memory, 81  
    transfer, 91, 157, 164  
Chromazonanol, 64  
Computational chemistry, 1, 81, 131  
Conia ene type reactions, 47  
Cycloadditions, 92, 225  
Cycloalkyne, 15  
Cyclobutyl carbocation, 33  
Cyclododecyne, 15  
Cycloheptatriene, 41  
Cycloheptyne–Au(I) complexes, 13  
1,4-Cyclohexadienes, 45  
Cyclohexane, 47  
Cyclohexyl isopropyl amine, 48  
Cycloisomerization, 6, 31, 157  
Cyclopentenylidene, 244  
Cyclopropanations, 25, 37, 95  
Cyclopropanes, 20  
Cyclopropyl carbene, 38  
Cyclopropyl carbenoids, 86  
Cyclopropyl metallocarbenoids, 18  
Cyclopropylallenyl esters, 163

**D**

Dewar–Chatt–Duncanson model, 9, 21  
DFT studies, 7, 82, 225  
Dictamnocide, 64  
1,3-Dienes, 37  
1,4-Dienes, 42  
Dienynes, Au-catalyzed reaction, 229  
    cycloisomerization, 58  
    domino hydroarylation/  
        cycloisomerization, 71  
1,5,9-Dienynes, phenoxylation/  
    cycloisomerization, 63  
*gem*-Digold, 24  
Dihydrofurans, 92

Dihydropyran, 92  
    cyclopropane-annulated, 50  
1,3-Dimethylallene, gold complexes, 166  
6,7-Dimethyl–3-azabicyclo[3.1.1]  
    heptanes, 178  
Dioxolane, 67  
Diphosphinocarbenes (PHCs) 22  
Domino carbonyl addition/  
    cycloisomerization, 66  
Domino cycloisomerization/oxidation, 67  
    / Prins cyclization, 65  
Domino enyne cycloisomerization-  
    nucleophile addition, 60  
Domino hydroamination/  
    cycloisomerization, 74  
Domino hydroarylation/  
    cycloisomerization, 72  
Domino processes, 90

**E**

Electron core potential (ECP) 90  
Electronic structure, 1  
Enamine intermediates, 48  
Ene acetoxo-vinylallenes, 119  
Energy decomposition analysis (EDA) 21  
Englerins, 67  
Enynes, 6, 31  
    cycloisomerizations, 37, 41, 92  
    propargylic, 85  
Epoxide propargyl acetates, 122  
Epoxides, 8  
Epoxyalkynes, 92  
Ethylene–metal-ion interaction, 9

**F**

Fischer-carbene, 20, 34  
Friedel–Crafts type hydroarylation, 7

**G**

Gold, 1, 3, 31, 157, 183  
    catalysis, 225  
    complexes, ion pairing, 139  
Gold-allene systems, 228  
Gold carbenes, 19, 36  
Gold–gold bonds, 4

Gold propargylic esters, 228  
Gold ylide, 19  
Gold(I) 4  
Gold(I) benzyldiene, 19  
Gold(I)-alkyne complexes, 15, 85  
Golden carousel, 88, 133

## H

Halides, 5  
*N*-Heterocyclic carbenes (NHC) 9, 131  
Heterocyclization, 183  
Homogeneous catalysis, 131  
Hydroarylation, 7

## I

Icetexone, 41  
Imidazol-1-ylidene, 21  
Indenes, 39  
*N*-heterocyclic carbene (NHC) ligands, 9  
Ion pairing, 139

## L

LACVP 90  
LANL2DZ 90  
LANL2TZ(f) 8  
Laurebiphenyl, 50  
Lewis acids, 1, 83  
    carbophilic, 32  
    properties, 1  
Lycopladine, 50

## M

Macrocycles, 41, 44  
Memory of chirality, 81  
Metacycloprodigiosin, 41  
Metal-alkene complexes, 9  
Metal-alkyne complexes, 10  
    bonding, 83  
Metal-ethylene complexes, 9  
Metal-vinylidene complex, 7

## N

Naphthalenes, 39  
Negishi alkyl-alkyl cross-coupling, 146

NHC ligands, 9  
Nitrogen nucleophiles, 73  
Nitroolefins, 93  
Noble metals, 81  
Nucleophiles, aromatic rings, 69  
Nucleophilic additions, 102

## O

Olefin cyclopropanation, 92  
Orientalol, 67  
Oxepane ether rings, 184  
4-Oxoazetidines-2-carbaldehydes, 183  
Oxygen nucleophiles, 60

## P

Palladium, 9  
    Pd-catalyzed aerobic oxidations, 141  
    Pd-catalyzed cross coupling  
        reactions, 145  
    Pd-catalyzed Negishi reaction, 146  
Palladium-NHC bond, 147  
3,4-Pentadienal, 93  
Pericyclic reactions, 104  
Phenanthrenes, 7  
Phosphane, 9  
Platencin, 50  
Platinum, 1, 31, 149, 183  
Podophyllotoxin, 64  
Post-lanthanide elements, 2  
Prodiginine antibiotics, 41  
Propargylcyclopropanols, 9  
Propargylic acetates, 8, 243  
    1,*n*-enynes, 94  
Propargylic enynes, 85  
Propargylic esters, 32, 85, 133  
Propargylic substrates, 81  
Pubinernoid B 67  
Pyrrolidine, bicyclic, 73

## R

Rautenstrauch reaction, 92  
Reaction pathways/mechanisms, 131,  
    183, 225  
Rearrangements, 81  
Relativistic effects, 2  
Roseophilin, 41

**S**

Sabinone, 50  
Salviasperanol, 41  
Selectivity, homogeneous catalysis, 5  
Silver tetrafluoroborate, 139  
Silyloxyenynes, 45, 48  
    cycloisomerization, 49  
Spiropyranones, 92  
Streptorubin B 41

**T**

Tetrahydrofurans, 93  
Tetrahydronaphthalenes, 40  
Tetrahydrooxepines, 209

Tol-binap-gold chloride, 64  
Transition metal catalysis, 131  
Trienynes, cycloisomerization, 58  
Triethynyl-based phosphines, 47  
Triflimidate gold catalyst, 47

**V**

Vinylaurate, 33  
    oxonium, 65  
Vinylidene, 7

**Z**

Zeise's salt, 13